4-10-2023 2:30 PM

New Aspects of Scattering Amplitudes, Higher-k Amplitudes, and Holographic Quark Gluon Plasmas

Bruno Giménez Umbert, *The University of Western Ontario*

Supervisor: Buchel, Alex, *The University of Western Ontario*

A thesis submitted in partial fulfillment of the requirements for the Doctor of Philosophy degree in Physics

Abstract

We present new results on different aspects of quantum field theory, which are divided into three main parts. In part I, we find and prove a new behavior of massless tree-level scattering amplitudes, including the biadjoint scalar theory, the U(N) non-linear sigma model, and the special Galileon, within specific subspaces of the kinematic space. We also derive new formulas for the double-ordered biadjoint scalar and ϕ^p amplitudes, which can be obtained as integrals over the positive tropical Grassmannian and under limiting procedures on the kinematic invariants. This reveals surprising connections with cubic amplitudes. We also present alternative versions of the formulas for ϕ^p amplitudes from combinatorial considerations in terms of non-crossing chord diagrams. In part II, we investigate the generalization of quantum field theory introduced by Cachazo, Early, Guevara and Mizera (CEGM) in 2019. We use soft limits to determine the number of singular solutions of the generalized scattering equations in certain cases and propose a general classification of all configurations that can support singular solutions. We also describe the generalized Feynman diagrams that compute CEGM amplitudes. These are planar arrays of Feynman diagrams satisfying certain compatibility conditions, and we propose combinatorial bootstrap methods to obtain them. Finally, in part III, we analyze different types of quark gluon plasmas in the presence of a background magnetic field using top-down holographic models. We explore conformal and nonconformal theories as consistent truncations of $\mathcal{N} = 8$ gauged supergravity and identify a universal behavior in the $\mathcal{N} = 2^*$ gauge theory.

Keywords: quantum field theory, scattering amplitude, Feynman diagram, CEGM amplitude, tropical Grassmannian, AdS/CFT, quark gluon plasma.

Summary for Lay Audience

Quantum field theory provides an excellent mathematical framework for explaining natural phenomena. In recent years, new approaches have emerged, allowing for the discovery of novel properties and alternative perspectives on the framework. This thesis investigates various aspects of quantum field theory. Firstly, we focus on scattering amplitudes, the primary physical observables of the theory that determine the likelihood of a scattering process, and which are tested in particle accelerators. Our research identifies new properties of scattering amplitudes for massless particles, and introduces new formulas for their computation using the positive tropical Grassmannian space. Our study is motivated by the fact that obtaining new information on the behavior and structure of scattering amplitudes is important in order to understand what makes such functions special and relevant to the physical world.

In addition, we explore the recent CEGM generalization of quantum field theory. Its physical relevance is still mysterious, but we study it with the aim of developing new tools for learning more about nature. Specifically, we analyze solutions to the equations that govern the CEGM formula and characterize the objects that compute the corresponding generalized amplitudes from a more familiar quantum field theoretic perspective.

Finally, we use the AdS/CFT correspondence, a duality between a quantum field theory and a gravitational theory, to study aspects of the quark gluon plasma, a state of matter similar to that which prevailed in the early universe and that can be reproduced in experiments. We identify a universal behavior in a theory with intrinsic scale which partially resembles the theory of quantum chromodynamics. This enables us to gain a better understanding of the properties of more realistic quark gluon plasmas.

Overall, this thesis presents new insights into quantum field theory observables, as well

as exploring aspects of the CEGM generalization and the potential of the AdS/CFT duality for enhancing our knowledge of the physical world.

Co-Authorship Statement

This thesis is based on articles [69], [85], [84], [74] and [62].

Chapter 2, together with the accompanying appendices A and B, are based on the article [69], which was coauthored with Freddy Cachazo and Nick Early and published in the Journal of High Energy Physics.

Chapter 3, together with the accompanying appendices C and D, are based on the article [85], which was coauthored with Freddy Cachazo and posted to the online arXiv. Exception is the section 3.8, which consists of results of mine and also in collaboration with Freddy Cachazo, and are as yet unpublished.

Chapter 4, together with the accompanying appendices E and F, are based on the article [84], which was coauthored with Freddy Cachazo and Yong Zhang and published in the Journal of High Energy Physics.

Chapter 5, together with the accompanying appendices G and H, are based on the article [74], which was coauthored with Freddy Cachazo, Alfredo Guevara and Yong Zhang and posted to the online arXiv.

Finally, chapter 6, together with the accompanying appendices I and J, are based on the article [62], which was coauthored with Alex Buchel and published in the Journal of High Energy Physics.

I am the sole author of all other parts of the thesis, including chapter 1 and chapter 7.

"*For beauty is the only thing that time cannot harm. Philosophies fall away like sand, and creeds follow one another like the withered leaves of Autumn; but what is beautiful is a joy for all seasons and a possession for all eternity.*"

Oscar Wilde

"*I've dreamt in my life dreams that have stayed with me ever after, and changed my ideas: they've gone through and through me, like wine through water, and altered the colour of my mind. And this is one: I'm going to tell it — but take care not to smile at any part of it.*"

Emily Brontë

Acknowledgements

First of all, I would like to express my heartfelt gratitude to Alex Buchel and Freddy Cachazo for their mentorship, guidance, patience and friendship. I have learned a lot from you and I can only feel deeply grateful for having shared your science with me.

I want to thank Alex Buchel for being an excellent advisor. You gave me complete freedom to pursue my research interests and provided invaluable support and kindness throughout the years. Thank you for teaching me about holography and for our collaboration. I truly enjoyed our physics conversations and your enthusiasm for the subject.

I am very grateful to Freddy Cachazo, whom I also consider an advisor, for our collaborations and for generously sharing your vast knowledge and your way of coming up with simple solutions to profound problems with me. Working with you was a truly exciting experience and I always felt at the frontier of the field. I greatly enjoyed our many stimulating conversations and exchange of ideas, which expanded my understanding of physics and made me become a better physicist. I would also like to thank you for your unwavering support and kindness during these years.

I wish to express my gratitude to the rest of my wonderful collaborators: Nick Early, Alfredo Guevara and Yong Zhang. I have learned a great deal from each of you, and you have been an endless source of inspiration and knowledge for me throughout our collaborations. Thank you also to Tibra Ali, Latham Boyle, Hugo Marrochio, Rob Myers, Andre Pereira, Nika Sokolova, Pedro Vieira and Beni Yoshida for discussions that have enriched my knowledge about physics. And thank you to Mina Arvanitaki, Davide Gaiotto and Daniel Gottesman for teaching very interesting courses.

Thank you Roberto Emparan, Tomeu Fiol and David Mateos for teaching me very interesting physics and for the hospitality when I visited the University of Barcelona.

It has been an enormous privilege to be part of the Perimeter Institute during all these years. I would like to thank all the amazing people there for providing such an inspiring and delightful environment every day. Thank you for making Perimeter feel like a second home, and for making this journey an unforgettable one. What a wonderful and special place to grow as a physicist and as a human being!

I would like to express my heartfelt appreciation to all the friends I have made at Perimeter. I am grateful to those already mentioned and, of course, to those that haven't been mentioned, but you know who you are. Thank you for all the wonderful times we have shared and for the many more we will continue to share. You have been and continue to be incredibly important and meaningful to me, and I cannot express my gratitude enough. Your friendship is the most valuable treasure I take from this entire experience.

Finally, I would like to thank my old friends from the Baix Montseny, as well as those in Barcelona and elsewhere. I am truly grateful for your presence in my life. And thank you to my family, for everything, especially my parents and my sister for all the love and support you have provided throughout my life. It's hard to put into words the depth of my gratitude. I dedicate this thesis to you.

Dedication

To my parents Lluís and Elena, to my sister Marián, and to the memory of all those who I wish were here to share this celebration with me.

Als meus pares Lluís i Elena, a la meva germana Marián, i en memòria de tots aquells amb qui hagués desitjat compartir aquesta celebració.

A mis padres Lluís y Elena, a mi hermana Marián, y en memoria de todos aquellos con quien hubiese querido compartir esta celebración.

Table of Contents

List of Tables

List of Figures

Chapter 1

Introduction

An important part of all the observed natural phenomena can be explained from quantum field theory. This theoretical framework seamlessly blends two foundational pillars of theoretical physics, quantum mechanics and special relativity, both of which were established in the early 20th century. Quantum field theory provides the foundation for our understanding of interacting physical systems, and its many remarkable scientific achievements include the prediction of the anomalous magnetic moment of the electron [173].

Among the most fundamental physical quantities we find scattering amplitudes, which determine the probability of a scattering process to happen, and as such they serve as the primary physical observables in quantum field theory. Scattering amplitudes can be tested at high energy colliders like the Large Hadron Collider (LHC), and thus build important bridges between theory and experiments. In fact, scattering of particles at the LHC is what triggered the discovery of the Higgs boson in 2012 [1].

In 1949 Feynman and Dyson introduced a robust way for computing scattering amplitudes perturbatively by summing over diagrams which make local interactions and unitary evolution in spacetime manifest [116, 100, 101]. Each of these diagrams represents a possible way the scattering could happen, and they evaluate to a mathematical expression. These are known by the name of *Feynman diagrams*. They were originally introduced to compute scattering between electrons and photons, described by the theory of quantum electrodynamics (QED). Later on, Feynman diagrams were also used for calculating collisions of other particles like quarks and gluons, which constitute the building blocks of atomic nuclei, governed by the non-Abelian theory of quantum chromodynamics (QCD).

However, this diagrammatic approach turns out to be most of the time impractical and, perhaps more crucially, it obscures properties inherent to scattering amplitudes. As a prime example, Parke and Taylor proposed in 1986 an extremely compact formula for the maximally helicity violating (MHV) sector of scattering amplitudes of gluons [176], in contrast with the huge number of terms that would appear from Feynman's method due to the introduction of spurious terms. This important result opened the door for new ideas for computing and understanding scattering amplitudes from different perspectives, making new properties manifest at the cost of obscuring already known ones, and some without even making any reference to spacetime [22]. In fact, it was in 2003, after Nair's work [171], when Witten introduced a groundbreaking method for computing scattering amplitudes [206] by formulating the S-matrix of $\mathcal{N} = 4$ super Yang-Mills (SYM) —a supersymmetric "relative" of QCD— from correlation functions of a certain string theory obtained by integrating over the moduli space of maps of punctured Riemann spheres to twistor space $\mathbb{CP}^{3|4}$ [182, 73, 79, 82]. Another major breakthrough in the field was due to Britto, Cachazo, Feng and Witten (BCFW) in 2005 [48], when they developed recursion relations for constructing scattering amplitudes just from knowledge about the their analytic structure, and other physical properties [35].

There has been an increasing interest in the study of massless particle scattering in the last years, one of the reasons being the simplifications they evoke. But there is a more fundamental motivation for studying them: most of the particles of the Standard Model are effectively considered massless at high enough energies, with the exception of the Higgs boson and probably the neutrinos[1] [179, 121]. Therefore, gaining a deeper understanding of the scattering of massless particles can be of significant physical importance.

1.1 S-matrices in QFT and CEGM amplitudes

One approach of particular interest for this thesis will come from the CHY formulation, proposed by Cachazo, He and Yuan in 2013 [75, 76, 77, 78]. This is a unifying formula that computes tree-level scattering amplitudes in arbitrary spacetime dimensions for different theories of massless particles, like scalars, gluons or gravitons. The CHY formula does not make use of Feynman diagrams, but is an integral defined in the moduli space $X(2,n)$[2] of n points on a one-dimensional complex projective space $\mathbb{CP}^1$. This formula extended Witten's approach to formulate various quantum field theory amplitudes from a worldsheet perspective. It has the form[3]

$$\mathcal{A}_n = \int d\mu_n \, \mathcal{I}_L \, \mathcal{I}_R$$

[1]Although the neutrinos were considered massless when the Standard Model of particle physics was established.

[2]This space is most famously known as $\mathcal{M}_{0,n}$, the moduli space of genus zero Riemann surfaces with n punctures.

[3]Throughout the thesis we will assume that momentum conservation holds, and will therefore not write the amplitude as a distribution.

where $\mathcal{I}_L$ and $\mathcal{I}_R$ are theory dependent "half-integrands", making properties like the double copy [37] manifest. The measure can be written as

$$d\mu_n = (|ij||jk||ki|)^2 \prod_{\substack{1\leq a\leq n \\ a\neq i,j,k}} d\sigma_a \, \delta\left(E_a\right) \,,$$

with $|ab| := \sigma_a - \sigma_b$ being the Plücker coordinates on $X(2,n)$ and σ_a the position of the punctures, and is independent of the choice of i, j, k [73]. A key element in the CHY formula are the scattering equations

$$E_a := \sum_{\substack{1\leq b\leq n \\ b\neq a}} \frac{s_{ab}}{\sigma_a - \sigma_b} = 0\,,$$

with $s_{ab} := (p_a + p_b)^2$, which connect the space of kinematic invariants to $X(2,n)$. These equations can also be computed as the critical points of an $\mathrm{SL}(2,\mathbb{C})$ invariant potential function

$$\mathcal{S} = \sum_{1\leq a<b\leq n} s_{ab} \log|ab|\,,$$

and have appeared in different contexts like in the tensionless regime of string scattering [113, 114, 127, 126, 14]. The scattering equations completely localize the CHY integral on their $(n-3)!$ solutions $\{\sigma_a^{(s)}\}_{s=1,\ldots,(n-3)!}$ and allow us to write the amplitude as

$$\mathcal{A}_n = \sum_{s=1}^{(n-3)!} \frac{(|ij||jk||ki|)^2}{\det\left(\frac{\partial E_a}{\partial \sigma_b}\right)} \mathcal{I}_L \, \mathcal{I}_R \Bigg|_{\sigma_a = \sigma_a^{(s)}} \,.$$

The weights of the measure and the half-integrands under $\mathrm{SL}(2,\mathbb{C})$ transformations on the punctures make the CHY integral $\mathrm{SL}(2,\mathbb{C})$ invariant.

There are plenty of theories known to have a CHY representation [78], and we will study some of them in chapter 2 in order to prove a new behavior developed by scattering amplitudes on certain subspaces of the kinematic space. The simplest scattering amplitudes that admit a CHY representation are those of the biadjoint scalar theory [77]. This is a theory with a $U(N) \times U(\tilde{N})$ flavour group and a scalar field in the biadjoint representation with cubic interactions. Its tree scattering amplitudes can be color-decomposed [161] in terms of partial amplitudes $m_n(\alpha, \beta)$, which depend on two orderings α and β. In their CHY representation, the half-integrands are given by the Parke-Taylor functions $\mathrm{PT}(\alpha)$ and $\mathrm{PT}(\beta)$, defined as

$$\mathrm{PT}(12\cdots n) = \frac{1}{|12||23|\cdots|n1|}\,.$$

These biadjoint scalar amplitudes have also shown to be important e.g. as key elements in the field-theory Kawai-Lewellen-Tye (KLT) relations between pure gravity and Yang-Mills scattering amplitudes [153, 38, 40, 75, 76, 77, 168]. They can also be defined in terms of Feynman diagrams or metric trees, as described later in chapters 2 and 3.

In 2019 Cachazo, Early, Guevara and Mizera (CEGM) proposed a natural generalization of the scattering equations to higher dimensional projective spaces $\mathbb{CP}^{k-1}$ [71], showing deep connections with tropical Grassmannians [195, 194, 140]. We will start exploring this connection in chapter 3 for $k = 2$, which is when the generalization reduces to the quantum field theory realm, where we will construct new formulas that compute scattering amplitudes for various massless scalar theories.

The generalized scattering equations are now computed as the critical points of an $\mathrm{SL}(k, \mathbb{C})$ invariant potential function

$$\mathcal{S}^{(k)} := \sum_{1\leq a_1<a_2<\ldots<a_k\leq n} \mathbf{s}_{a_1,a_2,\ldots,a_k} \log|a_1, a_2, \ldots, a_k|\,,$$

where $\mathbf{s}_{a_1,a_2,\ldots,a_k}$ are completely symmetric rank-k tensors corresponding to generalized kinematic invariants, which satisfy analogous momentum conservation and masslessness conditions. The moduli space on which the generalized scattering equations are defined can be written as a quotient of the Grassmannian $G(k,n)$ by the torus action on each of the columns of a matrix representative of a k-plane, i.e., $X(k,n) := G(k,n)/(\mathbb{C}^*)^n$, and $|a_1, a_2, ..., a_k|$ can be thought of as Plücker coordinates on $X(k,n)$. In chapter 4 we will study the generalized scattering equations, and in particular their number of solutions.

The CEGM generalization begs for an analogous definition of the CHY integral for the biadjoint theory, and in [71] CEGM proposed the following integral

$$m_n^{(k)}(\alpha,\beta) = \int d\mu_n^{(k)} \mathrm{PT}^{(k)}(\alpha)\mathrm{PT}^{(k)}(\beta)$$

to compute a "higher-k amplitude"[4], where the higher-k Parke-Taylor functions are defined as

$$\mathrm{PT}^{(k)}(12\cdots n) = \frac{1}{|12\cdots k||23\cdots k+1|\cdots|n1\cdots k-1|}\,.$$

In chapter 4 we will give a more extensive review of this formula, including the measure $d\mu_n^{(k)}$, and in chapter 5 we will describe the analogous objects to Feynman diagrams that compute these generalized CEGM amplitudes.

[4]Throughout this thesis we will use the terminology "higher-k amplitude", "CEGM amplitude" or "generalized amplitude" to refer to the CEGM generalization of biadjoint amplitudes. But it is well to keep in mind that there might exist an analogous generalization for other theories, especially after the recent introduction of color factors [72]. The study of this possibility is, however, beyond the scope of this thesis.

1.2 Holographic Quark-Gluon Plasmas

One of the peculiarities of QCD is that at low enough energies the theory becomes strongly coupled, and quarks and gluons find themselves forming hadrons. This phenomenon goes by the name of confinement, and in this situation perturbation theory is not useful anymore. It is at much higher energies when the coupling becomes very small (at energies way above a characteristic energy scale of roughly 300 MeV [207]) and perturbation theory can be used. Moreover, deep in the past the universe was in a very high temperature state, one in which quarks and gluons were deconfined and formed a strongly coupled state of matter known as the quark gluon plasma (QGP). In fact, this plasma is currently created at particle accelerators like RHIC or the LHC from high-energy collisions, where after some time it cools down back to the hadronic phase.

It is therefore important to use nonperturbative methods for studying strongly coupled non-Abelian plasmas if we want to have a better general understanding of QCD. For that purpose, one can resort to one of the deepest discoveries in theoretical physics of the last decades: the AdS/CFT correspondence, also known as *holography* or the gauge/string duality [160, 204, 129, 8]. AdS/CFT is a conjectured duality between a quantum field theory and a string theory living in a higher dimensional spacetime. The first example of an AdS/CFT correspondence was due to Maldacena in 1997 [160], which relied on the physics of D3-branes [178]. The duality involves $\mathcal{N} = 4$ $SU(N_c)$ SYM on 4-dimensional Minkowski spacetime, which is a conformal field theory (CFT), and type IIB string theory on $AdS_5 \times S^5$. This duality is an example of a theory of quantum gravity, which can be described in terms of an ordinary quantum field theory.

While $\mathcal{N} = 4$ SYM is characterized by the coupling constant g and the rank of the gauge group N_c (i.e. the number of colors), type IIB string theory on $AdS_5 \times S^5$ is characterized by the string scale l_s, in units of the curvature radius L, and Newton's constant G. One can show that the following relations between parameters follow[5]

$$\frac{L^8}{G} \sim \frac{L^8}{l_P^8} \sim N_c^2\,, \qquad \frac{L^4}{l_s^4} \sim \lambda$$

where l_P is the Planck length and $\lambda \equiv g^2 N_c$ is 't Hooft's coupling constant. One of the powers of AdS/CFT is that in the limit $g \to 0$ and $N_c \to \infty$, such that $\lambda \to \infty$, the theory simplifies and can be approximated by classical (super)gravity, i.e. described by Einstein's general relativity equations.

The duality suggests the following identity for the partition functions on both sides

$$Z_{\rm CFT}(\phi) = Z_{\rm string}(\Phi|_{\partial AdS})\,,$$

where ϕ is a source on the CFT side and $\Phi|_{\partial AdS} = \phi$ is the value of a string field Φ at the AdS boundary. Note that $Z_{\rm CFT}(\phi)$ allows for the computation of correlation functions of gauge invariant operators, and therefore includes all the physical information about the theory. Moreover, in the large N_c limit the right hand side reduces to $Z_{\rm string}(\Phi|_{\partial AdS}) \sim \exp[-S_{\rm grav}(\phi)]$, where $S_{\rm grav}(\phi)$ is the on-shell supergravity action. This means that we can study a strongly coupled gauge theory with a large number of colors, i.e. in the planar limit [200], from a classical theory of gravity living in a higher spacetime dimension. Since S^5 is a compact manifold, it is convenient to dimensionally reduce and get a tower of Kaluza-Klein modes in AdS_5. In this way the holographic principle is realized [201, 198, 44], with the extra dimension in the bulk being related to the direction of the renormalization group flow of the gauge theory.

Despite the fact that $\mathcal{N} = 4$ SYM is different than QCD, e.g. in the number of

[5]Here we are omitting numerical factors, which are irrelevant for the argument.

colors or in that it is conformal and highly supersymmetric, studying this theory and other holographic models has led people to infer important ideas in the understanding of the properties of the QGP and the strongly-coupled dynamics of QCD, including predictions for real world physics [155, 141, 50, 33, 156, 163, 193, 188, 158, 57, 58, 51, 34, 91, 111, 23, 24, 145, 130, 59, 164, 166, 165, 202, 184]. In fact, by introducing a finite temperature one obtains a deconfined thermal state for the strongly coupled gauge theory, keeping some qualitative resemblance with QCD, which is nowadays understood to be dual to a black brane background on the gravity side [128]. One can even generate confinement, e.g. from D4-branes followed by compactifying one dimension on a circle [205]. In chapter 6 we will perform an analysis for different QGPs under a background magnetic field, using holographic models for both conformal and nonconformal gauge theories with $\mathcal{N} = 4$ SYM as their ultraviolet fixed point. For example, we will focus on the $\mathcal{N} = 2^*$ gauge theory, which is a mass-deformed version of $\mathcal{N} = 4$ SYM, and is therefore nonconformal.

The advancements quantum field theory has brought into the understanding of the natural world can only be seen with admiration, and the unknown yet to be discovered is approached with excitement. In this thesis we take a modest step towards a better understanding of some quantum field theoretic aspects, from both the perturbative and the nonperturbative approach. The thesis is divided into three differentiated parts: part I consists of chapter 2, in which we discover and study a novel behavior developed by scattering amplitudes that we call 3-splits; and chapter 3, where we present novel formulas for computing scattering amplitudes from the positive tropical Grassmannian $\text{Trop}^+G(2, n)$. In part II we depart from the quantum field theory realm and analyze aspects of the CEGM generalization of quantum field theory, where we study the solutions of the generalized scattering equations using soft limits in chapter 4, and in chapter 5 we describe the generalized Feynman diagrams that compute CEGM amplitudes for any k. Finally, in part III we study strongly coupled QGPs from various holographic models under a background magnetic field, whose analysis is presented in chapter 6.

PART I

Scattering Amplitudes

The first part of the thesis will explore novel aspects of massless tree-level scattering amplitudes for different quantum field theories.

In the first chapter of this part we discover and present a novel behavior developed by certain tree-level scalar scattering amplitudes, including the biadjoint, the U(N) non-linear sigma model (NLSM), and the special Galileon, when a subset of kinematic invariants vanishes without producing a singularity. This behavior exhibits properties which we call *smooth splitting* and *semi-locality*. The former means that an amplitude becomes the product of exactly three amputated currents, while the latter means that any two currents share one external particle. We call these smooth splittings 3-splits. As they cannot be obtained from standard factorization, they are a new phenomenon in quantum field theory (QFT). Along the way, we also show how smooth splittings naturally lead to the discovery of mixed amplitudes in the NLSM and special Galileon theories and to novel BCFW-like recursion relations for NLSM amplitudes. Finally, we present a discussion of potential future research directions based on the insights gained from our results.

In the second chapter we present new formulas for computing tree-level scattering amplitudes as integrals over the positive tropical Grassmannian $\mathrm{Trop}^{+}G(2,n)$, thus producing a *global Schwinger parameterization*. In particular, we present formulas for the double-ordered partial biadjoint scalar and for ϕ^4 theories. The new formulas are obtained by applying a limiting procedure on the kinematic invariants. We perform a combinatorial study of this procedure, start the exploration of analogous formulas for general ϕ^p theories and discover that ϕ^p amplitudes can be expressed as a sum of products of cubic amplitudes. We also investigate physical properties like factorization and soft limits, and end with a discussion on various ideas related with our results.

Chapter 2

Smoothly Splitting Amplitudes and Semi-Locality

2.1 Introduction

Unitarity and locality are the basic pillars of quantum field theory. Using them as constraints on the S-matrix allows for the construction of scattering amplitudes using recursion relations such as the BCFW [48, 47, 46] or Berends-Giele [93] techniques. At tree-level[1], unitarity implies that scattering amplitudes have simple poles of the form $1/(P^2 - m^2 + i\epsilon)$, with P the sum of momenta of a subset of particles participating in the process and m the mass of a particle in the spectrum of the theory. Moreover, the residues are also completely determined to be the product of two smaller scattering amplitudes; this property is called *factorization*. The original set of particles is partitioned into two sets, often called

[1]Instead of restricting to tree-level, the correct way to describe this is by saying that one-particle states in the completeness relation imply the presence of poles. In this chapter we only work at tree-level so the restriction is enough.

"left" and "right". The two amplitudes in the residue only share an "internal" particle, with momentum P, which is taken to be on-shell, i.e. $P^2 = m^2$. Now, locality is the statement that tree-level amplitudes do not have any other kind of singularities which makes clear the power of the constraints in their computation. There is an important caveat; unitary and locality constrain singularities at finite momenta and unless emergent symmetries at large momenta are present [19], there could be singularities at infinite momenta which prevent the complete reconstruction of the amplitude [35, 110].

Scattering amplitudes in theories with color/flavour are dramatically simplified by the color decomposition into partial amplitudes [93]. The main reason for the simplification is that each partial amplitude can only contain a certain subset of all possible poles the full amplitude can have. These are called *planar poles*. For the canonical ordering $\mathbb{I} = (1, 2, \ldots, n)$, the only possible poles are of the form $1/(p_i + p_{i+1} + \ldots + p_{i+m})^2$. From now on we restrict our attention to massless theories and only to the canonical ordering. Therefore we will simply refer to it as the planar ordering.

Conventional wisdom would say that in regions where kinematic invariants of the form $(p_i + p_j)^2$ vanish and are not planar then a partial amplitude would not have any interesting behavior. In this chapter we show that in fact there are subspaces in the space of kinematic invariants where some non-planar kinematic invariants vanish and the partial amplitude becomes the product of lower point objects without becoming singular. We call the resulting behavior of amplitudes a *smooth splitting* and the corresponding subspace of kinematics invariants *split kinematics*.

Unlike standard factorizations, smooth splittings are semi-local, i.e., a particle can participate in two of the factors. Each factor is not an amplitude but an amputated Berends-Giele current (see e.g. [159]) as they possess one emerging leg which is off-shell. The current is said to be amputated because the propagator corresponding to the off-shell leg is not present.

We find that amplitudes factor in exactly three pieces and we call the corresponding behavior a 3-splitting. When one of the amputated currents only has two on-shell external legs, it becomes trivial, i.e. it is a constant. In such degenerate 3-splits, all original particles but one are either in the "left" or "right" currents while exactly one on-shell external particle is in both. In general 3-splits, each pair of currents shares an external on-shell particle. We call this phenomenon *semi-locality*.

A very important property of 3-splits is that they cannot be obtained from standard unitarity or factorization arguments and thus they do not have any close analog within the standard QFT literature. However, in the recent generalization of QFT amplitudes known as CEGM amplitudes [71], analogous 3-split behavior is common but it appears as the residue of a pole.

A simple way to define split kinematics is by using the structure of the matrix of Mandelstam invariants with entries $s_{a,b}$. Start by introducing three rows and columns labeled by (i,j,k) with $i<j<k$ with non-zero entries and not all three labels cyclically adjacent. Without loss of generality we often set $i=1$. This gives the matrix a "tic-tac-toe" structure. In other words, the matrix now has nine chambers. Split kinematics simply sets to zero the elements $s_{a,b}$ in the six non-diagonal chambers. A schematic representation is given in figure 2.1.

Here the dark entries are non-zero while white entries are zero. Of course, since we are dealing with massless particles any invariant of the form $s_{a,a}$ is zero and hence the white diagonal.

There are exactly $\binom{n}{3}-n$ 3-splits. Incidentally, this is also the dimension of the space of kinematic invariants of generalized $k=3$ CEGM amplitudes and in particular it is the

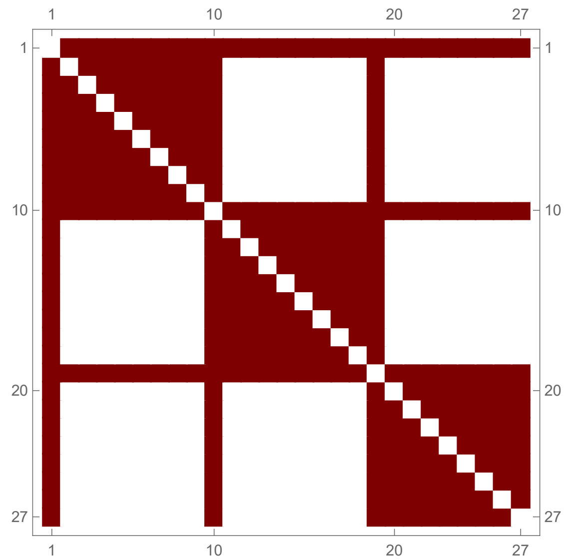

Figure 2.1: Matrix of Mandelstam invariants s_{ab} for the $n = 27$ split kinematics $(1, 10, 19)$, having set to zero all s_{ab}'s in the unshaded regions.

number of planar basis elements, each of which characterizes a pole [107]. Degenerate 3-splits are achieved when two of the labels (i, j, k) are consecutive in the canonical ordering.

The simplest non-trivial 3-split is obtained from the $n = 6$ biadjoint partial amplitude $m_6(\mathbb{I}, \mathbb{I})$ under the $(1, 3, 5)$ split kinematics, i.e, by setting $s_{24} = s_{46} = s_{62} = 0$ and the result is given by

$$m_6(\mathbb{I}, \mathbb{I})|_{\text{split kin.}} = \left(\frac{1}{s_{12}} + \frac{1}{s_{23}}\right)\left(\frac{1}{s_{34}} + \frac{1}{s_{45}}\right)\left(\frac{1}{s_{56}} + \frac{1}{s_{61}}\right). \tag{2.1}$$

This example is discussed in detail in section 2.2. Here we only point out the semi-local character of the expression since particle 3 participates in the first and second factor, particle 5 in the second and third, and particle 1 in the third and first. It is also clear that any of the three factors are obtained from a four-point (three on-shell) Berends-Giele current by amputating the propagator of the off-shell leg. For example, in the first factor the off-shell leg has momentum $P_I = -p_1 - p_2 - p_3$ and $P_I^2 = s_{123} \neq 0$.

2.1.1 Main Results

Now we present the main results in the chapter. We show that on the (i, j, k) split kinematics subspace, the biadjoint partial amplitude becomes the product

$$m_n(\mathbb{I}, \mathbb{I})\big|_{\text{split kin.}} = \mathcal{J}(i, i{+}1, \dots, j{-}1, j)\mathcal{J}(j, j{+}1, \dots, k{-}1, k)\mathcal{J}(k, k{+}1, \dots, i{-}1, i). \quad (2.2)$$

We further show that $\mathcal{J}(1, 2, \dots, m)$ denotes an amputated current with the off-shell leg carrying momentum $-(p_1 + p_2 + \cdots + p_m)$.

Surprisingly, we find that not only biadjoint amplitudes exhibit smooth splitting but so do non-linear sigma model (NLSM) [151] and special Galileon amplitudes [78]. The special Galileon theory does not have color/flavor ordering and thus it seems to be outside the scope of the construction. However, the derivative interactions manage to keep the amplitude finite in the limit as split kinematics is approached. In both NLSM and special Galileon amplitudes, smooth splitting produces currents in their corresponding *extended theories*, as defined by Cachazo, Cha, and Mizera (CCM) [65]. In fact, the smooth splitting behavior provides a new approach to discover the extended theories without resorting to soft limits.

In very schematic form, NLSM and special Galileon amplitudes split as follows,

$$A_n^{\text{NLSM}}(\mathbb{I})\big|_{\text{split kin.}} = \mathcal{J}^{\text{NLSM}}(\mathbb{I})\ \mathcal{J}^{\text{NLSM}\oplus\phi^3}(\mathbb{I}_1|\beta_1)\ \mathcal{J}^{\text{NLSM}\oplus\phi^3}(\mathbb{I}_2|\beta_2) \quad (2.3)$$

and

$$A_n^{\text{sGal}}\big|_{\text{split kin.}} = \mathcal{J}^{\text{sGal}}\ \mathcal{J}^{\text{sGal}\oplus\phi^3}(\beta_1)\ \mathcal{J}^{\text{sGal}\oplus\phi^3}(\beta_2) \quad (2.4)$$

where $\mathbb{I}_i$ and β_i are planar orderings of certain subsets of particle labels. These formulas are derived in section 2.4.

As explained above, having knowledge of the behavior of amplitudes in regions of the space of kinematic invariants can be used to partially or totally reconstruct them. Split kinematics provides novel regions that can be used in addition to unitarity to constrain amplitudes. In fact, NLSM amplitudes are examples where standard recursive techniques do not work [151]. This motivated the use of soft-limits in their recursive construction [87]. Here we show how smooth splitting leads to novel BCFW relations for NLSM amplitudes that do not require knowledge of soft limits.

More precisely, the new BCFW construction induces split kinematics at two points on the one-dimensional deformation space, chosen to be $z = 1$ and $z = -1$. We prove that the following formula,

$$A_n^{\text{NLSM}}(\mathbb{I}) = \frac{1}{2\pi i} \oint_{|z|=\epsilon} dz \frac{A^{\text{NLSM}}(z)}{z(1-z^2)},$$

provides a recursion relation without contributions at infinity. As an example we obtain a new formula for the six-point amplitude

$$\begin{aligned} A_6^{\text{NLSM}}(\mathbb{I}) = & \frac{(s_{12}+s_{23}-s_{123})(s_{45}+s_{56})}{s_{123}} + \frac{(s_{23}+s_{34})(s_{56}+s_{61}-s_{234})}{s_{234}} + \\ & \frac{(s_{34}+s_{45}-s_{345})(s_{61}+s_{12}-s_{345})}{s_{345}} + s_{34}+s_{45}-s_{345}. \end{aligned} \tag{2.5}$$

The chapter is organized as follows. We start in section 2.2 with examples that motivate and illustrate smooth splitting and split kinematics. This kinematics generically leads to smooth 3-splits but we also point out the border cases in which it produces smooth 3-splits with only two nontrivial factors. In section 2.3, we study 3-splits in the biadjoint theory. We prove the general formula in terms of three amputated currents using the CHY formalism. In section 2.4, we consider NLSM and special Galileon amplitudes. In section 2.5, we use smooth splittings to derive novel BCFW-like recursion relations for NLSM amplitudes in which soft limits are not required. In section 2.6 we discuss relations to soft limits, generalizations to other theories, soft triangulations and conncetions to CEGM amplitudes.

2.2 Split Kinematics

The purpose of this section is to give a presentation of our main results with the biadjoint theory as an example; further discussion and proofs are given in subsequent sections, including extensions to other theories.

We first introduce split kinematics in Definition 2.2.1 for Mandelstam invariants $s_{i,j}$ and later for planar basis invariants $s_{i,i+1,\ldots,j}$. We shall always assume that a triple (i, j, k) has the cyclic order $i < j < k$.

Definition 2.2.1. *Given any triple of distinct indices i, j, k that is not a (cyclic) interval in $\{1, \ldots, n\}$ of the form $(a, a + 1, a + 2)$, say with with $1 \leq i < j < k \leq n$, the split kinematics subspace is characterized by the following condition: $s_{a,b} = 0$ whenever the pair (a, b) interlaces the triple (i, j, k), having modulo cyclic rotation*

$$\begin{aligned} &a < i < b < j < k, \;\; \textit{or} \\ &a < j < b < k < i, \;\; \textit{or} \\ &a < k < b < i < j. \end{aligned} \tag{2.6}$$

For example, for $n = 7$ particles and the triple (1,3,6), the split kinematics subspace is cut out by the equations

$$s_{24} = 0,\ s_{25} = 0,\ s_{27} = 0,\ s_{47} = 0,\ s_{57} = 0.$$

We first formulate the notion of a smooth split in full generality, in the prototypical case, the biadjoint scalar partial amplitude $m_n(\mathbb{I}, \mathbb{I})$, and then show that only the case of a smooth 3-split can be achieved by a suitable restriction of the amplitude to a subspace of the kinematic space.

The definition of the biadjoint theory can be found e.g. in [78]. Here we only provide the definition of $m_n(\mathbb{I}, \mathbb{I})$ as it is our main object of study.

Definition 2.2.2. *Let $\mathcal{T}$ be the set of all planar unrooted binary trees with n leaves. A momentum vector, $p \in \mathbb{R}^{1,D-1}$ with $p^2 := p \cdot p = 0$, is assigned to each leaf such that $s_{ab} = (p_a + p_b)^2$ and $p_1 + p_2 + \ldots + p_n = 0$. Given a tree $T \in \mathcal{T}$, each edge e of T partitions the leaves into two sets $L_e \cup R_e = [n]$. Clearly,*

$$\left(\sum_{a \in L_e} p_a\right)^2 = \left(\sum_{a \in R_e} p_a\right)^2 := P_e^2.$$

The partial biadjoint amplitude then given by

$$m_n(\mathbb{I}, \mathbb{I}) := \sum_{T \in \mathcal{T}} \frac{1}{\prod_{e \in E(T)} P_e^2}, \tag{2.7}$$

where $E(T)$ is the edge set of T.

Definition 2.2.3. *For any $d \geq 2$, a smooth d-split is a decomposition*

$$m_n(\mathbb{I}, \mathbb{I})|_{\text{split kin.}} = \mathcal{J}(j_1, \ldots, j_2)\mathcal{J}(j_2, \ldots, j_3) \cdots \mathcal{J}(j_d, \ldots, j_1), \tag{2.8}$$

where each $\mathcal{J}(a, \ldots, b)$ is an amputated current, with exactly one off-shell leg.

In fact, we claim that in Definition 2.2.3, only the case $d = 3$ is possible. Assuming this for now, then we have the following cases.

1. No pair of labels is cyclically consecutive, that is

$$\{(j_1, j_2), (j_2, j_3), (j_3, j_1)\} \cap \{(1, 2), (2, 3), \ldots, (n, 1)\} = \emptyset.$$

   In this case, all three factors are nontrivial amputated currents.

2. If exactly one pair is cyclically consecutive, say $(j_3, j_1) = (j_3, j_3+1)$ (modulo n), then $\mathcal{J}(j_3, \ldots, j_1) = 1$ and equation (2.8) reduces to

$$m_n(\mathbb{I}, \mathbb{I})|_{\text{split kin.}} = \mathcal{J}(j_1, \ldots, j_2)\mathcal{J}(j_2, \ldots, j_1 - 1). \tag{2.9}$$

3. If two pairs are cyclically consecutive, so the triple is a single cyclic interval $(j, j + 1, j + 2)$, then no condition is imposed on the kinematics.

Evidently, the $\binom{n}{3} - n$ nontrivial smooth 3-splits are in in bijection with the interior tripods in a polygon with cyclic vertices, or equivalently, collections of triples (i, j, k) such that no two pairs of indices are cyclically adjacent.

Now we show that only $d = 3$ can be achieved by restricting $m_n(\mathbb{I}, \mathbb{I})$ to some subspace of the kinematic space[2].

The argument is very simple. First note that by equation (2.7), a biadjoint amplitude $m_n(\mathbb{I}, \mathbb{I})$ must have degree $-(n-3)$ in the Mandelstam invariants (or in physics terminology,

[2]Here we are assuming that the s_{ab} are formal variables; later we shall specialize to the case when they are inner products of momentum vectors.

mass dimension $-2(n-3)$). Now, an amputated current is nothing but an amplitude with one leg off-shell, i.e. such that one of the corresponding momentum vectors does not have zero Minkowski norm. Therefore the degree of a current agrees with that of an amplitude with the same number of legs.

Supposing that we had a smooth d-split as in equation (2.8), then the degree of the product would be

$$-\sum_{t=1}^{d}(j_{t+1}-j_t-1) = -(n-d), \tag{2.10}$$

where the indices are cyclic modulo n, which matches the degree of $m_n(\mathbb{I},\mathbb{I})$ only when $d=3$. Thus, smooth d-splits cannot occur for $d \neq 3$ as such.

2.2.1 Split Kinematics: Planar Poles

Here we describe how the conditions imposed by split kinematics translate into planar pole decomposition. All relations between planar basis elements that occur when imposing split kinematics have the form

$$s_{a_1,a_2,\ldots,a_m} = s_{a_1,a_2,\ldots,a_r} + s_{a_r,a_{r+1},\ldots,a_m}\,,$$

for $a_1 < a_r < a_m$ modulo n. To state the criterion determining which planar poles decompose in this way it is convenient to draw the n indices $1,\ldots,n$ on the boundary of a disk. Given a split (i,j,k), then we connect the three legs i,j,k in the center of the disk to form a *tripod*, as in figure 2.2, which partitions the disk into three connected components which we identify with the amputated currents themselves. The split kinematics conditions in terms of planar pole decomposition are given by the following. One has to draw all possible arcs joining two labels on the disk so that they cross one leg of the tripod. For example,

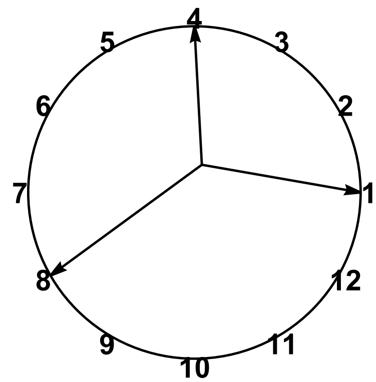

Figure 2.2: The tripod (1,4,8) for $n = 12$ particles.

an arc joining labels 2 and 6 in figure 2.2 is a valid arc since it crosses leg 4. If we call an arc joining labels a_1 and a_m as $\{a_1, a_2, ..., a_m\}$, with $a_1 < a_2 < \cdots < a_m$ modulo n, and provided the arc only crosses the tripod leg r, this corresponds to the condition

$$s_{a_1,a_2,...,a_m} = s_{a_1,a_2,...,a_r} + s_{a_r,a_{r+1},...,a_m} .$$

This is pictorially expressed in figures 2.3 and 2.4, where the arcs are represented in red curved lines.

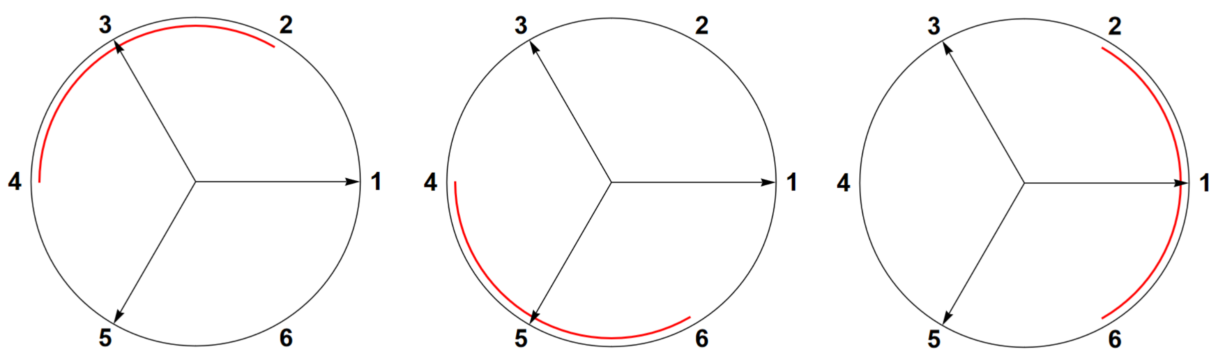

Figure 2.3: Planar basis relations for the $n = 6$ split kinematics given by the split $(1, 3, 5)$. The conditions are given by $s_{234} = s_{23} + s_{34}$, $s_{456} = s_{45} + s_{56}$, and $s_{612} = s_{61} + s_{12}$.

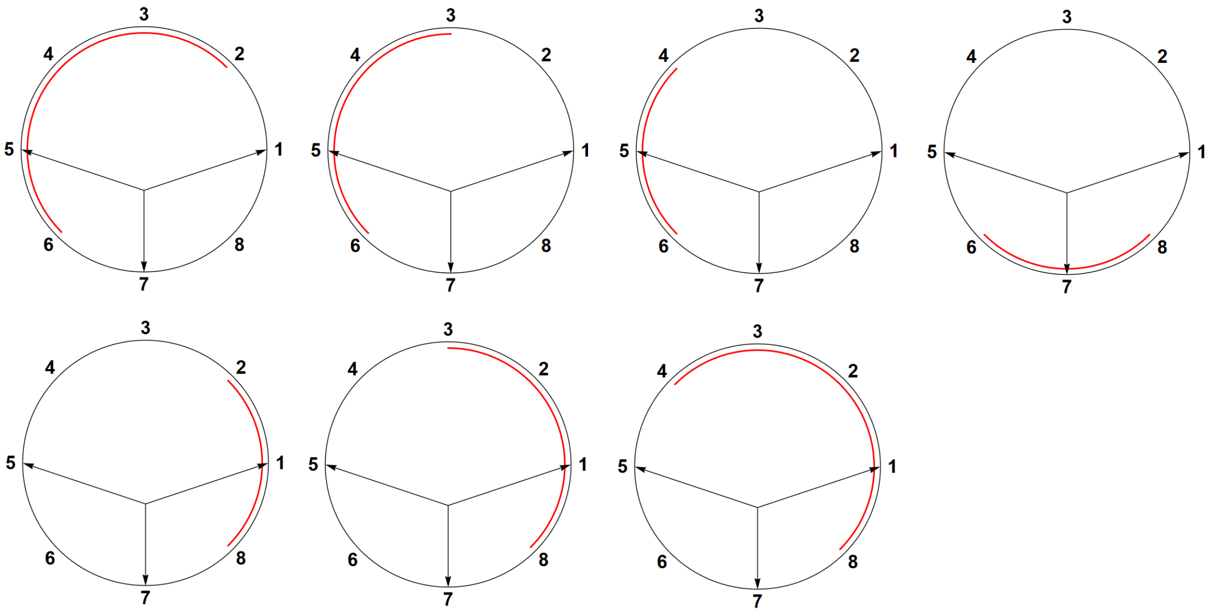

Figure 2.4: Conditions imposed in the planar kinematic invariants for the split $(1,5,7)$. These translate into $s_{23456} = s_{2345} + s_{56}$, $s_{3456} = s_{345} + s_{56}$, $s_{456} = s_{45} + s_{56}$, $s_{678} = s_{67} + s_{78}$, $s_{812} = s_{81} + s_{12}$, $s_{8123} = s_{81} + s_{123}$ and $s_{81234} = s_{81} + s_{1234}$.

We conclude our discussion of split kinematics with some issues that require further exploration. We caution that we know very little about the preimage of split kinematics as a subvariety of the Cartesian product of n copies of Minkowski space $\mathbb{R}^{1,D-1}$, as it is the intersection of a large number of hypersurfaces of the form

$$p_a \cdot p_b = -x_{a,1}x_{b,1} + \sum_{j=2}^{D} x_{a,j}x_{b,j} = 0,$$

where

$$p_a = (x_{a,1}, \ldots, x_{a,D})$$

for $a = 1, \ldots, n$. Moreover, we do not know in general the minimum dimension D which makes the intersection nontrivial, nor do we know the topology of the subvariety. Such questions are beyond the scope of this thesis and are left to future work.

2.3 Smoothly Splitting Biadjoint Amplitudes

In this section we prove the formula obtained by smoothly splitting biadjoint amplitudes. In many standard quantum field theory arguments Feynman diagrams make properties manifest and they are the standard tool for proofs. However, due to the semi-locality of smooth splits we choose to proceed using the Cachazo-He-Yuan (CHY) formalism, introduced in chapter 1.

Recall that in the CHY formalism, partial amplitudes $m_n(\mathbb{I},\mathbb{I})$ are obtained as an integration over the moduli space of n punctures on $\mathbb{CP}^1$, $\mathcal{M}_{0,n}$, using the scattering equations [75, 76, 77, 78]. Consider the following parameterization of $\mathcal{M}_{0,n}$ using inhomogeneous coordinates for the punctures

$$\begin{bmatrix} \sigma_1 & \sigma_2 & \sigma_3 & \sigma_4 & \cdots & \sigma_n \\ 1 & 1 & 1 & 1 & \cdots & 1 \end{bmatrix} /\mathrm{SL}(2,\mathbb{C}). \tag{2.11}$$

The CHY potential is defined as a function of the Plücker coordinates $|a\,b| = \sigma_a - \sigma_b$ and takes the form

$$\mathcal{S}_n = \sum_{a<b} s_{ab} \log|a\,b|\,. \tag{2.12}$$

It is not difficult to show that $\mathcal{S}_n$ is invariant under $\mathrm{SL}(2,\mathbb{C})$ transformations and therefore one can fix the location of three punctures.

We are interested in studying the behavior of amplitudes on the (i,j,k) split kinematic subspace. Therefore it is natural to fix $\sigma_i = 0$, $\sigma_j = 1$, and $\sigma_k = \infty$. Recall that $1 \leq i < j < k \leq n$.

Here it is convenient to set $i = 1$. Note that each term in the potential function (2.12) corresponds to an entry in the matrix of Mandelstam invariants shown schematically in figure 2.1. This already shows that the potential function splits into three parts, each corresponding to one of the diagonal blocks in figure 2.1 with extra terms corresponding to the rows and columns in the set $\{1, j, k\}$. More explicitly, the potential (2.12) can be written as

$$\mathcal{S}_n = \mathcal{B}_{(1,j)} + \mathcal{B}_{(j,k)} + \mathcal{B}_{(k,1)} + \mathcal{R}_1 + \mathcal{R}_j + \mathcal{R}_k + \mathcal{T}_{1j} + \mathcal{T}_{jk} + \mathcal{T}_{k1} \tag{2.13}$$

with the terms coming from the interior of the three blocks

$$\mathcal{B}_{(1,j)} := \sum_{1<a<b<j} s_{ab} \log|a\, b|, \quad \mathcal{B}_{(j,k)} := \sum_{j<a<b<k} s_{ab} \log|a\, b|, \quad \mathcal{B}_{(k,1)} := \sum_{k<a<b\leq n} s_{ab} \log|a\, b|, \tag{2.14}$$

and the extra terms

$$\mathcal{R}_1 := \sum_{a\notin\{1,j,k\}} s_{a1}\log|a\, 1|, \quad \mathcal{R}_j := \sum_{a\notin\{1,j,k\}} s_{aj}\log|a\, j|, \quad \mathcal{R}_k := \sum_{a\notin\{1,j,k\}} s_{ak}\log|a\, k|, \tag{2.15}$$

$$\mathcal{T}_{1j} := s_{1j}\log|1\, j|, \quad \mathcal{T}_{jk} := s_{jk}\log|j\, k|, \quad \mathcal{T}_{k1} := s_{k1}\log|k\, 1|. \tag{2.16}$$

Using the $\mathrm{SL}(2,\mathbb{C})$ gauge fixing described above, (2.15) and (2.16) become

$$\mathcal{R}_1 = \sum_{a\notin\{1,j,k\}} s_{a1}\log(\sigma_a), \quad \mathcal{R}_j = \sum_{a\notin\{1,j,k\}} s_{aj}\log(1-\sigma_a), \quad \mathcal{R}_k + \mathcal{T}_{k1} + \mathcal{T}_{jk} = 0, \quad \mathcal{T}_{1j} = 0. \tag{2.17}$$

In the last two equations we have used momentum conservation in the form $s_{1k} + s_{2k} +$

$\ldots + s_{nk} = 0$ and that $\log(\sigma_1 - \sigma_j) = \log(1) = 0$, respectively. The non-vanishing terms in (2.17) can be redistributed into the three parts from the blocks in (2.14) to define

$$\begin{aligned}
\mathcal{S}_{(1,j)} &:= \sum_{1<a<b<j} s_{ab} \log|a\, b| + \sum_{1<a<j} s_{a1} \log(\sigma_a) + \sum_{1<a<j} s_{aj} \log(1-\sigma_a), \\
\mathcal{S}_{(j,k)} &:= \sum_{j<a<b<k} s_{ab} \log|a\, b| + \sum_{j<a<k} s_{a1} \log(\sigma_a) + \sum_{j<a<k} s_{aj} \log(1-\sigma_a), \\
\mathcal{S}_{(k,1)} &:= \sum_{k<a<b\leq n} s_{ab} \log|a\, b| + \sum_{k<a\leq n} s_{a1} \log(\sigma_a) + \sum_{k<a\leq n} s_{aj} \log(1-\sigma_a).
\end{aligned} \tag{2.18}$$

Using this the CHY potential (2.12) can be written as

$$\mathcal{S}_n = \mathcal{S}_{(1,j)} + \mathcal{S}_{(j,k)} + \mathcal{S}_{(k,1)}. \tag{2.19}$$

Close inspection of this formula reveals something remarkable. Each term only depends on the location of the non-fixed punctures within the range specified by the labels. For example, $\mathcal{S}_{(j,k)}$ is only a function of σ_a with $j < a < k$. Having analysed the behavior of the CHY potential function, the next step is to study the CHY integral representation of the amplitude. We start by writing the formulation with σ_1, σ_j and σ_k set to generic values,

$$m_n(\mathbb{I}, \mathbb{I}) = \int \prod_{a=1}^{n}{}' d\sigma_a \delta\left(\frac{\partial \mathcal{S}}{\partial \sigma_a}\right) \left(|1\, j||j\, k||k\, 1|\, \mathrm{PT}_n(\mathbb{I})\right)^2 , \tag{2.20}$$

where the prime in the product means that $a \notin \{i, j, k\}$. Here PT stands for Parke-Taylor function or factor and it is defined as

$$\mathrm{PT}_n(\mathbb{I}) := \frac{1}{|1\, 2||2\, 3| \cdots |n-1\, n||n\, 1|}. \tag{2.21}$$

Let us write the combination that appears in the integrand of (2.20) more explicitly showing the locations of labels $1, j, k$,

$$|1\,j||j\,k||k\,1|\mathrm{PT}_n(\mathbb{I}) := \frac{|1\,j||j\,k||k\,1|}{|1\,2||2\,3|\cdots|j-1,j||j\,j+1|\cdots|k-1\,k||k\,k+1|\cdots|n-1\,n||n\,1|}. \tag{2.22}$$

Using the gauge fixing $\sigma_1 = 0$, $\sigma_j = 1$, and $\sigma_k = \infty$ one finds that (2.22) becomes

$$\begin{aligned}&\left(\frac{1}{\sigma_2|2\,3|\cdots|j-2\,j-1|(\sigma_{j-1}-1)}\right)\times\left(\frac{1}{(1-\sigma_{j+1})|j+1\,j+2|\cdots|k-2\,k-1|}\right)\times\\ &\left(\frac{1}{|k+1\,k+2|\cdots|n-1\,n|\sigma_n}\right).\end{aligned} \tag{2.23}$$

Once again, each of the factors depends only on the variables in one of the three sets defined by the potentials $\mathcal{S}_{(1,j)}$, $\mathcal{S}_{(j,k)}$, and $\mathcal{S}_{(k,1)}$. Reorganizing the CHY integral (2.20) one finds that it splits into three factors, i.e.

$$\begin{aligned}m_n(\mathbb{I},\mathbb{I})|_{\text{split kin.}} = &\left(\int\prod_{a=2}^{j-1} d\sigma_a\delta\left(\frac{\partial\mathcal{S}_{(1,j)}}{\partial\sigma_a}\right)\mathrm{PT}_{(1,j)}\right)\left(\int\prod_{a=j+1}^{k-1} d\sigma_a\delta\left(\frac{\partial\mathcal{S}_{(j,k)}}{\partial\sigma_a}\right)\mathrm{PT}_{(j,k)}\right)\\ &\left(\int\prod_{a=k+1}^{n} d\sigma_a\delta\left(\frac{\partial\mathcal{S}_{(k,1)}}{\partial\sigma_a}\right)\mathrm{PT}_{(j,k)}\right),\end{aligned} \tag{2.24}$$

with $\mathrm{PT}_{(1,j)}$, $\mathrm{PT}_{(j,k)}$ and $\mathrm{PT}_{(k,1)}$ defined as each of the factors in (2.23) respectively. The last step is the identification of each factor in (2.24) with amputated currents.

In order to complete the argument let us start by reinterpreting the potential functions $\mathcal{S}_{(1,j)}$, $\mathcal{S}_{(j,k)}$, and $\mathcal{S}_{(k,1)}$ in (2.18). The first function $\mathcal{S}_{(1,j)}$ can be thought of as the CHY potential for a current with one off-shell particle with momentum $P_K := -p_1 - p_2 - \ldots - p_j$ and gauge fixed so that $\sigma_1 = 0$, $\sigma_j = 1$ and $\sigma_K = \infty$. Here we follow the definition given by Naculich in [170] and reviewed in appendix A. Note that we have introduced the notation K for the off-shell leg and should not be confused with the k^{th} particle of the original amplitude.

The second function $\mathcal{S}_{(j,k)}$ requires a rearrangement before it can be identified. Note that

$$\sum_{j<a<k} s_{a1} \log(\sigma_a) = 2 \sum_{j<a<k} p_a \cdot p_1 \log(\sigma_a). \tag{2.25}$$

Using momentum conservation,

$$p_1 = -(p_2 + p_3 + \cdots p_{j-1}) - (p_j + p_{j+1} + \cdots + p_k) - (p_{k+1} + p_{k+2} + \cdots + p_n)$$

and noticing that on the $(1, j, k)$ split kinematic subspace

$$p_a \cdot p_1 = -p_a \cdot (p_j + p_{j+1} + \cdots + p_k) \quad \forall\, a :\; j < a < k$$

once can write $\mathcal{S}_{(j,k)}$ in (2.18) as

$$\mathcal{S}_{(j,k)} = \sum_{j<a<b<k} s_{ab} \log|a\, b| + \sum_{j<a<k} 2p_a \cdot P_I \log(\sigma_a) + \sum_{j<a<k} s_{aj} \log(1 - \sigma_a). \tag{2.26}$$

Comparing the formula (A.4) in the appendix it is straightforward to conclude that this is the CHY potential for a current with off-shell momentum $P_I := -p_j - p_{j+1} - \cdots - p_k$ and gauge fixed so that $\sigma_I = 0$, $\sigma_j = 1$ and $\sigma_k = \infty$. Finally, the function $\mathcal{S}_{(k,1)}$ in (2.18) can be written as

$$\mathcal{S}_{(k,1)} = \sum_{k<a<b\leq n} s_{ab} \log|a\, b| + \sum_{k<a\leq n} s_{a1} \log\left(\sigma_a\right) + \sum_{k<a\leq n} 2p_a \cdot P_J \log\left(1-\sigma_a\right), \tag{2.27}$$

where $P_J := -p_k - p_{k+1} - \cdots - p_n - p_1$. Comparing to (A.4) one has a current gauge fixed so that $\sigma_1 = 0$, $\sigma_J = 1$, and $\sigma_k = \infty$. Let us reinterpret the factors into which the Parke-Taylor function in equation (2.23) decomposed, i.e. $\mathrm{PT}_{(1,j)}$, $\mathrm{PT}_{(j,k)}$ and $\mathrm{PT}_{(k,1)}$. Consider

$$\mathrm{PT}_{(1,j)} = \left(\frac{1}{\sigma_2|2\,3|\cdots|j-2\,j-1|(\sigma_{j-1}-1)}\right). \tag{2.28}$$

This is indeed a standard $|1j||jK||K1|\mathrm{PT}(1,2,\ldots,j-1,j,K)$ with the gauge fixing $\sigma_1 = 0$, $\sigma_j = 1$ and $\sigma_K = \infty$. Likewise,

$$\mathrm{PT}_{(j,k)} = |jk||kI||Ij|\mathrm{PT}(j,j+1,\ldots,k-1,k,I)\big|_{\sigma_I=0,\sigma_j=1,\sigma_k=\infty}$$

and

$$\mathrm{PT}_{(k,1)} = |k1||1J||Jk|\mathrm{PT}(k,k+1,\ldots,n,1,J)\big|_{\sigma_1=0,\sigma_J=1,\sigma_k=\infty}.$$

Combining all these results the final form of the biadjoint amplitude on the $(1,j,k)$ split kinematic subspace is

$$m_n(\mathbb{I},\mathbb{I})|_{\text{split kin.}} = \mathcal{J}(1,2,...,j)\mathcal{J}(j,j+1,...,k)\mathcal{J}(k,k+1,...,n,1). \tag{2.29}$$

The three amputated currents were defined in terms of Feynman diagrams in section 2.2 and their CHY formulations are discussed in detail in appendix A.

2.4 Smoothly Splitting NLSM and Special Galileon Amplitudes

In this section we derive and study how split kinematics induces smooth splits in two other theories of scalars that admit a CHY formulation: the $U(N)$ non-linear sigma model (NLSM) and the special Galileon.

2.4.1 NLSM Amplitudes

Historically, interest in the NLSM started from studying an effective field theory of interactions of Goldstone bosons known as pions [125]. It is well-known that in this theory, when a single particle becomes soft, scattering amplitudes vanish implying that there must be a non-linearly realized symmetry. This phenomenon is known as the Adler zero [4, 199]. Instead, the double soft limit is the relevant one when one tries to obtain information about the spontaneously broken symmetries of the theory [13]. The lagrangian of the NLSM can be written as [78]

$$\mathcal{L}_{\text{NLSM}} = \frac{1}{8\lambda^2}\text{Tr}(\partial_\mu \text{U}^\dagger \partial^\mu \text{U})\,, \tag{2.30}$$

where we have used the Cayley transform to write $\text{U} = (\mathbb{I}_{N\times N} + \lambda\Phi)(\mathbb{I}_{N\times N} - \lambda\Phi)^{-1}$. Here $\Phi = \phi_I T^I$ where ϕ_I are the scalars carrying a flavour index, T^I are the $U(N)$ generators, and λ is a constant.

The CHY formula for NLSM amplitudes, which is non-vanishing only for an even number of particles, was proposed in [78] as

$$A_n^{\mathrm{NLSM}}(\mathbb{I}) = \int d\hat{\mu}_n \mathrm{PT}_n(\mathbb{I})\, \det{}'\mathbf{A}_n \,, \tag{2.31}$$

where we have defined the CHY measure[3]

$$d\mu_n \equiv \prod_{a\neq i,j,k} d\sigma_a \delta\left(\frac{\partial\mathcal{S}}{\partial\sigma_a}\right)$$

with $d\hat{\mu} := (|ij||jk||ki|)^2 d\mu$, where σ_i, σ_j and σ_k are the fixed punctures, and $\mathbf{A}_n$ is an $n\times n$ dimensional matrix with entries $A_{ab} \equiv \frac{s_{ab}}{\sigma_a-\sigma_b}$. In (2.31), $\det'\mathbf{A}_n$ is the reduced determinant of $\mathbf{A}_n$ and is defined as

$$\det{}'\mathbf{A}_n := \frac{1}{(\sigma_p-\sigma_q)^2}\,\det\mathbf{A}_n^{[p\,q]},$$

where $\mathbf{A}_n^{[p\,q]}$ is the submatrix of $\mathbf{A}_n$ defined by removing the p^{th} and q^{th} rows and columns. This reduction is necessary since the matrix $\mathbf{A}_n$ has co-rank 2 on the support of the delta functions in the measure. It is not difficult to show that $\det'\mathbf{A}_n$ is independent of the choice of p and q.

To start the study of the behaviour of NLSM amplitudes under split kinematics, let us first repeat the argument that led to the conclusion that only $d=3$-splits are possible for the biadjoint amplitude presented in (2.10). NLSM amplitudes have degree one in Mandelstam invariants (or equivalently, mass dimension two) for any values of n. This immediately implies that it is impossible to smoothly split NLSM amplitudes in terms of NLSM amputated currents which also have the same degree as the amplitudes. This leads to the expection that NLSM amplitudes should vanish on split kinematics. However, considering explicit examples reveals a surprising result. Directly evaluating the $n=8$

[3]The notation here slightly differs from the one introduced in chapter 1.

NLSM amplitude on split $(1,3,6)$ kinematics gives rise to

$$A_8^{\text{NLSM}}(\mathbb{I})|_{(1,3,6)} = (s_{12}+s_{23})\left(\frac{s_{34}+s_{45}}{s_{345}}+\frac{s_{45}+s_{56}}{s_{456}}-1\right)\left(\frac{s_{67}+s_{78}}{s_{678}}+\frac{s_{78}+s_{81}}{s_{781}}-1\right). \tag{2.32}$$

The first factor has the form of an $n=4$ NLSM amputated current and hence degree one. The second and third factors in the split do not have the form of NLSM amplitudes. In fact, five-point NLSM amplitudes vanish. These new currents therefore belong to a theory that extends the NLSM and have dimension zero leading to a consistent split. It is surprising that by simply exploring a region of the space of Mandelstam invariants one can find amplitudes of a different theory emerging from those of the original one. Exactly the same phenomenon was observed by Cachazo, Cha, and Mizera [65] when they computed the coefficient of the Adler zero and found exactly the same kind of extended amplitudes. These so-called *mixed amplitudes* involve NLSM particles (pions) and biadjoint scalars.

The particular currents in (2.32) correspond to mixed 5-point amputated currents of pions and biadjoint scalars [65], where particles 1, 3, 6 and the new off-shell ones with momenta $-(p_3+p_4+p_5+p_6)$ and $-(p_6+p_7+p_8+p_1)$ are identified with biadjoint scalars, while the rest are NLSM scalars. In fact, we will show that smoothly splitting NLSM amplitudes either vanish or produce one amputated current of the standard NLSM theory as well as two amputated currents in the extended NLSM theory, i.e. with an odd number of biadjoint scalars and an even number of NLSM scalars.

The CHY formulation of all mixed NLSM amplitudes corresponding to the extended theory was found in [65]. It contains an additional $U(\tilde{N})$ flavour group and a biadjoint scalar field. Its CHY formula is

$$A_n^{\mathrm{NLSM}\oplus\phi^3}(\mathbb{I}|\beta) = \int d\hat{\mu}_n \mathrm{PT}_n(\mathbb{I})\, \mathrm{PT}_\beta \, \det \mathbf{A}_{\bar{\beta}} \,. \tag{2.33}$$

The notation here requires some explanation. Both species of particles share the canonical ordering, $\mathbb{I}$, but the biadjoint scalars also respect the ordering β in the $U(\tilde{N})$ flavour group indices. Here $\bar{\beta}$ represents the particles in the complement of the set β in $[n]$. It is also common in the literature to use $\mathrm{PT}_\beta \equiv \mathrm{PT}(\beta)$ in order to avoid cluttering of the formulas.

Let us present the general result for 3-splits of NLSM amplitudes postponing the proof to section 2.4.4. At first sight there seem to be four cases to consider. As in previous sections, cyclic invariance allows us to study $(1, j, k)$-split kinematics without losing generality. The cases correspond to the different choices for the parity of j and k. However, one can check that all choices except for $j \in 2\mathbb{Z}+1$ and $k \in 2\mathbb{Z}+1$, lead to one current with an even number of points and two with an odd number of points. The case $j \in 2\mathbb{Z}+1$ and $k \in 2\mathbb{Z}+1$ requires all three currents to have an even number of points. This, however, is not possible as discussed above and leads to a vanishing result, i.e. a zero of the amplitude, as shown in section 2.4.3.

Let us present the explicit result for $j \in 2\mathbb{Z}+1$ and $k \in 2\mathbb{Z}$, knowing that other cases can be obtained by reflections and relabeling,

$$A_n^{\mathrm{NLSM}}(\mathbb{I})|_{\text{split kin.}} = \mathcal{J}_{j+1}^{\mathrm{NLSM}}(\mathbb{I}) \times \mathcal{J}_{k-j+2}^{\mathrm{NLSM}\oplus\phi^3}(\mathbb{I}|\beta_1) \times \mathcal{J}_{n-k+3}^{\mathrm{NLSM}\oplus\phi^3}(\mathbb{I}|\beta_2) \,, \tag{2.34}$$

Here $\beta_1 = \{I, j, k\}$, $\beta_2 = \{1, J, k\}$, with I, J denoting off-shell legs, and with the currents defined using the CHY formula (2.33) as explained in more detail in section 2.4.4. A simple argument using degree (or mass dimension) counting reveals that having three biadjoint particles in each mixed current is the only possibility[4].

2.4.2 Special Galileon Amplitudes

The second theory we study in this section is the special Galileon, which was discovered in [78] (see also [88, 143]) and whose CHY formula is given by

$$A_n^{\mathrm{sGal}} = \int d\hat{\mu}_n (\det{}' \mathbf{A}_n)^2 \,, \tag{2.35}$$

where $d\hat{\mu}_n$ is the same CHY measure used in other theories and $\det{}'\mathbf{A}_n$ is the same reduced determinant appearing in the NLSM CHY formula.

This theory is a special case of some scalar theories known as Galileon theories, which have appeared in different contexts, e.g. in cosmology and in the decoupling limit of massive gravity [142, 99, 152]. The general Galileon lagrangian is given by

$$\mathcal{L}_{\mathrm{Gal}} = -\frac{1}{2}\partial_\mu\phi\partial^\mu\phi + \sum_{m=3}^{\infty} g_m\,\phi\det\{\partial^{\mu_a}\partial_{\nu_b}\phi\}_{a,b=1}^{m-1} \,, \tag{2.36}$$

which computes non-vanishing amplitudes for any number of particles. However, the special Galileon amplitude (2.35) vanishes for an odd number of particles. It also vanishes when a single particle becomes soft.

Special Galileon amplitudes have degree $n-1$ in the kinematic invariants, i.e. they have mass dimension $2(n-1)$. Once again the same analysis as done in (2.10) reveals that it is impossible to find a smooth splitting of special Galileon amplitudes in terms of

[4]The reason why $|\beta_1| = |\beta_2| = 3$ is the following. The degree of an amputated mixed current is $3 - n + |\bar{\beta}_i|$ and that of a NLSM amputated currents is 1. Using this in (2.34) imposes the constraint $1 = j - n + 2 + |\bar{\beta}_1| + |\bar{\beta}_2|$. Since $|\beta_1| + |\bar{\beta}_1| = k - j + 2$ and $|\beta_2| + |\bar{\beta}_2| = n - k + 3$, it must be that $|\beta_1| + |\beta_2| = 6$. Mixed amplitudes only exist for $|\beta_i| > 2$ and therefore $|\beta_1| = |\beta_2| = 3$.

special Galileon amputated currents which also have the same degree as the amplitudes. This again leads to the expectation that special Galileon amplitudes should vanish on split kinematics. Another reason not to expect a smooth splitting is that, unlike biadjoint scalar and NLSM amplitudes, special Galileon particles do not have any flavour structure and hence no ordering, i.e., the complete permutation invariant amplitude must be considered[5]. This implies that it contains a permutation invariant set of poles. This means that the Mandelstam invariants set to zero in a given split kinematics point could be producing singularities in the amplitude. Indeed, this is the case: some individual Feynman diagrams do diverge. All this makes it surprising that special Galileon amplitudes smoothly split. Moreover, it is by using its CHY formulation, which re-sums Feynman diagrams, that the behavior on split kinematics is most easily understood. For this reason, we do not need to take a limit to produce smooth splits. Instead, smooth splits appear directly when imposing split kinematics to its CHY formula.

From the NSLM amplitude discussion it is reasonable to expect that special Galileon amplitudes split into products of mixed amputated currents. We recall the CHY formula for the most general mixed amplitudes, which now involve all three kinds of particles discussed so far [65],

$$A_n^{\mathrm{sGal}\oplus\mathrm{NLSM}^2\oplus\phi^3}(\alpha|\beta) = \int d\hat{\mu}_n \left(\mathrm{PT}_\alpha \det\mathbf{A}_{\bar{\alpha}}\right)\left(\mathrm{PT}_\beta \det\mathbf{A}_{\bar{\beta}}\right) . \tag{2.37}$$

This extended theory contains a $U(N)\times U(\tilde{N})$ biadjoint scalar and a NLSM field for each of the two flavour groups. Here the biadjoint scalars correspond to labels $\alpha\cap\beta$ while the special Galileon particles correspond to labels $\bar{\alpha}\cap\bar{\beta}$. The $U(N)$ and $U(\tilde{N})$ NLSM particles correspond to $\alpha\cap\bar{\beta}$ and $\bar{\alpha}\cap\beta$, respectively.

[5]Note that biadjoint and NLSM amplitudes are also permutation invariant since their fields are bosons. However, the flavour structure allows for a decomposition in terms of color-ordered partial amplitudes.

Once again, the behavior of sGal amplitudes on $(1, j, k)$-split kinematics depends on the parity of j and k. The amplitudes vanish when both j and k are odd and splits in terms of an amputated current of the original theory times two mixed currents corresponding to mixed amplitudes of the special form when $\alpha = \beta$ in (2.37), i.e.

$$A_n^{\mathrm{sGal}\oplus\phi^3}(\beta) = \int d\hat{\mu}_n \mathrm{PT}_\beta^2 (\det \mathbf{A}_{\bar{\beta}})^2 \,. \tag{2.38}$$

The final formula for $(1, j, k)$-split kinematics with $j \in 2\mathbb{Z}+1$ and $k \in 2\mathbb{Z}$, knowing that other cases can be obtained by reflections and relabeling, is

$$A_n^{\mathrm{sGal}}|_{\text{split kin.}} = \mathcal{J}_{j+1}^{\mathrm{sGal}} \times \mathcal{J}_{k-j+2}^{\mathrm{sGal}\oplus\phi^3}(\beta_1) \times \mathcal{J}_{n-k+3}^{\mathrm{sGal}\oplus\phi^3}(\beta_2) \,. \tag{2.39}$$

Here $\beta_1 = \{I, j, k\}$, $\beta_2 = \{1, J, k\}$, with I, J denoting off-shell legs. We present the proof of this formula in section 2.4.5.

2.4.3 Behavior of $\det{}'\mathrm{A}_n$ on Split Kinematics

In the following subsections we use the CHY argument seen for the biadjoint scalar theory in section 2.3 to derive how 3-splits appear in NLSM and special Galileon theories under split kinematics. In order to achieve it, we first have a look at the behavior of the reduced determinant that enters into the CHY formulation of these theories, under split kinematics.

Recall that the reduced determinant is independent of the choice of removing any two rows and columns. Therefore, we can remove row and column 1 and we still have to remove one more row and column.

Without loss of generality, consider again the split kinematics $(1, j, k)$. Under this

$$
\mathbf{A}_n^{[1]} = \left(\begin{array}{cccccccccccccc}
 & \mathbf{A}_{\{2,j-1\}} & & & \begin{matrix} A_{2,j} \\ A_{3,j} \\ \vdots \\ A_{-1+j,j} \end{matrix} & & & & & \begin{matrix} A_{2,k} \\ A_{3,k} \\ \vdots \\ A_{-1+j,k} \end{matrix} & & & & & \\
-A_{2,j} & -A_{3,j} & \cdots & -A_{-1+j,j} & 0 & A_{j,1+j} & A_{j,2+j} & \cdots & A_{j,-1+k} & A_{j,k} & A_{j,1+k} & A_{j,2+k} & A_{j,3+k} & \cdots & A_{j,n} \\
 & & & & \begin{matrix} -A_{j,1+j} \\ -A_{j,2+j} \\ \vdots \\ -A_{j,-1+k} \end{matrix} & & \mathbf{A}_{\{j+1,k-1\}} & & & \begin{matrix} A_{1+j,k} \\ A_{2+j,k} \\ \vdots \\ A_{-1+k,k} \end{matrix} & & & & & \\
-A_{2,k} & -A_{3,k} & \cdots & -A_{-1+j,k} & -A_{j,k} & -A_{1+j,k} & -A_{2+j,k} & \cdots & -A_{-1+k,k} & 0 & A_{k,1+k} & A_{k,2+k} & A_{k,3+k} & \cdots & A_{k,n} \\
 & & & & \begin{matrix} -A_{j,1+k} \\ -A_{j,2+k} \\ \vdots \\ -A_{j,-1+n} \\ -A_{j,n} \end{matrix} & & & & & \begin{matrix} -A_{k,1+k} \\ -A_{k,2+k} \\ \vdots \\ -A_{k,-1+n} \\ -A_{k,n} \end{matrix} & & & \mathbf{A}_{\{k+1,n\}} & &
\end{array}\right)
$$

Figure 2.5: General form of the matrix $\mathbf{A}_n^{[1]}$, i.e. when we remove row and column 1.

kinematics, the matrix $\mathbf{A}_n$ after removing row and column 1 has the form of the matrix in figure 2.5, where the entries are $A_{a,b} \equiv \frac{s_{ab}}{\sigma_a - \sigma_b}$ and $\mathbf{A}_{\{a,b\}}$ are matrices defined as

$$
\mathbf{A}_{\{a,b\}} = \begin{bmatrix} 0 & A_{a,a+1} & A_{a,a+2} & \cdots & A_{a,b} \\ -A_{a,a+1} & 0 & A_{a+1,a+2} & \cdots & A_{a+1,b} \\ \vdots & \vdots & \ddots & \vdots & \vdots \\ -A_{a,b} & -A_{a+1,b} & \cdots & -A_{b-1,b} & 0 \end{bmatrix}. \tag{2.40}
$$

We point out that $\mathbf{A}_{\{1,n\}} = \mathbf{A}_n$ in this notation. The rest of the entries are zero. For the argument we will use the following lemma:

Lemma 2.4.1. *Let $M \in \mathbb{C}^{2m\times 2m}$ be antisymmetric and $L \in \mathbb{C}^{r\times r}$ generic, then*

$$det\left[\begin{array}{ccccc|ccccc} & & & & & 0 & 0 & 0 & \cdots & 0 \\ & & & & & 0 & 0 & 0 & \cdots & 0 \\ & & M & & & \vdots & \vdots & \vdots & \ddots & \vdots \\ & & & & & 0 & 0 & 0 & \cdots & 0 \\ & & & & & c_1 & c_2 & c_3 & \cdots & c_r \\ \hline 0 & 0 & \cdots & 0 & d_1 & & & & & \\ 0 & 0 & \cdots & 0 & d_2 & & & L & & \\ \vdots & \vdots & \ddots & \vdots & \vdots & & & & & \\ 0 & 0 & \cdots & 0 & d_r & & & & & \end{array}\right] = det(M)\,det(L) \tag{2.41}$$

for any values of d_a and c_a.

The proof of the lemma is very simple and we present it in appendix B. Now recall from the CHY proof in the biadjoint scalar that the potential splits into three terms $\mathcal{S}_{(1,j)}$, $\mathcal{S}_{(j,k)}$ and $\mathcal{S}_{(k,1)}$, where $\mathcal{S}_{(1,j)}$ produces an amputated current with $j+1$ legs, $\mathcal{S}_{(j,k)}$ produces an amputated current with $k-j+2$ legs and $\mathcal{S}_{(k,1)}$ produces an amputated current with $n-k+3$ legs. Also recall that for non-vanishing NLSM and special Galileon amplitudes n is always even.

Let us consider the case in which $j \in 2\mathbb{Z}+1$ and $k \in 2\mathbb{Z}$. Motivated by the fact that in the following subsections we send puncture σ_k to infinity, here we remove row and column k from the matrix to end up with the that in figure 2.6, where the upper-left block $\mathbf{A}_{\{2,j\}}$ is $(j-1)\times(j-1)$ dimensional, and therefore even-dimensional. We also note that $\mathbf{A}_{\{j+1,k-1\}}$ has dimension $k-j-1$ and that $\mathbf{A}_{\{k+1,n\}}$ has dimension $n-k$. Given the statement (2.41) above, and the fact that the determinant of a block-diagonal matrix is the product of the determinants of each block, we know that $\det \mathbf{A}_n^{[1k]} = \det \mathbf{A}_{\{2,j\}} \det \mathbf{A}_{\{j+1,k-1\}} \det \mathbf{A}_{\{k+1,n\}}$.

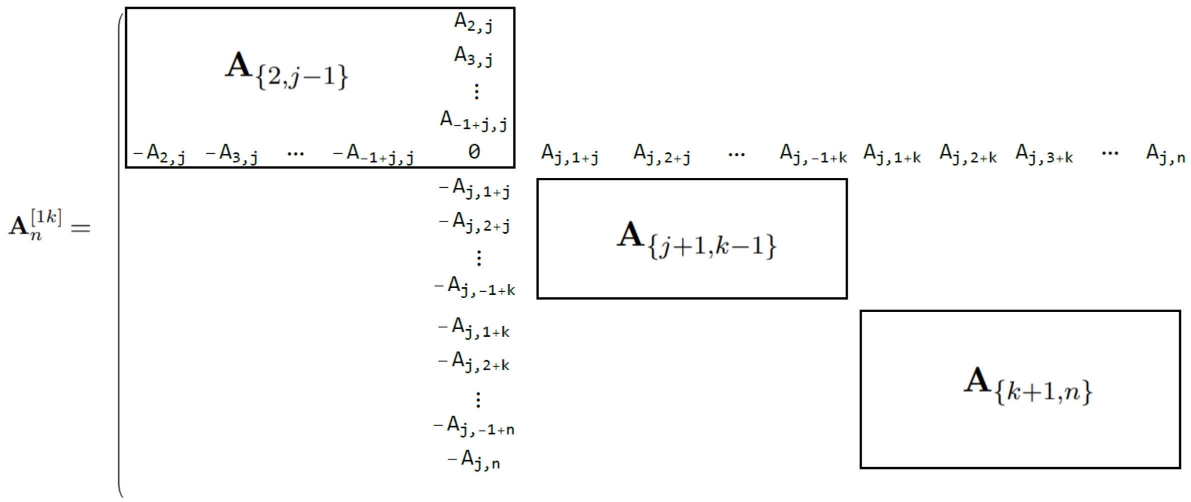

Figure 2.6: General form of the matrix $\mathbf{A}_n^{[1k]}$ where we emphasize the three different blocks that play the role in its determinant.

Now notice that if k is even then $\mathbf{A}_{\{j+1,k-1\}}$ and $\mathbf{A}_{\{k+1,n\}}$ are even-dimensional. In this case the block $\mathbf{A}_{\{2,j\}}$ will give rise to the NLSM or special Galileon amputated current, whilst each of the two blocks $\mathbf{A}_{\{j+1,k-1\}}$ and $\mathbf{A}_{\{k+1,n\}}$ that are embedded into a bigger one will give rise to the mixed amputated currents.

If k is odd then $\mathbf{A}_{\{j+1,k-1\}}$ and $\mathbf{A}_{\{k+1,n\}}$ are odd-dimensional and therefore the whole determinant vanishes since the determinant of an odd-dimensional antisymmetric matrix is zero. What this is telling us is the following. When j and k are odd, we know that all of the three amputated currents will have an even number of external particles, since n is even. Hence, the determinant is protecting the whole object from becoming a product of only non-mixed amputated currents!

2.4.4 Proof for NLSM Amplitudes

Now we are ready to prove how 3-splits are produced in NLSM amplitudes. Without loss of generality, we consider again the split kinematics $(1, j, k)$. Recall from section 2.3 that under this kinematics the CHY potential $\mathcal{S}_n$ splits into $\mathcal{S}_{(1,j)}$, $\mathcal{S}_{(j,k)}$ and $\mathcal{S}_{(k,1)}$, which are the potentials given by the parameterizations (2.42), (2.43) and (2.44), respectively, with their corresponding particle identifications

$$\mathcal{S}_{(1,j)} : \begin{array}{c} \begin{array}{cccccccc} 1 & 2 & 3 & 4 & & j-1 & j & K \end{array} \\ \begin{bmatrix} 0 & \sigma_2 & \sigma_3 & \sigma_4 & \cdots & \sigma_{j-1} & 1 & 1 \\ 1 & 1 & 1 & 1 & \cdots & 1 & 1 & 0 \end{bmatrix} \end{array}, \tag{2.42}$$

$$\mathcal{S}_{(j,k)} : \begin{array}{c} \begin{array}{ccccccc} I & j & j+1 & j+2 & & k-1 & k \end{array} \\ \begin{bmatrix} 0 & 1 & \sigma_{j+1} & \sigma_{j+2} & \cdots & \sigma_{k-1} & 1 \\ 1 & 1 & 1 & 1 & \cdots & 1 & 0 \end{bmatrix} \end{array} \tag{2.43}$$

and

$$\mathcal{S}_{(k,1)} : \begin{array}{c} \begin{array}{ccccccc} J & k & k+1 & k+2 & & n & 1 \end{array} \\ \begin{bmatrix} 1 & 1 & \sigma_{k+1} & \sigma_{k+2} & \cdots & \sigma_n & 0 \\ 1 & 0 & 1 & 1 & \cdots & 1 & 1 \end{bmatrix} \end{array}. \tag{2.44}$$

Let us consider again $j \in 2\mathbb{Z}+1$ and $k \in 2\mathbb{Z}$, without loss of generality. From section 2.4.3 we know that the determinant also splits like $\det \mathbf{A}_n^{[1k]} = \det \mathbf{A}_{\{2,j\}} \det \mathbf{A}_{\{j+1,k-1\}} \det \mathbf{A}_{\{k+1,n\}}$. Given the above separation of the moduli space and that of $\det \mathbf{A}_n^{[1k]}$, one can identify every factor in the smooth split with an amputated current. Namely, we will note that $\mathcal{S}_{(1,j)}$ generates an amputated current with an even number of particles. The other two factors, given by $\mathcal{S}_{(j,k)}$ and $\mathcal{S}_{(k,1)}$, will correspond to amputated currents with an odd number of particles, and therefore are mixed amputated currents.

Let us see this in more detail. Before going to the split kinematics subspace, and after gauge fixing the punctures $\sigma_1 = 0$, $\sigma_j = 1$ and $\sigma_k = \infty$, the NLSM CHY formula (2.31) picks up two copies of the Fadeev-Popov factor $|1j||jk||k1|$ and is expressed as

$$A_n^{\text{NLSM}}(\mathbb{I}) = \int d\mu_n(|1j||jk||k1|)^2 \text{PT}_n(\mathbb{I}) \det{}' \mathbf{A}_n^{[1k]} \,.$$

One copy of the Fadeev-Popov factor cancels with $\det{}'\mathbf{A}_n^{[1k]} = \frac{\det \mathbf{A}_n^{[1k]}}{(\sigma_1 - \sigma_k)^2}$ to produce a finite object. The second copy combines with the Parke-Taylor to produce the neat separation shown in equation (2.23), given by the product of Parke-Taylors $\text{PT}_{(1,j)} \times \text{PT}_{(j,k)} \times \text{PT}_{(k,1)}$ defined in section 2.3.

Now we go to the split kinematics subspace $(1, j, k)$ with $j \in 2\mathbb{Z} + 1$ and $k \in 2\mathbb{Z}$. Recall that in this kinematics the determinant of the original matrix splits as $\det \mathbf{A}_n^{[1k]} = \det \mathbf{A}_{\{2,j\}} \det \mathbf{A}_{\{j+1,k-1\}} \det \mathbf{A}_{\{k+1,n\}}$. This implies that in this subspace the NLSM amplitude separates into three pieces

$$\left(\int d\mu_{(1,j)} \text{PT}_{(1,j)} \det \mathbf{A}_{\{2,j\}} \right) \left(\int d\mu_{(j,k)} \text{PT}_{(j,k)} \det \mathbf{A}_{\{j+1,k-1\}} \right) \left(\int d\mu_{(k,1)} \text{PT}_{(k,1)} \det \mathbf{A}_{\{k+1,n\}} \right)$$

where $d\mu_{(a,b)}$ is the CHY measure defined by $\mathcal{S}_{(a,b)}$. Notice that any dependence on σ_k has disappeared.

Let us first analyze the first factor in detail. From (2.42) and the definition of the reduced determinant we know that $\det{}' \mathbf{A}_{\mathcal{S}_{(1,j)}} = \frac{\det \mathbf{A}_{\{2,j\}}}{(\sigma_1 - \sigma_K)^2}$ where $\mathbf{A}_{\mathcal{S}_{(1,j)}}$ is the matrix with elements $\frac{s_{ab}}{\sigma_a-\sigma_b}$ generated by (2.42). We also note that

$$\mathrm{PT}_{(1,j)} = |1j||jK||K1|\,\mathrm{PT}(12\cdots jK)|_{\sigma_1=0,\,\sigma_j=1,\,\sigma_K=\infty}\,.$$

This implies that if we start with the expression

$$\int d\mu_{(1,j)}(|1j||jK||K1|)^2\,\mathrm{PT}(12\cdots jK)\mathrm{det}'\mathbf{A}_{\mathcal{S}_{(1,j)}}$$

as we had gauge-fixed punctures σ_1, σ_j and σ_K, then $\frac{1}{(\sigma_1-\sigma_K)^2}$ is what is needed to combine with one copy of the Fadeev-Popov factor $|1j||jK||K1|$ to make the expression finite when $\sigma_K=\infty$, which becomes

$$\int d\mu_{(1,j)}\mathrm{PT}_{(1,j)}\mathrm{det}\mathbf{A}_{\{2,j\}}\,.$$

Additionally, from (2.43) one can see that if the set $\beta_1 = \{I, j, k\}$ is identified with the biadjoints, where the complement is given by $\bar{\beta}_1 = \{j+1, ..., k-1\}$, then we have $\mathrm{det}\mathbf{A}_{\bar{\beta}_1} = \mathrm{det}\mathbf{A}_{\{j+1,k-1\}}$. Similarly, from (2.44), if the set $\beta_2 = \{1, J, k\}$ is identified with the biadjoints, whose complement is given by $\bar{\beta}_2 = \{k+1, ..., n\}$, we have $\mathrm{det}\mathbf{A}_{\bar{\beta}_2} = \mathrm{det}\mathbf{A}_{\{k+1,n\}}$.

Hence, we see from (2.31) and (2.33) that we end up with the 3-split

$$\begin{aligned} A_n^{\mathrm{NLSM}}(\mathbb{I})|_{\text{split kin.}} = & \overbrace{\left(\int d\mu_{(1,j)}(|1j||jK||K1|)^2\,\mathrm{PT}(12\cdots jK)\mathrm{det}'\mathbf{A}_{\mathcal{S}_{(1,j)}}\right)}^{\mathcal{J}_{j+1}^{\mathrm{NLSM}}(\mathbb{I})} \\ & \times \underbrace{\left(\int d\mu_{(j,k)}\mathrm{PT}_{(j,k)}\mathrm{PT}_{\beta_1}\,\mathrm{det}\mathbf{A}_{\bar{\beta}_1}\right)}_{\mathcal{J}_{k-j+2}^{\mathrm{NLSM}\oplus\phi^3}(\mathbb{I}|\beta_1)} \times \underbrace{\left(\int d\mu_{(k,1)}\mathrm{PT}_{(k,1)}\mathrm{PT}_{\beta_2}\,\mathrm{det}\mathbf{A}_{\bar{\beta}_2}\right)}_{\mathcal{J}_{n-k+3}^{\mathrm{NLSM}\oplus\phi^3}(\mathbb{I}|\beta_2)}\,. \end{aligned} \tag{2.45}$$

To conclude, we note that, given that the only particles we identify with the biadjoint scalars are contained in the set $\{1, j, k, I, J, K\}$, since every current will contain three of these particles, it follows that we will always have 3 biadjoints in the mixed amputated currents. In fact, the only particle in this set which is not identified with a biadjoint scalar corresponds to the off-shell particle in the non-mixed current. This implies that the non-mixed current will contain two biadjoints and therefore its expression is equivalent to that of a current with only pions.

2.4.5 Proof for Special Galileon Amplitudes

In this subsection we show that special Galileon amplitudes smoothly split under split kinematics. We make use of the fact that special Galileon amplitudes admit a CHY formulation to derive this behavior in a similar fashion as with the NLSM amplitudes.

Let us consider again the case with $j \in 2\mathbb{Z}+1$ and $k \in 2\mathbb{Z}$ without loss of generality and recall the separation of moduli spaces given in (2.42), (2.43) and (2.44). From section 2.4.3 we know that the determinant also splits like $\det\mathbf{A}_n^{[1k]} = \det\mathbf{A}_{\{2,j\}} \det\mathbf{A}_{\{j+1,k-1\}} \det\mathbf{A}_{\{k+1,n\}}$. For the same reason as in the previous section, we identify again $\det'\mathbf{A}_{\mathcal{S}_{(1,j)}} = \frac{\det\mathbf{A}_{\{2,j\}}}{(\sigma_1-\sigma_K)^2}$. Also, given that $\beta_1 = \{I, j, k\}$ and $\beta_2 = \{1, J, k\}$, we can identify the determinants $\det\mathbf{A}_{\bar{\beta}_1} = \det\mathbf{A}_{\{j+1,k-1\}}$ and $\det\mathbf{A}_{\bar{\beta}_2} = \det\mathbf{A}_{\{k+1,n\}}$. A similar analysis as in section 2.4.4 leads to

$$
\begin{aligned}
A_n^{\mathrm{sGal}}\big|_{\text{split kin.}} = & \overbrace{\left(\int d\mu_{(1,j)} (|1j||jK||K1| \det{}'\mathbf{A}_{\mathcal{S}_{(1,j)}})^2\right)}^{\mathcal{J}^{\mathrm{sGal}}_{j+1}} \times \overbrace{\left(\int d\mu_{(j,k)} \mathrm{PT}^2_{\beta_1} (\det\mathbf{A}_{\bar{\beta}_1})^2\right)}^{\mathcal{J}^{\mathrm{sGal}\oplus\phi^3}_{k-j+2}(\beta_1)} \\
& \times \underbrace{\left(\int d\mu_{(k,1)} \mathrm{PT}^2_{\beta_2} (\det\mathbf{A}_{\bar{\beta}_2})^2\right)}_{\mathcal{J}^{\mathrm{sGal}\oplus\phi^3}_{n-k+3}(\beta_2)}
\end{aligned}
\tag{2.46}
$$

where we stress again that the fact that the only particles we identify with β_1 and β_2 are contained in the set $\{1, j, k, I, J, K\}$ shows why we will always have 3 biadjoints in the mixed amputated currents. Again, the only particle in this set which is not identified with a biadjoint scalar corresponds to the off-shell particle in the non-mixed current. This implies that the non-mixed current will contain two biadjoints and therefore its expression is equivalent to that of a current with only Galileons.

2.5 Applications: New Recursion Relations for NLSM Amplitudes

In this section we show how to use smooth splittings of NLSM amplitudes as data to build BCFW-like recursion relations. It is well-known that standard BCFW relations are not applicable to the NLSM. In order to explain the reason let us review the procedure. Consider some subset of momenta and introduce a one-complex parameter deformation $p_i(z) = p_i + zr_i$ such that $p_i(z)^2 = 0$ and momentum conservation remains valid for all z. This means that the amplitude evaluated on this new kinematics can be considered a function $A^{\text{NLSM}}(z)$ such that $A^{\text{NLSM}}(0) = A_n^{\text{NLSM}}(\mathbb{I})$, i.e. it agrees with the desired amplitude at $z = 0$. Now

$$A_n^{\text{NLSM}}(\mathbb{I}) = \frac{1}{2\pi i} \oint_{|z|=\epsilon} dz \frac{A^{\text{NLSM}}(z)}{z}.$$

Deforming the contour one gets a formula for $A_n^{\text{NLSM}}(\mathbb{I})$ in terms of residues where propagators give simple poles. These residues are determined via unitarity to be products of smaller amplitudes and hence the recursive structure. However, there is also the contribution of a pole at $z = \infty$ which is in general not known.

Thus, the condition for the recursion to work is that $A^{\text{NLSM}}(z)$ vanishes as $z \to \infty$. In general this is not the case in the NLSM due to the presence of contact terms. One possible solution is to design deformations such that the kinematics becomes that of a soft-limit for some $z = z^*$. Let us choose $z^* = 1$. The NLSM is known to vanish in a soft-limit and therefore one can consider

$$A_n^{\text{NLSM}}(\mathbb{I}) = \frac{1}{2\pi i} \oint_{|z|=\epsilon} dz \frac{A^{\text{NLSM}}(z)}{z(1-z)}.$$

Now, if the new deformation does not make the behaviour of $A^{\text{NLSM}}(z)$ worse as $z \to \infty$ then $\frac{A^{\text{NLSM}}(z)}{z(1-z)}$ has a better behavior while its residue at $z = 1$ vanishes. As it turns out, either a combination of several of these improvements are needed [87] or knowing the behavior of subleading terms in soft limits is needed so that $\frac{A^{\text{NLSM}}(z)}{z(1-z)^2}$ can be used [65]. Either way, new information is needed in order to construct a successful recursion relation.

The strategy we will use is therefore to introduce a complex deformation such that at some values $z = z^*$ split kinematics is achieved so that its behaviour can be used instead of soft limits. Given that split kinematics is completely defined in terms of Mandelstam invariants, it is convenient to introduce a version of the BCFW procedure for s_{ab} directly without starting with momentum vectors. In general, given a matrix of Mandelstam invariants, a BCFW deformation is achieved by

$$s_{ab}(z) = s_{ab} + z r_{ab}. \tag{2.47}$$

Imposing that $s_{ab}(z)$ is a valid matrix of Mandelstam invariants for any z simply implies that so must be r_{ab}. In a sense, (2.47) interpolates between two sets of Mandelstam invariants, the original one at $z = 0$ and the new one at $z = \infty$.

In order to construct the desired deformation let us select a particular 3-split (i,j,k). This is achieved by imposing that a certain subset of kinematic invariants vanish. Let us denote such set $\mathcal{V}_{(i,j,k)}$. For example, for $n=6$ and $(1,3,5)$ one has $\mathcal{V}_{(1,3,5)}=\{s_{24},s_{46},s_{62}\}$. Requiring the deformed kinematics to reach the 3-split kinematics at $z=1$ can be achieved by choosing $r_{ab}=-s_{ab}$ if $s_{ab}\in\mathcal{V}_{(i,j,k)}$. More explicitly, one finds

$$s_{ab}(z)=\begin{cases}(1-z)s_{ab} & \text{if} \quad s_{ab}\in\mathcal{V}_{(i,j,k)}\\ s_{ab}+zr_{ab} & \quad\text{otherwise.}\end{cases} \tag{2.48}$$

as discussed above, one must require that momentum conservation is satisfied and this means that

$$\sum_{b=1}^{n} r_{ab}=0 \quad \text{for} \quad a\in\{1,2,\ldots,n\}.$$

Let us consider the NLSM amplitude under the deformation (2.48). Using the CHY formulation it is easy to show that the mass dimension of $A_n^{\mathrm{NLSM}}(\mathbb{I})$ is 2, i.e. it is of degree one in Mandelstam invariants. This gives

$$A^{\mathrm{NLSM}}(z)=\mathcal{O}(z) \quad \text{as} \quad z\to\infty. \tag{2.49}$$

This behavior implies that even the modified function $A^{\mathrm{NLSM}}(z)/z(1-z)$ still has a pole at $z=\infty$. The way to solve this problem is to change the deformation so that in addition to reaching (i,j,k)-split kinematics at $z=1$ it reaches a different split kinematics point, say

(r,p,q), at a different point, say $z=-1$. A straightforward way of doing this is by using

$$s_{ab}(z) = \begin{cases} (1-z)s_{ab} & \text{if} \quad s_{ab} \in \mathcal{V}_{(i,j,k)} \quad \text{and} \quad s_{ab} \notin \mathcal{V}_{(r,p,q)} \\ (1+z)s_{ab} & \text{if} \quad s_{ab} \notin \mathcal{V}_{(i,j,k)} \quad \text{and} \quad s_{ab} \in \mathcal{V}_{(r,p,q)} \\ (1-z)(1+z)s_{ab} & \text{if} \quad s_{ab} \in \mathcal{V}_{(i,j,k)} \quad \text{and} \quad s_{ab} \in \mathcal{V}_{(r,p,q)} \\ s_{ab} + z r_{ab} & \qquad\qquad \text{otherwise.} \end{cases} \tag{2.50}$$

However, this has the problem of making every Mandelstam invariant $s_{ab} \in \mathcal{V}_{(i,j,k)} \cap \mathcal{V}_{(r,p,q)}$ a polynomial of degree 2 in z. Such polynomials would spoil the counting and the construction. Therefore we must require that $\mathcal{V}_{(i,j,k)} \cap \mathcal{V}_{(r,p,q)} = \emptyset$. A simple choice that achieves the desired deformation is $(1,2,4)$ and $(1,3,4)$. It is easy to prove that $\mathcal{V}_{(1,2,4)} \cap \mathcal{V}_{(1,3,4)} = \emptyset$. More explicitly,

$$\mathcal{V}_{(1,2,4)} = \{s_{3a} \ : \ a = 5,6,\ldots,n\},$$
$$\mathcal{V}_{(1,3,4)} = \{s_{2a} \ : \ a = 5,6,\ldots,n\}.$$

Now we are ready to present the BCFW-like construction. Consider the complex deformation:

$$s_{ab}(z) = \begin{cases} (1-z)s_{2b} & \text{if} \quad a=2, \ \ b \in \{5,6,\ldots,n\} \\ (1+z)s_{3b} & \text{if} \quad a=3, \ \ b \in \{5,6,\ldots,n\} \\ s_{ab} + z r_{ab} & \qquad\qquad \text{otherwise.} \end{cases} \tag{2.51}$$

Here we are using momentum conservation

$$\sum_{b=1}^{n} s_{ab}(z) = 0. \tag{2.52}$$

The function $A^{\mathrm{NLSM}}(z)$ has poles at finite values of z exactly where planar kinematic invariants involving an odd number of particles vanish. This is because the theory possesses interactions vertices with only an even number of legs. Let us call the set of planar invariants in poles

$$\mathcal{P}_n := \{s_{i,i+1,\ldots,i+m-1} \ : i \in [n],\ m \in 2\mathbb{Z}\}. \tag{2.53}$$

The choice of r_{ab} in (2.51) is arbitrary as long as all invariants in $\mathcal{P}_n$ become polynomials of degree exactly one under the deformation (2.51).

The BCFW-like formula for the NLSM is then obtained by deforming the contour of

$$A_n^{\rm NLSM}(\mathbb{I}) = \frac{1}{2\pi i}\oint_{|z|=\epsilon} dz \frac{A^{\rm NLSM}(z)}{z(1-z^2)},$$

giving rise to[6]

$$A_n^{\rm NLSM}(\mathbb{I}) = \frac{1}{2}A^{\rm NLSM}(1) + \frac{1}{2}A^{\rm NLSM}(-1) + \sum_{s(z^*)=0\,:\, s\in\mathcal{P}_n} A_L^{\rm NLSM}(z^*)\frac{1}{(1-(z^*)^2)s}A_R^{\rm NLSM}(z^*). \tag{2.54}$$

In this formula

$$A^{\rm NLSM}(1) = A_n^{\rm NLSM}(\mathbb{I})\big|_{\text{split kin. (1,3,4)}} = \mathcal{J}^{{\rm NLSM}\oplus\phi^3}(5,\ldots,n|1,I(1),4)\times(s_{12}+s_{23})\,, \tag{2.55}$$

where $\mathcal{J}^{{\rm NLSM}\oplus\phi^3}(5,\ldots,n|1,I(1),4)$ stands for the $(n-1)$-point current evaluated on $s_{ab}(1)$. Likewise,

$$A^{\rm NLSM}(-1) = A_n^{\rm NLSM}(\mathbb{I})\big|_{\text{split kin. (1,2,4)}} = \mathcal{J}^{{\rm NLSM}\oplus\phi^3}(5,\ldots,n|1,I(-1),4)\,(s_{23}+s_{34})\,. \tag{2.56}$$

[6]Clearly the original contour $|z|=\epsilon$ is defined to be counterclockwise. The contour deformation leads to contours around the poles at $z=1$, $z=-1$, etc., which are clockwise and therefore the residues pick up an extra minus sign. Also, for contours $|s(z)|=\epsilon$, note that the pole in the amplitude is of the form $1/s(z)\equiv 1/(s+az)$ for some a. This means that the residue of $1/z(1-z^2)(s+az)$ is $-1/(1-(z^*)^2)s$. The minus sign cancels the one needed to make the contour counterclockwise.

Finally, $A_L^{\text{NLSM}}(z^*)$ and $A_R^{\text{NLSM}}(z^*)$ are the amplitudes that result from the standard factorization at the planar poles of the deformed amplitude.

2.5.1 Example: Six-Point NLSM Amplitude

In order to illustrate the BCFW formula (2.54) let us apply it to the six-point NLSM amplitude. The complex deformation is given by

$$s_{ab}(z) = \begin{cases} (1-z)s_{2b} & \text{if} \quad a=2, \quad b \in \{5,6\} \\ (1+z)s_{3b} & \text{if} \quad a=3, \quad b \in \{5,6\} \\ s_{ab} + z r_{ab} & \quad \text{otherwise.} \end{cases} \tag{2.57}$$

Momentum conservation only imposes six constrains and we find that the remaining freedom can be used to make the following choice

$$\begin{aligned} \{ \; & r_{12} \to 0,\, r_{13} \to 0,\, r_{14} \to 0,\, r_{15} \to 0, r_{16} \to 0, \\ & r_{24} \to -s_{25} - s_{26} - \Lambda^2,\, r_{34} \to s_{35} + s_{36} - \Lambda^2, \\ & r_{45} \to s_{26} - s_{36} + \Lambda^2,\, r_{46} \to s_{25} - s_{35} + \Lambda^2, \\ & r_{56} \to -s_{25} - s_{26} + s_{35} + s_{36} - \Lambda^2,\, r_{23} \to \Lambda^2 \big\}\,. \end{aligned} \tag{2.58}$$

Recall that the original s_{ab} are assumed to satisfy momentum conservation. In order to use the recursion formula (2.54) it is convenient to introduce the planar invariants $s_{123}(z), s_{234}(z)$ and $s_{345}(z)$. These are deformations of the usual planar invariants, e.g.

$$s_{123}(z) = s_{12}(z) + s_{13}(z) + s_{23}(z) = s_{123} + z\Lambda^2. \tag{2.59}$$

Now we list the contribution from each of the poles in $\mathcal{P}_6$. The first contribution is from $s_{123}(z^*) = 0$, i.e. $z^* = -s_{123}/\Lambda^2$. This is given by

$$(s_{12}(z^*) + s_{23}(z^*)) \frac{1}{s_{123}(1-(z^*)^2)} (s_{45}(z^*) + s_{56}(z^*)) \,. \tag{2.60}$$

The other two contributions are similar. Instead of presenting their expressions as functions of Λ we use the fact that the final answer must be Λ independent and then present their limit as $\Lambda \to \infty$. In the order $s_{123}(z^*) = 0, s_{234}(z^*) = 0$ and $s_{345}(z^*) = 0$ the contributions are:

$$\begin{aligned} &\frac{(s_{12}+s_{23}-s_{123})(s_{45}+s_{56})}{s_{123}} + \frac{(s_{23}+s_{34})(s_{56}+s_{61}-s_{234})}{s_{234}} + \\ &\frac{(s_{34}+s_{45}-s_{345})(s_{61}+s_{12}-s_{345})}{s_{345}}. \end{aligned} \tag{2.61}$$

Finally, the contributions from split kinematic points $z = 1$ and $z = -1$ are computed using mixed currents in the NLSM $\oplus\, \phi^3$ theory defined in [65],

$$\mathcal{J}(4,5|1,I(z),3) = \frac{s_{34}(z)+s_{45}(z)}{s_{345}(z)} + \frac{s_{45}(z)+s_{51}(z)}{s_{451}(z)} - 1. \tag{2.62}$$

This means that

$$A^{\rm NLSM}(1) = \mathcal{J}(5,6|1,I(1),3) \times (s_{23}(1) + s_{34}(1)), \tag{2.63}$$

$$A^{\rm NLSM}(-1) = \mathcal{J}(5,6|1,I(-1),3) \times (s_{12}(-1) + s_{23}(-1)). \tag{2.64}$$

We also present these results in the limit $\Lambda \to \infty$,

$$\frac{1}{2}A^{\rm NLSM}(1) = 0, \quad \frac{1}{2}A^{\rm NLSM}(-1) = s_{34} + s_{45} - s_{345}. \tag{2.65}$$

Adding all five contributions gives the expression

$$
\begin{aligned}
A_6^{\mathrm{NLSM}}(\mathbb{I}) = & \frac{(s_{12}+s_{23}-s_{123})(s_{45}+s_{56})}{s_{123}} + \frac{(s_{23}+s_{34})(s_{56}+s_{61}-s_{234})}{s_{234}} + \\
& \frac{(s_{34}+s_{45}-s_{345})(s_{61}+s_{12}-s_{345})}{s_{345}} + s_{34}+s_{45}-s_{345},
\end{aligned}
\tag{2.66}
$$

which agrees with the well-known result

$$
A_6^{\mathrm{NLSM}}(\mathbb{I}) = \left(\frac{1}{2} \frac{(s_{12}+s_{23})(s_{45}+s_{56})}{s_{123}} - s_{12} \right) + \text{perm.} \tag{2.67}
$$

where the permutations indicate five other terms obtained from the one shown by sending all labels $i \to i+m \bmod 6$ with $m \in \{1,2,3,4,5\}$.

2.6 Discussion

In this chapter we have uncovered a new behavior of tree-level scattering amplitudes on subspaces of the kinematic space. Smoothly splitting amplitudes on the (i,j,k) split kinematic subspace leads to a product of three amputated currents in which the particle set does not partition. This semi-locality is what makes smooth splits different from standard factorization and as far as we know not derivable from unitarity arguments. In fact, the closest behavior in the literature to smoothly splitting an amplitude seems to be the soft limit.

Obtaining new information on the behavior of amplitudes on subspaces of the kinematic space is important in order to understand what makes such functions special and relevant to the physical world. The semi-local behavior we have found involves currents which have to be turned into amplitudes in order to be observables. It is interesting to note that when further conditions on the kinematic space are imposed in order to require the currents to become amplitudes at least one of them vanishes. It would be interesting to further explore this phenomenon and perhaps associated with a mechanism for ensuring locality in observables.

In this chapter we have only scratched the surface of this fascinating topic and therefore there are many directions to be explored. Here we only provide a partial list (see also [69] for more).

2.6.1 Comparison with the Soft Limit

As mentioned above, the closest behavior to semi-locality seems to be the soft limit. It is therefore instructive to consider the similarities and differences. In a soft limit the momentum of a particle, say the n^{th} particle, is taken to zero, i.e. $p_n \to \tau \hat{p}_n$ with $\tau \to 0$. In this limit

$$m_n(\mathbb{I}_n, \mathbb{I}_n) \to \left(\frac{1}{s_{n-1,n}} + \frac{1}{s_{n,1}} \right) m_n(\mathbb{I}_{n-1}, \mathbb{I}_{n-1}) + \mathcal{O}(\tau^0). \tag{2.68}$$

The so-called soft factor is reminiscent of a four-particle amplitude. Of course, we have seen in this work, this expectation is not correct since $s_{n-1,n,1}/s_{n-1,n} \neq 0$, i.e. the momentum of the fourth leg is off-shell. The ratio is needed in order to remove the trivial τ dependence. Nevertheless, this soft factor can be thought of as an amputated current $\mathcal{J}(n-1,n,1)$ and once again we get a semi-local factorization

$$m_n(\mathbb{I}_n, \mathbb{I}_n) \to \mathcal{J}(n-1,n,1) m_n(\mathbb{I}_{n-1}, \mathbb{I}_{n-1}) + \mathcal{O}(\tau^0)\,, \tag{2.69}$$

in which particles $n-1$ and 1 participate in both factors.

While the semi-local feature is similar to that of smooth splits the main difference is that this is achieved in a singular limit and there are subleading corrections.

In order to compare let us consider the $(1, n-2, n-1)$ split kinematic subspace. This is simply defined as the subspace with $s_{an} = 0$ for $a \in \{2, 3, \ldots, n-3\}$. Here the biadjoint amplitude smoothly splits as

$$m_n(\mathbb{I}_n, \mathbb{I}_n)|_{\text{split kin.}} = \mathcal{J}(n-1, n, 1)\mathcal{J}(1, 2, \ldots, n-2). \tag{2.70}$$

Note that in order to reach the soft limit subspace from the $(1, n-2, n-1)$ split kinematic subspace one has to impose the additional constrains $s_{n-2,n} = s_{n-1,n} = s_{n,1} = \mathcal{O}(\tau)$ with $\tau \to 0$. In this limit the off-shell leg of $\mathcal{J}(1, 2, \ldots, n-2)$ which has momentum $P_I = p_{n-1} + p_n$ becomes $P_I \to p_{n-1}$ and therefore on-shell, turning the current into the amplitude $m_n(\mathbb{I}_{n-1}, \mathbb{I}_{n-1})$. It is also worth noticing that the direction in which the soft limit subspace is approached is important. If we were to take the limit $s_{n-2,n} \to 0$ first, then $s_{n-1,n} + s_{n,1} \to 0$ due to momentum conservation and therefore the current $\mathcal{J}(n-1, n, 1)$ would vanish.

We interpret this close connection between soft limits and how an amplitude smoothly splits as saying that the $(1, n-2, n-1)$ split kinematic subspace provides a "pre-soft limit". It would be interesting to explore this connection further.

2.6.2 Generalization to Other Theories

One of the most pressing questions is to find out if there are other theories with amplitudes that smoothly split. In this work only scalar theories that admit a CHY representation were considered. One of the key ingredients was the behavior of the matrix $\mathbf{A}_n$ on the split kinematic subspace. There are other theories with CHY formulations based on the same matrix, such as the Born-Infeld theory. In such theories a new element is also present, it is a matrix that combines momenta and polarization vectors, known as $\Psi(p_a, \epsilon_a)$. It seems reasonable to expect that imposing conditions on the polarization vectors one could smoothly split such amplitudes. Of course, if the Pfaffian of Ψ shows a good behavior then a whole new branch of theories could also smoothly split, such as Yang-Mills.

The attentive reader might have noticed that neither Born-Infeld nor Yang-Mills amplitudes can split solely in terms of currents within the corresponding theories as a degree (dimension) counting argument reveals. This means that currents outside the theories are needed. It is known that the Born-Infeld (BI) theory admits an extension in which BI photons interact with emergent YM gluons. It would be interesting to further explore this connection.

2.6.3 Relation to Causal Diamonds and the Soft-Limit Triangulation

A surprising connection between solutions to the wave equations and the space of planar Mandelstam invariants was uncovered in [16]. Properties of scattering amplitudes, such as factorization, can be translated into properties of the causal structure of an emergent space-time.

It is natural to consider what conditions on the causal structure are imposed on the (i, j, k)-split kinematic subpsace. Somehow the conditions that planar invariants which involve a chain of labels, which in the notation of [16] correspond to $X_{a,b} = s_{a,a+1,\ldots,b,b+1}$ or $X_{a,b} = \eta_{a+1,b+1}$, can split into, e.g., $X_{a,b} = X_{a,i-1} + X_{i,b}$, must have a meaning in terms of how different regions interact with each other. It would be interesting to find a geometric interpretation of the semi-local property in this context.

In order to give more evidence that there are interesting connections, note that a recursion for biadjoint scattering amplitudes was presented in [136, 186, 16] using a novel soft-limit triangulation. For the reader's convenience we rewrite Equation 16 of [16] below,

$$m_n = \sum_{i=4}^{n} \left(\frac{1}{X_{1,3}} + \frac{1}{X_{2,i}} \right) \hat{m}_{n_L} \times \hat{m}_{n_R}. \tag{2.71}$$

In this equation the hatted amplitudes are the smaller amplitudes into which m_n factors near the $X_{2,i} = 0$ region with variables shifted so that $X_{2,j} \to X_{2,j} - X_{2,i}$.

Let us consider the $n = 5$ and $n = 6$ cases in order to show how degenerate 3-splits can naturally appear from (2.71) by setting to zero all but one of the terms. The explicit form of (2.71) for $n = 5$ reads (see also [16, eq. 17]),

$$m_5(\mathbb{I}, \mathbb{I}) = \left(\frac{1}{s_{12}} + \frac{1}{s_{23}} \right) \left(\frac{1}{s_{51} - s_{23}} + \frac{1}{s_{45}} \right) + \left(\frac{1}{s_{12}} + \frac{1}{s_{51}} \right) \left(\frac{1}{s_{34}} + \frac{1}{s_{23} - s_{51}} \right). \tag{2.72}$$

Requiring the first term to vanish by setting the second factor to zero implies that we are exploring the subspace of kinematics space where $s_{23} = s_{45} + s_{51}$. Using that for $n = 5$ $s_{23} = s_{451}$ we get the condition of a $(2, 3, 5)$-split which is a degenerate 3-split, i.e.

$$s_{451} = s_{45} + s_{51}$$

or $s_{41} = 0$. Evaluating the second term in (2.72) on this subspace gives

$$m_5(\mathbb{I}, \mathbb{I})|_{\text{split kin.}} = \left(\frac{1}{s_{12}} + \frac{1}{s_{51}} \right) \left(\frac{1}{s_{34}} + \frac{1}{s_{45}} \right) = \mathcal{J}(5, 1, 2)\mathcal{J}(3, 4, 5). \tag{2.73}$$

Of course, this is a degenerate 3-split because the third amputated current is trivial, i.e. $\mathcal{J}(2, 3) = 1$.

Let us now consider the $n = 6$ case. The formula (2.71) becomes

$$
\begin{aligned}
m_6(\mathbb{I}, \mathbb{I}) = &\left(\frac{1}{s_{12}} + \frac{1}{s_{23}}\right) \hat{m}(4,5,6,1,I) + \left(\frac{1}{s_{12}} + \frac{1}{s_{234}}\right) \hat{m}(2,3,4,I)\hat{m}(5,6,1,I)+ \\
&\left(\frac{1}{s_{12}} + \frac{1}{s_{61}}\right) \hat{m}(2,3,4,5,I).
\end{aligned} \tag{2.74}
$$

As explained in the definition of (2.71) each hatted amplitude must be appropriately shifted and the meaning of the emergent particle I is different in each term. Let us select kinematic invariants that set to zero the second and third terms in (2.74). This is achieved by

$$
s_{234} = s_{23} + s_{34}, \quad s_{2345} = s_{23} + s_{345} \tag{2.75}
$$

which is clearly the $(6, 1, 3)$-split kinematic subspace, i.e., $s_{24} = s_{25} = 0$. As expected, the first term in (2.74) gives the expected answer, i.e.

$$
m_6(\mathbb{I}, \mathbb{I})|_{\text{split kin.}} = \left(\frac{1}{s_{12}} + \frac{1}{s_{23}}\right) \mathcal{J}(3,4,5,6). \tag{2.76}
$$

A similar analysis shows that setting to zero the first and third terms in (2.74) by only imposing linear constrains leads to subspace in which the second term vanishes as well and therefore we do not get any interesting split.

We have also considered each term in (2.74) evaluated on the $(1, 3, 5)$-split and $(2, 4, 6)$-split kinematic subspaces and found that the second term always vanishes while the other two are non-trivial functions which have to be added in order to exhibit the 3-split behavior.

2.6.4 CEGM Amplitudes: Connections and Prospects

Let us now point out an intriguing similarity between the smooth splitting in equation (2.1) and a particular residue of the generalized biadjoint scalar partial amplitudes $m_n^{(k)}(\mathbb{I},\mathbb{I})$, proposed by Cachazo, Early, Guevara and Mizera (CEGM) in [71] and introduced in chapter 1.

Recall that the CEGM construction starts with a generalization of the CHY formula for the biadjoint theory which is an integral over the space of n marked points on $\mathbb{CP}^1$, also known as $X(2,n)$, to an integral over the space of n marked points in $\mathbb{CP}^{k-1}$, i.e. $X(k,n)$. The CEGM generalization of the CHY potential function is

$$\mathcal{S}^{(k)} := \sum_{j_1<j_2<\ldots<j_k} \mathfrak{s}_{j_1,j_2,\ldots,j_k} \log|j_1,j_2,\ldots,j_k| \tag{2.77}$$

where $|a_1,a_2,\ldots a_k|$ denote Plücker coordinates of $X(k,n)$. There are several important novelties in the theory, which we recall, for the reader's convenience. First, the kinematic invariants for the theory are higher rank-k analogs of Mandelstam invariants s_{ij}; they are indexed by k-element subsets, and we use the notation $\mathfrak{s}_J = \mathfrak{s}_{j_1,\ldots,j_k}$. Here, the generalization of masslessness is imposed by requiring $\mathfrak{s}_J$ be zero whenever an index is repeated. One also has the n linear relations which generalize momentum conservation,

$$\sum_{J\ni a} \mathfrak{s}_J = 0$$

for each $a = 1,\ldots,n$.

In [71], the generalized biadjoint scalar $m_n^{(k)}(\mathbb{I},\mathbb{I})$ was constructed as follows

$$m_n^{(k)}(\mathbb{I},\mathbb{I}) := \int \prod_{\alpha=1}^{(k-1)(n-k-1)} dx_\alpha\, \delta\left(\frac{\partial \mathcal{S}_n^{(k)}}{\partial x_\alpha}\right) \times (\mathrm{PT}^{(k)}(\mathbb{I}))^2 \tag{2.78}$$

where $\mathrm{PT}^{(k)}(\mathbb{I})$ is the $X(k,n)$ analog of the Parke-Taylor function $\mathrm{PT}(\mathbb{I})$ presented in equation (2.21) and x_α is some parameterization of $X(k,n)$. In the same way that the $k=2$ formula controls the leading order in an expansion around $\alpha'=0$ of string theory integrals, (2.78) has been shown to control the leading order in generalized string integrals [14].

In order to present the connection with the smooth splitting of biadjoint amplitudes let us specialize to the case $k=3$ and $n=6$. Following [71], one finds that the kinematic invariant $\tilde{R}$, defined by

$$\tilde{R} = \mathfrak{s}_{156} + \mathfrak{s}_{256} + \mathfrak{s}_{345} + \mathfrak{s}_{346} + \mathfrak{s}_{356} + \mathfrak{s}_{456}, \tag{2.79}$$

is a pole of $m_6^{(3)}(\mathbb{I},\mathbb{I})$; it is the residue at $\tilde{R}=0$ that is now of interest. In terms of the planar basis of kinematic invariants, introduced and developed by Early in [108, 107, 106] in the context of permutohedral and hypersimplicial blades, equation (2.79) can be rewritten as $\tilde{R} = \eta_{246}(\mathfrak{s})$, where

$$\begin{aligned} \eta_{246} \;=\; & \frac{1}{6}\,(6\mathfrak{s}_{123} + 5\mathfrak{s}_{124} + 4\mathfrak{s}_{125} + 3\mathfrak{s}_{126} + 4\mathfrak{s}_{134} + 3\mathfrak{s}_{135} + 2\mathfrak{s}_{136} + 2\mathfrak{s}_{145} + \mathfrak{s}_{146} + 6\mathfrak{s}_{156} \\ +\; & 3\mathfrak{s}_{234} + 2\mathfrak{s}_{235} + \mathfrak{s}_{236} + \mathfrak{s}_{245} + 5\mathfrak{s}_{256} + 6\mathfrak{s}_{345} + 5\mathfrak{s}_{346} + 4\mathfrak{s}_{356} + 3\mathfrak{s}_{456})\,. \end{aligned} \tag{2.80}$$

For the biadjoint scalar, which corresponds here to the case $k=2$, one recovers the planar kinematic invariants, as

$$\eta_{ij} = s_{i+1\cdots j}\,.$$

One can check directly (see for instance [71, 42, 107]), that the residue of $m_6^{(3)}(\mathbb{I},\mathbb{I})$ at $\eta_{246}=0$ is a product of three factors

$$\mathrm{Res}_{\eta_{246}=0}(m_6^{(3)}(\mathbb{I},\mathbb{I})) \quad = \quad \left(\frac{1}{\eta_{236}}+\frac{1}{\eta_{124}}\right)\left(\frac{1}{\eta_{256}}+\frac{1}{\eta_{146}}\right)\left(\frac{1}{\eta_{346}}+\frac{1}{\eta_{245}}\right). \qquad (2.81)$$

This expression is intriguingly similar to that of (2.1). Looking forward, we focus on an important outcome of this chapter: we have established, using the CHY formalism, that the kind of novel behavior for residues of generalized CEGM amplitudes that has been observed in [71], with more progress in [14, 134], has an analog in three different quantum field theories, as a semi-local "shadow". This shadow appears not only for the cubic scalar partial amplitude, but also for NLSM and, more surprisingly, the special Galileon amplitudes where a planar order is not present. One of the most significant – and intriguing – contrasts is that the semi-local smooth 3-splits into amputated currents that we have explored in this paper do not occur at residues of the amplitude but on certain subspaces of the kinematic space where the amplitude does not have a singularity; but for $m_n^{(3)}(\mathbb{I},\mathbb{I})$ it has been observed directly to occur on residues where one (or more) compatible planar basis elements $\eta_{j_1j_2j_3}$ vanishes [107]. The 3-splitting behavior is not very well-understood, and in fact it remains a very pressing open question whether it continues to occur in any generality. What lessons need to be learned here?

Another interesting direction would be to study split kinematics in the context of likelihood geometry and in particular likelihood degenerations [197, 6]. It is natural to propose generalizations of split kinematics for higher rank $k \geq 3$; could one describe what happens to the solutions to the CEGM scattering equations as one approaches the split kinematics subspace, not only for $k=2$, but for $k=3$ and beyond? In the next section we sketch a promising and related direction for future research.

2.6.5 CEGM Amplitudes: Smooth Splits at $k=3$

Here we show how generalized $k=3$ amplitudes smoothly split when restricted to a kinematic subspace analogous to the one previously studied for quantum field theory amplitudes.

In order to study smooth splits in generalized amplitudes we will use the CEGM formulation [71]. Without loss of generality, we consider the $k=3$ split kinematics subspace $(1,2,j,j{+}1)$ defined by setting to zero any $\mathfrak{s}_{abc}$ whose indices do not satisfy $1\leq a,b,c\leq j{+}1$ or $j\leq a,b,c\leq 2$, where the indices are understood modulo n. Due to the existing $\mathrm{SL}(3,\mathbb{C})$ redundancy we can fix four particles, and a natural choice is the gauge fixing

$$\begin{array}{c} \begin{array}{cccc} 1 & 2 & j & j+1 \end{array} \\ \begin{bmatrix} 0 & 0 & 1 & 1 \\ 0 & 1 & 0 & 1 \\ 1 & 0 & 0 & 1 \end{bmatrix} \end{array} \tag{2.82}$$

where punctures 2 and j are sent to infinity. Let us however start by writing the $k=3$ CEGM formula for punctures 1, 2, j and $j+1$ fixed to generic values

$$m_n^{(3)}(\mathbb{I},\mathbb{I})=\int {\prod_{a=1}^{n}}' \prod_{t=1}^{2} dx_{t,a}\delta\left(\frac{\partial\mathcal{S}^{(3)}}{\partial x_{t,a}}\right)(V_{1,2,j,j+1}\,\mathrm{PT}_n^{(3)}(\mathbb{I}))^2 \tag{2.83}$$

where $V_{1,2,j,j+1}\equiv|1,2,j||2,j,j+1||j,j+1,1||j+1,1,2|$ and the prime in the product means $a \notin \{1,2,j,j+1\}$. The $k=3$ Parke-Taylor function is given by

$$\mathrm{PT}_n^{(3)}(\mathbb{I}) = \frac{1}{|123||234|\cdots|n12|}\,.$$

Using the gauge fixing (2.82) the factor $V_{1,2,j,j+1}\,\mathrm{PT}_n^{(3)}(\mathbb{I})$ can be written as the product

$$\begin{aligned}
&\overbrace{\left(\frac{|12j||2,j,j+1||j,j+1,1||j+1,1,2|}{|123||234|\cdots|j-2,j-1,j||j-1,j,j+1||j,j+1,1||j+1,1,2|}\right)}^{V_{1,2,j,j+1}\,\mathrm{PT}^{(3)}_{(1,2,\dots,j,j+1)}}\\
&\times\underbrace{\left(\frac{|j,j+1,1||j+1,1,2||12j||2,j,j+1|}{|j,j+1,j+2||j+1,j+2,j+3|\cdots|n-1,n,1||n12||12j||2,j,j+1|}\right)}_{V_{j,j+1,1,2}\,\mathrm{PT}^{(3)}_{(j,j+1,\dots,n,1,2)}},
\end{aligned} \tag{2.84}$$

where $V_{1,2,j,j+1} = V_{j,j+1,1,2}$. The first factor corresponds to the Parke-Taylor function for a generalized amplitude with the double ordering $(1,2,...,j+1)$ multiplied by the Fadeev-Popov factor $V_{1,2,j,j+1}$ that appears from the fixing of punctures 1, 2, j and $j+1$. Similarly, the second factor corresponds to the Parke-Taylor function for the double ordering $(j,j+1,...,n,1,2)$ multiplied by the same Fadeev-Popov factor. Notice that the variables in each factor and after the gauge fixing (2.82) have completely decoupled.

Now let us have a look at the $k=3$ CEGM potential

$$\mathcal{S}_n^{(3)} := \sum_{1\le a<b<c\le n} \mathfrak{s}_{abc}\log|abc|$$

in the split kinematics subspace $(1,2,j,j+1)$. Note that in this kinematics the potential splits into

$$\mathcal{S}_n^{(3)} = \mathcal{S}_{j+1}^{(3)} + \mathcal{W}$$

where the first term

$$\mathcal{S}^{(3)}_{j+1} := \sum_{1\leq a<b<c\leq j+1} \mathfrak{s}_{abc} \log|abc|$$

is the $k=3$ CEGM potential for a generalized amplitude with particles $(1, 2, ..., j+1)$ and the second term $\mathcal{W}$ is an object that we still have to identify. Let us look at it in more detail. This term can be written as

$$\begin{aligned}\mathcal{W} := \sum_{j\leq a<b<c\leq 2} \mathfrak{s}_{abc} \log|abc| - \mathfrak{s}_{12j}\log|12j| - \mathfrak{s}_{1,2,j+1}\log|1,2,j+1| - \mathfrak{s}_{1,j,j+1}\log|1,j,j+1| \\ - \mathfrak{s}_{2,j,j+1}\log|2,j,j+1|\end{aligned} \tag{2.85}$$

where the indices in the sum are understood modulo n. After using the gauge fixing (2.82) we have

$$\log|12j| = \log|1,2,j+1| = \log|1,j,j+1| = \log|2,j,j+1| = 0$$

and the variables in the two terms $\mathcal{S}^{(3)}_{j+1}$ and $\mathcal{W}$ completely decouple. Moreover, we can now identify $\mathcal{W}|_{(2.82)}$ with the $k=3$ CEGM potential for a generalized amplitude with particles $(j, j+1, ..., n, 1, 2)$, i.e.

$$\mathcal{W}|_{(2.82)} \equiv \mathcal{S}^{(3)}_{(j...n12)}|_{(2.82)} \,.$$

Putting all the pieces together one can see that with the gauge fixing (2.82) the CEGM integral (2.83) under the split kinematics $(1,2,j,j+1)$ splits into

$$
\begin{aligned}
m_n^{(3)}(\mathbb{I},\mathbb{I})|_{(1,2,j,j+1)} = & \left(\int \prod_{a=3}^{j-1}\prod_{t=1}^{2} dx_{t,a}\delta\left(\frac{\partial \mathcal{S}^{(3)}_{j+1}|_{(2.82)}}{\partial x_{t,a}}\right)(V_{1,2,j,j+1}\,\mathrm{PT}^{(3)}_{(1,2,\ldots,j,j+1)})^2|_{(2.82)}\right) \\
& \times\left(\int \prod_{a=j+2}^{n}\prod_{t=1}^{2} dx_{t,a}\delta\left(\frac{\partial \mathcal{S}^{(3)}_{(j\ldots n12)}|_{(2.82)}}{\partial x_{t,a}}\right)(V_{j,j+1,1,2}\,\mathrm{PT}^{(3)}_{(j,\ldots,n,1,2)})^2|_{(2.82)}\right)
\end{aligned}
\tag{2.86}
$$

where from (2.83) one can see that the first factor is identified with an object that resembles the generalized amplitude $m^{(3)}_{j+1}(\alpha_1,\alpha_1)$ with $\alpha_1=(1,2,\ldots,j+1)$, while the second factor is identified with an object that resembles the generalized amplitude $m^{(3)}_{n-j+3}(\alpha_2,\alpha_2)$ with $\alpha_2=(j,\ldots,n,1,2)$. However, these two factors in the split are not amplitudes since their particles do not satisfy momentum conservation. We leave the interpretation of these resulting objects for future research.

The CEGM construction turned out to reveal a rich connection between physical and combinatorial ideas through the mathematics of the tropical spaces and, in particular, the positive tropical Grassmannian $\mathrm{Trop}^+G(k,n)$ [98]. In the following chapter, we will examine part of its potential for gaining insights into quantum field theory when $k=2$.

Chapter 3

Global Schwinger Formulae

3.1 Introduction

The positive tropical Grassmannian $\mathrm{Trop}^+G(2,n)$ [195] is the space of all planar metric trees with n leaves and vertices of any degree. Hence, in some sense it governs the singularity structure of any planar tree-level scattering amplitude of massless scalar fields with arbitrary polynomial interactions.

For example, tree-level partial amplitudes of massless scalars in the biadjoint representation of $U(N) \times U(\tilde{N})$ with only cubic interactions, $m_n(\alpha, \beta)$, are computed by summing over all n-particle cubic Feynman diagrams which are planar with respect to both, α and β, orderings. The partial amplitudes with the largest number of diagrams are the ones where both orderings coincide, e.g., $m_n(\mathbb{I}, \mathbb{I})$. In a recent work by Cachazo and Early [66], a formula for $m_n(\mathbb{I}, \mathbb{I})$ as a single integral over $\mathrm{Trop}^+G(2,n)$ was presented,

$$m_n(\mathbb{I}, \mathbb{I}) = \int_{\mathbb{R}^{n-3}} d^{n-3}x \exp(-F_n(x)) \,. \tag{3.1}$$

Here the function $F_n(x) = \sum_{a,b} t_{[a,b]} f_{[a,b]}(x)$ is a piece-wise linear function defined on $\text{Trop}^+G(2,n)$ via the "tropical cross-ratios" $f_{[a,b]}(x)$, and $t_{[a,b]} := (p_a + p_{a+1} + \cdots + p_b)^2$ are standard planar kinematic invariants. This construction is reviewed in detail in section 3.2.

When restricted to a single cone of $\text{Trop}^+G(2,n)$, the corresponding integral becomes nothing but the Schwinger parameterization of a single Feynman diagram. In this sense, $\text{Trop}^+G(2,n)$ provides a global Schwinger parameterization of the amplitude. The regions in $\text{Trop}^+G(2,n)$ corresponding to trees with one or more higher-degree vertices are of measure zero and therefore do not contribute to the integral.

In this chapter we continue the study of global Schwinger parameterizations by extending the construction to all partial amplitudes $m_n(\alpha,\beta)$ and to amplitudes in scalar theories with ϕ^p-interactions and $p > 3$. In both cases, our construction starts with the global Schwinger formulation of $m_n(\mathbb{I},\mathbb{I})$ and proceeds with a limiting procedure on the planar kinematic invariants to obtain amplitudes in other theories.

In the case of $m_n(\alpha,\mathbb{I})$ partial amplitudes, the limiting procedure on kinematic invariants produces indicator functions in the integrand. These indicator functions describe the regions of the original $\text{Trop}^+G(2,n)$ that intersect with $\text{Trop}^+G_\alpha(2,n)$, defined with the ordering α. Our first result is the following,

$$m_n(\alpha,\mathbb{I}) = \int_{\mathbb{R}^{n-3}} d^{n-3}x \exp\left(-G_\alpha(x)\right) \mathbf{1}_{S(H_\alpha)}(x)\,, \tag{3.2}$$

where $G_\alpha(x)$ is a piece-wise linear function that depends on the ordering α, and $\mathbf{1}_{S(H_\alpha)}(x)$ is an indicator function. We provide a derivation and examples of this formula in section 3.3.

The next set of theories we study are a straightforward generalization of $m_n(\mathbb{I},\mathbb{I})$ in which one sums over only planar Feynman diagrams with ϕ^p-interaction vertices. We denote such amplitudes by $A_n^{\phi^p}$. In this work we only consider planarity with respect to the cannonical ordering $\mathbb{I}$ and therefore there is no need to specify it. Of course, $A_n^{\phi^p}$ is defined to be zero if no Feynman diagram exists for the particular number of external particles.

In order to obtain the global Schwinger formulation of $A_n^{\phi^p}$, the limiting procedure on kinematic invariants produces distributions in the integrand. In particular, the Dirac delta functions localize the integral over $\mathbb{R}^{n-3}$ to regions of measure zero[1], those where trees with higher-degree vertices live. For example, for ϕ^4 amplitudes we find

$$A_n^{\phi^4} = \int_{\mathbb{R}^{n-3}} d^{n-3}x \exp\left(-\sum_{a<b}^{\text{even}} t_{[a,b]} f_{[a,b]}(x)\right) Q(x)\,, \tag{3.3}$$

where $Q(x)$ is the distribution obtained from the limiting procedure and the sum is over $b - a \equiv 0 \mod 2$. This procedure, together with the derivation of the global Schwinger formula for $A_n^{\phi^4}$, is developed in section 3.4. In section 3.5 we provide several examples.

Our global Schwinger formula for ϕ^4 amplitudes reveals surprising connections to cubic amplitudes: we find that each of the $\mathrm{C}_{n/2-1}$ regions that define the support of the distributions in the integrand is in bijection with a $m_{n/2+1}(\alpha, \mathbb{I})$ amplitude. We study this feature in section 3.6, where we propose a combinatorial procedure to obtain such regions from non-crossing chord diagrams. This implies that $A_n^{\phi^4}$ can also be expressed as a sum over regions. These results motivate a formula for the general *schematic* structure of $A_n^{\phi^4}$

[1]Each corresponds to a polyhedral cone in $\mathrm{Trop}^+G(2,n)$.

in terms of cubic amplitudes based on the Lagrange inversion procedure

$$A_n^{\phi^4} = \left(\frac{2}{n\, h_0^{n/2-1}}\right) \frac{1}{2\pi i} \oint_{|z|=\epsilon} dz \left(\frac{h(z)}{z}\right)^{n/2} \quad \text{with} \quad h(x) = \sum_{i=0}^{\infty} m_{i+2}(\mathbb{I},\mathbb{I})\, x^i \,. \tag{3.4}$$

Here $h_0 = m_2(\mathbb{I},\mathbb{I}) := P^2$ and $m_3(\mathbb{I},\mathbb{I}) := 1$.

The fact that $A_n^{\phi^4}$ is computed as a sum over regions is very reminiscent of the recent constructions based on Stokes polytopes [30, 29, 149, 9, 186, 196], which were motivated by the connection between ϕ^3 amplitudes and the associahedron [167, 12]. It is known that some Stokes polytopes are associahedra and therefore their contribution could coincide with that of some of the regions we find. However, we find that only associahedra or intersections of associahedra [64] appear in our construction.

In section 3.7 we start the exploration of ϕ^p amplitudes in general. We propose an analogous limiting procedure and obtain the corresponding global Schwinger formula

$$A_n^{\phi^p} = \int_{\mathbb{R}^{n-3}} d^{n-3}x \exp\left(-\sum_{a<b}^{\mathcal{K}_p} t_{[a,b]} f_{[a,b]}(x)\right) Q(x)\,. \tag{3.5}$$

where $\mathcal{K}_p$ indicates that the sum is over ordered pairs (a,b) such that $b-a \equiv 0 \bmod p-2$.

We also propose a diagrammatic construction to find the regions that compute $A_n^{\phi^p}$ as non-crossing $(p-2)$-chord diagrams (these are counted by the Fuss-Catalan numbers[2] $\mathrm{FC}_{(n-2)/(p-2)}(p-2,1)$). The sum over all contributions leads to the expected number of trees in $A_n^{\phi^p}$, which is also given by Fuss-Catalan numbers, $\mathrm{FC}_{(n-2)/(p-2)}(p-1,1)$. Moreover,

[2] Here $\mathrm{FC}_m(q,r)$ is the Fuss-Catalan number given by

$$\mathrm{FC}_m(q,r) \equiv \frac{r}{mq+r}\binom{mq+r}{m}\,.$$

we point out a connection to $m_{(n+2(p-3))/(p-2)}(\alpha, \mathbb{I})$ amplitudes and provide some examples. We also propose a formula giving the general structure of $A_n^{\phi^p}$ in terms of cubic amplitudes.

Of course, $A_n^{\phi^p}$ amplitudes have also been recently studied and found to be related to a class of polytopes known as accordiohedra [162, 181, 10, 154, 150, 147, 148, 146] (see also [25, 26] for related work). Some accordiohedra are associahedra and therefore as in the case of ϕ^4 we suspect that contributions from such accordiohedra could coincide with that of some of our regions.

In section 3.8 we explore physical properties like factorization and soft limits for the partial biadjoint amplitude and for CEGM amplitudes using their global Scwhinger formulas. We conclude in section 3.9 with discussions on possible future research directions including connections between our schematic formulas for $A_n^{\phi^p}$ and those that express general Green functions in terms of connected Green functions in planar theories, a way to connect to accordiohedra constructions, and possible extensions to CEGM generalized amplitudes.

3.2 Global Schwinger Formula for $m_n(\mathbb{I}, \mathbb{I})$

In this section we review the construction of the global Schwinger formula for $m_n(\mathbb{I}, \mathbb{I})$ introduced and proved in [66]. Consider a single metric tree $\mathcal{T}$ with n leaves and all internal vertices of degree three. We follow the mathematical convention and call these binary trees[3]. Label the leaves of $\mathcal{T}$ so that it is planar with respect to the ordering $\mathbb{I} := (1, 2, \ldots, n)$. Its contribution to an amplitude can be constructed as follows. First,

[3]The name stems from the fact that when a leaf is selected as a root, then walking up along the tree implies that at each internal vertex there are exactly two possible edges to choose from in order to continue the walk.

define the function

$$\mathcal{F}(\mathcal{T}) := -\sum_{1\leq a,b\leq n} d_{ab}s_{ab}\,, \tag{3.6}$$

where d_{ab} represents the matrix of distances, i.e., the distance from leaf a to leaf b. Mandelstam invariants $s_{ab} := (k_a + k_b)^2$ satisfy

$$s_{ab} = s_{ba}, \quad s_{aa} = 0, \quad \text{and} \quad \sum_{b=1}^{n} s_{ab} = 0 \quad \forall a. \tag{3.7}$$

Let e_a be the length of the edge containing the a^{th} leaf and write $d_{ab} = e_a + e_b + d_{ab}^{\text{int}}$ where d_{ab}^{int} is the length of the internal edges along the unique path connecting a and b. Due to momentum conservation (3.7), e_a drops out from the function $\mathcal{F}(\mathcal{T})$ and it can be written as

$$\mathcal{F}(\mathcal{T}) = \sum_{i=1}^{n-3} f_{I_i}t_{I_i}\,, \tag{3.8}$$

where f_I denotes the length of an internal edge that partitions the set leaves of $\mathcal{T}$ as $I \cup I^{\text{c}} = [n]$. The kinematic invariant multiplying f_I is defined as the square of the momentum flowing through the edge under consideration, i.e.,

$$t_I := \left(\sum_{a\in I} k_a\right)^2 = \sum_{\{a,b\}\subset I} s_{ab}\,. \tag{3.9}$$

The conditions (3.7) guarantee that $t_I = t_{I^{\text{c}}}$. Finally, the contribution to the amplitude is

$$\mathcal{R}(\mathcal{T}) = \int_{O^+} d^{n-3}f \exp(-\mathcal{F}(\mathcal{T})) = \prod_{i=1}^{n-3}\int_0^\infty df_{I_i} \exp(-f_{I_i}t_{I_i}) = \prod_{i=1}^{n-3}\frac{1}{t_{I_i}}\,. \tag{3.10}$$

where $O^+ := (\mathbb{R}^+)^{n-3}$ is the positive orthant in $\mathbb{R}^{n-3}$. Of course, the integral formulas are only defined for $t_{I_i} > 0$ but once the answer is in the rational function form, it is valid for any values $t_{I_i} \neq 0$. Note that the second integral in (3.10) is the standard Schwinger formula and the edge lengths f_I are the Schwinger parameters.

Denoting the set of all binary trees which are planar with respect to an ordering of the leaves $\alpha := (\alpha_1, \alpha_2, \ldots, \alpha_n)$ by $\mathtt{Pl}_n(\alpha)$, the amplitude is computed as

$$m_n(\mathbb{I}, \mathbb{I}) = \sum_{\mathcal{T} \in \mathtt{Pl}_n(\mathbb{I})} \mathcal{R}(\mathcal{T})\,. \tag{3.11}$$

In [194], Speyer and Sturmfels introduced the tropical Grassmannian $\operatorname{Trop} G(2,n)$ and showed that it agrees with the moduli space of phylogenetic trees studied by Billera, Holmes and Vogtmann (BHV) [39]. Motivated by the work of Postnikov [180] on totally positive Grassmannians, Speyer and Williams introduced positive tropical Grassmannians [195]. In particular, $\operatorname{Trop}^+ G(2,n)$ parameterizes the space of planar trees on n leaves. This means that $\operatorname{Trop}^+ G(2,n)$ must provide a global definition of Schwinger parameters which unifies all the individual Schwinger representations into a single integral.

In order to present the formula, one starts with $G^+(2,n)$ and then tropicalizes the Plücker coordinates. Such a positive parameterization of $G^+(2,n)$ is given by[4]

$$\begin{pmatrix} 1 & 0 & -1 & -(1+\tilde{x}_1) & -(1+\tilde{x}_1+\tilde{x}_2) & \cdots & -(1+\tilde{x}_1+\cdots+\tilde{x}_{n-3}) \\ 0 & 1 & 1 & 1 & 1 & \cdots & 1 \end{pmatrix} \tag{3.12}$$

where $\tilde{x}_a \in \mathbb{R}^+$. Note that any minor Δ_{ab} with $a < b$ is positive. The tropicalization of a minor Δ_{ab} of (3.12) proceeds by replacing addition, $\tilde{x}_i + \tilde{x}_j$, with the min-function, $\min(x_i, x_j)$, and multiplication $\tilde{x}_i\tilde{x}_j$ with addition $x_i + x_j$. Note that we drop the tilde to

[4]Here we suppress the torus coordinates which under tropicalization map to the e_a's which drop out.

differentiate the two sets of variables. This is important since while $\tilde{x}_a \in \mathbb{R}^+$, the tropical variables are unconstrained, i.e., $x_a \in \mathbb{R}$.

The connection to the space of planar trees is simply the identification of (minus) the distance matrix d_{ab} with the tropical Plücker coordinates. It is not difficult to evaluate $\Delta_{ab}^{\mathrm{Trop}}(x)$ and find

$$-d_{ab} \leftrightarrow \Delta_{ab}^{\mathrm{Trop}}(x) = \begin{cases} \min(x_{a-2}, x_{a-1}, \ldots, x_{b-3}) & 2 \leq a \leq b-1,\, 4 \leq b \leq n \\ 0 & \text{otherwise} \end{cases}, \tag{3.13}$$

where $x_0 := 0$ and whenever there is a single argument $\min(x) := x$. It might seem strange that some d_{ab} are sent to zero, however, recall that momentum conservation makes the physics independent of the lengths e_a which can then be used to set to zero some of the entries d_{ab}. The choice corresponds to a choice of frame in (3.12). Using this in (3.6) one defines the "tropical potential function"

$$F_n(x) := \sum_{1 \leq a < b \leq n} s_{ab}\, \Delta_{ab}^{\mathrm{Trop}}(x) = \sum_{b=4}^{n} \sum_{a=2}^{b-1} s_{ab} \min(x_{a-2}, x_{a-1}, \ldots, x_{b-3})\,. \tag{3.14}$$

The scattering amplitude (3.11) now has a single integral representation [66]

$$m_n(\mathbb{I}, \mathbb{I}) = \int_{\mathbb{R}^{n-3}} d^{n-3}x \exp(-F_n(x))\,. \tag{3.15}$$

Note that the integral is over all $\mathbb{R}^{n-3}$. Of course, the integral in (3.15) might not exist for some values of kinematic invariants. Let us discuss the regions of convergence. The best approach is to write the tropical potential function $F_n(x)$ in terms of planar kinematic invariants. This is easily done by introducing the notation $t_{[a,b]}$ to denote t_I with $I =$

$\{a, a+1, \ldots, b-1, b\}$, a set of consecutive labels, and using

$$s_{ab} = t_{[a,b]} - t_{[a+1,b]} - t_{[a,b-1]} + t_{[a+1,b-1]}\,. \tag{3.16}$$

Here one defines $t_{[c,d]} = 0$ whenever $c \geq d$. For example, $s_{14} = t_{[1,4]} - t_{[2,4]} - t_{[1,3]} + t_{[2,3]}$ while $s_{23} = t_{[2,3]}$. Using (3.16) in $F_n(x)$ and arranging by planar kinematic invariants one finds

$$F_n(x) = \sum_{a<b} t_{[a,b]} \left(\Delta^{\text{Trop}}_{a,b}(x) - \Delta^{\text{Trop}}_{a,b+1}(x) - \Delta^{\text{Trop}}_{a-1,b}(x) + \Delta^{\text{Trop}}_{a-1,b+1}(x) \right)\,. \tag{3.17}$$

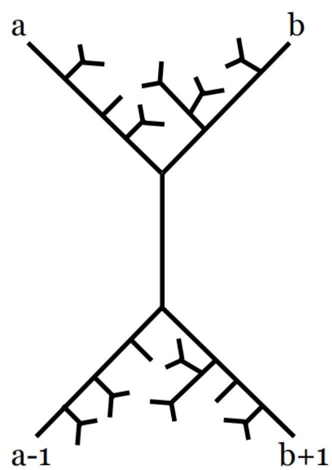

Figure 3.1: In a generic tree, the combination of distances $-d_{a,b} + d_{a,b+1} + d_{a-1,b} - d_{a-1,b+1}$ equals twice the length of the edge which removal would split the diagram into two parts, one containing a and b and the other $a-1$ and $b+1$.

The quantity in brackets has a very beautiful interpretation when thought of as $-d_{a,b} + d_{a,b+1} + d_{a-1,b} - d_{a-1,b+1}$ for a single planar Feynman diagram. This is nothing but twice the length of the edge partitioning the labels as $\{a, a+1, \ldots, b-1, b\} \cup \{b+1, b+2, \ldots, a-2, a-1\}$, i.e., what used to be $f_{[a,b]}$, see figure 3.1. Of course, for this to be the case, it better be that it is always non-negative. This is easily seen to be the case by noticing the following general property for any three real numbers A, B, C,

$$A - \min(A, B) - \min(A, C) + \min(A, B, C) \geq 0\,. \tag{3.18}$$

The proof is left as an exercise to the reader[5]. It is important to mention that the condition

$$\Delta^{\text{Trop}}_{a,b}(x) + \Delta^{\text{Trop}}_{a-1,b+1}(x) \geq \Delta^{\text{Trop}}_{a,b+1}(x) + \Delta^{\text{Trop}}_{a-1,b}(x) \tag{3.19}$$

is part of what is referred to as a positive tropical Plücker relation and it must be satisfied in order to be in $\text{Trop}^+G(2,n)$.

Finally, the condition for the integral formula (3.15) to exist is simply that all planar kinematic invariants be positive. In the rest of this work, only the formula with planar invariants will be used. This why it is convenient to introduce special notation for the combination of tropical minors in (3.17),

$$f_{[a,b]}(x) := \Delta^{\text{Trop}}_{a,b}(x) - \Delta^{\text{Trop}}_{a,b+1}(x) - \Delta^{\text{Trop}}_{a-1,b}(x) + \Delta^{\text{Trop}}_{a-1,b+1}(x)\,, \tag{3.20}$$

so that $F_n(x) = \sum_{a,b} t_{[a,b]} f_{[a,b]}(x)$ and we arrive at the final form of the global Schwinger formula [66]

$$m_n(\mathbb{I}, \mathbb{I}) = \int_{\mathbb{R}^{n-3}} d^{n-3}x \exp\left(-\sum_{a<b} t_{[a,b]} f_{[a,b]}(x)\right)\,. \tag{3.21}$$

Figures 3.2 and 3.3 qualitatively represent how the standard Schwinger parameterization is related to the global Schwinger parameterization.

[5] Hint: $A - \min(A, B) = -\min(A - A, B - A) = -\min(0, B - A) \geq 0$. Repeated use leads to $-\min(0, B - A) - \min(0, (B - A) - \min(0, C - A))$.

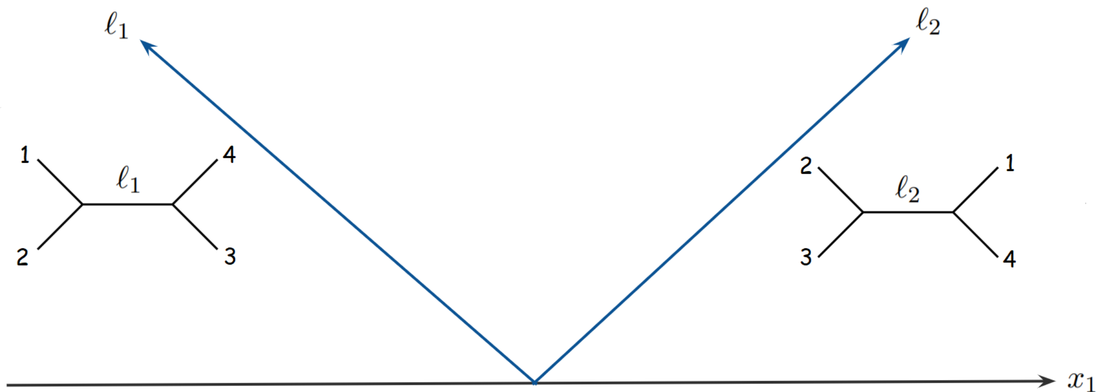

Figure 3.2: In the standard Schwinger parameterization for $n = 4$, the amplitude equals to the sum of two integrals, each of them given by integrating over the positive internal length ℓ_a of the corresponding metric tree, and weighted by the Mandelstam associated to the propagator, i.e. $m_4(\mathbb{I}, \mathbb{I}) = \int_0^{+\infty} d\ell_1 \exp(-s_{12}\ell_1) + \int_0^{+\infty} d\ell_2 \exp(-s_{23}\ell_2)$. The global Schwinger formula can be understood as the projection onto a single line, given by the integral over e.g. x_1 of the piece-wise linear function $F_4(x)$, i.e. $m_4(\mathbb{I}, \mathbb{I}) = \int_{-\infty}^{+\infty} dx_1 \exp(-(s_{24}\min(0, x_1) + s_{34}x_1))$.

3.3 From $m_n(\mathbb{I}, \mathbb{I})$ to $m_n(\alpha, \beta)$

In order to extend the global Schwinger formula (3.21) for $m_n(\mathbb{I}, \mathbb{I})$ to all other partial amplitudes, $m_n(\alpha, \beta)$, let us first review their definition. Recall that $\mathtt{Pl}_n(\alpha)$ denotes the set of all binary trees which are planar with respect to the ordering of the leaves defined by $\alpha = (\alpha_1, \alpha_2, \ldots, \alpha_n)$. Given a second ordering $\beta = (\beta_1, \beta_2, \ldots, \beta_n)$, one can determine the set of trees which are planar with respect to both orderings by simply finding the intersection $\mathtt{Pl}_n(\alpha) \cap \mathtt{Pl}_n(\beta)$, and therefore,

$$m_n(\alpha, \beta) = \sum_{\mathcal{T} \in \mathtt{Pl}_n(\alpha) \cap \mathtt{Pl}_n(\beta)} \mathcal{R}(\mathcal{T})\,. \tag{3.22}$$

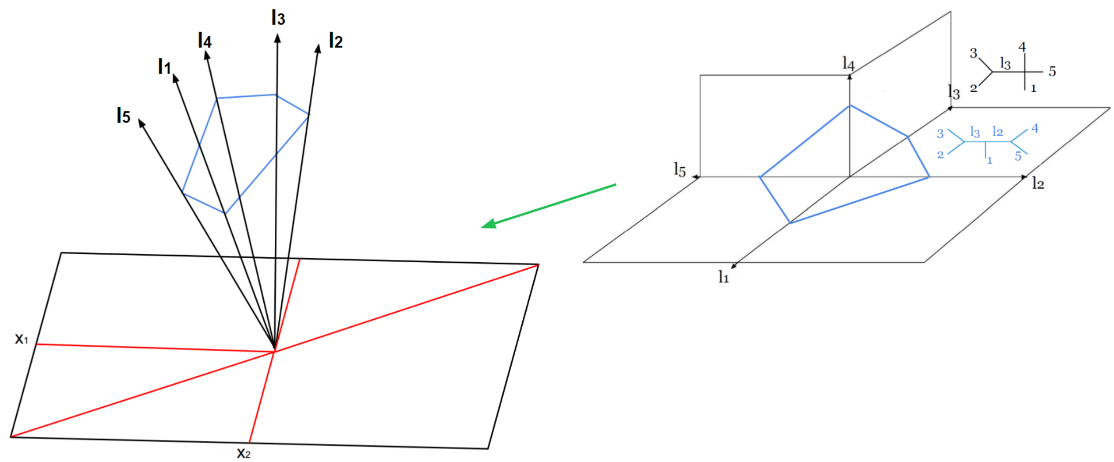

Figure 3.3: The global Schwinger parameterization for $n = 5$ viewed as a projection of $\text{Trop}^+G(2,5)$. *Right*: A positive part of the space of binary metric trees with 5 leaves. A point in each quadrant is in correspondence with a metric tree where the internal lengths are the Schwinger parameters, and a point in each semi-ray is therefore in correspondence with a planar kinematic invariant. *Left*: The global Schwinger formula as a unification of 5 integrals into a single two-dimensional integral, parametrized by two tropical variables x_1 and x_2. The red lines on the plane define the domains where the tropical potential $F_5(x)$ becomes linear.

Depending on conventions, there might be an overall sign which depends on the two orderings chosen. Since our main concern is the kinematic dependence of the amplitude, we refer the reader to [77] for details on the definition of the sign[6].

Without loss of generality we assume that $\beta = \mathbb{I} = (1, 2, \ldots, n)$. Now, recall that t_I is planar with respect to an ordering if the set I coincides with the set of labels of an interval in the ordering. For example, if $\alpha = (1, 2, 5, 4, 3, 6)$ then $I = \{1, 2, 5\}$ is planar with respect to α but not with respect to $\mathbb{I}$ while $I = \{3, 4, 5\}$ is planar with respect to both orderings. Let $\texttt{PK}(\alpha)$ denote the set of all planar kinematic invariants with respect to α.

[6]For example, one could decide to define partial amplitudes so that the sign is included in the traces of the flavour groups. While convenient when individual partial amplitudes are considered, this makes properties such as the $U(1)$-decoupling identity, which involves several partial amplitudes, cumbersome.

Proposition 3.3.1. *Consider the set of planar kinematic invariants* $\mathtt{PK}(\mathbb{I})$*, set* $t_I = 1/\epsilon$ *whenever* $t_I \notin \mathtt{PK}(\alpha)$*, and evaluate* $m_n(\mathbb{I}, \mathbb{I})$ *on it to get a function of* ϵ *and kinematic invariants in* $\mathtt{PK}(\alpha) \cap \mathtt{PK}(\mathbb{I})$*,* $m_n^{(\epsilon)}(\mathbb{I}, \mathbb{I})$*. Then*

$$m_n(\alpha, \mathbb{I}) = \lim_{\epsilon \to 0} m_n^{(\epsilon)}(\mathbb{I}, \mathbb{I}) \,. \tag{3.23}$$

Proof. Since all trees in $m_n^{(\epsilon)}(\mathbb{I}, \mathbb{I})$ that do not contribute to $m_n(\alpha, \mathbb{I})$ contain at least one kinematic invariant that has been set to $1/\epsilon$, in the limit their contribution to the amplitude vanishes. Since invariants in $\mathtt{PK}(\alpha) \cap \mathtt{PK}(\mathbb{I})$ are ϵ-independent, so are the corresponding Feynman diagram contributions $\mathcal{R}(\mathcal{T})$ to (3.22). $\square$

The construction of the global Schwinger formula for $m_n(\alpha, \mathbb{I})$ proceeds in exactly the same way. Let us define the ϵ-dependent tropical potential function, $F_n(x, \epsilon)$, by starting with $F_n(x)$ and restricting to the kinematic space of Proposition 3.3.1. More explicitly,

$$F_n(x) := \sum_{I \in \mathtt{PK}(\mathbb{I})} t_I \, f_I(x) \to F_n(x, \epsilon) := \sum_{I \in \mathtt{PK}(\alpha) \cap \mathtt{PK}(\mathbb{I})} t_I \, f_I(x) + \frac{1}{\epsilon} \left(\sum_{I \notin \mathtt{PK}(\alpha) \cap \mathtt{PK}(\mathbb{I})} f_I(x) \right) . \tag{3.24}$$

Let us define the finite and divergent parts to be $F_n(x, \epsilon) = G_\alpha(x) + \frac{1}{\epsilon} H_\alpha(x)$, i.e.,

$$G_\alpha(x) := \sum_{I \in \mathtt{PK}(\alpha) \cap \mathtt{PK}(\mathbb{I})} t_I \, f_I(x) \,, \quad H_\alpha(x) := \sum_{I \notin \mathtt{PK}(\alpha) \cap \mathtt{PK}(\mathbb{I})} f_I(x) \,. \tag{3.25}$$

Note that we have chosen to add the subscript α to indicate that the form of the functions depends on the α-ordering. Using (3.23) and (3.15) one finds

$$m_n(\alpha, \mathbb{I}) = \lim_{\epsilon \to 0^+} \int_{\mathbb{R}^{n-3}} d^{n-3}x \, \exp(-F_n(x, \epsilon)) \,. \tag{3.26}$$

Defining the limit as a directional limit from above is necessary for the convergence of the integral since all planar kinematic invariants must be positive. Moreover, it also allows the limit to be taken inside the integral. Using (3.25) one finds

$$m_n(\alpha, \mathbb{I}) = \int_{\mathbb{R}^{n-3}} d^{n-3}x \exp\left(-G_\alpha(x)\right) \lim_{\epsilon\to 0^+} \exp\left(-\frac{1}{\epsilon} H_\alpha(x)\right) . \tag{3.27}$$

The function resulting from computing the limit is nothing but an indicator function. In general, given two sets S, U such that $S \subset U$,

$$\mathbf{1}_S : U \to \{0,1\}, \quad \mathbf{1}_S(x) = \begin{cases} 1 & \text{if } x \in S, \\ 0 & \text{otherwise.} \end{cases} \tag{3.28}$$

In the case at hand, we define the set $S(H_\alpha) := \{x \in \mathbb{R}^{n-3} : H_\alpha(x) = 0\} \subset \mathbb{R}^{n-3}$. This leads to the final formula for the global Schwinger formula,

$$m_n(\alpha, \mathbb{I}) = \int_{\mathbb{R}^{n-3}} d^{n-3}x \exp\left(-G_\alpha(x)\right) \mathbf{1}_{S(H_\alpha)}(x) . \tag{3.29}$$

Example 3.3.2. *Consider* $\alpha = (1324)$. *In this case*

$$G_\alpha(x) = -s_{23} \min(0, x_1) , \quad H_\alpha(x) = x_1 - \min(0, x_1) . \tag{3.30}$$

The set $S(H_\alpha) = \{x_1 : x_1 \leq 0\} = (-\infty, 0]$ *and therefore,*

$$m_4(1324, \mathbb{I}) = \int_{-\infty}^{\infty} dx_1 \exp\left(s_{23} \min(0, x_1)\right) \mathbf{1}_{(-\infty,0]}(x_1) = \int_{-\infty}^{0} dx_1 \exp\left(s_{23}\, x_1\right) = \frac{1}{s_{23}} . \tag{3.31}$$

Let us present a more interesting example.

Example 3.3.3. *Consider* $\alpha = (123654)$. *In this case*

$$\begin{aligned} G_\alpha(x) =& s_{12}\left(x_1 - \min\left(0, x_1\right)\right) - s_{23}\,\min\left(0, x_1\right) + s_{45}\left(x_2 - \min\left(x_2, x_3\right)\right) + \\ & s_{56}\left(x_3 - \min\left(x_2, x_3\right)\right) + t_{123}\left(\min\left(x_2, x_3\right) - x_1\right), \\ H_\alpha(x) =& x_1 - \min(x_1, x_2, x_3)\,. \end{aligned} \tag{3.32}$$

In the expression for $G_\alpha(x)$ *we have already used that* $x_1 \leq \min(x_2, x_3)$ *is the condition imposed by requiring* $H_\alpha(x) = 0$ *in order to simplify the expression. The set* $S(H_\alpha) = \{x_1 : x_1 \leq \min(x_2, x_3)\}$. *In this case it is convenient to write the indicator function as a product of two Heaviside step functions* $\theta(x_2 - x_1)\theta(x_3 - x_1)$ *so that*

$$m_6(123654, \mathbb{I}) = \int_{\mathbb{R}^3} d^3x \exp\left(-G_\alpha(x_1, x_2, x_3)\right)\theta(x_2 - x_1)\theta(x_3 - x_1)\,. \tag{3.33}$$

This integral is easily evaluated to give the expected result

$$m_6(123654, \mathbb{I}) = \left(\frac{1}{s_{12}} + \frac{1}{s_{23}}\right)\left(\frac{1}{s_{45}} + \frac{1}{s_{56}}\right)\frac{1}{t_{123}}\,. \tag{3.34}$$

3.4 From ϕ^3 Amplitudes to ϕ^4 Amplitudes

The positive tropical Grassmannian $\operatorname{Trop}^+ G(2, n)$ is the space of all planar metric trees. In other words, trees with vertices of any degree $3 \leq d \leq n$ are part of the space. In the previous section, amplitudes of theories where only Feynman diagrams corresponding to binary trees were discussed. At first it might be puzzling that a formula for $m_n(\mathbb{I}, \mathbb{I})$ involves an integration over the entire $\operatorname{Trop}^+ G(2, n)$. However, this is easily understood by noticing that the regions in $\operatorname{Trop}^+ G(2, n)$ which correspond to trees with at least one vertex of degree $d > 3$ are of measure zero and do not contribute to the integral.

In this section we extend the idea used to obtain $m_n(\alpha, \mathbb{I})$ from $m_n(\mathbb{I}, \mathbb{I})$ by a limiting procedure in order to obtain a global Schwinger formula for $A_n^{\phi^4}$. The main difference is that while the limiting procedure produced indicator functions leading to $m_n(\alpha, \mathbb{I})$, here it produces Dirac delta functions that localize the integral to the regions of measure zero where ϕ^4 planar trees are located. The process unearths a surprising connection to $m_{n/2+1}(\alpha, \mathbb{I})$ amplitudes.

Proposition 3.4.1. *Consider the space of kinematic invariant of $n = 2m$ massless particles with $t_{[a,b]} = 1/\epsilon$ whenever $b - a \equiv 1 \bmod 2$ and let $m_n^{(\epsilon)}(\mathbb{I}, \mathbb{I})$ denote $m_n(\mathbb{I}, \mathbb{I})$ evaluated on it. Then*

$$A_n^{\phi^4} = \lim_{\epsilon \to 0} \frac{1}{(2\epsilon)^{n/2-1}} m_n^{(\epsilon)}(\mathbb{I}, \mathbb{I})\,. \tag{3.35}$$

Proof. Consider any Feynman diagram $\mathcal{T}^{(4)}$ contributing to $A_n^{\phi^4}$, that is, any completely ternary planar tree on n-leaves. Such a diagram has $n/2 - 1$ vertices of degree 4. The strategy is to find out how many planar binary trees give rise to $\mathcal{T}^{(4)}$ by collapsing edges, i.e., taking their length to zero. This is easily done by realizing that for each degree-four vertex of $\mathcal{T}^{(4)}$ there are exactly two ways, compatible with planarity, of growing an edge to produce two degree-three vertices. This means that there are $2^{n/2-1}$ binary trees that give rise to $\mathcal{T}^{(4)}$. Of course, not all binary trees descend to a ternary diagram. Note that under the kinematics in the proposition, ϕ^3 Feynman diagrams that collapse to ϕ^4 diagrams have exactly $n/2-2$ ϵ-independent propagators and $(n-3)-(n/2-2) = n/2-1$ which become $1/t = \epsilon$. Diagrams that do not produce a ϕ^4 diagram have at least one extra propagator of the form $1/t = \epsilon$. Therefore, in the limit $\epsilon \to 0$ the ϕ^4 amplitude is recovered. $\square$

3.4.1 Global Schwinger Formula for $A_n^{\phi^4}$

Following the same steps as in section 3.3 we start the derivation of the global Schwinger formulation of $A_n^{\phi^4}$ by using Proposition 3.4.1 and the representation for $m_n(\mathbb{I},\mathbb{I})$ given in (3.21), i.e.

$$A_n^{\phi^4} = \lim_{\epsilon\to 0^+} \frac{1}{(2\epsilon)^{n/2-1}} \int_{\mathbb{R}^{n-3}} d^{n-3}x \exp\left(-\sum_{a<b} t_{[a,b]}(\epsilon) f_{[a,b]}(x)\right) . \tag{3.36}$$

Rewrite

$$F_n(x,\epsilon) = \sum_{a<b} t_{[a,b]} f_{[a,b]}(x) = G(x) + \frac{1}{\epsilon} H(x) \tag{3.37}$$

with

$$G(x) = \sum_{a<b}^{\text{even}} t_{[a,b]} f_{[a,b]}(x)\,, \quad H(x) = \sum_{a<b}^{\text{odd}} f_{[a,b]}(x)\,, \tag{3.38}$$

where the sums are over ordered pairs (a,b) such that $b-a \equiv 0 \mod 2$ (even) or $b-a\equiv 1 \mod 2$ (odd).

Unlike the cases considered in the previous section, the limit $\epsilon \to 0$ of $m_n^{(\epsilon)}(\mathbb{I},\mathbb{I})$ does not lead to a finite answer and therefore commuting the limit and the integration in (3.36) must be carefully defined. We take the approach in which

$$Q(x) := \lim_{\epsilon\to 0^+} \frac{1}{(2\epsilon)^{n/2-1}} \exp\left(-\frac{1}{\epsilon}H(x)\right) \tag{3.39}$$

is to be treated as a distribution. Since $H(x)\geq 0$, it is clear that $Q(x)$ only has support in regions where $H(x)=0$. In the next section we show that solutions to $H(x)=0$ are regions of dimension $n/2-1$ in $\mathbb{R}^{n-3}$ which are classified by non-crossing chord diagrams.

Here we show the explicit form of $H(x)$,

$$H(x) = \sum_{a=0}^{n-3} x_a + 2 \sum_{a=0}^{n-4} \sum_{b=a+1}^{n-3} (-1)^{b-a} \min(x_a, x_{a+1}, ..., x_b) \,. \tag{3.40}$$

Thus, the distribution $Q(x)$ becomes a sum over distributions that localize the integral to the regions. This gives the first form of the global Schwinger formula for the ϕ^4 theory,

$$A_n^{\phi^4} = \int_{\mathbb{R}^{n-3}} d^{n-3}x \exp\left(- \sum_{a<b}^{\text{even}} t_{[a,b]} f_{[a,b]}(x) \right) Q(x) \,. \tag{3.41}$$

In the next section we present some examples that motivate a second version of the formula as a sum over regions labelled by non-crossing chord diagrams.

3.5 Computing ϕ^4 Amplitudes Using the Global Schwinger Formula

In this section we illustrate the use of the global Schwinger formula (3.41) by considering several examples.

3.5.1 Four-Point Amplitude

The four-particle kinematic space is only two dimensional, s_{12}, s_{23}. Therefore $G(x) = 0$ and

$$H(x) = x_1 - 2\min(0, x_1) = |x_1|. \tag{3.42}$$

The distribution in the integral is

$$Q(x) = \lim_{\epsilon \to 0^+} \frac{1}{2\epsilon} \exp\left(-\frac{1}{\epsilon}|x_1|\right) = \delta(x_1)\,. \tag{3.43}$$

This implies that (3.41) becomes

$$A_4^{\phi^4} = \int_{\mathbb{R}} dx_1 \delta(x_1) = 1\,. \tag{3.44}$$

3.5.2 Six-Point Amplitude

The six-particle kinematic space is nine dimensional, $s_{12}, s_{23}, \ldots, s_{61}, t_{[1,3]}, t_{[2,4]}, t_{[3,5]}$. Evaluating $H(x)$ one finds

$$\begin{aligned} H(x) = {} & x_1 + x_2 + x_3 - 2\min(0, x_1) - 2\min(x_1, x_2) - 2\min(x_2, x_3) \\ & + 2\min(0, x_1, x_2) + 2\min(x_1, x_2, x_3) - 2\min(0, x_1, x_2, x_3)\,. \end{aligned} \tag{3.45}$$

Setting $H(x)$ to zero gives rise to two regions,

$$R_1 = \{x_1 = 0,\ x_2 = x_3\}\,, \quad R_2 = \{x_1 = x_2 > 0,\ x_3 = 0\}\,. \tag{3.46}$$

The distribution $Q(x)$ then becomes

$$Q(x) = Q_1(x) + Q_2(x)\,,\ \text{with } Q_1(x) := \delta(x_1)\delta(x_2 - x_3)\,,\ Q_2(x) := \theta(x_1)\delta(x_1 - x_2)\delta(x_3)\,. \tag{3.47}$$

Instead of computing (3.41) as a single object, let us split it by regions

$$A_6^{\phi^4:(1)} = \int_{\mathbb{R}^3} d^3x \exp(-G(x)) Q_1(x) = \frac{1}{t_{123}} + \frac{1}{t_{234}}\,. \tag{3.48}$$

$$A_6^{\phi^4:(2)} = \int_{\mathbb{R}^3} d^3x \exp(-G(x)) Q_2(x) = \frac{1}{t_{345}} . \tag{3.49}$$

Adding up the two contributions leads to the amplitude

$$A_4^{\phi^4} = \frac{1}{t_{123}} + \frac{1}{t_{234}} + \frac{1}{t_{345}} . \tag{3.50}$$

3.5.3 Eight-Point Amplitude

The eight-particle kinematic space is twenty dimensional, $s_{12}, s_{23}, \ldots, s_{81}$, $t_{123}, t_{234}, \ldots, t_{812}$, and $t_{[1,4]}, t_{[2,5]}, t_{[3,6]}, t_{[4,7]}$. Evaluating $H(x)$ using (3.40) one finds five regions:

$$\begin{aligned}
R_1 =& \{x_1 = 0,\, x_2 = x_3,\, x_4 = x_5\} , \\
R_2 =& \{x_1 = 0,\, x_2 = x_5,\, x_3 = x_4,\, x_2 < x_3\} , \\
R_3 =& \{x_5 = 0,\, x_1 = x_2,\, x_3 = x_4,\, x_1 > 0,\, x_3 > 0\} , \\
R_4 =& \{x_3 = 0,\, x_1 = x_2,\, x_4 = x_5,\, x_1 > 0\} , \\
R_5 =& \{x_5 = 0,\, x_1 = x_4,\, x_2 = x_3,\, x_2 > x_1 > 0\} .
\end{aligned} \tag{3.51}$$

The distribution $Q(x)$ then becomes

$$Q(x) = Q_1(x) + Q_2(x) + Q_3(x) + Q_4(x) + Q_5(x) \tag{3.52}$$

with

$$
\begin{aligned}
Q_1(x) &:= \delta(x_1)\delta(x_2 - x_3)\delta(x_4 - x_5)\,, \\
Q_2(x) &:= \theta(x_3 - x_2)\delta(x_1)\delta(x_2 - x_5)\delta(x_3 - x_4)\,, \\
Q_3(x) &:= \theta(x_1)\theta(x_3)\delta(x_5)\delta(x_1 - x_2)\delta(x_3 - x_4)\,, \\
Q_4(x) &:= \theta(x_1)\delta(x_3)\delta(x_1 - x_2)\delta(x_4 - x_5)\,, \\
Q_5(x) &:= \theta(x_1)\theta(x_2 - x_1)\delta(x_5)\delta(x_1 - x_4)\delta(x_2 - x_3)\,.
\end{aligned}
$$

The contributions from each region are:

$$
\begin{aligned}
A_8^{\phi^4:(1)} &= \frac{1}{t_{123}t_{456}} + \frac{1}{t_{456}t_{781}} + \frac{1}{t_{781}t_{234}} + \frac{1}{t_{234}t_{678}} + \frac{1}{t_{678}t_{123}}\,, \\
A_8^{\phi^4:(2)} &= \frac{1}{t_{567}}\left(\frac{1}{t_{123}} + \frac{1}{t_{234}}\right)\,, \\
A_8^{\phi^4:(3)} &= \frac{1}{t_{812}}\left(\frac{1}{t_{345}} + \frac{1}{t_{567}}\right)\,, \\
A_8^{\phi^4:(4)} &= \frac{1}{t_{345}}\left(\frac{1}{t_{678}} + \frac{1}{t_{781}}\right)\,, \\
A_8^{\phi^4:(5)} &= \frac{1}{t_{456}t_{812}}\,.
\end{aligned}
\tag{3.53}
$$

The amplitude $A_8^{\phi^4}$ is the sum over all five contributions and gives rise to the familiar expression in terms of 12 Feynman diagrams.

3.5.4 One Region for All n

In the next section we provide a diagrammatic technique for finding all regions contributing to $A_n^{\phi^4}$. In this last example, we study the contribution from the analog to R_1 for all n.

The region is defined in the following proposition.

Proposition 3.5.1. *The function*

$$H(x) = \sum_{a<b}^{\text{odd}} f_{[a,b]}(x)\,, \tag{3.54}$$

defined in (3.38)*, vanishes in the region*

$$R_1 = \{x_0 = x_1,\, x_2 = x_3,\, x_4 = x_5, \dots,\, x_{n-4} = x_{n-3}\}\,. \tag{3.55}$$

Proof. Since $H(x)$ is the sum of non-negative functions, $f_{[a,b]}(x)$, we have to show that each such function vanishes on R_1. Using the definitions (3.20), (3.13), one has

$$\begin{aligned} f_{[a,b]}(x) &= \min(x_{a-2}, x_{a-1}, \dots, x_{b-3}) - \min(x_{a-2}, x_{a-1}, \dots, x_{b-3}, x_{b-2}) \\ &\quad - \min(x_{a-3}, x_{a-2}, \dots, x_{b-3}) + \min(x_{a-3}, x_{a-2}, \dots, x_{b-3}, x_{b-2})\,. \end{aligned} \tag{3.56}$$

By definition, $H(x)$ only contains $f_{[a,b]}(x)$ with $b - a \equiv 1 \mod 2$. This means that on R_1, either $x_{a-3} = x_{a-2}$ or $x_{b-3} = x_{b-2}$. This is easily seen by considering two cases: If $a \in 2\mathbb{Z}$ then $b \in 2\mathbb{Z}+1$ and therefore $a-3 \in 2\mathbb{Z}+1$, $b-3 \in 2\mathbb{Z}$, and $x_{b-3} = x_{b-2}$ on R_1. The same can be repeated when $a \in 2\mathbb{Z}+1$ to conclude that $x_{a-3} = x_{a-2}$. Finally, note that if $x_{a-3} = x_{a-2}$ then the first and third terms in (3.56) cancel each other while the second and fourth do too. If $x_{b-3} = x_{b-2}$ then the first and second cancel while the third and fourth do too. $\square$

In order to evaluate the contribution from R_1 it is convenient to define the following combination of kinematic invariants,

$$r_{ab} := s_{ab} + s_{a,b+1} + s_{a+1,b} + s_{a+1,b+1} \,. \tag{3.57}$$

It is also useful to write r_{ab} in terms of planar invariants using (3.16),

$$r_{ab} = -t_{[a,b-1]} + t_{[a,b+1]} + t_{[a+2,b-1]} - t_{[a+2,b+1]} \,. \tag{3.58}$$

Note that if $a \in 2\mathbb{Z}$ and $b \in 2\mathbb{Z}+1$, then all four invariants in (3.58) belong to the set of ϕ^4 invariants. Restricting the tropical potential function (3.14) to R_1 one finds

$$F_n(x) = G_n(x) = \sum_{a=2}^{\text{even}} \sum_{b=5}^{\text{odd}} r_{ab} \min(x_{a-2}, x_a, \ldots, x_{b-5}, x_{b-3}) + \sum_{a=2}^{\text{even}} t_{a,a+1,a+2} x_{a-2} \,. \tag{3.59}$$

In sums labeled "even" ("odd") the index only takes even (odd) values. The first equality is due to the fact that on R_1 the function $H_n(x) = 0$.

The function $G_n(x)$ has exactly the structure of a tropical potential for $m_{n/2+1}(\mathbb{I},\mathbb{I})$ if the labels are identified as $x_a \to x_{a/2}$. This is well-defined since a only takes even values in (3.59). Instead of using the mapping, we keep the original labels and write the tropical potential for $m_{n/2+1}(\mathbb{I},\mathbb{I})$ as

$$F^{\phi^3}_{n/2+1}(x_0, x_2, \ldots, x_n) := \sum_{a=2}^{\text{even}} \sum_{b=5}^{\text{odd}} s_{a,b+1} \min(x_{a-2}, x_a, \ldots, x_{b-5}, x_{b-3}) + \sum_{a=2}^{\text{even}} s_{a,a+2} x_{a-2} \,. \tag{3.60}$$

Matching the coefficients gives the map of kinematic invariants,

$$r_{ab} = s_{a,b+1} \,, \quad t_{a,a+1,a+2} = s_{a,a+2} \,, \quad a \in \{2,4,6\ldots\} \,,\ b \in \{5,7,9,\ldots\} \,. \tag{3.61}$$

We conclude that the contribution of region R_1 to $A_n^{\phi^4}$ is nothing but $m_{n/2+1}(\mathbb{I},\mathbb{I})$ with kinematic invariants given by (3.61). This result prompts the following proposition.

Proposition 3.5.2. *Consider $A_n^{\phi^4}$ evaluated on the following subspace of kinematic invariants,*

$$t_{[a,b]} = \frac{1}{\epsilon}\,, \quad a \in \{3,5,\ldots,n-3\}\,,\; b \in \{a+2, a+4, \ldots, n-1\}\,. \tag{3.62}$$

to produce a function $A_n^{\phi^4(\epsilon)}$. Then,

$$\lim_{\epsilon\to 0} A_n^{\phi^4(\epsilon)} = m_{n/2+1}(\mathbb{I},\mathbb{I}), \tag{3.63}$$

for some bijection of the set of planar kinematic invariants.

Proof. Let us start by proving the spaces of kinematic invariants possess the same cardinality. The set of planar kinematic invariants of $A_n^{\phi^4}$ has cardinality of $n(n-4)/4$. For example, it is $0,3,8,15$ for $n=4,6,8,10$. In the statement of the proposition, $(n-2)(n-4)/8$ of the kinematic invariants are set to $1/\epsilon$ so there are only $(n-4)(n+2)/8$ left. Let us introduce $n_3 := n/2+1$, then $(n-4)(n+2)/8 = n_3(n_3-3)/2$ which is the cardinality of the set of planar kinematic invariants for $m_{n_3=n/2+1}(\mathbb{I},\mathbb{I})$.

The rest of the proof is based on the fact that in the kinematic space of interest and the corresponding limit, only region R_1 contributes to the amplitude. Since the result from region R_1 was shown to be $m_{n_3=n/2+1}(\mathbb{I},\mathbb{I})$ for some bijetion of the kinematic invariants in this subsection, then the statement of the proposition follows. In order to actually complete the proof, we first need to classify all regions and this is done in the next section. We therefore postpone the completion of the proof to the end of the next section in subsection 3.6.3.

□

3.6 Combinatorial Description of Regions

In the previous section we provided some examples of how the global Schwinger formula for $A_n^{\phi^4}$ is evaluated. The result decomposes as a sum over regions (cones) which are in bijection with noncrossing chord diagrams. In this section we provide a systematic study of the structure of the regions. The unexpected appearance of $m_{n/2+1}(\mathbb{I},\mathbb{I})$ in the contribution from one of the regions, explained in section 3.5.4, motivates a similar interpretation for the other regions. Indeed, in all examples we have studied we find that all contributions are related to $m_{n/2+1}(\alpha,\mathbb{I})$ for some choice of ordering α. In order to make the study systematic, we propose a diagrammatic procedure for finding all the regions that contribute to $A_n^{\phi^4}$ and show how each such region is in bijection with a cubic $m_{n/2+1}(\alpha,\mathbb{I})$ amplitude.

3.6.1 Regions for $A_n^{\phi^4}$: Non-Crossing Chord Diagrams

Let us start by defining non-crossing chord diagrams in our context.

Definition 3.6.1. *Place $n-2$ points labeled $0,1,\ldots,n-3$ in increasing order on the real line. A non-crossing chord diagram is a perfect matching of the points such that all edges can be drawn as chords on the upper half plane without any crossings. Let us denote the chord connecting points a and b as θ_{ab}.*

Conjecture 3.6.2. *The regions contributing to $A_n^{\phi^4}$ are in bijection with the set of all $C_{n/2-1}$ possible non-crossing chord diagrams defined in 3.6.1. Moreover, the region R corresponding to a particular diagram is obtained as follows:*

- *For each chord θ_{ab} set $x_a = x_b$.*
- *If a chord θ_{ab} surrounds another chord θ_{cd}, then $x_a = x_b < x_c = x_d$.*

In other words, the regions defined by non-crossing chord diagrams are all the solutions to $H(x) = 0$.

Let us note that the case in which no chord surrounds any other chord corresponds to

$$R = \{x_0 = x_1,\, x_2 = x_3,\, \ldots,\, x_{n-4} = x_{n-3}\}\,. \tag{3.64}$$

This is nothing but the region R_1 which was proven to set $H(x) = 0$ in Proposition (3.5.1).

Example 3.6.3. *Consider two of the examples presented in section 3.5. For $n = 4$ there is a single chord diagram. It has a single chord θ_{01} and therefore the region is given by $x_0 = x_1$. Recall that $x_0 = 0$ and so $x_1 = 0$. For $n = 6$ there are two non-crossing chord diagrams as shown in figure 3.4. The corresponding regions can be seen to match R_1 and*

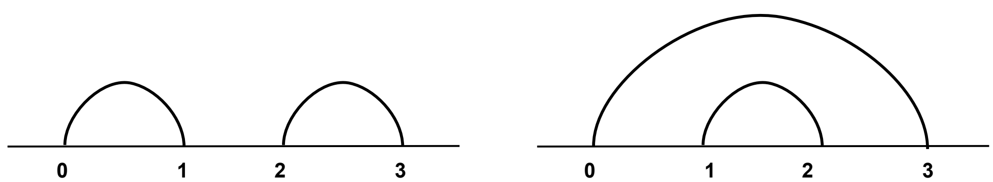

Figure 3.4: Non-crossing chord diagrams for $n = 6$. On the right, the chord θ_{03} surrounds the chord θ_{12} and therefore the condition $x_0 < x_1$ is imposed.

R_2 in (3.46), i.e.,

$$R_1 = \{x_0 = x_1,\, x_2 = x_3\}\,, \quad R_2 = \{x_0 = x_3,\, x_1 = x_2,\, x_0 < x_1\}\,. \tag{3.65}$$

Finally, we leave as an exercise to the reader to check that the five regions for $n = 8$ presented in (3.51) correspond to the diagrams in figure 3.5.

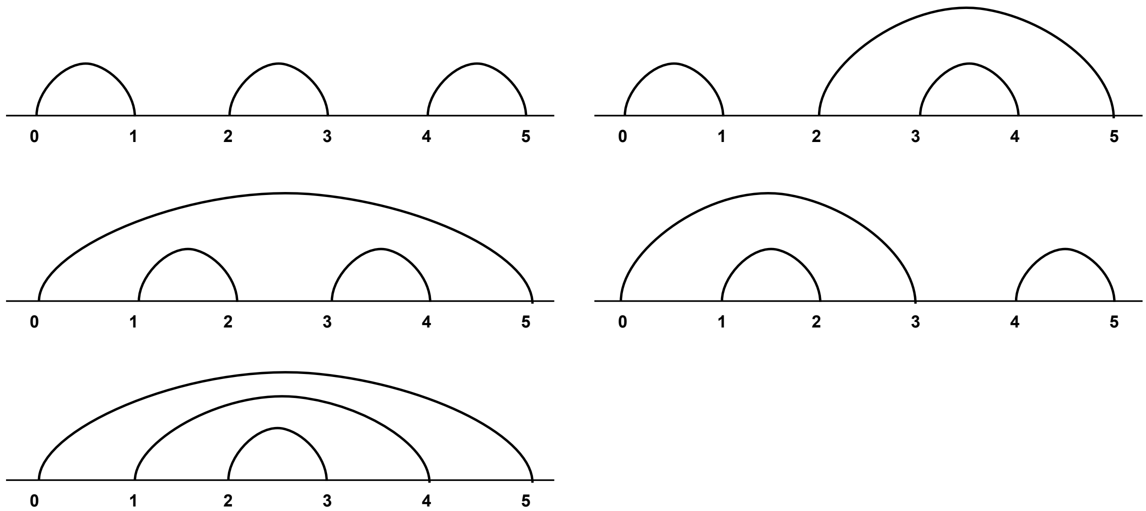

Figure 3.5: Non-crossing chord diagrams for $n = 8$. In the second diagram θ_{25} surrounds θ_{34} and therefore $x_2 < x_3$. In the third diagram θ_{05} surrounds both θ_{12} and θ_{34} and therefore $x_0 < x_1$ and $x_0 < x_3$. In the fourth diagram θ_{03} surrounds θ_{12} so $x_0 < x_1$. Finally, in the fifth diagram θ_{05} surrounds θ_{14} which surrounds θ_{23} so $x_0 < x_1 < x_2$.

In the last example of section 3.5 we found that the contribution to region R_1 was computed by a biadjoint ϕ^3 amplitude with $n/2+1$ particles, i.e., $m_{n/2+1}(\mathbb{I}, \mathbb{I})$. The attentive reader might have noticed that in all examples provided so far, the structure of the answer resembles that of $m_{n/2+1}(\alpha, \mathbb{I})$ for some permutation α. We leave the precise connection between α and a region for future work and here we concentrate on the schematic structure of $A_n^{\phi^4}$ for which we have an all n proposal.

3.6.2 Products of ϕ^3 Amplitudes: Towards $m_{n/2+1}(\alpha, \mathbb{I})$

In order to understand the structure of each region, it is useful to introduce an additional chord to the non-crossing chord diagrams described above. More precisely, we introduce two new points, which could be denoted -1 and $n-2$, and we always draw a chord between them. The point -1 is located to the left of 0 and $n-2$ is to the right of $n-3$

so that the chord $\theta_{-1,n-2}$ surrounds the whole diagram. This can be understood as a way of introducing into the figure the fixed particles 1 and 2 in the parameterization (3.12).

Definition 3.6.4. *An extended non-crossing chord diagram (also known as indecomposable non-crossing chord diagram) associated to $A_n^{\phi^4}$ is a non-crossing chord diagram on n points labeled by $\{-1,0,1,2,\ldots,n-3,n-2\}$ in which $\theta_{-1,n-2}$ is always included. We also define a meadow of an extended non-crossing chord diagram as any region in the diagram delimited by more than one chord and by the line where the points lie.*

The claim is that a meadow delimited by m chords and the real line corresponds to a biadjoint $(m+1)$-subamplitude participating in $m_{n/2+1}(\alpha,\mathbb{I})$. Moreover, we also claim that any chord θ_{ab} shared by *two* meadows corresponds to a propagator in $m_{n/2+1}(\alpha,\mathbb{I})$ of the form $1/t_{[a+3,b+2]}$. This also fixes the topology of the cubic double-ordered amplitude.

Before describing the consequences of this proposal, let us give some examples to illustrate it.

Example 3.6.5. *Consider the region described by the diagram in figure 3.6 for $n=10$. Using the diagram it is easy to recognize the region as*

$$R=\{x_0=x_1,\,x_2=x_5,\,x_3=x_4,\,x_6=x_7,\,x_2<x_3\}\,. \tag{3.66}$$

Since the green meadow is delimited by 4 chords and the real line then it corresponds to a 5-particle subamplitude of $m_6(\alpha,\mathbb{I})$, while the blue meadow is delimited by 2 chords and the real line and thus corresponds to a 3-particle subamplitude. The disk diagram on the right is intended to represent the topology of $m_6(\alpha,\mathbb{I})$ given the diagram on the left. The reader familiar with the CHY description of biadjoint partial amplitudes would recognize the disk diagram as encoding the two orderings α and $\mathbb{I}$. Finally, notice that the chord θ_{25} is shared

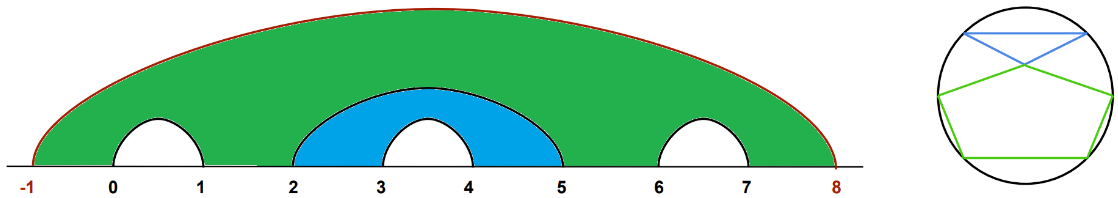

Figure 3.6: *Left:* An extended non-crossing chord diagram for $n = 10$ where the meadows have been coloured. The additional points -1 and 8 together with the chord $\theta_{-1,8}$ joining them are coloured in magenta. *Right:* Disc diagram of an $m_6(\alpha, \mathbb{I})$ amplitude corresponding to the contribution of the region on the left.

by two meadows, hence it generates the propagator $1/t_{567}$ *in* $m_6(\alpha, \mathbb{I})$*. The conclusion is that the contribution of this region to* $A_{10}^{\phi^4}$ *is schematically given by*

$$m_3 \times m_5 \times \frac{1}{t_{567}}\,. \tag{3.67}$$

Example 3.6.6. *Consider another region contributing to* $A_{10}^{\phi^4}$*, described by the diagram in figure 3.7. In this case we have two 4-particle subamplitudes and one propagator of the*

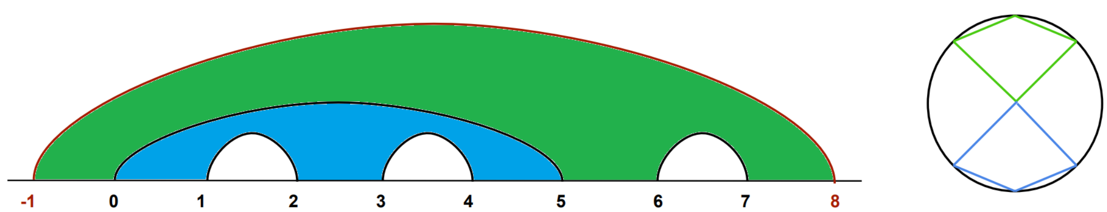

Figure 3.7: *Left:* An extended non-crossing chord diagram for $n = 10$ where the meadows have been coloured. *Right:* Disc diagram of an $m_6(\alpha, \mathbb{I})$ amplitude corresponding to the contribution of the region on the left.

form $1/t_{[3,7]}$*. The contribution of this region to* $A_{10}^{\phi^4}$ *is schematically given by*

$$(m_4)^2 \times \frac{1}{t_{[3,7]}}\,. \tag{3.68}$$

Note that $(m_4)^2$ stands for the product of two distinct four-point ϕ^3 amplitudes. Since we are only interested in the schematic structure, i.e. in the number of amplitudes of a given type, we keep track of that using exponents.

Example 3.6.7. *Consider now a region contributing to $A_8^{\phi^4}$. The region is defined by the diagram in figure 3.8. We leave as an exercise for the reader to show that this corresponds to region R_5 in the example given in section 3.5.3. The extended non-crossing chord diagram*

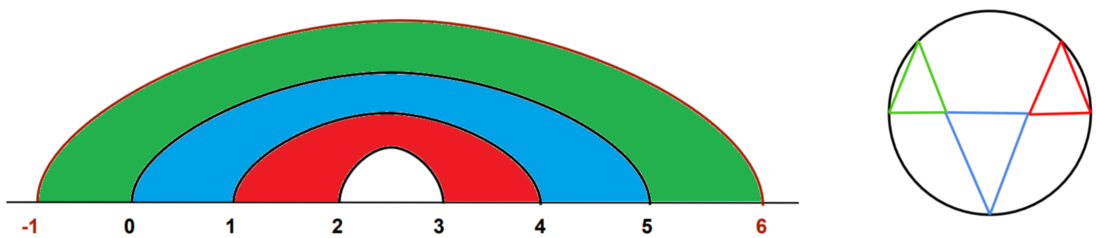

Figure 3.8: *Left:* An extended non-crossing chord diagram for $n = 8$ where the meadows have been coloured. *Right:* Disc diagram of an $m_5(\alpha, \mathbb{I})$ amplitude corresponding to the contribution of the region on the left.

contains three meadows delimited by two chords (i.e. three 3-particle subamplitudes) and two propagators corresponding to the chords θ_{05} and θ_{14}. Accoding to our proposal, these propagators are $1/t_{[3,7]} = 1/t_{812}$ and $1/t_{456}$, respectively. Once again, the schematic form of the contribution is

$$(m_3)^3 \times \frac{1}{t_{812}} \times \frac{1}{t_{456}} \,. \tag{3.69}$$

If we define $m_3 := 1$ this is exactly the contribution $A_8^{\phi^4:(5)}$ presented in (3.53).

Based on these and many other examples, we have found a formula that reproduces the schematic structure of $A_n^{\phi^4}$ in every case. The formula is based on the Lagrange inversion procedure relating the series expansion of a function $f(x)$ with that of its compositional inverse. We review some related material in appendix C. Here we simply present the final form of the proposal. Let

$$h(x) = \sum_{i=0}^{\infty} h_i x^i := \sum_{i=0}^{\infty} m_{i+2} x^i \,, \tag{3.70}$$

where m_{i+2} represents a generic $(i+2)$-particle amplitude in the biadjoint ϕ^3 scalar theory of the form $m_{i+2}(\mathbb{I},\mathbb{I})$. Since the mass dimension of $m_{i+2}(\mathbb{I},\mathbb{I})$ is $-2(i-1)$ we are motivated to define $m_2 := P^2$ and $m_3 := 1$. Here $1/P^2$ represents a generic propagator.

The claim is that the schematic form of the amplitude $A_n^{\phi^4}$ is given by

$$A_n^{\phi^4} = \left(\frac{2}{n\, h_0^{n/2-1}}\right) \frac{1}{2\pi i} \oint_{|z|=\epsilon} dz \left(\frac{h(z)}{z}\right)^{n/2} . \tag{3.71}$$

Let us compute the first few cases of (3.71),

$$\begin{aligned}
A_4^{\phi^4} &= h_1 = m_3 \,, \\
A_6^{\phi^4} &= \frac{h_0^2 h_2 + h_0 h_1^2}{h_0^2} = m_4 + m_3^2 \frac{1}{P^2} \,, \\
A_8^{\phi^4} &= \frac{h_3 h_0^3 + 3 h_1 h_2 h_0^2 + h_1^3 h_0}{h_0^3} = m_5 + 3 m_3 m_4 \frac{1}{P^2} + m_3^3 \left(\frac{1}{P^2}\right)^2 , \\
A_{10}^{\phi^4} &= m_6 + 4 m_5 m_3 \frac{1}{P^2} + 2 m_4^2 \frac{1}{P^2} + 6 m_4 m_3^2 \left(\frac{1}{P^2}\right)^2 + m_3^4 \left(\frac{1}{P^2}\right)^3 .
\end{aligned}$$

There are several consistency checks that can be done on (3.71). The first is that the number of non-crossing chord diagrams with $n/2-1$ chords is $\mathrm{C}_{n/2-1}$. Therefore if we set all $m_r := 1$ so that the contribution from each region is unity, one must find that

$A_n^{\phi^4} = \mathrm{C}_{n/2-1}$. This means that we must set

$$h(x) = \sum_{i=1}^{\infty} x^i = \frac{1}{1-x}\,, \tag{3.72}$$

and evaluate

$$A_n^{\phi^4} = \left(\frac{2}{n}\right) \frac{1}{2\pi i} \oint_{|z|=\epsilon} dz \left(\frac{1}{z(1-z)}\right)^{n/2} = \mathrm{C}_{n/2-1}\,. \tag{3.73}$$

The last equality follows from the Lagrange inversion formula with $f(x) = x(1-x)$ and $g(x) = xB_2(x)$, where $B_2(x)$ is the generating function of Catalan numbers.

The second check is that if $A_n^{\phi^4}$ is evaluated on "planar kinematics" [77, 107, 66], i.e. on the kinematic point where all planar Mandelstam invariants that participate in $A_n^{\phi^4}$ are unity, $t_{[a,b]} = 1$, then $A_n^{\phi^4}$ simply counts the number of planar ternary trees (with all internal vertices of degree four). The numbers are known to be given by the Fuss-Catalan sequence, $\mathrm{FC}_{n/2-1}(3,1)$. For $n = 4, 6, 8, 10$ one has $\mathrm{FC}_{n/2-1}(3,1) = 1, 3, 12, 55$. This check can be done by realizing that on planar kinematics $m_n = \mathrm{C}_{n-2}$ and therefore

$$h(x) = \sum_{i=1}^{\infty} \mathrm{C}_i\, x^i = B_2(x) = \frac{1-\sqrt{1-4x}}{2x}\,. \tag{3.74}$$

As shown in appendix C in (C.8), it is indeed the case that

$$\mathrm{FC}_r(3,1) = \frac{1}{2\pi i} \oint_{|z|=\epsilon} \frac{dz}{r+1} \left(\frac{1-\sqrt{1-4z}}{2z^2}\right)^{r+1}\,, \tag{3.75}$$

which gives the required relation when $r = n/2 - 1$.

3.6.3 Completing the Proof of Proposition 3.5.2

In order to complete the proof of Proposition 3.5.2 we have to show that all regions that contribute to $A_n^{\phi^4}$, except for R_1, are $\mathcal{O}(\epsilon)$ when

$$t_{[a,b]} = \frac{1}{\epsilon}\,, \quad a \in \{3, 5, \ldots, n-3\}\,,\ b \in \{a+2, a+4, \ldots, n-1\}\,. \tag{3.76}$$

Recall that R_1 is the region corresponding to $n/2-1$ non-crossing chords so that none is surrounded by any other. According to the rules explained in this section, this means that no propagator is generated. One the other hand, every single other region has at least one chord surrounded by another, say θ_{ef} and therefore there is at least one propagator in the region's contribution to the amplitude. The propagator is $1/t_{[e+3,f+2]}$. Clearly $f-e \geq 3$ so that the chord can contain at least another one. This means that the chords of interest can only have $e \in \{0, 1, \ldots, n-6\}$ and $f \in \{e+3, e+4, \ldots, n-3\}$. Therefore each region different from R_1 contains at last one propagator of the form $1/t_{[a,b]}$ with $a \in \{3, 4, \ldots, n-3\}$ and $b \in \{a+2, a+3, \ldots, n-1\}$. But this is exactly the range of propagators set to ϵ and this concludes the proof.

3.7 From ϕ^3 Amplitudes to ϕ^p Amplitudes

In this section we extend the limiting procedure used to obtain $A_n^{\phi^4}$ from $m_n(\mathbb{I},\mathbb{I})$ to make a general conjecture for any $A_n^{\phi^p}$ amplitude and its global Schwinger formulation. We also propose a diagrammatic procedure for finding all the regions that contribute to $A_n^{\phi^p}$ and point out a connection with $m_{(n+2(p-3))/(p-2)}(\alpha,\mathbb{I})$ amplitudes. To start with, the limiting procedure that generates $A_n^{\phi^p}$ from $m_n(\mathbb{I},\mathbb{I})$ is the following.

Proposition 3.7.1. *Consider the region of the kinematic space of n massless particles where $t_{[a,b]} = 1/\epsilon$ whenever $b - a \not\equiv 0 \mod p-2$ and let $m_n^{(\epsilon)}(\mathbb{I},\mathbb{I})$ denote $m_n(\mathbb{I},\mathbb{I})$ evaluated on it. Then*

$$A_n^{\phi^p} = \lim_{\epsilon\to 0} \frac{1}{\left(C_{p-2}\,\epsilon^{p-3}\right)^{\frac{n-2}{p-2}}} m_n^{(\epsilon)}(\mathbb{I},\mathbb{I}), \tag{3.77}$$

where C_m is the m^{th} Catalan number.

Proof. The proof is analogous to that of Proposition 3.4.1. First, consider any Feynman diagram $\mathcal{T}^{(p)}$ of $A_n^{\phi^p}$, that is, any $(p-1)$-ary planar tree on n-leaves. Such a diagram has $(n-2)/(p-2)$ vertices of degree p. The strategy is again to find out how many planar binary trees give rise to $\mathcal{T}^{(p)}$ by collapsing edges, i.e., taking their length to zero. This is easily done by realizing that for each degree-p vertex of $\mathcal{T}^{(p)}$ there are exactly C_{p-2} ways, compatible with planarity, of growing a tree to produce C_{p-2} degree-three vertices. This means that there are $\mathrm{C}_{p-2}^{(n-2)/(p-2)}$ binary trees that give rise to $\mathcal{T}^{(p)}$. Of course, not all binary trees descend to a $(p-1)$-ary diagram. Note that under the kinematics in the proposition, ϕ^3 Feynman diagrams that collapse to ϕ^p diagrams have exactly $(n-p)/(p-2)$ ϵ-independent propagators and therefore $(n-3)-(n-p)/(p-2) = (p-3)(n-2)/(p-2)$ which become $1/t = \epsilon$. Diagrams that do not produce a ϕ^p diagram have at least one extra propagator of the form $1/t = \epsilon$. Therefore, in the limit $\epsilon \to 0$ the ϕ^p amplitude is recovered. □

As in section 3.4, one can write the global Schwinger formula for $A_n^{\phi^p}$ as a single integral

$$A_n^{\phi^p} = \int_{\mathbb{R}^{n-3}} d^{n-3}x \exp\left(-\sum_{a<b}^{\mathcal{K}_p} t_{[a,b]} f_{[a,b]}(x)\right) Q(x)\,, \tag{3.78}$$

where $\mathcal{K}_p$ means that the sum is over ordered pairs (a,b) such that $b-a \equiv 0 \mod p-2$.

Here $Q(x)$ is defined as

$$Q(x) := \lim_{\epsilon \to 0^+} \frac{1}{\left(\mathrm{C}_{p-2}\, \epsilon^{p-3}\right)^{\frac{n-2}{p-2}}} \exp\left(-\frac{1}{\epsilon} H(x)\right) \tag{3.79}$$

with

$$H(x) = \sum_{a<b:(a,b)\notin \mathcal{K}_p} f_{[a,b]}(x)\,. \tag{3.80}$$

Note that due to the non-negativity of $H(x)$, $Q(x)$ only has support in regions where $H(x) = 0$. Again, the distribution $Q(x)$ becomes a sum over distributions that localize the integral to these regions. This means that equation (3.78) can also be understood as a sum over regions, where these as associated to diagrams as explained in the next subsection.

3.7.1 Combinatorial Description of Regions

In this subsection we conjecture that the solutions of $H(x) = 0$ are regions of dimension $n/(p-2) - 1$ in $\mathbb{R}^{n-3}$ which are classified by non-crossing $(p-2)$-chord diagrams. The definition of non-crossing $(p-2)$-chord diagrams, in our context, is the following.

Definition 3.7.2. *Place $n-2$ points labeled $0, 1, \ldots, n-3$ on the real line in increasing order. A non-crossing $(p-2)$-chord diagram is a perfect matching of the points such that each matching involves $(p-2)$ points joined by a $(p-2)$-chord and drawn on the upper half plane without any crossings. Let us denote the $(p-2)$-chord connecting points $a_1, a_2, \ldots, a_{p-2}$ as $\theta_{a_1,a_2,\ldots,a_{p-2}}$ (for general k-chord diagrams see e.g. [208].)*

Conjecture 3.7.3. *The regions contributing to $A_n^{\phi^p}$ are in bijection with the set of all*

$FC_{(n-2)/(p-2)}(p-2,1)$[7] *possible non-crossing $(p-2)$-chord diagrams. Moreover, the region R corresponding to a particular diagram is obtained as follows:*

- *For each $(p-2)$-chord $\theta_{a_1,a_2,\ldots,a_{p-2}}$ set $x_{a_1} = x_{a_2} = \cdots = x_{a_{p-2}}$.*
- *If a $(p-2)$-chord $\theta_{a_1,a_2,\ldots,a_{p-2}}$ surrounds another $(p-2)$-chord $\theta_{b_1,b_2,\ldots,b_{p-2}}$, then $x_{a_1} = x_{a_2} = \cdots = x_{a_{p-2}} < x_{b_1} = x_{b_2} = \cdots = x_{b_{p-2}}$.*

In other words, the regions defined by the non-crossing $(p-2)$-chord diagrams are all the solutions to $H(x) = 0$, where $H(x)$ is given by (3.80), and the sum of their contributions produces all the $FC_{(n-2)/(p-2)}(p-1,1)$ trees of ϕ^p.

Example 3.7.4. *Consider the $n = 10$ amplitude for ϕ^6. There are four non-crossing 4-chord diagrams and are shown in figure 3.9.*

Reading from top to bottom and recalling that $x_0 = 0$, the four regions generated by these diagrams correspond, respectively, to

$$
\begin{aligned}
R_1 =& \{x_1 = x_2 = x_3 = 0,\, x_4 = x_5 = x_6 = x_7\}\,, \\
R_2 =& \{x_1 = x_2 = x_7 = 0,\, x_3 = x_4 = x_5 = x_6,\, x_3 > 0\}\,, \\
R_3 =& \{x_1 = x_6 = x_7 = 0,\, x_2 = x_3 = x_4 = x_5,\, x_2 > 0\}\,, \\
R_4 =& \{x_5 = x_6 = x_7 = 0,\, x_1 = x_2 = x_3 = x_4,\, x_1 > 0\}\,.
\end{aligned}
$$

[7] Recall that $\mathrm{FC}_m(q,r)$ is the Fuss-Catalan number given by

$$\mathrm{FC}_m(q,r) \equiv \frac{r}{mq+r}\binom{mq+r}{m}\,.$$

Note that for $q = 2$ and $r = 1$ the Fuss-Catalan numbers coincide with the Catalan numbers, i.e. $\mathrm{FC}_m(2,1) = \mathrm{C}_m$.

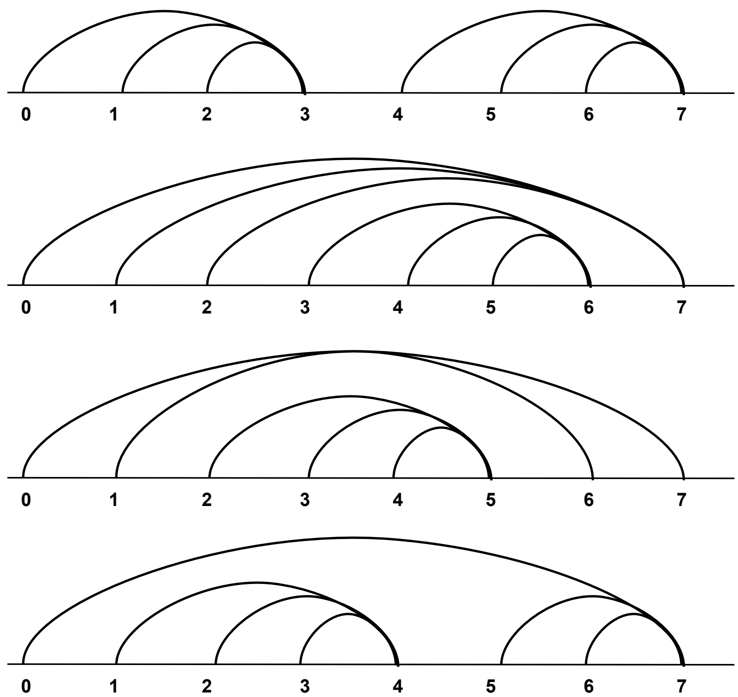

Figure 3.9: All possible non-crossing 4-chord diagrams for $n = 10$ and $p = 6$. Each diagram contains exactly two 4-chords. In the top diagram one 4-chord joins points $0, 1, 2, 3$ while the second 4-chord joins $4, 5, 6, 7$. In the second diagram the 4-chord θ_{0127} surrounds θ_{3456}. In the third, θ_{0167} surrounds θ_{2345}. In the last diagram, θ_{0567} surrounds θ_{1234}.

Therefore, the distribution $Q(x)$ is given by

$$Q(x) = Q_1(x) + Q_2(x) + Q_3(x) + Q_4(x)$$

with

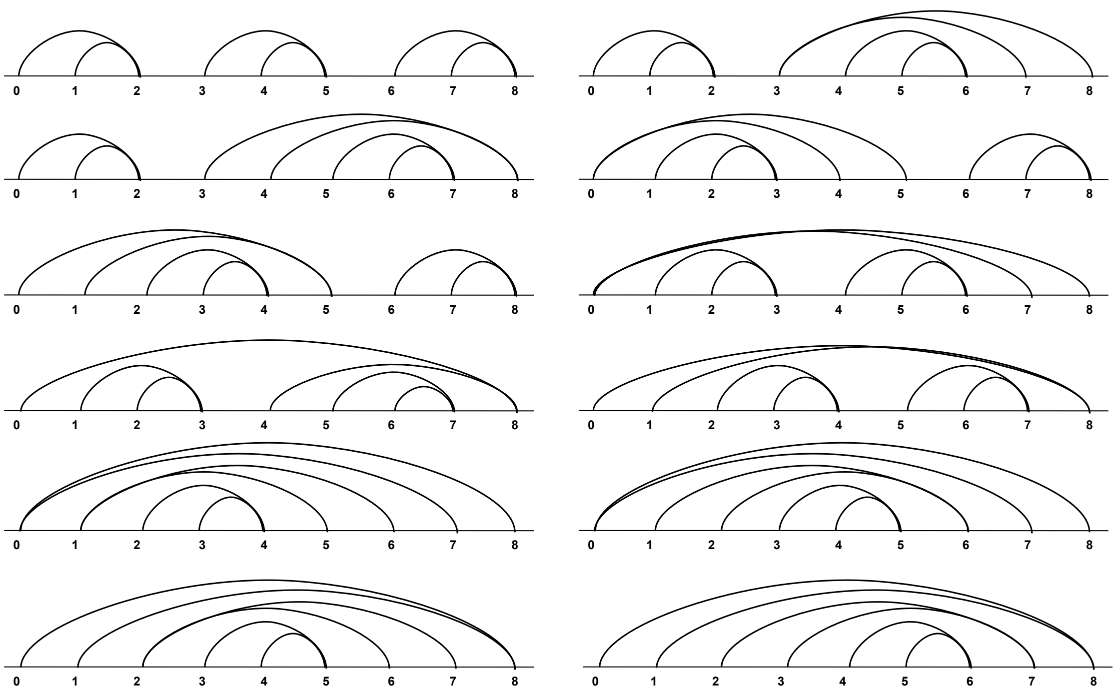

Figure 3.10: All possible non-crossing 3-chord diagrams for $n = 11$ and $p = 5$.

$$Q_1 := \delta(x_1)\delta(x_2)\delta(x_3)\delta(x_4 - x_5)\delta(x_5 - x_6)\delta(x_6 - x_7)\,,$$

$$Q_2 := \theta(x_3)\delta(x_1)\delta(x_2)\delta(x_7)\delta(x_3 - x_4)\delta(x_4 - x_5)\delta(x_5 - x_6)\,,$$

$$Q_3 := \theta(x_2)\delta(x_1)\delta(x_6)\delta(x_7)\delta(x_2 - x_3)\delta(x_3 - x_4)\delta(x_4 - x_5)\,,$$

$$Q_4 := \theta(x_1)\delta(x_5)\delta(x_6)\delta(x_7)\delta(x_1 - x_2)\delta(x_2 - x_3)\delta(x_3 - x_4)\,.$$

The contributions from each region are

$$\begin{aligned} A_{10}^{\phi^6:(1)} &= \frac{1}{t_{[1,5]}} + \frac{1}{t_{[2,6]}}\,, \qquad & A_{10}^{\phi^6:(2)} &= \frac{1}{t_{[5,9]}}\,, \\ A_{10}^{\phi^6:(3)} &= \frac{1}{t_{[4,8]}}\,, & A_{10}^{\phi^6:(4)} &= \frac{1}{t_{[3,7]}}\,. \end{aligned} \tag{3.81}$$

The amplitude $A_{10}^{\phi^6}$ *is the sum over all* $FC_2(4,1) = 4$ *contributions and gives rise to the familiar expression with* $FC_2(5,1) = 5$ *Feynman diagrams.*

Example 3.7.5. *Consider now the* $n = 11$ *case for* ϕ^5*. There are 12 non-crossing* 3*-chord diagrams and are represented in figure 3.10. Reading from left to right and top to bottom, the 12 regions generated by these diagrams correspond, respectively, to*

$$
\begin{aligned}
R_1 &= \{x_1 = x_2 = 0,\, x_3 = x_4 = x_5,\, x_6 = x_7 = x_8\}\,,\\
R_2 &= \{x_1 = x_2 = 0,\, x_3 = x_7 = x_8,\, x_4 = x_5 = x_6,\, x_3 < x_4\}\,,\\
R_3 &= \{x_1 = x_2 = 0,\, x_5 = x_6 = x_7,\, x_3 = x_4 = x_8,\, x_3 < x_5\}\,,\\
R_4 &= \{x_4 = x_5 = 0,\, x_1 = x_2 = x_3,\, x_6 = x_7 = x_8,\, x_1 > 0\}\,,\\
R_5 &= \{x_1 = x_5 = 0,\, x_2 = x_3 = x_4,\, x_6 = x_7 = x_8,\, x_2 > 0\}\,,\\
R_6 &= \{x_7 = x_8 = 0,\, x_1 = x_2 = x_3,\, x_4 = x_5 = x_6,\, x_1 > 0,\, x_4 > 0\}\,,\\
R_7 &= \{x_4 = x_8 = 0,\, x_1 = x_2 = x_3,\, x_5 = x_6 = x_7,\, x_1 > 0,\, x_5 > 0\}\,,\\
R_8 &= \{x_1 = x_8 = 0,\, x_2 = x_3 = x_4,\, x_5 = x_6 = x_7,\, x_2 > 0,\, x_5 > 0\}\,,\\
R_9 &= \{x_7 = x_8 = 0,\, x_1 = x_5 = x_6,\, x_2 = x_3 = x_4,\, x_2 > x_1 > 0\}\,,\\
R_{10} &= \{x_7 = x_8 = 0,\, x_1 = x_2 = x_6,\, x_3 = x_4 = x_5,\, x_3 > x_1 > 0\}\,,\\
R_{11} &= \{x_1 = x_8 = 0,\, x_2 = x_6 = x_7,\, x_3 = x_4 = x_5,\, x_3 > x_2 > 0\}\,,\\
R_{12} &= \{x_1 = x_8 = 0,\, x_2 = x_3 = x_7,\, x_4 = x_5 = x_6,\, x_4 > x_2 > 0\}\,.
\end{aligned}
$$

We leave as an exercise to the reader to find the distributions associated to these regions *and to show that the contributions from each region are:*

$$
\begin{aligned}
A_{11}^{\phi^5:(1)} &= \frac{1}{t_{[2,5]}t_{[8,11]}} + \frac{1}{t_{[2,5]}t_{[2,8]}} + \frac{1}{t_{[5,8]}t_{[2,8]}} + \frac{1}{t_{[5,8]}t_{[5,11]}} + \frac{1}{t_{[8,11]}t_{[5,11]}}\,, \\
A_{11}^{\phi^5:(2)} &= \frac{1}{t_{[6,9]}}\left(\frac{1}{t_{[2,5]}} + \frac{1}{t_{[5,11]}}\right), \quad A_{11}^{\phi^5:(3)} = \frac{1}{t_{[7,10]}}\left(\frac{1}{t_{[2,5]}} + \frac{1}{t_{[5,11]}}\right), \\
A_{11}^{\phi^5:(4)} &= \frac{1}{t_{[3,6]}}\left(\frac{1}{t_{[8,11]}} + \frac{1}{t_{[2,8]}}\right), \quad A_{11}^{\phi^5:(5)} = \frac{1}{t_{[4,7]}}\left(\frac{1}{t_{[8,11]}} + \frac{1}{t_{[2,8]}}\right), \\
A_{11}^{\phi^5:(6)} &= \frac{1}{t_{[3,9]}}\left(\frac{1}{t_{[3,6]}} + \frac{1}{t_{[6,9]}}\right), \quad A_{11}^{\phi^5:(7)} = \frac{1}{t_{[7,10]}t_{[3,6]}}\,, \\
A_{11}^{\phi^5:(8)} &= \frac{1}{t_{[4,10]}}\left(\frac{1}{t_{[4,7]}} + \frac{1}{t_{[7,10]}}\right), \quad A_{11}^{\phi^5:(9)} = \frac{1}{t_{[4,7]}t_{[3,9]}}\,, \\
A_{11}^{\phi^5:(10)} &= \frac{1}{t_{[5,8]}t_{[3,9]}}\,, \quad A_{11}^{\phi^5:(11)} = \frac{1}{t_{[5,8]}t_{[4,10]}}\,, \quad A_{11}^{\phi^5:(12)} = \frac{1}{t_{[6,9]}t_{[4,10]}}\,.
\end{aligned}
\tag{3.82}
$$

The amplitude $A_{11}^{\phi^5}$ is the sum over all $FC_3(3,1) = 12$ contributions and gives rise to the familiar expression with $FC_3(4,1) = 22$ Feynman diagrams.

From these examples note that even for $p > 4$ the structure of the contribution of each region also resembles that of a cubic amplitude. In particular, it has the structure of $m_{(n+2(p-3))/(p-2)}(\alpha, \mathbb{I})$ for some permutation α. Here we will only concentrate on the schematic structure of $A_n^{\phi^p}$ for all n, leaving again the precise connection between α and the region to future work.

3.7.2 Products of ϕ^3 Amplitudes: Towards $m_{(n+2(p-3))/(p-2)}(\alpha, \mathbb{I})$

As in the $p = 4$ case, in order to understand the structure of each region it is useful to introduce an additional $(p-2)$-chord to the non-crossing $(p-2)$-chord diagrams from Definition 3.7.2. This is done by adding $p-2$ new points labelled $-p+3, -p+4, \ldots, -1$

and $n-2$ so that the new set of points is $\{-p+3, -p+4, \ldots -1, 0, 1, 2, \ldots, n-3, n-2\}$ and points are located in increasing order on the real line[8].

Definition 3.7.6. *An extended non-crossing $(p-2)$-chord diagram is a non-crossing $(p-2)$-chord diagram on n points labelled by $\{-p+3, -p+4, \ldots -1, 0, 1, 2, \ldots, n-3, n-2\}$ in which $\theta_{-p+3,-p+4,\ldots,-1,n-2}$ is always included. We also define a meadow of an extended non-crossing $(p-2)$-chord diagram as any region in the diagram delimited by more than one $(p-2)$-chord and by the line where the points lie.*

From now on we will abuse notation and use θ_{ab} to refer to the unique path in a $(p-2)$-chord joining two points a and b. Therefore, the general claim is that a meadow delimited by m such paths and the real line corresponds to a biadjoint $(m+1)$-subamplitude participating in $m_{(n+2(p-3))/(p-2)}(\alpha, \mathbb{I})$. We also claim that the upper boundary of a meadow, θ_{ab}, corresponds to a propagator in $m_{(n+2(p-3))/(p-2)}(\alpha, \mathbb{I})$ of the form $1/t_{[a+3,b+2]}$, with the exception of the pair $\{a, b\} = \{-1, n-2\}$. This also fixes the topology of the cubic double-ordered amplitude.

Let us again give some examples to illustrate the proposal.

Example 3.7.7. *Consider the extended non-crossing 4-chord diagram of ϕ^6 for $n = 14$ shown in figure 3.11.*

In this extended diagram the points -3, -2, -1 and 12 together with the 4-chord $\theta_{-3,-2,-1,12}$ that joins them are coloured in magenta. One can see that there are two meadows coloured in green and blue. The green meadow is delimited by the real line and by 2 paths $\theta_{-1,12}$ and $\theta_{0,11}$, thus it corresponds to a 3-point subamplitude appearing in $m_5(\alpha, \mathbb{I})$. Similarly, the blue meadow is delimited by 3 paths $\theta_{2,11}$, θ_{36} and $\theta_{7,10}$ and the real line,

[8] In fact, any choice where at least one point is on the left of 0 and one point is on the right on $n-3$ is valid.

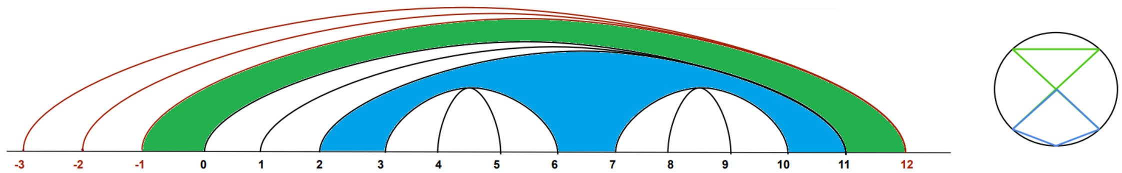

Figure 3.11: *Left:* An extended non-crossing chord diagram of ϕ^6 for $n = 14$ where the meadows have been coloured. *Right:* Disc diagram of an $m_5(\alpha, \mathbb{I})$ amplitude corresponding to the contribution of the region on the left.

thus it corresponds to a 4-point subamplitude of $m_5(\alpha, \mathbb{I})$*. The upper boundary of the blue meadow is* $\theta_{2,11}$ *and this means that there is a propagator of the form* $1/t_{[5,13]}$*. The upper boundary of the green meadow is of the form* $\theta_{-1,n-2}$ *and it does not generate a propagator. Therefore, the schematic form of the contribution is*

$$m_3 \times m_4 \times \frac{1}{t_{[5,13]}}\,.$$

Example 3.7.8. *Now consider another extended non-crossing 4-chord diagram of* ϕ^6 *for* $n = 14$ *shown in figure 3.12. As in the previous example, one can see that there are*

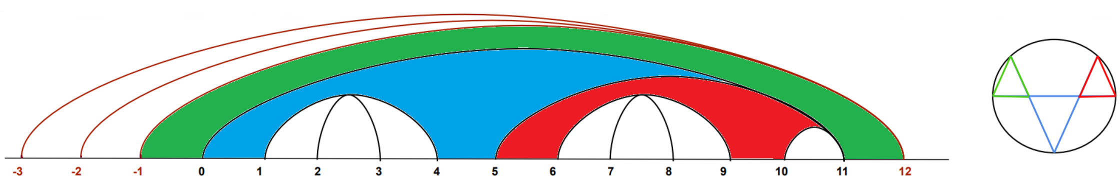

Figure 3.12: *Left:* An extended non-crossing chord diagram of ϕ^6 for $n = 14$ where the meadows have been coloured. *Right:* Disc diagram of an $m_5(\alpha, \mathbb{I})$ amplitude corresponding to the contribution of the region on the left.

three meadows coloured in green, blue and red. The green meadow is delimited by the real line and by 2 paths $\theta_{-1,12}$ *and* $\theta_{0,11}$ *and gives rise to a 3-point subamplitude appearing in* $m_5(\alpha, \mathbb{I})$*. Similarly, the blue meadow is delimited by the real line and 2 paths* θ_{05} *and* θ_{14}*, thus it corresponds to a 3-point subamplitude of* $m_5(\alpha, \mathbb{I})$*. Likewise, the red meadow is* *delimited by the real line and 2 paths $\theta_{5,10}$ and θ_{69} and gives rise to a 3-point subamplitude of $m_5(\alpha, \mathbb{I})$. We also have two propagators of the form $1/t_{[3,7]}$ and $1/t_{[8,12]}$. Therefore, the schematic form of the contribution is*

$$(m_3)^3 \times \frac{1}{t_{[3,7]}} \times \frac{1}{t_{[8,12]}}\,.$$

3.7.3 Schematic Structure of $A_n^{\phi^p}$

Before proposing a Lagrange inversion-like formula to reproduce the schematic structure of $A_n^{\phi^p}$, we present more examples:

$$\begin{aligned}
A_8^{\phi^5} &= m_4 + 2m_3^2\frac{1}{P^2}\,, \quad A_{11}^{\phi^5} = m_5 + 6m_3m_4\frac{1}{P^2} + 5m_3^3\left(\frac{1}{P^2}\right)^2,\\
A_{14}^{\phi^5} &= m_6 + 4m_4^2\frac{1}{P^2} + 8m_5m_3\frac{1}{P^2} + 28m_4m_3^2\left(\frac{1}{P^2}\right)^2 + 14m_3^4\left(\frac{1}{P^2}\right)^3,\\
A_{10}^{\phi^6} &= m_4 + 3m_3^2\frac{1}{P^2}\,, \quad A_{14}^{\phi^6} = m_5 + 9m_3m_4\frac{1}{P^2} + 12m_3^3\left(\frac{1}{P^2}\right)^2,\\
A_{12}^{\phi^7} &= m_4 + 4m_3^2\frac{1}{P^2}\,,\\
A_{14}^{\phi^8} &= m_4 + 5m_3^2\frac{1}{P^2}\,.
\end{aligned} \tag{3.83}$$

Let us make a proposal for the all n structure of $A_n^{\phi^p}$ amplitudes in terms of biadjoint cubic amplitudes and then perform the same consistency check as done for ϕ^4. The proposal is motivated by the fact, proven in appendix C, that $f(x) = x/B_{k-1}(x)$ and $g(x) = xB_k(x)$ are compositional inverses of each other if $B_r(x)$ is the generating function of the Fuss-Catalan numbers $\mathrm{FC}_m(r,1)$. This led us to propose a recursive structure in which we define

$$h_3(x) := \sum_{i=0}^{\infty} m_{i+2} x^i \tag{3.84}$$

and

$$h_k(x) = \sum_{j=0}^{\infty} h_{k,j} x^j := \sum_{j=0}^{\infty} \frac{1}{2\pi i} \oint_{|z|=\epsilon} \frac{dz}{j+1} \left(\frac{h_{k-1}(z)}{z} \right)^{j+1} x^j \,. \tag{3.85}$$

The structure of the $A_n^{\phi^p}$ amplitude is then given by

$$A_n^{\phi^p} = \frac{h_{p,(n-2)/(p-2)}}{h_0^{(p-3)(n-2)/(p-2)}} \,. \tag{3.86}$$

The first consistency check is that the number of non-crossing $(p-2)$-chord diagrams with $(n-2)/(p-2)$ chords is $\mathrm{FC}_{(n-2)/(p-2)}(p-2,1)$. Therefore if one sets all $m_{i+2} := 1$ so that the contribution from each region is unity, one must find that $A_n^{\phi^p} = \mathrm{FC}_{(n-2)/(p-2)}(p-2,1)$. In section 3.6.2 we showed that setting

$$h_3(x) = \sum_{i=1}^{\infty} x^i = \frac{1}{1-x} = B_1(x) \,, \tag{3.87}$$

turns $h_4(x)$ into the generating function of the numbers $\mathrm{FC}_m(3,1)$. Iterating the procedure one finds that $h_k(x)$ turns into the generating function of the numbers $\mathrm{FC}_m(k-1,1)$.

The second check is evaluating $A_n^{\phi^p}$ on planar kinematics so that $A_n^{\phi^p}$ counts the number of unrooted planar $(p-1)$-ary trees (with all internal vertices of degree p). The numbers are known to be given by the Fuss-Catalan sequence, $\mathrm{FC}_{(n-2)/(p-2)}(p-1,1)$. This check can again be done by realizing that on planar kinematics $m_n = \mathrm{C}_{n-2}$ and therefore

$$h_3(x) = \sum_{i=1}^{\infty} \mathrm{C}_i \, x^i = B_2(x) = \frac{1-\sqrt{1-4x}}{2x} \,. \tag{3.88}$$

Iterating one finds that $h_k(x) = B_{k-1}(x)$, the generating function of the Fuss-Catalan numbers $\mathrm{FC}_m(k-1,1)$ as required. In appendix C we provide several examples that illustrate the iteration procedure and the resulting formulas for $A_n^{\phi^p}$.

3.8 Factorization and Soft Limits

In this section we study how physical properties like factorization and soft limits are realized in the partial biadjoint amplitude $m_n(\mathbb{I},\mathbb{I})$ by using the global Schwinger formula. We also study soft limits in the CEGM amplitude from its analogous global Schwinger formulation presented in [66].

3.8.1 Factorization

One of the basic features of tree-level scattering amplitudes is that unitarity and locality constrain them so that the only existing poles have the schematic form $1/P^2$, where P is the sum of momenta of a subset of particles participating in the scattering, and the residues at these poles correspond to the product of two lower-point amplitudes.

In this section we initiate a qualitative study of how factorization is realized from the global Schwinger formulation perspective for the partial biadjoint amplitude. For example, we can consider the residue of $m_n(\mathbb{I},\mathbb{I})$ when $s_{34\ldots r} = 0$, which corresponds to a factorization of the form

$$m_{r-1}(3,4,...,r,I|3,4,...,r,I) \times m_{n-r+2}(I,r+1,...,1,2|I,r+1,...,1,2)\,,$$

where I is a new intermediate particle carrying momentum $-(p_3 + p_4 + \cdots + p_r)$.

From the global Schwinger formula point of view, what we want to find is the region that produces a divergence when $s_{34\dots r}$ is small. We start by recalling the global Schwinger formula

$$m_n(\mathbb{I},\mathbb{I}) = \int_{\mathbb{R}^{n-3}} d^{n-3}x \exp(-F_n(x))\,, \tag{3.89}$$

where the tropical potential can be written as

$$F_n(x) := \sum_{b=4}^{n}\sum_{a=2}^{b-1} s_{ab} \min(x_{a-2}, x_{a-1}, \dots, x_{b-3})\,. \tag{3.90}$$

If we apply the change of variables $x_1 = \tau^{-1}$ and $x_a = \tau^{-1} + u_a$, for $a \in \{2, ..., r-3\}$, we claim that the factorization is produced when $\tau \to 0^+$. This means that one of the tropical directions is flattened in the factorization limit. The way to see this is by noticing that after applying the change of variables, using momentum conservation considering that now $s_{34\dots r} \to 0$[9], and at leading order in τ we have

$$F_n(x) \to \tau^{-1} s_{34\dots r} + F_L(u) + F_R(x)\,, \tag{3.91}$$

where

$$F_L(u) = \sum_{b=5}^{r}\sum_{a=3}^{b-1} s_{ab}\min(u_{a-2}, u_{a-1}, \cdots, u_{b-3})\,, \tag{3.92}$$

[9]For example, we will have $(s_{3,r+1} + \cdots + s_{r,r+1}) = -(s_{r+2,r+1} + \cdots + s_{n,r+1} + s_{1,r+1} + s_{2,r+1}) = s_{I,r+1}$.

with $u_1 := 0$ and

$$\begin{aligned} F_R(x) =& s_{2,r+1}\text{min}(0, x_{r-2}) + s_{I,r+1}x_{r-2} \\ & + s_{2,r+2}\text{min}(0, x_{r-2}, x_{r-1}) + s_{I,r+2}\text{min}(x_{r-2}, x_{r-1}) + s_{r+1,r+2}x_{r-1} \\ & \dots \\ & + s_{2,n}\text{min}(0, x_{r-2}, ..., x_{n-3}) + s_{I,n}\text{min}(x_{r-2}, ..., x_{n-3}) + \cdots + s_{n-1,n}x_{n-3}\,. \end{aligned} \tag{3.93}$$

Here we have expanded $F_R(x)$ for clarity. This implies that (3.89) becomes

$$-\int d\tau\tau^{-2}\text{exp}(-\tau^{-1}s_{34\ldots r})\int_{\mathbb{R}^{r-4}} d^{r-4}u\,\text{exp}(-F_L(u))\int_{\mathbb{R}^{n-r-2}} d^{n-r-2}x\,\text{exp}(-F_R(x))\,. \tag{3.94}$$

Comparing to (3.89), we see that the second and third integrals give rise to the amplitudes $m_{r-1}(3, 4, ..., r, I|3, 4, ..., r, I)$ and $m_{n-r+2}(I, r+1, ..., 1, 2|I, r+1, ..., 1, 2)$, respectively. The limits of integration of the integral over τ are from 0 to τ_0, where τ_0 is positive and arbitrarily small. After integrating, if we expand in $s_{34\ldots r}/\tau_0$ we find that the leading order produces the desired pole $1/s_{34\ldots r}$. Hence the factorization. In order to complete the proof, one should show that the region considered here is the only one that produces the divergence. We leave this as an exercise for the reader.

3.8.2 Soft Limits: Biadjoint Scalar Amplitudes

In order to study soft limits from the global Schwinger formula we proceed in a similar way as in the factorization case. Now, we consider a soft particle, e.g. particle n, such that $s_{an} = \tau\hat{s}_{an}$ with $\tau \to 0$, and look for the regions that produce a divergence. Namely, we consider the part of (3.89) which depends on x_{n-3}, since it is the part in which particle n

appears

$$\int_{-\infty}^{\infty} dx_{n-3} \exp\left(-\sum_{a=2}^{n-1} s_{an}\min(x_{a-2}, x_{a-1}, ..., x_{n-2})\right), \tag{3.95}$$

with $x_0 = 0$ and $x_{n-2} = \infty$. There are two regions that contribute to the pole as $\tau \to 0$. One is when $x_{n-3} \in (-\infty, \min(x_0, x_1, ..., x_{n-4}))$. If we use momentum conservation we find that in this region we have

$$\int_{-\infty}^{\min(x_0,x_1,...,x_{n-4})} dx_{n-3}\exp(s_{1n}x_{n-3}) = \frac{\exp(s_{1n}\min(x_0, x_1, ..., x_{n-4}))}{s_{1n}} = \frac{1}{\tau\hat{s}_{1n}} + \mathcal{O}(\tau^0)\,.$$

The second region that contributes to the pole is $x_{n-3} \in (\max(x_0, x_1, ..., x_{n-4}), \infty)$. In this case we find that the contribution will come from

$$\int_{\max(x_0,x_1,...,x_{n-4})}^{\infty} dx_{n-3}\exp(-s_{n-1,n}x_{n-3}) = \frac{\exp(-s_{n-1,n}\max(x_0, x_1, ..., x_{n-4}))}{s_{n-1,n}} = \frac{1}{\tau\hat{s}_{n-1,n}} + \mathcal{O}(\tau^0)\,.$$

The remaining regions of integration will contribute $\mathcal{O}(\tau^0)$. Therefore, the amplitude in the soft limit behaves as expected

$$m_n(\mathbb{I}, \mathbb{I}) = \frac{1}{\tau}\left(\frac{1}{\hat{s}_{1n}} + \frac{1}{\hat{s}_{n-1,n}}\right) m_{n-1}(\mathbb{I}, \mathbb{I}) + \mathcal{O}(\tau^0)\,. \tag{3.96}$$

3.8.3 Soft Limits: CEGM Amplitudes

One of the many fascinating properties of the still mysterious CEGM generalized amplitudes is their behavior in soft limits. Using the CHY representation and the global residue theorem, García-Sepúlveda and Guevara proved that $k = 2$, i.e. biadjoint scalar, amplitudes are the leading soft factors of $k > 2$ amplitudes, after some relabellings in the generalized kinematic invariants [123]. In particular, they showed that in the soft limit[10] $\mathsf{s}_{a_1 a_2 \ldots a_{k-1} n} = \tau \hat{\mathsf{s}}_{a_1 a_2 \ldots a_{k-1} n}$, with $\tau \to 0$, the higher-k amplitude becomes

$$m_n^{(k)}(\mathbb{I}, \mathbb{I}) \to \frac{1}{\tau^{k-1}} m_{k+2}^{(2)}(\mathbb{I}, \mathbb{I}) \times m_{n-1}^{(k)}(\mathbb{I}, \mathbb{I}) + \mathcal{O}(\tau^{-k+2})\,. \tag{3.97}$$

Now we will perform a similar analysis than the one we did for the partial biadjoint scalar amplitude, using the global Schwinger formula for higher-k amplitudes

$$m_n^{(k)}(\mathbb{I}, \mathbb{I}) = \int_{\mathbb{R}^{(k-1)(n-k-1)}} d^{(k-1)(n-k-1)} x \exp(-F_n^{(k)}(x))\,. \tag{3.98}$$

In order to obtain the tropical potential $F_n^{(k)}(x)$, one starts with $G^+(k,n)$ and then tropicalizes the Plücker coordinates to define the function

$$F_n^{(k)}(x) := \sum_{1 \leq a_1 < a_2 < \ldots < a_k \leq n} \mathsf{s}_{a_1, a_2, \ldots, a_k} \Delta^{\text{Trop}}_{a_1, a_2, \ldots, a_k}(x)\,,$$

where $\mathsf{s}_{a_1, a_2, \ldots, a_k}$ are the generalized kinematic invariants and $\Delta^{\text{Trop}}_{a_1, a_2, \ldots, a_k}(x)$ are the tropicalized Plücker coordinates. We refer the reader to the original paper [66] for more details.

In order to study soft limits using the global Schwinger formula for CEGM amplitudes, it is instructive to start with the simplest example, i.e. $k = 3$

$$m_n^{(3)}(\mathbb{I}, \mathbb{I}) = \int_{\mathbb{R}^{2(n-4)}} d^{n-4} x d^{n-4} y \exp(-F_n^{(3)}(x))\,. \tag{3.99}$$

Consider the soft limit for particle n and the part of the integral over $\text{Trop}^+ G(3,n)$ which depends on x_{n-4} and y_{n-4}, since it is the part in which particle n appears. We now

[10] Here we will say that the soft limit is for particle n. However, it is important to stress that the physical notion of what a particle is in the CEGM generalization is not clear yet.

want to separate the integral into regions that will contribute to the pole as $\tau \to 0$ when $\mathsf{s}_{abn} = \tau \hat{\mathsf{s}}_{abn}$. We claim that these regions will be given by the large x_{n-4} and large y_{n-4} behavior, since x_a and y_a for $a < n-4$ will only affect subleading order contributions. Thus we can set them to zero without affecting the leading order, and the part $\mathcal{F}^{(3)}$ of the tropical potential that we are interested in is given by

$$
\begin{aligned}
\mathcal{F}^{(3)} =& \sum_{a=3}^{n-2} \mathsf{s}_{1an} \min(0, x_{n-4}) + \mathsf{s}_{1,n-1,n} x_{n-4} + \sum_{\substack{a=2 \\ a<b<n-1}}^{n-3} \mathsf{s}_{abn} \min(0, x_{n-4}, x_{n-4} + y_{n-4}) \\
&+ \sum_{a=2}^{n-3} \mathsf{s}_{a,n-1,n}(x_{n-4} + \min(0, y_{n-4})) + \mathsf{s}_{n-2,n-1,n}(x_{n-4} + y_{n-4})\,.
\end{aligned}
\tag{3.100}
$$

This tropical function has 5 regions where it becomes linear. These correspond to

$$
\{x_{n-4} < 0, y_{n-4} < 0\}\,,\ \{x_{n-4} < 0, y_{n-4} > 0\}\,,\ \{x_{n-4} > 0, y_{n-4} > 0\}\,,
$$

$$
\{x_{n-4} > 0, y_{n-4} < 0, x_{n-4} + y_{n-4} > 0\}\,,\ \{x_{n-4} > 0, y_{n-4} < 0, x_{n-4} + y_{n-4} < 0\}\,.
$$

Integrating over the five regions one obtains the expected leading soft factor

$$
\frac{1}{\tau^2}\left(\frac{1}{\hat{\mathsf{s}}_{12n}\hat{\mathbf{t}}_{2,\ldots,n-1}} + \frac{1}{\hat{\mathsf{s}}_{12n}\hat{\mathsf{s}}_{n-2,n-1,n}} + \frac{1}{\hat{\mathsf{s}}_{n-2,n-1,n}\hat{\mathbf{t}}_{1,\ldots,n-2}} + \frac{1}{\hat{\mathbf{t}}_{1,\ldots,n-2}\hat{\mathsf{s}}_{n-1,n,1}} + \frac{1}{\hat{\mathsf{s}}_{n-1,n,1}\hat{\mathbf{t}}_{2,\ldots,n-1}}\right),
\tag{3.101}
$$

where we have used

$$
\mathbf{t}_{1,\ldots,n-2} := \sum_{a=1}^{n-2} \mathsf{s}_{a,n-1,n}\,, \qquad \mathbf{t}_{2,\ldots,n-1} := -\sum_{\substack{a=2 \\ a<b<n}}^{n-2} \mathsf{s}_{abn}\,.
$$

The rest of the regions contribute to subleading orders.

The attentive reader may have noticed the similarity between $\mathcal{F}^{(3)}$ and the $k = 2$ tropical potential for 5 particles[11]

$$F_5(w) = s_{24}\text{min}(0, w_1) + s_{34}w_1 + s_{25}\text{min}(0, w_1, w_2) + s_{35}\text{min}(w_1, w_2) + s_{45}w_2 \,.$$

In fact, if we define $w_1 = x_{n-4}$ and $w_2 = x_{n-4} + y_{n-4}$, both $\mathcal{F}^{(3)}$ and $F_5(w)$ map to each other. Let us write the coefficients in $F_5(w)$ in terms of the planars poles, and using the map we find the following identification

$$s_{51} = \mathbf{t}_{2,\ldots,n-1} \,, s_{12} = \mathbf{t}_{1,\ldots,n-2} \,, s_{23} = \mathsf{s}_{12n} \,, s_{34} = \mathsf{s}_{n-1,n,1} \,, s_{45} = \mathsf{s}_{n-2,n-1,n} \,.$$

By substituting the planar poles into the $n = 5$ biadjoint amplitude

$$m_5(\mathbb{I}, \mathbb{I}) = \frac{1}{s_{12}s_{34}} + \frac{1}{s_{23}s_{45}} + \frac{1}{s_{34}s_{51}} + \frac{1}{s_{45}s_{12}} + \frac{1}{s_{51}s_{23}}$$

we recover the expected soft factor. This provides an alternative way to compute the leading soft factor without having to evaluate the integral for each region.

In general, we expect that an analogous procedure will work. More concretely, if we consider the part of the integral over $\text{Trop}^{+}G(k, n)$ that only depends on $x^{(1)}_{n-(k+1)}$, $x^{(2)}_{n-(k+1)}$, ..., $x^{(k-1)}_{n-(k+1)}$ (where, e.g., for $k = 3$ we have $x^{(1)}_{n-4} = x_{n-4}$ and $x^{(2)}_{n-4} = y_{n-4}$) and set the other variables to zero without affecting the leading order, we end up with a tropical function $\mathcal{F}^{(k)}$ that splits into C_k[12] regions where it becomes linear. Evaluating this part of the integral over all the regions will produce the leading soft factor.

[11]We will now use variables w for the $k = 2$ tropical integral to avoid confusion with the notation for higher-k.

[12]Where C_m is the m^{th} Catalan number.

Equivalently, we can map $\mathcal{F}^{(k)}$ with the $k=2$ tropical potential $F_{k+2}(x)$ by defining

$$w_i = \sum_{a=1}^{i} x^{(a)}_{n-(k+1)}\,.$$

Then we solve for the coefficients and substitute into the $n = k+2$ partial biadjoint amplitude to obtain the leading soft factor.

We have checked that this works up to $k=5$, and we conjecture that it holds in general.

3.9 Discussions

In this chapter we have extended the global Schwinger formulation to all partial amplitudes $m_n(\alpha,\beta)$, and also to amplitudes in ϕ^p theories. $A_n^{\phi^p}$ is given as a sum over regions, each of which is proposed to be in bijection with a ϕ^3 biadjoint partial amplitude. This leads to the statement that $A_n^{\phi^p}$ amplitudes can be understood as a sum of products of cubic amplitudes.

A very simple diagrammatic procedure for listing all regions contributing to an amplitude was found in terms of non-crossing k-chord diagrams. Given one such diagram, we have provided an algorithm for determining the structure of the contribution in terms of ϕ^3 amplitudes (meadows) and propagators ("frontiers" separating meadows). Every meadow can be seen to be related to a cubic amplitude participating in $m_{(n+2(p-3))/(p-2)}(\alpha,\mathbb{I})$. Our identification so far is lacking a direct way of determining the permutation α from the non-chord diagram. It would also be very important to find a purely combinatorial method to determine the precise bijection between the set of planar kinematic invariants in each object.

Our main focus has been on a combinatorial prescription for ϕ^p amplitudes. However, it would be interesting to find a diagrammatic procedure, in the lines of that for ϕ^p amplitudes, to determine the regions that compute $m_n(\alpha, \beta)$ so that $H_\alpha(x) = 0$ in (3.25).

We end the chapter with three topics for future research.

3.9.1 Relation to Green Functions in Planar Theories

The standard way of computing Green functions, G_n, from connected Green functions, G_n^c, is via an exponentiation procedure. However, it is well-known that in planar theories this does not work [45]. This is because planarity forces points of the Green function $G_n(x_1, x_2, \ldots, x_n)$, to be on the boundary of a disk and a connected Green function for points in a subset $J \subset \{x_1, x_2, \ldots, x_n\}$ can be thought of as cutting the disk into regions so that one of them only contains the points in J. Having done this, another connected Green function can only be constructed from the pieces left, and so on. In [45], a theory that only admits Green functions with an even number $n = 2q$ of points was considered and gave rise to the following combinatorial problem: in how many ways can $2q$ points on a disk be clustered in non-overlapping sets so that there are r_1 pairs, r_2 quadruplets, etc. As shown in [45] this is solved by the coefficients of the formula relating Green functions

$$G_{2q} = \sum_{r_i \geq 0} \delta_{q,(\sum_i i\, r_i)} \frac{(2q)!}{(2q+1-\sum_i r_i)!} \frac{(G_2^c)^{r_1}}{r_1!} \frac{(G_4^c)^{r_2}}{r_2!} \cdots \frac{\left(G_{2q}^c\right)^{r_q}}{r_q!} . \tag{3.102}$$

Here the Kronecker delta guarantees that each of the $2q$ points participates in each term.

Up to this point, this discussion seems to be completely independent of the formulas found in this work. In order to see the connection, let us list the first few cases as done in eq. (31) of [45],

$$
\begin{aligned}
G_4 &= G_4^c + 2\,(G_2^c)^2\,, \\
G_6 &= G_6^c + 6\,G_4^c G_2^c + 5\,(G_2^c)^3\,, \\
G_8 &= G_8^c + 4\,(G_4^c)^2 + 8\,G_6^c G_2^c + 28\,G_4^c\,(G_2^c)^2 + 14\,(G_2^c)^4\,.
\end{aligned}
$$

Comparing to the expressions for ϕ^5 amplitudes in (3.83), i.e.

$$
\begin{aligned}
A_8^{\phi^5} &= m_4 + 2m_3^2 \frac{1}{P^2}\,, \\
A_{11}^{\phi^5} &= m_5 + 6m_3 m_4 \frac{1}{P^2} + 5m_3^3 \left(\frac{1}{P^2}\right)^2\,, \\
A_{14}^{\phi^5} &= m_6 + 4m_4^2 \frac{1}{P^2} + 8m_5 m_3 \frac{1}{P^2} + 28 m_4 m_3^2 \left(\frac{1}{P^2}\right)^2 + 14 m_3^4 \left(\frac{1}{P^2}\right)^3\,,
\end{aligned}
$$

it is clear that there must be a relation. The fact that the coincidence of the structure continues to all multiplicities is shown using the Lagrange inversion formula in appendix C. It is natural to expect that the relation extends to all ϕ^p amplitudes as follows. Let $m = p - 3$, and place mq points on a disk. Now count all possible ways of clustering the points in non-overlapping sets so that there are r_1 groups of m points each, r_2 groups of $2m$ points, etc. Then the formula that relates $A_n^{\phi^p}$ amplitudes and Green functions is given by the natural generalization of (3.102),

$$
G_{mq} = \sum_{r_i \geq 0} \delta_{q,(\sum_i i\, r_i)} \frac{(mq)!}{(mq + 1 - \sum_i r_i)!} \frac{(G_m^c)^{r_1}}{r_1!} \frac{(G_{2m}^c)^{r_2}}{r_2!} \cdots \frac{\left(G_{mq}^c\right)^{r_q}}{r_q!}\,. \tag{3.103}
$$

We leave it as an exercise for the reader to check that the coefficients we have presented in the text and the ones in appendix C are indeed the correct values of the combinatorial problem and the coefficients in (3.103).

It would be very interesting to explore this connection further, in particular to matrix models with Φ^{p-1} interactions as the one studied in [45].

3.9.2 Possible Connection with Stokes Polytopes

Recent work on the computation of ϕ^p amplitudes as a sum over contributions obtained from various polytopes known as accordiohedra is very reminiscent of the structures we have uncovered using the global Schwinger formulation. Developing a connection between the two approaches is certainly an important problem. Here we restrict to ϕ^4 amplitudes and therefore to Stokes polytopes in order to point out some possible directions. Most of the formulations using Stokes polytopes construct the amplitudes as (see e.g equation (5) of [181])

$$A_n^{\phi^4} = \sum_{\text{Symmetry:}\,\sigma} \sum_{\text{Primitive:}\,P} \alpha_P\, m_{P,n}^{(\sigma.P)} \tag{3.104}$$

where the sum is over all primitive Stokes polytopes and the symmetry classes into which they fall. The $m_{P,n}^{(\sigma.P)}$ are the contributions obtained from the corresponding polytope. Here the α_P are the so-called *weights*, which are in general rational numbers.

Consider for example,

$$A_6^{\phi^4} = \alpha_1 \left(\frac{1}{X_{1,4}} + \frac{1}{X_{3,6}} \right) + \alpha_2 \left(\frac{1}{X_{2,5}} + \frac{1}{X_{1,4}} \right) + \alpha_3 \left(\frac{1}{X_{3,6}} + \frac{1}{X_{2,5}} \right) . \tag{3.105}$$

Here there are three polytopes and the weights have to be chosen to be $\alpha_a = 1/2$.

In [186], Salvatori and Stanojevic propose a way to simplify (3.104) by reducing the redundancy by taking certain limits of kinematic invariants in each term. Let us rewrite

Eq. 4.8 of [186] for $n = 6$,

$$A_6^{\phi^4} = \left(\frac{1}{X_{1,4}} + \frac{1}{X_{3,6}}\right) + \lim_{X_{1,4}\to\infty}\left(\frac{1}{X_{2,5}} + \frac{1}{X_{1,4}}\right). \tag{3.106}$$

In this formula, the first bracket comes from the Stokes polytope with reference $1,4$ while the second bracket comes from the reference $2,5$. Here $X_{i,j}$ can be identified with the planar invariants $t_{[a,b]}$ in a simple way. Note that (3.106) groups the three terms in the same way as that found in our construction (3.48) and (3.49) coming from the two possible non-crossing chord diagrams. In [186], the $n = 8$ amplitude is also computed. The amplitude is given as a sum over five Stokes polytopes. Our formula (3.53) also has five regions. However, while our regions all contribute with a factor of one, Eq. 4.10 of [186] has four terms with coefficient $+1$ and one with -1. In fact, only the first region can be matched directly; it coincides with the first polytope, i.e. the one with no limits and which gives rise, in our language, to $m_5(\mathbb{I},\mathbb{I})$. We suspect that there exist other combinations with different limits which could match our formula term by term. One hint is that every one of our terms is isomorphic to either an associahedron or to intersections of two associahedra.

3.9.3 Towards Generalized ϕ^p Amplitudes

Another intriguing feature of our procedure for constructing the regions from the extended non-crossing chord diagrams for ϕ^4 is the introduction of two additional points (-1 and $n-2$) and a chord joining them. The relevance of this additional chord lies in the way each meadow is associated to a cubic amplitude. For now we have conceived these diagrams simply as combinatorial objects, but if one attempts to relate each of the labels $0, 1, \ldots, n-3$ in the diagram to the particles $3, 4, \ldots, n$ respectively, then the new chord $\theta_{-1,n-2}$ has the interpretation of identifying particles 1 and 2, which in their tropicalized variables are set to $-\infty$ and $+\infty$. However, one has to be careful in that the variable x_{a-3} coming from the parameterization (3.12) does not exactly correspond to a single particle a as it appears in all rows $r \geq a$. It might seem puzzling that for a general value of p, we introduce $p-2$ additional points to the non-crossing $(p-2)$-chord diagrams and join them with another $(p-2)$-chord. Strikingly, $p-2$ is precisely the number of particles with tropicalized variables set at infinity that appear in the higher-k version of the global Schwinger parameterization using $\mathrm{Trop}^{+}G(k,n)$ for $k = p-2$ (see [66] for its construction). It would be interesting to explore if there is a connection with these generalized objects and CEGM generalized amplitudes [71]. One direction to tackle is to try and find an analog of ϕ^p amplitudes for higher-k theories, using a similar limiting procedure on the *planar arrays* of Feynman diagrams that will be described in chapter 5. We provided a first step in the original paper [74], and we refer the reader to it for details.

We will now start the second part of the thesis, in which we explore some aspects of the CEGM generalization of quantum field theory. In fact, we will take a mathematical detour and extend the study to higher-k amplitudes and their connection to some of the topics presented in part I.

PART II

Higher-k Amplitudes

The second part of the thesis will explore aspects of the CEGM generalization of quantum field theory introduced in chapter 1.

In the first chapter of this second part we study the generalization of the scattering equations on $X(2,n)$, the configuration space of n points on $\mathbb{CP}^1$, to higher dimensional projective spaces. One of the new features of the scattering equations in $X(k,n)$ with $k>2$ is the presence of both regular and singular solutions in a soft limit. Here we study soft limits in $X(3,7)$, $X(4,7)$, $X(3,8)$ and $X(5,8)$, find all singular solutions, and show their geometrical configurations. We also propose a classification of all configurations that can support singular solutions for general $X(k,n)$ and comment on their contribution to soft expansions of generalized biadjoint amplitudes.

In the second chapter of this part we find and describe the analogous objects to Feynman diagrams that compute CEGM amplitudes. Planar collections of Feynman diagrams were first proposed by Borges and Cachazo as the natural generalization of Feynman diagrams for the computation of $k=3$ biadjoint amplitudes. In the second chapter we introduce planar matrices of Feynman diagrams as the objects that compute $k=4$ biadjoint amplitudes. These are symmetric matrices of metric trees satisfying compatibility conditions. We also introduce two notions of combinatorial bootstrap techniques for finding collections from Feynman diagrams and matrices from collections. As applications of the first, we find all 693, 13 612, and 346 710 collections for $(k, n) = (3, 7), (3, 8)$, and $(3, 9)$ respectively. As applications of the second kind, we find all 90 608 and 30 659 424 planar matrices that compute $(k, n) = (4, 8)$ and $(4, 9)$ biadjoint amplitudes respectively. We also start the study of higher dimensional arrays of Feynman diagrams, including the combinatorial version of the duality between (k, n) and $(n - k, n)$ objects.

Chapter 4

Singular Solutions in Soft Limits

4.1 Introduction

Recall that in 2019, Cachazo, Early, Guevara and Mizera (CEGM) introduced and studied a natural generalization of the scattering equations, which connect the space of Mandelstam invariants to that of points on $\mathbb{CP}^1$ [113, 114, 75, 76], to higher dimensional projective spaces $\mathbb{CP}^{k-1}$ [71]. The equations are obtained by computing the critical points of a potential function

$$\mathcal{S}_k \equiv \sum_{1\leq a_1<a_2\cdots<a_k\leq n} \mathsf{s}_{a_1a_2\cdots a_k} \log{(a_1, a_2, \ldots, a_k)}. \tag{4.1}$$

Here $\mathsf{s}_{a_1a_2\cdots a_k}$ are a generalization of Mandelstam invariants while $(a_1, a_2, \cdots, a_k)$ can be thought of as Plücker coordinates on $G(k, n)$. The configuration space of n points on $\mathbb{CP}^{k-1}$ is obtained by modding out by a torus action $\mathbb{C}^*$ on each of the points, i.e., $X(k, n) := G(k, n)/(\mathbb{C}^*)^n$ [190].

The kinematic invariants are completely symmetric tensors satisfying

$$\mathsf{s}_{aabc\cdots} = 0, \qquad \sum_{a_2,a_3,\ldots,a_k} \mathsf{s}_{a_1a_2\cdots a_k} = 0 \qquad \forall\, a_1. \tag{4.2}$$

These are the analogs of masslessness and momentum conservation conditions. These conditions guarantee that the potential function is invariant under the torus action and therefore one can choose inhomogeneous coordinates for points on $\mathbb{CP}^{k-1}$. For example, when $k = 3$ one can use (x_i, y_i) while the Plücker coordinates are then replaced by

$$|abc| := \det \begin{pmatrix} 1 & 1 & 1 \\ x_a & x_b & x_c \\ y_a & y_b & y_c \end{pmatrix}. \tag{4.3}$$

Having a higher-k version of the scattering equations, the most natural question is to determine the number of solutions, i.e. the number of critical points of the potential $\mathcal{S}_k$. The standard scattering equations, i.e. $k = 2$, possess $(n-3)!$ solutions and the original proof given in [77] uses that a soft particle decouples from the rest and proceeds by induction. The argument relies on the fact that as the soft limit is approached, all solutions stay away from boundaries of $X(2, n)$, i.e. the n points are in a generic configuration. These solutions are known as *regular* solutions. The terminology comes from the study of factorization limits, i.e. when a physical kinematic invariant vanishes. In such a limit, some solutions give rise to configurations where the Riemann sphere degenerates into two spheres joined by a single, emergent puncture. Such solutions are called *singular* solutions.

In [71] it was found that when $k \geq 3$ regular solutions in a soft limit cannot possibly account for all solutions. This was deduced by computing the regular solutions for $X(3, 7) \to X(3, 6)$ and $X(4, 7) \to X(4, 6)$. The numbers were shown to be 1 092 and

1 152 respectively. Since $X(3,7)$ and $X(4,7)$ are isomorphic, they must possess the same number of total solutions. Motivated by this, Cachazo and Rojas designed a technique for determining the number of missing solutions for $X(4,7)$ as the rank of a matrix built out of generalized biadjoint amplitudes thus finding 120 [81]. This implies that the total number of solutions is exactly 1 272 and that the number of singular solutions for $X(3,7)$ and $X(4,7)$ must be 180 and 120 respectively.

For $X(3,8) \to X(3,7)$ and $X(5,8) \to X(5,7)$ one can also compute the number of regular solutions and find them to be 128 472 and 129 312 respectively. Once again, since $X(3,8)$ is isomorphic to $X(5,8)$ there must be singular solutions. At this point there is no technique for computing the total number of solutions from the scattering equations or generalized biadjoint scalar amplitudes. However, the total number of solutions can be related to the number of uniform matroids over finite fields [6]. Using this one can reproduce the correct number for $X(2,n)$, $X(3,6)$, and $X(3,7)$. Moreover, it also predicts 188 112 solutions for $X(3,8)$.

In this chapter we study the soft limits of scattering equations on $X(3,7)$, $X(4,7)$, $X(3,8)$, and $X(5,8)$ and find all singular solutions. In each case, singular solutions correspond to configurations where the soft particle develops some linear dependence with subsets of the hard particles while every minor containing only hard particles remains finite. Such linear dependencies prevent the decoupling of the soft particle from the rest. The simplest example corresponds to $X(3,7)$ when particle 7 is taken to be soft and a configuration where $|147|$, $|257|$ and $|367|$ vanish. This means that the terms containing s_{147}, s_{257} and s_{367} cannot be dropped in the scattering equations for the hard particles as it is usually the case for regular solutions.

We find that in every case it is possible to define a new set of scattering equations in the strict soft limit. This is a completely novel phenomenon. The strict soft limit scattering equations can be solved or its solutions counted using some of the same techniques developed for the original scattering equations. In fact, using a soft-limit approach one finds again regular and singular solutions.

Based on these examples we propose a general classification of all configurations that can support singular solutions in $X(k,n)$ for general k and n. For example, when $k=3$ there are $\left\lfloor \frac{n-1}{2} \right\rfloor - 2$ distinct topologies corresponding to 3, ..., $\left\lfloor \frac{n-1}{2} \right\rfloor$ lines intersecting at the soft particle position. For higher k, there are configurations that are inherited from lower k values as well as new ones corresponding to at least k $(k-2)$-planes intersecting at the soft particle location. The general structure hints at a recursive structure for $X(k,n)$ similar to that found for $X(2,n)$.

An elegant structure of soft theorems was unearthed by García-Sepúlveda and Guevara in generalized biadjoint amplitudes [123] in 2019, as reviewed in section 3.8 of chapter 3. One of the surprising results is the fact that standard $k=2$ biadjoint amplitudes serve as soft factors for $k>2$ amplitudes. They computed the leading order behavior of amplitudes in the soft limit, i.e., as $\tau \to 0$ with $\mathsf{s}_{abn} = \tau \hat{\mathsf{s}}_{abn}$, assuming a decoupling of the soft particle from the scattering equations governing the hard particles. We find that in all examples we studied their assumption is indeed correct as singular solutions can at most contribute to subleading terms in the soft limit expansion.

This chapter is organized as follows: In section 4.2 we review the standard argument for $k=2$ adding an explanation for why no singular solutions are found. In section 4.3 we review what it is known regarding regular solutions, in particular, how this led to the prediction of the existence of singular solutions. In section 4.4 we find all singular solutions in the soft limits $X(3,7) \to X(3,6)$ and $X(4,7) \to X(4,6)$. In section 4.5 we find all singular solutions in the soft limits $X(3,8) \to X(3,7)$ and $X(5,8) \to X(5,7)$. In the latter we find for the first time topologically distinct configurations leading to singular solutions. In section 4.6, we make our proposal for all configurations that can support singular solutions and explain the evidence supporting it. We end in section 4.7 with discussions regarding the contribution of singular solutions to the soft expansion of generalized biadjoint scalar amplitudes. Moreover, in appendix E we show how the counting of the number of singular solutions works from the bounded chambers method in some particular cases for $k = 3$, and in appendix F we comment on the geometrical interpretation of some of the singular configurations in $X(5, 8)$.

4.2 Soft Limits in $X(2, n)$

Scattering equations on $X(2, n)$ have provided a direct connection between locality and unitarity constraints in tree-level scattering amplitudes and properties of the moduli space of punctured Riemann spheres. The way this happens is somewhat surprising. The scattering equations for n particles possess $\mathcal{N}_n = (n-3)!$ solutions and when a factorization channel, in which particles separate into two sets L, R, containing $n_L > 1$ and $n_R > 1$ particles, is approached, $\mathcal{N}_n^{\text{singular}} := (n_L-2)! \times (n_R-2)!$ solutions become singular. More explicitly, all punctures in L (or R) approach each other[1]. However, cross ratios involving only particles on L (or R) remain finite and lead to the blow up picture where two Riemann spheres are joined by a new puncture with one containing particles in L and the other particles in R.

The singular solutions are the most relevant to ensure the correct physical behavior of scattering amplitudes in the Cachazo-He-Yuan (CHY) formulation as they produce the kinematic pole while the remaining $\mathcal{N}_n^{\text{regular}} := (n-3)! - \mathcal{N}_n^{\text{singular}}$ are regular. This means that the CHY formula remains finite on them. This is precisely the opposite to what

[1]This is in some $\mathrm{SL}(2, \mathbb{C})$ gauge choice.

happens in a soft limit. Indeed, in $X(2,n)$ one finds only regular solutions and they are the ones responsible for the leading order behavior of amplitudes in the limit and control the corresponding soft theorems [203, 83, 189, 5]. In this section we review the soft limit analysis as preparation for $X(k,n)$ with $k>2$.

4.2.1 Regular Solutions

Let us write the scattering equations in a form that manifestly exhibits the dependence on particle n:

$$E_a := \sum_{b=1}^{n-1} \frac{s_{ab}}{x_{ab}} + \frac{s_{an}}{x_{an}} \quad \text{with} \quad 1 \leq a \leq n-1 \quad \text{and} \quad E_n := \sum_{b=1}^{n-1} \frac{s_{nb}}{x_{nb}} \tag{4.4}$$

with $x_{ab} = x_a - x_b$ and the equations are obtained by requiring $E_a = 0$ for all a.

The soft limit in particle n is defined by taking $s_{an} = \tau \hat{s}_{an}$ with $\tau \to 0$. Regular solutions are defined as those where none of the punctures approach another. More explicitly, $x_{ab} \neq 0$ for all values of a and b. Under this assumption it is easy to see from (4.4) that all n dependence can be dropped from the first $n-1$ equations. This set of equations precisely corresponds to that of a system of $n-1$ particles and therefore can be solved to find $\mathcal{N}_{n-1}$ solutions. In other words, in the soft limit, the n^{th} particle decouples from the equations that control the rest. However, the possible values of x_n are not arbitrary since τ drops from the last equation in (4.4) to give

$$\sum_{b=1}^{n-1} \frac{\hat{s}_{nb}}{x_n - x_b^I} = 0 \tag{4.5}$$

where x_b^I is any one of the $\mathcal{N}_{n-1}$ solutions for the hard particles. At first sight this equation leads to a polynomial in x_n of degree $n-2$ but the coefficient of x_n^{n-2} vanishes due to momentum conservation and hence it leads to $n-3$ solutions for x_n. Since this is true for each x_b^I one finds $\mathcal{N}_n^{\text{regular}} = (n-3)\mathcal{N}_{n-1}$.

Under the assumption that $\mathcal{N}_n^{\text{singular}} = 0$ one finds the recursion relation $\mathcal{N}_n = (n-3)\mathcal{N}_{n-1}$ with $\mathcal{N}_4 = 1$ and whose solution is $\mathcal{N}_n = (n-3)!$. Now we turn to proving that $\mathcal{N}_n^{\text{singular}} = 0$.

4.2.2 Absence of Singular Solutions

A singular solution is one which does not obey the condition for decoupling the soft particle from the equations determining the rest. This can only happen when $x_{in} = \tau\hat{x}_{in}$, i.e. vanishes in the soft limit for some values of i. Let us denote the set of such particles $\mathcal{D}$. Clearly $\mathcal{D}$ must contain more than one element for if $|\mathcal{D}| = 1$ then the last equation in (4.4) becomes $E_n = \hat{s}_{in}/\hat{x}_{in} = 0$ which has no solutions.

Let us assume that $|\mathcal{D}| \geq 2$ and parameterize $x_i = x_n + \tau u_i$ for $i \in \mathcal{D}$. Here we follow an argument originally presented in [75] for factorization limits but perfectly applicable to the situation at hand. It is simple to show that for any $a \notin \mathcal{D}$

$$x_{an}E_a = \sum_{b\notin\mathcal{D}} \frac{x_{an}}{x_{ab}} s_{ab} + \sum_{b\in\mathcal{D}} \left(1 + \tau\frac{u_b}{x_{ab}}\right) s_{ab}. \tag{4.6}$$

Of course, this must be zero when the scattering equations are imposed. Adding all these equations one finds

$$\sum_{a\notin\mathcal{D}} x_{an}E_a = 0 \quad \Rightarrow \quad \left(\sum_{a\notin\mathcal{D}} k_a\right)^2 = \mathcal{O}(\tau). \tag{4.7}$$

However, an implicit assumption in a soft limit is that the kinematics of the system of $n-1$

particles is generic and therefore no kinematic invariant involving only hard particles is allowed to vanish. This means that (4.7) is a contradiction and therefore singular solutions do not exist in the soft limit $X(2,n) \to X(2,n-1)$.

4.3 Regular Solutions in $X(k,n) \to X(k,n-1)$

In this section we review the known results for the counting of regular solutions in the soft limits $X(k,n) \to X(k,n-1)$. As discussed in the previous section, regular solutions are defined as those for which the soft particle decouples from the equations determining the configuration of the others. This means that we can assume that the system $X(k,n-1)$ has been solved and $\mathcal{N}_{n-1}^{(k)}$ solutions have been found. The task at hand is then to determine the number of solutions for the position of particle n from the equations

$$\nabla_n \mathcal{S}_k = 0. \tag{4.8}$$

Here the gradient is taken only with respect to the coordinates of particle n since all other particle positions are assumed to have been found. Let us denote the number of solutions to (4.8) as $\mathrm{Soft}_{k,n}$. The notation is motivated by soft theorems. This means that the number of regular solutions is $\mathcal{N}_n^{(k)\text{:regular}} = \mathrm{Soft}_{k,n} \times \mathcal{N}_{n-1}^{(k)}$.

In the soft limit $X(2,n) \to X(2,n-1)$ we have seen that (4.8) is a single equation with $\mathrm{Soft}_{2,n} = n-3$ solutions and therefore $\mathcal{N}_n^{(2)\text{:regular}} = (n-3) \times \mathcal{N}_{n-1}^{(2)}$. Of course, we have seen that $\mathcal{N}_n^{(2)\text{:regular}}$ is also equal to the total number of solutions $\mathcal{N}_n^{(2)}$.

The only other case that is known for all n is the soft limit $X(3,n) \to X(3,n-1)$. In

[71] it was found that

$$\mathrm{Soft}_{3,n} = \frac{1}{8}(n-4)(n^3 - 6n^2 + 11n - 14). \tag{4.9}$$

The first few values are $\mathrm{Soft}_{3,5} = 2, \mathrm{Soft}_{3,6} = 13, \mathrm{Soft}_{3,7} = 42$, and $\mathrm{Soft}_{3,8} = 101$. By explicit computations it was found in [71] that $\mathcal{N}_5^{(3)} = 2$ and $\mathcal{N}_6^{(3)} = 2 \times 13 = 26$. This means that there are no singular solutions for $n \leq 6$. Therefore the number of regular solutions for $n = 7$ is $\mathcal{N}_7^{(3):\text{regular}} = 42 \times 26 = 1\,092$. In [81], it was proven that the total number of solutions for $n = 7$ is $\mathcal{N}_7^{(3)} = 1\,272$ and with this the number of regular solutions in the soft limit $X(3,8) \to X(3,7)$ is $\mathcal{N}_8^{(3):\text{regular}} = 101 \times 1\,272 = 128\,472$. In section 4.5 we show that the total number of solutions for $X(3,8)$ is $\mathcal{N}_8^{(3)} = 188\,112$. Therefore the number of regular solutions for $n = 9$ is $\mathcal{N}_9^{(3):\text{regular}} = 205 \times 188\,112 = 38\,562\,960$. Since the total number of solutions for $X(3,9)$ is not presently known we cannot determine $\mathcal{N}_n^{(3):\text{regular}}$ for $n \geq 10$.

In [71], the number of regular solutions was identified with the number of bounded chambers by real hyperplanes when the kinematics was chosen in a special region known as the positive region (reviewed in section 4.4.1). This identification is also based on the assumption that all solutions are real in the positive region. Using this approach $\mathrm{Soft}_{4,6} = 6$, $\mathrm{Soft}_{4,7} = 192$ and $\mathrm{Soft}_{4,8} = 1\,858$ were computed. Here we have pushed the computation of bounded chambers up to $n = 16$ leading to the following proposal

$$\mathrm{Soft}_{4,n} = \frac{1}{1296}(n-5)(n^8-13n^7-5n^6+1019n^5-7934n^4+29198n^3-57510n^2+57276n-20736). \tag{4.10}$$

These results imply that

$$\mathcal{N}_7^{(4):\text{regular}} = 6 \times 192 = 1\,152, \quad \mathcal{N}_8^{(4):\text{regular}} = 1\,272 \times 1\,858 = 2\,363\,376. \tag{4.11}$$

For $k = 5$ much less is known: $\text{Soft}_{5,7} = 24$, $\text{Soft}_{5,8} = 5\,388$ and $\text{Soft}_{5,9} = 204\,117$. This leads to

$$\mathcal{N}_8^{(5):\text{regular}} = 24 \times 5\,388 = 129\,312, \quad \mathcal{N}_9^{(5):\text{regular}} = 204\,117 \times 188\,112. \tag{4.12}$$

The last result uses that the total number of solutions of the scattering equations on $X(5,8)$ is $\mathcal{N}_8^{(5)} = \mathcal{N}_8^{(3)} = 188\,112$.

4.4 Singular Solutions in $X(3,7) \to X(3,6)$ and $X(4,7) \to X(4,6)$

We have already seen that there cannot be singular solutions for $k = 2$. For higher k, however, it is possible to keep all minors without the soft particle finite while sending some of the minors involving the soft particle to zero. This makes singular solutions possible for $k > 2$. In this section we study the first examples where singular solutions appear, which correspond to $X(3,7) \to X(3,6)$ and $X(4,7) \to X(4,6)$. This analysis also explains why there are not singular solutions for $X(3,6) \to X(3,5)$ explaining the agreement of the regular soft counting of solutions with the total number of solutions found in [71].

4.4.1 Singular Solutions in $X(3,7) \to X(3,6)$

The first explicit example where we have singular solutions is in $X(3,7)$. In order to obtain the singular solutions, we study the soft limit for, e.g., particle $n = 7$, *i.e.* $\mathsf{s}_{ab7} \to \tau \hat{\mathsf{s}}_{ab7}$ (with $\tau \to 0$). The singular solutions arise from configurations where three lines[2] in $\mathbb{CP}^2$ (or

[2] In this chapter we use the word "line" to refer to a complex line, i.e., $\mathbb{CP}^1$, or to a real line. The meaning should be clear from the context.

$\mathbb{RP}^2$ if all solutions are real), each defined by two hard particles, meet at the soft particle.

One such configuration is where lines $\overline{14}$, $\overline{25}$ and $\overline{36}$ meet at the particle 7 as shown in figure 4.1. This implies that all three determinants $|147|$, $|257|$ and $|367|$ vanish. There exist $\binom{6}{2}\binom{4}{2}\binom{4}{2}/3! = 15$ different such configurations.

For each configuration, it is possible to choose coordinates to find equations governing the system at $\tau = 0$. The new scattering equations have 12 solutions. Therefore there are $\mathcal{N}_7^{(3):\text{singular}} = 12 \times 15 = 180$ singular solutions.

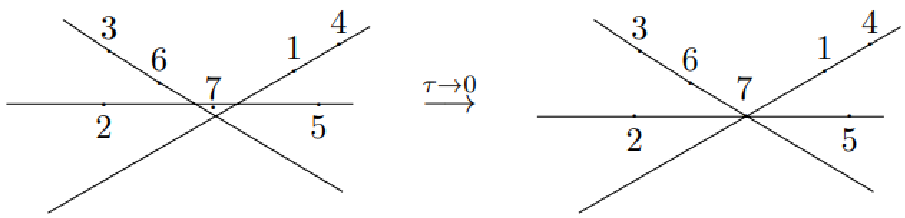

Figure 4.1: Configuration of singular solutions in $X(3,7)$. *Left*: Near the soft limit three lines $\overline{14}$, $\overline{25}$ and $\overline{36}$ almost cross the soft particle. *Right*: In the strict soft limit the three lines meet at the soft particle.

The way to get the solutions is the following. Take the configuration where $|147|$, $|257|$ and $|367|$ vanish as an example. A convenient choice of gauge fixing in projective space is

$$\begin{pmatrix} 1 & 0 & 0 & 1 & 1 & 1 & 1 \\ x_1 & x_2 & x_3 & x_4 & x_5 & x_6 & x_7 \\ y_1 & y_2 & y_3 & y_4 & y_5 & y_6 & y_7 \end{pmatrix} \xrightarrow{\text{gauge fixing}} \begin{pmatrix} 1 & 0 & 0 & 1 & 1 & 1 & 1 \\ 0 & 1 & 0 & 1 & x_5 & x_6 & x_7 \\ 0 & 0 & 1 & 1 & y_5 & y_6 & y_7 \end{pmatrix}. \tag{4.13}$$

Under the parametrization $\mathsf{s}_{ab7} \to \tau\hat{\mathsf{s}}_{ab7}$, terms containing s_{147}, s_{257} and s_{367} cannot be dropped in the equations for the hard particles

$$\frac{\partial\tilde{\mathcal{S}}_3}{\partial x_a}+\sum_{b\neq a,7}\frac{\tau\hat{\mathsf{s}}_{ab7}}{|ab7|}\frac{\partial|ab7|}{\partial x_a}=0,\quad \frac{\partial\tilde{\mathcal{S}}_3}{\partial y_a}+\sum_{b\neq a,7}\frac{\tau\hat{\mathsf{s}}_{ab7}}{|ab7|}\frac{\partial|ab7|}{\partial y_a}=0,\quad \text{for}\ \ a=1,\ldots 6 \tag{4.14}$$

where $\tilde{\mathcal{S}}_3$ is the potential of hard particles, $\tilde{\mathcal{S}}_3\equiv\sum_{1\leq a<b<c\leq 6}\mathsf{s}_{abc}\log(a,b,c)$. They also dominate in the two scattering equations for the soft particle

$$\begin{aligned}\frac{\partial\mathcal{S}_3}{\partial x_7}&=\frac{\tau\hat{\mathsf{s}}_{147}}{|147|}\frac{\partial|147|}{\partial x_7}+\frac{\tau\hat{\mathsf{s}}_{257}}{|257|}\frac{\partial|257|}{\partial x_7}+\frac{\tau\hat{\mathsf{s}}_{367}}{|367|}\frac{\partial|367|}{\partial x_7}+\mathcal{O}(\tau)=0\,,\\ \frac{\partial\mathcal{S}_3}{\partial y_7}&=\frac{\tau\hat{\mathsf{s}}_{147}}{|147|}\frac{\partial|147|}{\partial y_7}+\frac{\tau\hat{\mathsf{s}}_{257}}{|257|}\frac{\partial|257|}{\partial y_7}+\frac{\tau\hat{\mathsf{s}}_{367}}{|367|}\frac{\partial|367|}{\partial y_7}+\mathcal{O}(\tau)=0\,.\end{aligned} \tag{4.15}$$

The subleading terms $\mathcal{O}(\tau)$ in the above equations (4.14) and (4.15) can be omitted in the soft limit[3]. In contrast to regular solutions, where we solve the equations for hard particles first, here the equations for the soft particle (4.15) are simpler and we solve them first. Note that there are three dominating terms in each of the equations (4.15). Algebraically, one can check that there would be no solutions for x_7 and y_7 if there were only two dominating terms in each of the equations (4.15). In fact, this is the reason why there are no singular solutions for $X(3,6)\to X(3,5)$. The fact that at least three terms are needed has a more intuitive geometric explanation which we give in the next subsection.

We then parametrize each determinant as $|147|=\tau u$, $|257|=\tau v$ and $|367|=\tau p$, that is

$$x_6=y_5-\tau(u+v+p),\quad x_7=y_5-\tau(u+v),\quad y_7=y_5-\tau v. \tag{4.16}$$

[3]This is because the terms shown explicitly in (4.15) are of order $\mathcal{O}(\tau^0)$ since the minors in the denominators vanish as $\mathcal{O}(\tau)$ thus canceling the explicit factor of τ in the numerators.

In the soft limit, the new set of scattering equations, with variables x_5, y_5, y_6, u, v and p is

$$\lim_{\tau\to 0} \frac{\partial \mathcal{S}_3}{\partial x_i}\bigg|_{(4.16)} = 0, \quad \lim_{\tau\to 0} \frac{\partial \mathcal{S}_3}{\partial y_i}\bigg|_{(4.16)} = 0, \quad \text{for} \;\; i = 1, \ldots 7. \tag{4.17}$$

Among the 14 equations (4.17), only 6 of them are independent. Furthermore, we can separately solve for u, v and p from (4.17) and obtain equations involving only hard particles

$$\Big(\frac{\partial \tilde{\mathcal{S}}_3}{\partial y_5} + \frac{\partial \tilde{\mathcal{S}}_3}{\partial x_6}\Big)\bigg|_{x_6\to y_5} = 0, \quad \frac{\partial \tilde{\mathcal{S}}_3}{\partial x_5}\bigg|_{x_6\to y_5} = 0, \quad \frac{\partial \tilde{\mathcal{S}}_3}{\partial y_6}\bigg|_{x_6\to y_5} = 0\,. \tag{4.18}$$

Solving these equations we find that, compared to the original scattering equations for 6 particles, which have 26 solutions, now the requirement that lines $\overline{14}$, $\overline{25}$ and $\overline{36}$ pass through a common point reduces the number of solutions to 12.

Singular Solutions on Positive Kinematics

We have seen the kind of configurations that produce singular solutions in $X(3,7) \to X(3,6)$. However, a purely algebraic approach sheds little light on why such configurations can produce singular solutions while others cannot. Moreover, unless a more geometric understanding is reached, it seems hopeless to uncover the general structure for all soft limits $X(k,n) \to X(k,n-1)$.

In this subsection, we make use of kinematic data in what is known as the positive region $\mathcal{K}^+_{3,n}$ to study and visualize the solutions (for more the details on $\mathcal{K}^+_{3,n}$ see [80, 71]). The main advantage is that one can develop intuition on why there are singular solutions through explicit geometric pictures.

Let us briefly review the construction of kinematic data in the positive region $\mathcal{K}^+_{k,n}$ for general k. We start by selecting $k+1$ particles A_1, A_2, $\cdots$, A_{k+1} to be fixed by the action of

SL$(k,\mathbb{C})$. This time $k-1$ particles, say A_2, A_3, $\cdots$, A_k, can be sent to infinity in $k-1$ different directions by setting their homogeneous coordinates to $(0,1,0,\cdots,0)$, $(0,0,1,\cdots,0)$, $\cdots$, $(0,0,\cdots,0,1)$, respectively. The other two are chosen to be, in inhomogeneous coordinates, at the origin and at $(1,1,\cdots,1)$ on the plane $(x_1,x_2,\cdots,x_{k-1})\in\mathbb{R}^{k-1}$.

Since interactions in the potential function are controlled by the determinants $|a_1a_2...a_k|$, a given particle is not directly sensitive to the location of any other particle but only sensitive to the $(k-2)$-planes defined by any other $k-1$ particles. In order to find the analog of the positive region, let us again consider the potential function

$$\mathcal{S}_k = \sum_{\substack{1\leq a_1<a_2<\cdots<a_k\leq n \\ |\{a_1,a_2,\cdots,a_k\}\cap\{A_1,A_2,\cdots,A_{k+1}\}|\leq k-1 \\ |\{a_1,a_2,\cdots,a_k\}\cap\{A_2,A_3,\cdots,A_k\}|\leq k-2}} \mathsf{s}_{a_1,a_2,\cdots,a_k} \log|a_1,a_2,\cdots,a_k|\,. \tag{4.19}$$

Therefore, this positive region $\mathcal{K}^+_{k,n}$ is defined by requiring all invariants that explicitly appear in (4.19) to be positive. This is possible because the set of all such invariants form a basis of the kinematic space. Since critical points of the potential correspond to equilibrium points, they can only lie inside the bounded chambers of this space, assuming they are all real.

Let us define the subregion of $\mathcal{K}^+_{k,n}$ where all solutions to the scattering equations are real by $\mathcal{K}^{+,\mathbb{R}}_{k,n}$. When $k=2$, it is known that $\mathcal{K}^{+,\mathbb{R}}_{2,n}=\mathcal{K}^+_{2,n}$. Moreover, since $\mathcal{K}^+_{2,n}$ contains all soft limits, it is possible to smoothly go from one to another without ever leaving $\mathcal{K}^{+,\mathbb{R}}_{2,n}$. In [71], it was argued that for $k=3$ it turns out that $\mathcal{K}^{+,\mathbb{R}}_{3,n}\subset\mathcal{K}^+_{3,n}$ is disconnected. In fact, each soft limit seems to live in its own region. For our present problem of $X(3,7)$, it is enough to know that sufficiently near the soft limit of particle 7 all solutions are real.

Singular solutions are called singular because they make some minors $|ab7|$ containing particle 7 vanish. Geometrically, this means that lines $\overline{ab}$ in $\mathbb{RP}^2$ space will dominate. The remaining lines can be omitted for the soft particle at first. Therefore, in order to bound particle 7 in $\mathbb{RP}^2$ space, we need at least 3 such dominating lines. That is, we need at least three vanishing minors involving particle 7 while keeping the other minors still finite. For $n = 7$, this can be achieved for example by letting $|147|$, $|257|$ and $|367|$ vanish. There are 15 such kind of configurations. In appendix E, we further find out that there are 12 bounded chambers to bound the soft particle 7, which means there are 12 solutions for each of the configurations.

4.4.2 Singular Solutions in $X(4,7) \to X(4,6)$

Another simple example is $X(4,7)$. Taking again particle 7 to be soft, *i.e.* $\mathsf{s}_{abc7} \to \tau\hat{\mathsf{s}}_{abc7}$ (with $\tau \to 0$), all singular solutions come from 30 different configurations where determinants of the form $|1237|$, $|3457|$, $|1567|$ and $|2467|$ vanish. We can geometrically interpret this configuration in the soft limit as having the soft particle as the intersection of four planes, and each hard particle lying on the intersection of two of those planes. We give a very schematic representation, i.e. drawing $\mathbb{RP}^3$ on a plane, of this in figure 4.2.

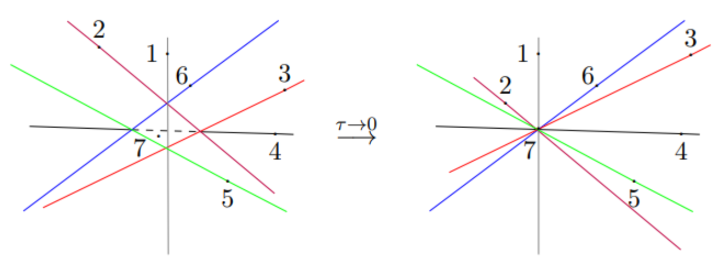

Figure 4.2: A configuration of singular solutions in $X(4,7)$. *Left*: Near the soft limit four 2-planes $\overline{123}$, $\overline{345}$, $\overline{561}$ and $\overline{246}$ almost cross the soft particle. *Right*: In the strict soft limit the soft particle lies in the intersection of the four 2-planes.

There are 4 solutions for each of these configurations, so we obtain a total amount of

$\mathcal{N}_7^{(4):\text{singular}} = 4 \times 30 = 120$ singular solutions.

The way to get the solutions is the following. For a configuration where $|1237|$, $|3457|$, $|1567|$ and $|2467|$ vanish, a convenient choice of gauge fixing in projective space is

$$\begin{pmatrix} 1 & 0 & 1 & 0 & 0 & 1 & 1 \\ x_1 & x_2 & x_3 & x_4 & x_5 & x_6 & x_7 \\ y_1 & y_2 & y_3 & y_4 & y_5 & y_6 & y_7 \\ z_1 & z_2 & z_3 & z_4 & z_5 & z_6 & z_7 \end{pmatrix} \overset{\text{gauge fixing}}{\longrightarrow} \begin{pmatrix} 1 & 0 & 1 & 0 & 0 & 1 & 1 \\ 0 & 1 & 1 & 0 & 0 & x_6 & x_7 \\ 0 & 0 & 1 & 1 & 0 & y_6 & y_7 \\ 0 & 0 & 1 & 0 & 1 & z_6 & z_7 \end{pmatrix}. \tag{4.20}$$

We then parameterize each determinant as $|1237| = \tau u, \quad |3457| = \tau v, \quad |5617| = \tau p$, and $|2467| = \tau q$, that is

$$x_6 = \frac{\tau(v y_6 + p) + y_6}{\tau(q-u) + z_6}, \quad x_7 = \tau v + 1, \quad y_7 = \tau(q-u) + z_6, \quad z_7 = \tau q + z_6\,. \tag{4.21}$$

When we plug this into the original scattering equations and take the strict soft limit $\tau \to 0$, we obtain a new set of scattering equations with variables u, v, p, q, y_6 and z_6

$$\lim_{\tau\to 0} \frac{\partial \mathcal{S}_4}{\partial x_i}\bigg|_{(4.21)} = 0, \quad \lim_{\tau\to 0} \frac{\partial \mathcal{S}_4}{\partial y_i}\bigg|_{(4.21)} = 0, \quad \lim_{\tau\to 0} \frac{\partial \mathcal{S}_4}{\partial z_i}\bigg|_{(4.21)} = 0, \quad \text{for} \;\; i = 1, \ldots 7. \tag{4.22}$$

Among the above 21 equations, only 6 of them are independent. The system is simple enough that all variables except one can be eliminated using resultants producing an irreducible polynomial of degree 4 for the left over variable. This means that there are 4 solutions. Note that in this case one can again eliminate u, v, p and q in the new scattering equations (4.22) first and then reduce the system to one only involving hard particles

$$\left(\frac{\partial \tilde{\mathcal{S}}_4}{\partial x_6} + z_6 \frac{\partial \tilde{\mathcal{S}}_4}{\partial y_6}\right)\bigg|_{x_6 \to \frac{y_6}{z_6}} = 0, \quad \left(\frac{\partial \tilde{\mathcal{S}}_4}{\partial z_6} + x_6 \frac{\partial \tilde{\mathcal{S}}_4}{\partial y_6}\right)\bigg|_{x_6 \to \frac{y_6}{z_6}} = 0, \tag{4.23}$$

where $\tilde{\mathcal{S}}_4$ is the potential of hard particles, $\tilde{\mathcal{S}}_4 \equiv \sum_{1\leq a<b<c<d\leq 6} \mathsf{s}_{abcd} \log |a,b,c,d|$. Here we just present two independent equations and the remaining variables are y_6 and z_6. Compared to the original scattering equations for 6 particles, which has 6 solutions, now the requirement that the planes $\overline{123}$, $\overline{345}$, $\overline{561}$ and $\overline{246}$ pass through a common point reduces the number of solutions to 4. Therefore, the number of singular solutions for $X(4,7)$ is $\mathcal{N}_7^{(4)\text{:singular}} = 30 \times 4 = 120$, as expected.

Singular Solutions on Positive Kinematics

Now, we make the use of kinematic data in the positive region $\mathcal{K}^+_{4,n}$ (or more precisely in $\mathcal{K}^{+,\mathbb{R}}_{4,n}$) (4.19) to study the solutions. Singular solutions make some minors of the form $|abc7|$, i.e. containing particle 7, vanish. Geometrically, this means that planes $\overline{abc}$ in $\mathbb{RP}^3$ space will dominate. The remaining planes can be omitted for the soft particle at first. Therefore, in order to bound particle 7 in $\mathbb{RP}^3$ space, we need at least 4 such dominating planes. That is, we need at least four vanishing minors involving particle 7 while keeping the other minors still finite. For $n = 7$, this can be achieved for example by letting $|1237|$, $|3457|$, $|1567|$ and $|2467|$ vanish. In figure 4.2 the soft particle is bounded inside a tetrahedron whose volume is of order τ when we use the kinematic data from the positive region. It is not trivial for six hard particles to form such a tetrahedron while any four of them are not allowed to lie in a common plane. One can check that this is the only kind of configuration, up to relabelling, that achieves this goal for $X(4,7)$.

Here we introduce another description of the tetrahedron, which can be generalized to describe more complicated polytopes. We view each vertex of the tetrahedron as an auxiliary point and give each of them a label, ranging from 8 to 11, see figure 4.3.

Note that particle labels are from 1 to 7. Hard particles 1-6 lie on the lines determined by

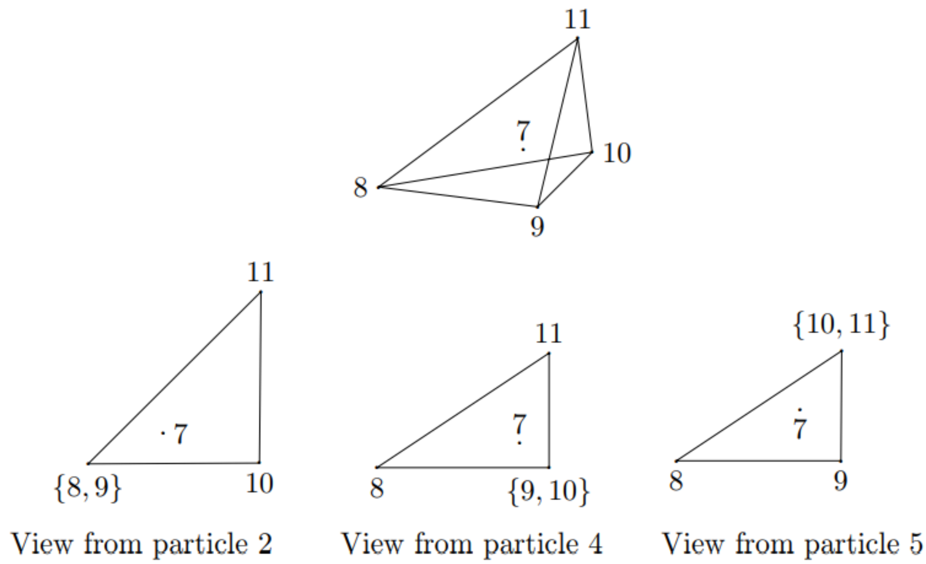

Figure 4.3: *Top*: The soft particle lies inside a tetrahedron. *Bottom*: Three projections of the tetrahedron from the point of view of particles 2, 4 and 5, respectively, when these are sent to infinity. In the strict soft limit, the tetrahedron as well as its three projections collapse to a point.

{8,11}, {8,9}, {9,11}, {9,10}, {10,11} and {8,10} respectively. Using the auxiliary points, we can understand the relative positions of the hard particles. Alternatively, now we can ignore the auxiliary points and imagine how these hard particles form some dominating planes to bound the soft particle.

We can also describe this tetrahedron through its projections from 3 orthogonal directions. As particles 2, 4 and 5 are sent to infinity in different directions, we can say that the three projections in figure 4.3 are just what the tetrahedron would look like if one stands at the position of 2, 4 and 5 respectively. In the first projection, vertices 8 and 9 are pinched from the view of particle 2, which has been sent to infinity. We can say that particle 2 lies on the lines determined by {8,9}. The remaining two projections are completely analogous.

There are 4 solutions for this particular configuration. For generic points in $\mathcal{K}^+_{4,7}$ there are complex solutions. However, the region $\mathcal{K}_{4,7}^{+;\mathbb{R}}$ is non-empty and therefore restricting to it one can find all four real solutions. Looking at the new equations (4.22) for $X(4,7)$, it is very hard to see whether there are solutions. Using the positive kinematic data in $\mathcal{K}_{4,7}^{+;\mathbb{R}}$ and viewing the solutions as equilibrium points, we see at least that there are possible solutions for the soft particle 7.

A beautiful way to count the number of solutions is from the dual limit in the dual space $X(3,7)$ as we explain now.

Singular Solutions from a Dual Hard Limit

One new feature of $k > 2$ kinematics is that in addition to soft limits there are also "hard limits". In fact, these are dual to each other under the isomorphism $X(k,n) \sim X(n-k,n)$ with the corresponding action on kinematic invariants [71, 123]. In the case at hand, the soft limit of particle 7 in $X(4,7)$ is dual to the hard limit of particle 7 in $X(3,7)$. It is important not to confuse it with the soft limit of particle 7 in $X(3,7)$ analyzed at the beginning of the section.

The reason for the name is easily seen from the relation among kinematic invariants. Consider $X(4,7) \sim X(3,7)$ and the relation $\mathsf{s}_{abcd} = \mathsf{s}_{efg}$ with $\{e,f,g\} = \{1,2,\ldots,7\} \setminus \{a,b,c,d\}$. This means that the soft limit in $X(4,7)$, i.e. $\mathsf{s}_{abc7} \to 0$ with the rest finite, implies $\mathsf{s}_{abc} \to 0$ if $7 \notin \{a,b,c\}$ and finite for any invariant containing 7, i.e. s_{ab7}. Going back to the singular solutions in $X(4,7)$, one can explicitly visualize the four solutions for each of the 30 configurations by using the dual hard limit in $X(3,7)$. Recall that the singular solutions in $X(4,7)$ come from configurations where the determinants of the form $|1237|$, $|3457|$, $|1567|$ and $|2467|$ vanish. Just as for kinematic invariants, this corresponds to having the determinants $|456|$, $|126|$, $|234|$ and $|135|$ vanishing in $X(3,7)$.

If we gauge fix the homogeneous coordinates of particles 3 and 6 to infinity as $(0,0,1)$ and $(0,1,0)$, and of particles 4 and 1 to be the origin $(1,0,0)$ and $(1,1,1)$, then the configurations that give rise to singular solutions automatically fix particles 2 and 5 to be at $(1,0,1)$ and $(1,1,0)$ respectively.

Therefore, for generic positive kinematics in $\mathbb{RP}^2$ we are left with four bounded chambers, which correspond to equilibrium points where particle 7 can be. These points correspond to the 4 solutions of the system. We give a graphical representation in figure 4.4.

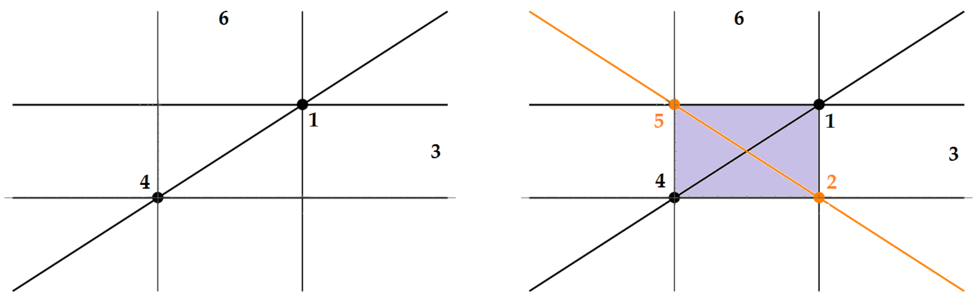

Figure 4.4: Four bounded chambers from the hard limit in $X(4,7)$. *Left:* the gauge-fixed particles 1, 3, 4 and 6 create repelling black lines. *Right:* the singular configurations automatically fix the position of particles 2 and 5 to be in the two remaining vertices of the square $[0,1]^2$, and create a new repelling (orange) line. This produces four bounded chambers (shown in grey) where particle 7 can be.

4.5 Singular Solutions in $X(3,8) \to X(3,7)$ and $X(5,8) \to X(5,7)$

Now we move on to two more complicated cases, $X(3,8)$ and $X(5,8)$, each of which have their own new features. In the former, the equations are complicated enough that counting solutions directly is not straightforward as in previous cases. Instead we use that the new scattering equations at $\tau = 0$ can also be analysed in soft limits to count solutions. The new equations also turn out to have both regular and singular solutions. In the latter case, we find the first example in which several topologically distinct configurations contribute to singular solutions. Of course, we expect this to be the generic behavior for higher k and n.

4.5.1 Singular Solutions in $X(3,8) \to X(3,7)$

In order to obtain the singular solutions, we study the soft limit for, e.g., particle $n = 8$, *i.e.* $\mathsf{s}_{ab8} \to \tau\hat{\mathsf{s}}_{ab8}$ (with $\tau \to 0$). The singular solutions arise from configurations where three lines in $\mathbb{CP}^2$, each defined by two hard particles, meet at the soft particle. In the same spirit as for $X(3,7)$, we let e.g. $|148|$, $|258|$ and $|368|$ vanish and we find 568 singular solutions. The large number of the solutions is the reason this case resists a direct approach as mentioned above. There are $\binom{7}{2}\binom{5}{2}\binom{3}{2}/3! = 105$ different configurations of this kind and therefore $\mathcal{N}_8^{(3)\text{:singular}} = 105 \times 568 = 59\,640$.

Let us now explain how to count the solutions for each singular configuration. The 568 solutions can be counted by taking a second soft limit, say that of particle 7. The solutions to the new scattering equations come in three different types. The first corresponds to regular solutions and the other two to singular solutions. Since the three kinds come from the singular solutions for the particle 8 we can denote them as $(\texttt{regular}_7, \texttt{singular}_8)$ and $(\texttt{singular}_7, \texttt{singular}_8)$ of type A and type B.

The first class of solutions, $(\texttt{regular}_7, \texttt{singular}_8)$, come from decoupling particle 7 from the remaining hard particles. We obtain 12 solutions for the hard particles and each gives 41 solutions for particle 7 leading to $12 \times 41 = 492$ such solutions.

The first kind of ($\texttt{singular}_7, \texttt{singular}_8$) solutions come from configurations in which particle 7 belongs to one of the already existing three lines and lies in the intersection of two other new lines (see left side of figure 4.5). For instance, this would correspond to vanishing determinants of the form $|147|$, $|267|$ and $|357|$. We find 6 solutions for each of the 6 possible configurations of this kind.

The second kind of ($\texttt{singular}_7, \texttt{singular}_8$) solutions corresponds to the case where three new lines intersect at particle 7 (see right side of figure 4.5). For instance, this would correspond to vanishing determinants of the form $|167|$, $|247|$ and $|357|$. We find 5 solutions for each of the 8 possible configurations of this kind.

Notice that in these last two cases there is a symmetry between particles 7 and 8. Combining these results one finds that the number of solutions to the equations that arise in a particular singular configuration in the soft limit of particle 8 is $41 \times 12 + 8 \times 5 + 6 \times 6 = 568$.

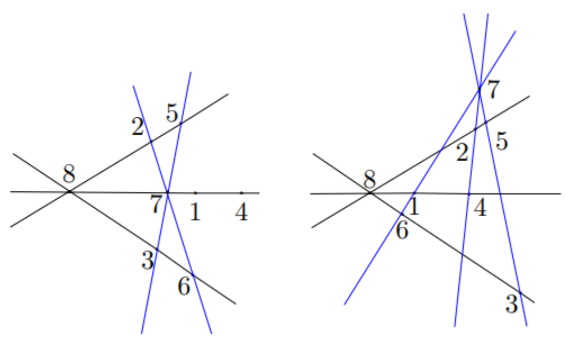

Figure 4.5: *Left*: representation of ($\texttt{singular}_7, \texttt{singular}_8$) type A configurations. *Right*: representation of ($\texttt{singular}_7, \texttt{singular}_8$) type B configurations.

Let us now explain how the procedure is implemented. We can again use a similar gauge fixing as in previous cases and parameterize the space as

$$x_6 = y_4 - \tau(u + v + p), \quad x_8 = y_4 - \tau(u + v), \quad y_8 = y_4 - \tau v. \tag{4.24}$$

When we take the strict soft limit $\tau \to 0$ we obtain a set of new equations with 8 variables: u, v, p, x_5, y_5, y_6, x_7 and y_7. The equations are given by

$$\lim_{\tau\to 0} \frac{\partial \mathcal{S}_3}{\partial x_i}\bigg|_{(4.24)} = 0, \quad \lim_{\tau\to 0} \frac{\partial \mathcal{S}_3}{\partial y_i}\bigg|_{(4.24)} = 0, \quad \text{for} \quad i = 1, \ldots 8. \tag{4.25}$$

More explicitly, we have

$$\begin{aligned} &\lim_{\tau\to 0} \frac{\partial \mathcal{S}_3}{\partial x_8}\bigg|_{(4.24)} = \frac{\mathsf{s}_{368}}{p} - \frac{\mathsf{s}_{148}}{u}\,, \quad \lim_{\tau\to 0} \frac{\partial \mathcal{S}_3}{\partial x_8}\bigg|_{(4.24)} = \frac{\mathsf{s}_{148}}{u} - \frac{\mathsf{s}_{258}}{v}\,, \\ &\lim_{\tau\to 0} \frac{\partial \mathcal{S}_3}{\partial y_5}\bigg|_{(4.24)} = \frac{\mathsf{s}_{258}}{v} + \frac{\partial \tilde{\mathcal{S}}_3}{\partial y_5}\bigg|_{x_6\to y_5}\,, \quad \lim_{\tau\to 0} \frac{\partial \mathcal{S}_3}{\partial x_6}\bigg|_{(4.24)} = -\frac{\mathsf{s}_{368}}{p} + \frac{\partial \tilde{\mathcal{S}}_3}{\partial y_5}\bigg|_{x_6\to y_5}\,, \end{aligned} \tag{4.26}$$

with $\tilde{\mathcal{S}}_3$ defined as the potential $\tilde{\mathcal{S}}_3 \equiv \sum_{1\le a<b<c\le 7} \mathsf{s}_{abc} \log(a,b,c)$. This allows us to easily eliminate u, v and p and reduce the new set of equations (4.25) to ones involving fewer particles,

$$\left\{ \frac{\partial \tilde{\mathcal{S}}_3}{\partial y_5} + \frac{\partial \tilde{\mathcal{S}}_3}{\partial x_6}\,, \quad \frac{\partial \tilde{\mathcal{S}}_3}{\partial x_5}\,, \quad \frac{\partial \tilde{\mathcal{S}}_3}{\partial y_6}\,, \quad \frac{\partial \tilde{\mathcal{S}}_3}{\partial x_7}\,, \quad \frac{\partial \tilde{\mathcal{S}}_3}{\partial y_7} \right\}\bigg|_{x_6\to y_5} = 0\,. \tag{4.27}$$

Now we have 5 independent equations and the remaining variables are x_5, y_5, y_6, x_7 and y_7. So we have reduced a problem of 8 particles to one of 7 particles.

This means we can now start with the set of equations (4.27) and study them independently of where they came from, i.e. the eight-particle problem, just like we did in the $X(3,7)$ case. As mentioned above, when the soft limit $\mathsf{s}_{ab7} \to \epsilon \hat{\mathsf{s}}_{ab7}$ (with $\epsilon \to 0$) is taken, there are again both regular and singular solutions for (4.27).

For the $(\texttt{regular}_7, \texttt{singular}_8)$ solutions, all terms involving particle 7 can be omitted in the first three equations in (4.27), which become exactly the same equations as (4.18) and give 12 solutions for x_5, y_5 and y_6. We plug each solution into the last two equations in (4.27) and obtain 41 solutions for x_7 and y_7. Compared to the regular solutions in $X(3,7)$, roughly speaking, we can see that the requirement $x_6 = y_5$ reduces the number of solutions for x_7 and y_7 from 42 to 41. In total, we obtain $12 \times 41 = 492$ solutions from this sector. We give a graphical representation and counting of these solutions in appendix E.

For the ($\texttt{singular}_7, \texttt{singular}_8$) solutions, note that the three lines $\overline{12}$, $\overline{34}$ and $\overline{56}$ already intersect at the same point (i.e. the position of particle 8, but this fact is irrelevant for our present problem). Now we need another 3 lines intersecting at the position of particle 7 in the $\mathbb{CP}^2$ in the strict second soft limit $\epsilon \to 0$. There are 2 different kinds of configurations that we graphically represented in figure 4.5.

For the first configuration, which corresponds to requiring $|147|$, $|267|$ and $|357|$ to vanish, we re-parameterize the $\mathbb{CP}^2$ space using the constraints

$$|147| = \epsilon\, q, \quad |267| = \epsilon\, r, \quad |357| = \epsilon\, s, \tag{4.28}$$

that is

$$y_6 = \epsilon(q + r + s) + x_5, \quad x_7 = s\epsilon + x_5, \quad y_7 = \epsilon(q + s) + x_5. \tag{4.29}$$

If one plugs them in into (4.27) and takes the strict soft limit $\epsilon \to 0$, a new set of scattering equations with variables q, r, s, x_5 and y_5 arises. Again we can easily eliminate q, r and s and reduce the new set of equations to those only involving the six hard particles

$$\left.\frac{\partial \hat{\mathcal{S}}_3}{\partial y_5} + \frac{\partial \hat{\mathcal{S}}_3}{\partial x_6}\right|_{x_6 \to y_5, y_6 \to x_5} = 0\,, \quad \left.\frac{\partial \hat{\mathcal{S}}_3}{\partial x_5} + \frac{\partial \hat{\mathcal{S}}_3}{\partial y_6}\right|_{x_6 \to y_5, y_6 \to x_5} = 0\,, \tag{4.30}$$

with $\hat{\mathcal{S}}_3$ defined as the potential of 6 particles, i.e. $\hat{\mathcal{S}}_3 \equiv \sum_{1 \le a < b < c \le 6} \mathsf{s}_{abc} \log(a, b, c)$. It turns out that there are 6 solutions to these equations.

For the second type of configuration, i.e., where $|167|$, $|247|$ and $|357|$ are taken to vanish, we re-parameterize the $\mathbb{CP}^2$ space using the constraints

$$|167| = \epsilon\, q, \quad |247| = \epsilon\, r, \quad |357| = \epsilon\, s, \tag{4.31}$$

that is

$$x_7 = \epsilon s + x_5, \quad y_7 = 1 - \epsilon r, \quad y_6 = \frac{-\epsilon(q + r y_5) + y_5}{\epsilon s + x_5}. \tag{4.32}$$

When we plug this into (4.27) and take the strict soft limit $\epsilon \to 0$, we obtain a set of new scattering equations with variables q, r, s, x_5 and y_5. Again we can easily eliminate q, r and s and reduce the new set of equations to those only involving 6 hard particles

$$\left.\frac{\partial \hat{\mathcal{S}}_3}{\partial y_5} + \frac{\partial \hat{\mathcal{S}}_3}{\partial x_6} + \frac{x_5}{y_5}\frac{\partial \hat{\mathcal{S}}_3}{\partial x_5}\right|_{x_6 \to y_5, y_6 \to x_5} = 0\,, \quad \left.\frac{x_5^2}{y_5}\frac{\partial \hat{\mathcal{S}}_3}{\partial x_5} + \frac{\partial \hat{\mathcal{S}}_3}{\partial y_6}\right|_{x_6 \to y_5, y_6 \to x_5} = 0. \tag{4.33}$$

These equations have 5 solutions. Therefore, we obtain a total of $6 \times 6 + 8 \times 5 = 76$ $(\texttt{singular}_7, \texttt{singular}_8)$ solutions.

Summarizing, we have proven that there are 568 solutions for the new set of equations (4.27). Therefore, as mentioned above, we find that the total number of singular solutions for $X(3,8)$ is $\mathcal{N}_8^{(3)\text{:singular}} = 105 \times 568 = 59\,640$. Together with the already known 128 472 regular solutions, mentioned in section 4.3, we get a total of $\mathcal{N}_8^{(3)\text{:total}} = 188\,112$ solutions, which is consistent to a proposal made by Lam that this should be related to the number of representations of uniform matroids as defined in [192].

Of course, the challenge now is to reproduce the same number of total solutions for the dual space $X(5,8)$. Confirming that $\mathcal{N}_8^{(5)\text{:total}} = 188\,112$ would be a very strong consistency check on our constructions and on the number itself.

4.5.2 Singular Solutions in $X(5,8) \to X(5,7)$

Unlike any case considered previously, the soft limit $X(5,8) \to X(5,7)$ has four kinds of topologically distinct singular solutions. In order to describe them let particle 8 be soft. As summarized in table 4.1, the four kinds of singular solutions come from the configurations where either 4, 5, 6, or 7 minors involving particle 8 vanish. Each class has 210, 420, 210, and 840 different configurations, respectively. For each of them, there are 96, 24, 8, and 32 solutions respectively, as we show below. Thus we obtain $\mathcal{N}_8^{(5):\text{singular}} = 210 \times 96 + 420 \times 24 + 210 \times 8 + 840 \times 32 = 58\,800$ singular solutions.

Topology type	Vanishing minors	Number of configurations	Number of solutions
1	$\|57238\|, \|57148\|, \|53468\|, \|51268\|$	210	96
2	$\|12358\|, \|12468\|, \|15678\|, \|23478\|, \|34568\|$	420	24
3	$\|12378\|, \|12458\|, \|13568\|, \|23468\|, \|25678\|, \|34578\|$	210	8
4	$\|12348\|, \|12358\|, \|12368\|, \|12378\|, \|14568\|, \|24578\|, \|34678\|$	840	32

Table 4.1: Four different topologies of singular configurations for $X(5,8)$ defined by the list of vanishing minors.

Type 1 Configuration

The first configuration in table 4.1 is slightly subtler than the remaining ones so we describe it in a separate subsection. The soft particle 8 can be thought of as being projected from $\mathbb{CP}^4$ space to $\mathbb{CP}^3$ space through the particle 5 and then being crossed by four 2-planes in the projection space just like the case $X(4,7)$. We give a very schematic representation, i.e. drawing $\mathbb{RP}^3$ on a plane, of the projection in figure 4.6, where particle 5 is sent to infinity. The four vertices of the tetrahedron in this projection actually correspond to four parallel lines in $\mathbb{RP}^4$ space. We can think of these four lines intersecting at the infinity point, particle 5.

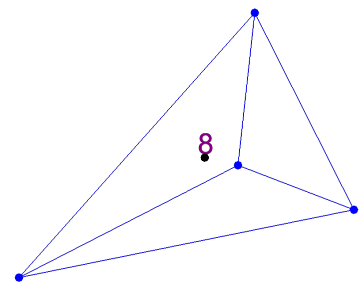

Figure 4.6: The geometrical interpretation of the topology type 1 near the soft limit, from the point of view of particle 5, is that the projection of the soft particle lies inside a tetrahedron just like in $X(4,7)$. In the strict soft limit, in projection space, the tetrahedron collapses to a point where the projection of the soft particle 8 lies while in $\mathbb{CP}^4$ space, the four 3-planes $\overline{5723}$, $\overline{5714}$, $\overline{5346}$, and $\overline{5128}$ share a common line that crosses particles 5 and 8.

There are no analogs to this case for $k = 3$ because there are no singular solutions for $k = 2$. Starting at $k = 4$, however, the soft particle can be projected into a lower-dimensional space and its projection satisfies the requirement of that particular dimension as long as n is large enough.

The way to obtain the solutions in the soft limit $\mathsf{s}_{abcd8} \to \tau \hat{\mathsf{s}}_{abcd8}$ (with $\tau \to 0$) is the following. First, we parameterize $X(5,8)$ as

$$\begin{pmatrix} 1 & 0 & 0 & 0 & 0 & 1 & 1 & 1 \\ x_1 & x_2 & x_3 & x_4 & x_5 & x_6 & x_7 & x_8 \\ y_1 & y_2 & y_3 & y_4 & y_5 & y_6 & y_7 & y_8 \\ z_1 & z_2 & z_3 & z_4 & z_5 & z_6 & z_7 & z_8 \\ w_1 & w_2 & w_3 & w_4 & w_5 & w_6 & w_7 & w_8 \end{pmatrix} \xrightarrow{\text{gauge fixing}} \begin{pmatrix} 1 & 0 & 0 & 0 & 0 & 1 & 1 & 1 \\ 0 & 1 & 0 & 0 & 0 & 1 & x_7 & x_8 \\ 0 & 0 & 1 & 0 & 0 & 1 & y_7 & y_8 \\ 0 & 0 & 0 & 1 & 0 & 1 & z_7 & z_8 \\ 0 & 0 & 0 & 0 & 1 & 1 & w_7 & w_8 \end{pmatrix}. \tag{4.34}$$

Notice that a direct consequence of sending particle 5 to infinity in the direction of w is that all vanishing minors $|57238|$, $|57148|$, $|53468|$ and $|51268|$ become independent of w_8.

Next, we make a reparameterization under the constraints

$$|57238| = \tau u, \;\; |57148| = \tau v, \;\; |53468| = \tau p, \;\; |51268| = \tau q\,, \tag{4.35}$$

that is

$$y_7 = \frac{\tau(-qx_7 + ux_7 - v) + x_7 z_7}{\tau p + 1}, \;\; x_8 = \tau p + 1, \;\; y_8 = \tau(u-q) + z_7, \;\; z_8 = \tau u + z_7. \tag{4.36}$$

We then plug this into the original scattering equations and take the strict soft limit $\tau \to 0$

$$\left\{ \lim_{\tau\to 0} \frac{\partial \mathcal{S}_5}{\partial x_i}\,, \quad \lim_{\tau\to 0} \frac{\partial \mathcal{S}_5}{\partial y_i}\,, \quad \lim_{\tau\to 0} \frac{\partial \mathcal{S}_5}{\partial z_i}\,, \quad \lim_{\tau\to 0} \frac{\partial \mathcal{S}_5}{\partial w_i} \right\}\Bigg|_{(4.36)} = 0, \quad \text{for} \;\; i = 1, \ldots 8. \tag{4.37}$$

Since all vanishing minors are independent of w_8, the above 32 equations only depend on 7 variables u, v, p, q, x_7, z_7 and w_7. Correspondingly, only 7 of these equations are independent since e.g. the leading order of $\frac{\partial \mathcal{S}_5}{\partial w_8}$ in τ vanishes. Hence, we must require its subleading contribution to vanish

$$\lim_{\tau\to 0} \frac{1}{\tau} \frac{\partial \mathcal{S}_5}{\partial w_8}\Bigg|_{(4.36)} = 0. \tag{4.38}$$

One can solve the equations for the leading order in (4.37) and obtain 16 solutions for u, v, p, q, x_7, z_7 and w_7. When each of these solutions is plugged into the subleading term (4.38), we find 6 solutions for w_8. Therefore, the total number of solutions is $16 \times 6 = 96$ as shown in table 4.1.

Now we can again use the kinematic data from the positive region (4.19), assuming all solutions are real, to interpret the singular solutions. Singular solutions make some minors $|abcd8|$ containing particle 8 become singular. Geometrically, this means that 3-

planes $\overline{abcd}$ in $\mathbb{RP}^4$ space will dominate. The remaining planes can be omitted for the soft particle at first. Therefore, in order to bound particle 8 in $\mathbb{RP}^4$ space, it seems we need at least five such dominating planes. This is the case for the remaining 3 configurations in table 4.1. However, it is not the case for type 1 configuration described now. The four dominating 3-planes do not bound the soft particle. They produce equilibrium lines instead of equilibrium points for the soft particle.

As shown in figure 4.6, any equilibrium point in the projection space will correspond to an equilibrium line in $\mathbb{RP}^4$ space. The soft particle 8 can lie at any point of these equilibrium lines and won't be pushed to infinity by the dominating 3-planes. This corresponds to the fact that the leading order of $\frac{\partial \mathcal{S}_5}{\partial w_8}$ in τ vanishes. It has no constraints on the positions of particle 8 in the direction from which 5 is sent to infinity.

The position of the soft particle 8 is finally determined by considering the normal 3-planes determined by the hard particles as well. This corresponds to equation (4.38). In each of the equilibrium lines, there are 6 equilibrium points considering both dominating and non-dominating minors.

Other Three Types of Configurations

For the second configuration in table 4.1, we make a reparameterization of (4.34) under the constraints

$$|12358| = \tau u,\ |12468| = \tau v,\ |15678| = \tau p,\ |23478| = \tau q,\ |34568| = \tau r\,, \tag{4.39}$$

that is

$$\begin{aligned}
w_7 &= -\frac{\tau(-ry_7+rz_7-qx_7+qz_7+ux_7-uy_7+vx_7-vz_7+p)-y_7+z_7}{x_7-z_7},\\
x_8 &= \tau r+1, \quad y_8 = -\frac{\tau(rz_7+ux_7-ry_7-uy_7+p)-y_7+z_7}{x_7-z_7}, \qquad z_8=-\tau u,\\
w_8 &= -\frac{\tau(-ry_7+rz_7+ux_7-uy_7+vx_7-vz_7+p)-y_7+z_7}{x_7-z_7}\,.
\end{aligned} \tag{4.40}$$

When this is plugged into the original scattering equations and the strict soft limit $\tau \to 0$ is taken, we obtain a new set of scattering equations with variables u, v, p, q, y_6 and z_6

$$\left\{\lim_{\tau\to 0}\frac{\partial \mathcal{S}_5}{\partial x_i}, \quad \lim_{\tau\to 0}\frac{\partial \mathcal{S}_5}{\partial y_i}, \quad \lim_{\tau\to 0}\frac{\partial \mathcal{S}_5}{\partial z_i}, \quad \lim_{\tau\to 0}\frac{\partial \mathcal{S}_5}{\partial w_i}\right\}\Bigg|_{(4.21)} = 0, \quad \text{for} \quad i=1,\ldots 8. \tag{4.41}$$

Among the above 32 equations, only 8 of them are independent. One can find that there are 24 solutions by solving the system above. We can also easily eliminate u, v, p , q and r in the new scattering equations (4.41) and then reduce the system to one only involving hard particles

$$\left\{\frac{\partial \tilde{\mathcal{S}}_5}{\partial y_7}+\frac{x_7-z_7}{y_7-z_7}\frac{\partial \tilde{\mathcal{S}}_5}{\partial x_7}, \quad \frac{\partial \tilde{\mathcal{S}}_5}{\partial z_7}+\frac{y_7-x_7}{y_7-z_7}\frac{\partial \tilde{\mathcal{S}}_5}{\partial x_7}, \quad \frac{\partial \tilde{\mathcal{S}}_5}{\partial w_7}+\frac{(x_7-z_7)^2}{z_7-y_7}\frac{\partial \tilde{\mathcal{S}}_5}{\partial x_7}\right\}\Bigg|_{w_7,y_8,w_8\to\frac{y_7-z_7}{x_7-z_7}} = 0, \tag{4.42}$$

where $\tilde{\mathcal{S}}_5$ is the potential for hard particles, $\tilde{\mathcal{S}}_5 \equiv \sum_{1\le a<b<c<d<e\le 7} \mathsf{s}_{abcde} \log|a,b,c,d,e|$. In (4.42) we presented only three independent equations for the three remaining variables y_7, z_7 and w_7. Notice that even though the equations in (4.42) are different from the original scattering equations for $X(5,7)$, they share the same number of solutions.

It is not obvious that there are solutions for the new equations (4.41). Let's use the positive kinematic data to clarify it. Recall that, in the soft limit for $X(3,7)$, the soft particle is bounded by a 2-simplex, i.e. a triangle, formed by three lines in $\mathbb{RP}^2$. For $X(4,7)$, the soft particle is bounded by a 3-simplex, i.e. a tetrahedron, formed by four planes in $\mathbb{RP}^3$ space. It turns out that for $X(5,8)$, we can geometrically interpret the second configuration in table 4.1 as having the soft particle bounded by a 4-simplex formed by five 3-planes in $\mathbb{RP}^4$. Its four projections are shown in figure 4.7.

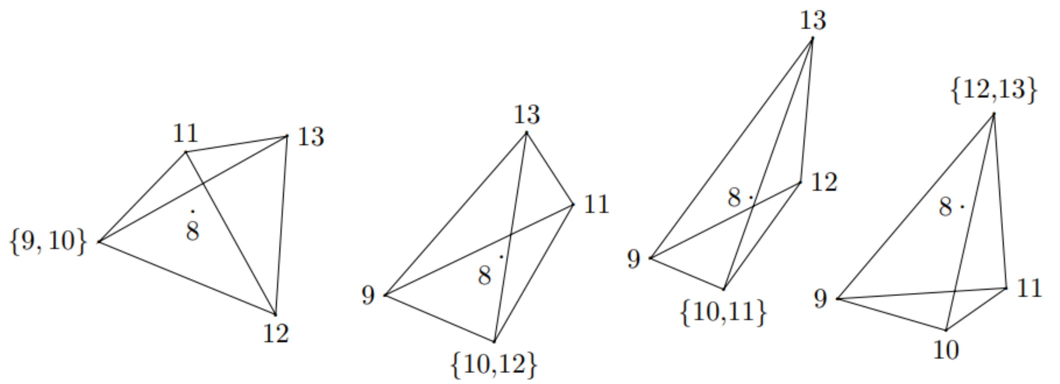

Figure 4.7: Geometrical interpretation for the topology type 2 near the soft limit. The soft particle is bounded by a 4-simplex. Here we show four projections of the 4-simplex from the viewpoint of particles 2, 3, 4 and 5, respectively. In the strict soft limit the 4-simplex collapses to a point where the soft particle lies.

The five vertices of the 4-simplex can be seen as auxiliary points, each of them having a label ranging from 9 to 13. The five facets of the 4-simplex, each of them corresponding to a tetrahedron, have vertices labelled by $\{9,10,12,13\}$, $\{9,10,11,13\}$, $\{9,11,12,13\}$, $\{9,10,11,12\}$ and $\{10,11,12,13\}$, respectively. They are passed by the five dominating 3-planes $\overline{1235}$, $\overline{1246}$, $\overline{1567}$, $\overline{2347}$ and $\overline{3456}$, respectively.

In the first projection shown in figure 4.7, two points $\{9,10\}$ are pinched from the viewpoint of particle 2, which has been sent to infinity. We can say that particle 2 lies on the line determined by $\{9{,}10\}$. Particles 1 and 6 lie on the line determined by $\{9{,}13\}$

and {11,13} respectively. Particle 7 lies on a 2-plane determined by three vertices of the 4-simplex $\{9, 11, 12\}$. The remaining three projections are completely analogous.

The polytopes in the remaining two configurations in table 4.1 are slightly more complicated. Actually, now there are two bounded chambers formed by the dominating 3-planes for the configurations type 3 and type 4. The soft particle can lie in either of the two bounded chambers. See appendix F for more details. In the following, we just show how to get the solutions for general kinematic data.

For type 3, we make a reparameterization of (4.34) under the constraints

$$|12378| = \tau u,\ |12458| = \tau v,\ |13568| = \tau p,\ |23468| = \tau q,\ |25678| = \tau r,\ |34578| = \tau s\,, \tag{4.43}$$

that is

$$\begin{aligned} &y_7 = \frac{\tau(s+r-v+vz_7-p)+x_7-z_7}{\tau(s-p)+x_7-1}, \quad w_7 = \frac{\tau(qz_7+u)-z_7}{\tau(p-s)-x_7}, \\ &x_8 = \tau s + x_7, \quad y_8 = \tau v, \quad z_8 = \tau(s-p)+x_7, \quad w_8 = 1-\tau q. \end{aligned} \tag{4.44}$$

When this is plugged into the original scattering equations and the strict soft limit $\tau \to 0$ is taken, we obtain a new set of scattering equations which has 8 solutions.

Likewise for type 4, we make a reparameterization of (4.34) under the constraints

$$|12348| = \tau u,\ |12358| = \tau v,\ |12378| = \tau p,\ |14568| = \tau q,\ |24578| = \tau r,\ |34678| = \tau s\,, \tag{4.45}$$

that is

$$
\begin{aligned}
z_7 &= \frac{\tau(rv - rp + qv - qp + uv + sv - uvx_7) + vx_7 - vy_7 + wy_7 - w}{u\left(-\tau(r+q) + y_7 - 1\right)}, \\
w_7 &= \frac{\tau(r + q + u + s - ux_7) + x_7 - y_7}{\tau(r+q) - y_7 + 1}, \\
x_8 &= -\tau(q+r) + y_7, \quad y_8 = y_7 - \tau r, \quad z_8 = -\tau v, \quad w_8 = \tau u\,,
\end{aligned}
\tag{4.46}
$$

which will make $|12368| = \tau(u+v)$ vanish as well. When we plug this into the original scattering equations and take the strict soft limit $\tau \to 0$, we obtain a new set of scattering equations which has 32 solutions.

As mentioned before, combining all these results we obtain $\mathcal{N}_8^{(5)\text{:singular}} = 420 \times 24 + 210 \times 8 + 840 \times 32 + 210 \times 96 = 58\,800$ singular solutions. In addition to the already known $\mathcal{N}_8^{(5)\text{:regular}} = 24 \times 5388 = 129\,312$ regular solutions, the total number of solutions for $X(5,8)$ is $\mathcal{N}_8^{(5)} = 188\,112$, which is exactly the same as the result obtained for $X(3,8)$.

4.6 General Configurations that Support Singular Solutions

In this section we explain what we believe are all configurations of points that lead to singular solutions in soft limits $X(k,n) \to X(k,n-1)$ for general k and n. Our proposal is based on the examples already computed and on many other configurations for which we have been able to compute particular solutions.

In general, recall that singular solutions will make some minors involving the soft particle vanish while keeping all other minors non-vanishing. In particular, no subset of only hard particles should develop any linear dependence detected by the vanishing of a single minor as this would imply that the hard-particle kinematics is not generic. We start by assigning each hard particle a position in the $\mathbb{CP}^{k-1}$ and each vanishing minor will correspond to a $(k-2)$-plane determined by $(k-1)$ particles.

We state our conjecture distinguishing $k = 3$ from $k > 3$. The reason is that $k = 3$ is the base case for the rest since $k = 2$ does not have singular solutions.

For $k = 3$ and $n = 2m + 1$ or $n = 2m + 2$ with $m \geq 3$, we conjecture that singular solutions come from configurations where $3, 4, \cdots, m$ lines meet at the soft particle respectively. Each line is determined by two hard particles and of course no subset of three hard particles are allowed to be collinear. We have checked that up to $n = 14$ there are indeed solutions supported by all such configurations. In figure 4.8, we show all three configurations for $n = 11$.

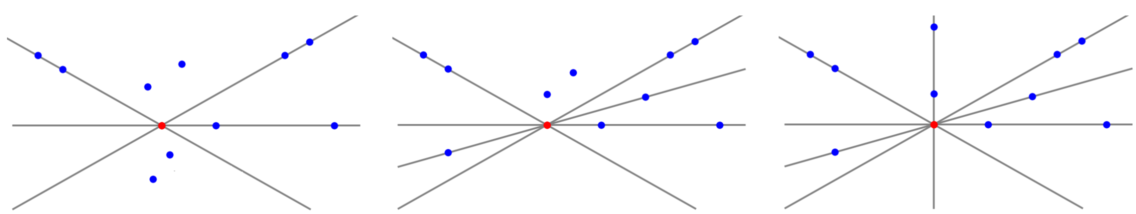

Figure 4.8: All configurations of singular solutions in $n = 11$. The soft particle is represented as a red point and the hard particles are represented as blue points. *Left*: one possible situation is when we have 3 vanishing minors involving the soft particle. Namely, we have three lines, each one passing through two hard particles, intersecting at the soft particle. The rest of the hard particles do not develop any linear dependence. *Center*: another possible situation is when we have 4 vanishing minors involving the soft particle, i.e. 4 lines. *Right*: the last possibility in $n = 11$ is when we have $m = 5$ vanishing minors involving the soft particle, i.e. 5 lines.

For $k \geq 4$, we conjecture that singular solutions come from two kinds of configurations. The first kind of configurations is obtained from the cases with lower k and n. More explicitly, this kind requires that all vanishing minors share a set of hard particles. Besides, the remaining hard particles together with the soft particle are projected by the common hard particles to a lower dimension space and their projections satisfy the requirement of that particular dimension.

For example, we already know there are singular solutions where three minors of the form $|14n|$, $|25n|$ and $|36n|$ vanish for $k = 3$ and $n \geq 7$. Thus we expect that for any $k \geq 4$ and $n \geq k+4$, there will always be solutions coming from configurations where three minors of the form $|1478\cdots k+3, n|$, $|2578\cdots k+3, n|$ and $|3678\cdots k+3, n|$ vanish. The hard particles 1-6 together with the soft particle are projected to a lower dimension space through the hard particles 7, 8, $\cdots$, $k+3$ one by one. Finally, they are projected to $\mathbb{CP}^2$ and the projection of the soft particle is crossed by three lines. We have numerically checked that for any $n \leq 12$ and $4 \leq k \leq n-4$, there are indeed solutions of this kind.

Similarly, we already know there are singular solutions where four minors of the form $|123n|$, $|345n|$, $|561n|$ and $|246n|$ vanish for $k = 4$ and $n = 7$. Thus we expect that for any $k \geq 4$ and $n \geq k+3$, there will always be solutions coming from configurations where four minors of the form $|12378\cdots k+2, n|$, $|34578\cdots k+2, n|$, $|56178\cdots k+2, n|$ and $|24678\cdots k+2, n|$ vanish. The hard particles 1-6 together with the soft particle are projected to a lower dimension space through the hard particles 7, 8, $\cdots$, $k+2$ one by one. Finally, they are projected to $\mathbb{CP}^3$ and the projection of the soft particle is crossed by four planes. We have numerically checked that for any $n \leq 11$ and $4 \leq k \leq n-3$, there are indeed solutions of this kind.

The second kind of configurations correspond to those where at least k $(k-2)$-planes meet at the soft particle location. Each of the $(k-2)$-planes are determined by $k-1$ hard particles. Besides, by slightly changing the position of hard particles, these $(k-2)$-planes can form a polytope with infinitesimal volume around the position of the soft particle without any hard particle as one of its vertices. Of course, no subset of k hard particles can lie on a single $(k-2)$-plane as this would imply an unwanted linear dependence. In particular, any configuration that supports singular solutions must still support singular ones for higher n and the same k.

For example, for $k = 4$ and $n = 8$, we find 7 different topologies of configurations that satisfy the requirements to support singular solutions, as shown in table 4.2. We have

I	$\|1478\|, \|2578\|, \|3678\|$		
II	$\|1238\|, \|3458\|, \|5618\|, \|2468\|$	III	$\|1238\|, \|3458\|, \|5678\|, \|2468\|$
IV	$\|1478\|, \|2578\|, \|3678\|, \|1238\|, \|4568\|$	V	$\|1238\|, \|1458\|, \|1678\|, \|2468\|, \|2578\|$
VI	$\|1238\|, \|1458\|, \|1678\|, \|2468\|, \|2578\|, \|3478\|$		
VII	$\|1238\|, \|1248\|, \|1258\|, \|1268\|, \|1278\|, \|3458\|, \|3678\|$		

Table 4.2: Seven different topologies of singular configurations for $X(4,8)$ defined by the list of vanishing minors.

numerically checked that there are solutions for each of them.

The first topology belongs to the first kind of configurations which are related to that of $X(3,7)$ through projection. For the remaining six topologies, there are at least 4 planes meeting at the soft particle location.

The second topology is the same configuration that supports the singular solutions in $X(4,7)$. The third topology has one hard particle changed in the third vanishing minor with respect to the second topology. Note that no matter what hard particle in a single minor in the second configuration is changed as 7, they all lead to the configuration of the same topology.

Comparing the first and fourth topology, we see in addition to three common minors $|1478|, |2578|, |3678|$, the fourth topology has two more vanishing ones $|1238|, |4568|$, which supports singular solutions. However, if we just add one more vanishing minor, such as

$|1238|$, to those of the first topology, there will be no singular solutions. This is because by slightly changing the position of hard particles, the four planes $\overline{147}$, $\overline{257}$, $\overline{367}$ and $\overline{123}$ can form a polytope with infinitesimal volume around the position of the soft particle but with the hard particle 7 as one of the vertices, which is forbidden.

Another way to think about it is to use the geometry description using positive kinematic data (4.19). For the first configuration, three planes $\overline{147}$, $\overline{257}$ and $\overline{367}$ share a common line that crosses particles 7 and 8. The final position of the soft particle 8 in the line is determined by both vanishing and finite minors. However, we can also fix the position of 8 in the line by imposing two more vanishing minors. That is the case of the fourth configuration. One can imagine that we cannot just impose one more vanishing minor as this will push the particle 8 in the line into infinity, i.e. there will be no singular solutions where only 4 minors of the form $|1478|$, $|2578|$, $|3678|$ and $|1238|$ vanish.

We have also checked many other examples up to $k = 6$, all of them having solutions (see table 4.3).

k	n	Vanishing minors
4	9	$\|123n\|, \|345n\|, \|567n\|, \|781n\|$
4	9	$\|123n\|, \|124n\|, \|126n\|, \|127n\|, \|345n\|, \|368n\|$
4	10	$\|123n\|, \|345n\|, \|567n\|, \|789n\|$
4	10	$\|123n\|, \|145n\|, \|167n\|, \|246n\|, \|257n\|, \|347n\|, \|389n\|$
5	9	$\|1235n\|, \|1246n\|, \|1567n\|, \|2347n\|, \|3458n\|$
6	10	$\|12358n\|, \|12468n\|, \|15678n\|, \|23478n\|, \|34589n\|$

Table 4.3: Some explicit examples supporting singular solutions, where particle n is the soft one.

4.7 Discussions

In this chapter we started the study of singular solutions in soft limits. This is a new phenomenon for scattering equations on $X(k,n)$ with $k>2$. We computed all singular solutions for all cases with $n<9$, except for $X(4,8)$. This proved that studying singular solutions is an effective technique for computing the number of solutions in cases where other known techniques cannot be applied. For example, we have proven that $\mathcal{N}_8^{(3)} = \mathcal{N}_8^{(5)} = 188\,112$. Also, even in cases where indirect approaches are possible, singular solutions prove to be a much simpler route as seen in the alternative determination of $\mathcal{N}_7^{(3)} = \mathcal{N}_7^{(4)} = 1\,272$.

One of the most pressing issues is to extend our study to all $X(3,n) \to X(3,n-1)$ cases with $n>8$. In section 4.6, we presented a conjecture for all configurations that can support singular solutions. It is very tempting to suggest that in this case, it would be possible to count solutions using a recursive approach. Recall that in $X(3,8) \to X(3,7)$ we resorted to a second soft limit in order to count solutions. Such "fibration" structure is familiar in the $k=2$ case where $X(2,n)$ can be thought of as a fibration over $X(2,n-1)$ (see e.g. [169]). For $k=3$ the structure we have uncovered is much more interesting and we leave its study for future work.

The scattering equations have been a powerful tool for studying properties of scattering amplitudes via the CHY formalism [76, 77]. The quantum field theory whose amplitudes have the simplest CHY formulation is a theory with a $U(N)\times U(\tilde{N})$ flavour group and a scalar field in the biadjoint representation with cubic interactions (for related developments see e.g. [78, 49, 94, 168, 167, 12, 120, 185, 29, 181, 96, 42]). It is not surprising that this is the first theory to have been generalized so that it has a CHY representation based on $X(k,n)$ with $k>2$ [81]. We now turn to a discussion on such biadjoint amplitudes and their soft limit behavior on singular solutions using the explicit cases we have computed and the conjecture regarding the general configurations that can support them.

4.7.1 Generalized Biadjoint Scalar Soft Limit

Recall the generalized biadjoint scalar amplitude [81]

$$m_n^{(k)}[\alpha|\beta] = \int \left[\frac{1}{\mathrm{Vol}[\mathrm{SL}(k,\mathbb{C})]} \prod_{a=1}^{n} \prod_{i=1}^{k-1} dx_a^i\right] \prod_{a=1}^{n} {\prod_{i=1}^{k-1}}' \delta\left(\frac{\partial \mathcal{S}}{\partial x_a^i}\right) \mathrm{PT}_n^{(k)}[\alpha]\mathrm{PT}_n^{(k)}[\beta], \tag{4.47}$$

where the Parke-Taylor functions correspond to

$$\mathrm{PT}_n^{(k)}[12\cdots n] = \frac{1}{|12\cdots k||23\cdots k+1|\cdots|n1\cdots k-1|}. \tag{4.48}$$

Now consider the soft limit for one particle, for instance $\mathsf{s}_{abn} = \tau\hat{\mathsf{s}}_{abn}$. Following our conjecture in section 4.6, one can analytically show that when $\tau \to 0$ the singular solutions for $k = 3$ and general n can at most contribute to order $\mathcal{O}(\tau^{-1})$ to the amplitude. The argument goes as follows. For $k = 3$ and $n \geq 7$ we have seen that there is always one singular configuration with 3 vanishing minors involving the soft particle. If we choose e.g. particle n to be the soft one, we parameterize the vanishing minors as $|abn| \sim u\tau$. This means that the Jacobian for the change of variables will give an $\mathcal{O}(\tau^3)$ factor in the amplitude[4]. Moreover, given the form of the singular configurations, we can at most have two vanishing determinants in the Parke-Taylor functions. This produces an $\mathcal{O}(\tau^{-4})$ factor in the amplitude. Hence, the leading contribution of the singular solutions to the biadjoint scalar amplitude in $k = 3$ is of order $\mathcal{O}(\tau^{-1})$.

[4]Note that for singular configurations with m vanishing minors the Jacobian gives orders of $\mathcal{O}(\tau^m)$. That's why having only 3 vanishing minors corresponds to the leading contribution.

Now we move on to explain the contribution to the amplitude for the cases $k = 4$ and $n = 7$, and $k = 5$ and $n = 8$ in the soft limit. Consider again the biadjoint scalar amplitude (4.47). For $k = 4$ and $n = 7$ the singular configurations are those where 4 vanishing minors involve the soft particle. The Jacobian for the change of variables thus gives an order $\mathcal{O}(\tau^4)$ to the amplitude. From the Parke-Taylor functions (4.48) we again obtain a factor of $\mathcal{O}(\tau^{-4})$, hence the contribution to the amplitude in this case is of the order $\mathcal{O}(\tau^0)$.

For $k = 5$ and $n = 8$ the analysis is slightly different. In this case the configuration that gives a more dominant contribution to the amplitude is the one with only 4 vanishing minors. Following the same procedure as for $k = 4$ and $n = 7$, this would naively give us again a total contribution of order $\mathcal{O}(\tau^0)$ to the amplitude. However, recall that the leading order in τ for one of the soft scattering equations vanished in this configuration. This means that we get an extra factor of $\mathcal{O}(\tau^{-1})$ in the amplitude, coming from the subleading term of the vanishing soft scattering equation (4.38). Therefore, the contribution to the amplitude in this case is of the order $\mathcal{O}(\tau^{-1})$[5].

We haven't obtained the whole set of singular solutions for higher values of k and n, but in what follows we make a prediction on their contribution to the biadjoint scalar amplitudes in the soft limit expansion based on our conjecture in section 4.6.

For any $k \geq 4$ and $n \geq k+3$, as we have already explained, there will always be some singular solutions from configurations where four minors of the form $|12378 \cdots k+2, n|$, $|34578 \cdots k+2, n|$, $|56178 \cdots k+2, n|$ and $|24678 \cdots k+2, n|$ vanish. We can use the gauge redundancy of $\mathrm{SL}(k, \mathbb{C})$ to send 7, 8, $\cdots$, $k+2$ to infinity in different directions. A direct consequence is that the leading order for the scattering equations of the soft particle corresponding to these directions vanish. See section 4.5.2 as an example. This means

[5]Singular configurations with 5, 6 and 7 vanishing minors give orders of $\mathcal{O}(\tau^1)$, $\mathcal{O}(\tau^2)$ and $\mathcal{O}(\tau^1)$, respectively.

that we get a factor of $\mathcal{O}(\tau^{4-k})$ from the subleading term of the vanishing soft scattering equations. The Jacobian for the change of variables in this case gives an order $\mathcal{O}(\tau^4)$ and the Parke-Taylor functions (4.48) also give a factor of $\mathcal{O}(\tau^{-4})$. Thus we expect that the contribution to the amplitude in this case is at most of the order $\mathcal{O}(\tau^{4-k})$. Besides $X(5,8)$, we have numerically checked the existence of such kind of solutions for $X(6,9)$.

Similarly, for any $k \geq 3$ and $n \geq k+4$, singular solutions from configurations where three minors of the form $|1278\cdots k+3,n|$, $|3478\cdots k+3,n|$ and $|5678\cdots k+3,n|$ vanish will contribute to the amplitude with order $\mathcal{O}(\tau^{2-k})$ at most. The reason is as follows. Consider the second kind of configurations conjectured in section 4.6. The Jacobian for the change of variables in this case gives an order $\mathcal{O}(\tau^k)$ at most since there are at least k vanishing minors. Although any Parke-Taylor function has k minors involving the soft particles, there can be at most $(k-1)$ vanishing ones, otherwise some minors only involving hard particles must vanish. Since in this case all the scattering equations keep their leading terms, the upper bound of the contribution of the singular solutions is of order $\mathcal{O}(\tau^{2-k})$. We have numerically checked the existence of such kind of solutions for $X(4,8)$ and $X(5,9)$.

The leading contribution to the biadjoint scalar theory amplitude is $\mathcal{O}(\tau^{1-k})$. This actually implies that singular solutions do not contribute to leading order. We summarize these results in table below:

	$\mathbf{k=3}$	$\mathbf{k=4}$	$\mathbf{k=5}$
Regular solutions	$\mathcal{O}(\tau^{-2})$	$\mathcal{O}(\tau^{-3})$	$\mathcal{O}(\tau^{-4})$
Singular solutions for $\mathbf{n=7}$	$\mathcal{O}(\tau^{-1})$	$\mathcal{O}(\tau^{0})$	-
Singular solutions for $\mathbf{n=8}$	$\mathcal{O}(\tau^{-1})$	$\mathcal{O}(\tau^{-2})$	$\mathcal{O}(\tau^{-1})$
Singular solutions for $\mathbf{n\geq 9}$	$\mathcal{O}(\tau^{-1})$	$\mathcal{O}(\tau^{-2})$	$\mathcal{O}(\tau^{-3})$

Table 4.4: Leading order contribution in the soft limit expansion. The results in black are obtained from analytic derivation. The results in red come from what we conjecture.

From table 4.4 one can notice an interesting pattern. For $k \geq 4$ the singular solutions for $n = k+3$ do not contribute to the subleading term. For $n > k+3$, though, the singular solutions will always be relevant, i.e. will contribute to the subleading term in the biadjoint scalar amplitude. This special case $k \geq 4$ and $n = k+3$ is nothing but the case that just comes after $n = k+2$, i.e. when no singular solutions arise. This phenomenon does not appear in $k = 3$ since for $n = 6$ there are no singular solutions, as explained before. Therefore, for $k = 3$ the singular solutions will always contribute to the subleading term.

These results in fact resonate with the recent work of García-Sepúlveda and Guevara [123]. More precisely, they computed the leading order behavior of biadjoint scalar amplitudes in the limit when a soft particle decouples from the scattering equations of the hard particles. Hence, no singular configurations were taken into account. With this assumption, they found that the leading soft factor for the $m_n^{(k)}$ amplitude is

$$S_n^{(k)} = m_{k+2}^{(k)}(\mathbb{I}|\mathbb{I})(\hat{\mathbf{T}}_{k+2}^{(p,q)} \to \hat{\mathbf{T}}_n^{(p,q)}) \tag{4.49}$$

where the canonical ordering is assumed and

$$\hat{\mathbf{T}}_n^{(p,q)} := \sum_{a_1,\ldots,a_r=1}^{n} \hat{\mathbf{s}}_{12\ldots q a_1\ldots a_r (n-k+q+r+1)\ldots n-1n} \tag{4.50}$$

are planar kinematic invariants, $0 \leq r \leq k-2$ and $1 \leq q \leq k-r$, and r denotes the number of summed indices. The fact that singular solutions do not contribute to the leading order in the soft limit expansion of the biadjoint scalar amplitudes serves to corroborate their statement (4.49) for the cases already mentioned. Indeed, they numerically checked that only regular solutions contribute to leading order for $k = 3$ and $n = 7$, 8, for $k = 4$ and $n = 7$ and for $k = 5$ and $n = 8$.

Chapter 5

Generalized Feynman Diagrams

5.1 Introduction

In this chapter, we conclude our exploration of the CEGM generalization of quantum field theory by approaching it from a viewpoint that is more familiar to physicists. Specifically, we will identify the analogous objects to Feynman diagrams that contribute to CEGM amplitudes and utilize them to perform calculations for some examples.

As pointed out in [71], these higher-k "biadjoint amplitudes" were shown to have deep connections to tropical Grassmannians. This led to the proposal that generalized Feynman diagrams could be identified with facets of the corresponding $\operatorname{Trop} G(k,n)$ [71]. Motivated by the connection (as described in chapter 3) between $\operatorname{Trop} G(2,n)$ with metric trees, which can be identified as Feynman diagrams, and that of $\operatorname{Trop} G(3,n)$ with metric arrangements of trees [140], Cachazo and Borges introduced a generalization to $k=3$ called planar collections of Feynman diagrams as the objects that compute $k=3$ biadjoint amplitudes [42].

The computation of a $k = 3$ biadjoint amplitude is completely analogous to that of the standard $k = 2$ amplitude but defined as a sum over planar collections of Feynman diagrams

$$m_n^{(3)}(\alpha, \beta) = \sum_{\mathcal{C} \in \Omega(\alpha) \cap \Omega(\beta)} \mathcal{R}(\mathcal{C}), \tag{5.1}$$

with $\Omega(\alpha)$ the set of all collections of Feynman diagrams which are planar with respect to the α-ordering [42]. More explicitly, the i^{th} tree in a collection is a tree with $n-1$ leaves $\{1, 2, \ldots, n\} \setminus i$ which is planar with respect to the ordering induced by deleting i from α. This is why the collection is called *planar* and not the individual trees. The value $\mathcal{R}(\mathcal{C})$ of a planar collection $\mathcal{C}$ is obtained from the following function

$$\mathcal{F}(\mathcal{C}) = \sum_{i,j,k} \pi_{ijk} \, \mathsf{s}_{ijk} \tag{5.2}$$

defined in terms of the metrics of the trees in the collection $d_{jk}^{(i)}$ which satisfy a compatibility condition $d_{jk}^{(i)} = d_{ik}^{(j)} = d_{ij}^{(k)}$, thus defining a completely symmetric rank three tensor $\pi_{ijk} := d_{jk}^{(i)}$ [140]. Recall that s_{ijk} is the $k = 3$ generalization of Mandelstam invariants, defined as completely symmetric rank-three tensors satisfying

$$\mathsf{s}_{iij} = 0, \quad \sum_{j,k=1}^{n} \mathsf{s}_{ijk} = 0, \quad \forall i \in \{1, 2, \ldots, n\}. \tag{5.3}$$

The explicit value is then computed as

$$\mathcal{R}(\mathcal{C}) = \int_{\Delta} d^{2(n-4)} f_I \exp \mathcal{F}(\mathcal{C}) \,, \tag{5.4}$$

where the domain Δ is defined by the requirement that all internal lengths of all Feynman diagrams in the collection be positive [42]. Figure 5.1 is an example of a planar collection

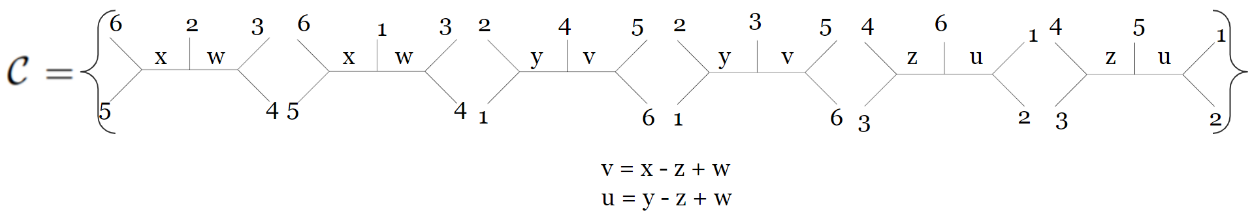

Figure 5.1: An example of a planar collection of Feynman diagrams for $n = 6$ and with relations between the internal lengths after imporsing the compatibility conditions $\pi_{ijk} := d^{(j)}_{kl} = d^{(k)}_{jl} = d^{(l)}_{jk}$.

that corresponds to a bypiramidal facet in Trop$G(3, 6)$, and integrates to

$$\mathcal{R}(\mathcal{C}) = \int_{\Delta} dxdydzdw \exp(-\sum_{a<b<c} \mathsf{s}_{abc}\pi_{abc}) = \frac{R + \tilde{R}}{R\tilde{R}\mathbf{t}_{1234}\mathbf{t}_{3456}\mathbf{t}_{5612}}\,, \tag{5.5}$$

where $\Delta = \{x > 0, y > 0, z > 0, w > 0, u > 0, v > 0\}$ and R, $\tilde{R}$, $\mathbf{t}_{1234}$, $\mathbf{t}_{3456}$ and $\mathbf{t}_{5612}$ are planar poles of the $(k, n) = (3, 6)$ CEGM amplitude given by

$$\mathbf{t}_{a_1,a_2,\ldots,a_m} := \sum_{\{a,b,c\}\subset\{a_1,a_2,\ldots,a_m\}} \mathsf{s}_{abc}\,,$$

$$R := \mathbf{t}_{1234} + \mathsf{s}_{345} + \mathsf{s}_{346}\,, \qquad \tilde{R} := \mathbf{t}_{1234} + \mathsf{s}_{125} + \mathsf{s}_{126}\,.$$

In this chapter we continue the study of planar collections of Feynman diagrams by exploiting an algorithm proposed in [42] for determining all collections for $k = 3$ and n points by a "combinatorial bootstrap" starting from $k = 2$ and n-point planar Feynman diagrams. We review in detail the algorithm in section 5.2 and use it to construct all 693, 13 612, and 346 710 collections for $(k, n) = (3, 7)$, $(3, 8)$ and $(3, 9)$ respectively. The 693 collections for $(k, n) = (3, 7)$ were already obtained in [42] by imposing a planarity condition on the metric tree arrangements presented by Herrmann, Jensen, Joswig, and Sturmfels in their study of the tropical Grassmannian $\operatorname{Trop} G(3,7)$ in [140]. Also, there are deep connections between positive tropical Grassmannians and cluster algebras as explained by Speyer and Williams in [195] and explored by Drummond, Foster, Gürdogan, and Kalousios in [96]. In the latter work it was found that $\operatorname{Trop}^+ G(3,8)$ can be described in terms of 25 080 clusters. Here we show that our 13 612 planar collections for $(3,8)$ encode exactly the same information as their 25 080 clusters. The cluster algebra analysis of $\operatorname{Trop}^+ G(3,9)$ has not appeared in the literature but it should be possible to obtain them from our 346 710 collections.

We also start the exploration of the next layer of generalizations of Feynman diagrams in section 5.3 and propose that $k = 4$ biadjoint amplitudes are computed using planar matrices of Feynman diagrams. In a nutshell, an n-point planar matrix of Feynman diagrams $\mathcal{M}$ is an $n \times n$ matrix with Feynman diagrams as entries. The $\mathcal{M}_{ij}$ entry is a Feynman diagram with $n-2$ leaves $\{1,2,\ldots,n\} \setminus \{i,j\}$. Each tree has a metric defined by the minimum distance between leaves, $d^{(ij)}_{kl}$. Here we use superscripts to denote the entry in the matrix of trees and subscripts for the two leaves whose distance is given. Planar matrices of Feynman diagrams must satisfy a compatibility condition on the metrics

$$d^{(ij)}_{kl} = d^{(ik)}_{jl} = d^{(il)}_{kj} = d^{(kl)}_{ij} = d^{(jl)}_{ik} = d^{(kj)}_{il}. \tag{5.6}$$

This means that the collection of all metrics defines a completely symmetric rank four tensor $\pi_{ijkl} := d^{(ij)}_{kl}$.

Using this we generalize the prescription for computing the value $R(T)$ and $\mathcal{R}(\mathcal{C})$ of $k = 2$ and $k = 3$ "diagrams" to $\mathcal{R}(\mathcal{M})$ for $k = 4$ and therefore their contribution to generalized $k = 4$ amplitudes. Moreover, we find that a second class of combinatorial bootstrap approach can be efficiently used to simplify the search for matrices of diagrams that satisfy the compatibility conditions (5.6). The idea is that any column of a planar matrix of Feynman diagrams must also be a planar collection of Feynman diagrams but with one less particle. In the first of our two main examples, any matrix for $(k,n)=(4,8)$ must have columns taken from the set of 693 $(k,n)=(3,7)$ planar collections. Using that the matrix must be symmetric, one can easily find 91 496 matrices of trees satisfying this purely combinatorial condition. Therefore the set of all valid planar matrices for $(k,n)=(4,8)$ must be contained in the set of those 91 496 matrices. Surprisingly, we find that only 888 such matrices do not admit a generic metric satisfying (5.6). This means that there are exactly 90 608 planar matrices of Feynman diagrams for $(k,n)=(4,8)$. We also find efficient ways of computing their contribution to $m_8^{(4)}(\mathbb{I},\mathbb{I})$. As the second main example of the technique, we used the $(3,8)$ planar collections to construct candidate matrices in $(4,9)$. We found 33 182 763 such symmetric objects. Computing their metrics we found that 2 523 339 of them are degenerate and therefore the total number of planar matrices of Feynman diagrams for $(4,9)$ is 30 659 424. We presented all these results in the original paper [74] and in this chapter we will only comment on them. The 888 degenerate matrices also appeared as good non-regular triangulations of the $m=2$ amplituhedron, as described by Łukowski, Parisi and Williams [157].

After identifying collections with $(3,n)$ amplitudes and matrices with $(4,n)$, it is natural to introduce planar $(k-2)$-dimensional arrays of Feynman diagrams as the objects relevant for the computation of (k,n) biadjoint amplitudes. In section 5.4 we discuss these objects and explain the combinatorial version of the duality connecting (k,n) and $(n-k,n)$ biajoint amplitudes at the level of the arrays. We end in section 5.5 with some discussions.

5.2 Planar Collections of Feynman Diagrams

In this section we give a short review of the definition and properties of planar collections of Feynman diagrams [42]. Emphasis is placed on a technique for constructing n-particle planar collections starting from special ones obtained by "pruning" n-point planar Feynman diagrams and then applying a "mutation" process. Here we borrow the terminology *mutation* from the cluster algebra literature [117, 118, 36]. The reason for this becomes clear below. This pruning-mutating technique is the first combinatorial bootstrap approach we use in this work. The second kind is introduced in section 5.3 as a way of constructing planar matrices of Feynman diagrams from planar collections.

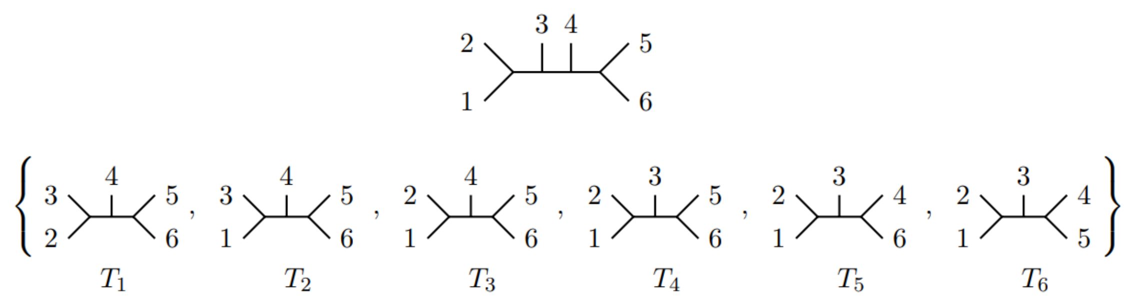

Figure 5.2: An example for an initial planar collection obtained by pruning a 6-point Feynman diagram. Above is the 6-point Feynman diagram to be pruned. Below is the planar collection of 5-point Feynman diagrams obtained by pruning the leaves $1, 2, ..., 6$ of the above Feynman diagram, respectively.

Without loss of generality, from now on we only consider the canonical ordering $\mathbb{I} := (1, 2, \ldots, n)$ and every time an object is said to be planar, it means with respect to $\mathbb{I}$. Recall that for $k = 2$ the objects of interest are n-particle planar Feynman diagrams in a ϕ^3 scalar theory. There are exactly C_{n-2} such diagrams[1]. When Feynman diagrams are thought of

[1] C_m is the m^{th} Catalan number.

as metric trees, a length is associated to each edge and if any of the $n-3$ internal lengths becomes zero we say that the tree degenerates. Here is where the power of restricting to planar objects comes into play; once a given planar tree degenerates, there is exactly one more planar tree that shares the same degeneration. These two planar Feynman diagrams only differ by a single pole and we say that they are related by a mutation. Starting from any planar Feynman diagram, one can get all other planar Feynman diagrams by repeating mutations. If no new Feynman diagrams are generated, we are sure we have obtained all of the Feynman diagrams of certain ordering. Here the terminology *mutation* precisely coincides with the one used in cluster algebras since planar Feynman diagrams are known to be in bijection with clusters of an A-type cluster algebra and mutations connect clusters in exactly the same way as degenerations connect planar metric trees. This precise connection between objects connected via degenerations and cluster mutations does not hold for higher k and therefore we hope the abuse of terminology will not cause confusion [42].

For the computation of $k=3$ biadjoint amplitudes, planar n-point Feynman diagrams are replaced by planar collections of $(n-1)$-point Feynman diagrams. Each collection is made out of n Feynman diagrams with the i^{th} tree defined on the set $\{1,2,\cdots,n\}\setminus i$ and planar the respect to the ordering $(1,2,\cdots,i-1,i+1,\cdots,n)$. Each tree has its own metric defined as the matrix of minimal lengths from one leaf to another. The metric for the i^{th}-tree is denoted as $d^{(i)}_{jk}$ with $j,k\in\{1,2,\cdots,n\}\setminus i$. Moreover, the metrics have to satisfy a compatibility condition $d^{(j)}_{kl}=d^{(k)}_{jl}=d^{(l)}_{jk}$. A necessary condition for two planar collections of Feynman diagrams to be related is that their individual elements, i.e. the $(n-1)$-point Feynman diagrams, are either related by a mutation or are the same. Of course, in order to prove that the collections are actually related it is necessary to study the space of metrics and show that the two share a common degeneration. The key idea is that we can get all planar collections of Feynman diagrams by repeated mutations, starting at any single collection. What is more, we can tell whether we have obtained all of the collections when there are no new collections produced by mutations [2].

A more efficient variant of the mutation procedure described above is obtained by introducing multiple initial collections. In fact there is a canonical set of planar collections which are easily obtained from n-point planar Feynman diagrams. Let us define the *initial planar collections* as those obtained via the following procedure. Consider any n-point planar Feynman diagram T and denote the tree obtained by pruning (or removing) the i^{th} leaf by T_i. Then the set $\{T_1, T_2, \ldots, T_n\}$ is a planar collection of Feynman diagrams. Let us illustrate this with a simple example seen in figure 5.2.

(k,n)	Number of collections	Numbers of collections for each kind					Number of layers
(3,5)	5	2-mut. 5					0
(3,6)	48	4-mut. 46	6-mut. 2				3
(3,7)	693	6-mut. 595	7-mut. 28	8-mut. 70			4
(3,8)	13 612	8-mut. 9 672	9-mut. 1 488	10-mut. 2 280	11-mut. 96	12-mut. 76	8
(3,9)	346 710	10-mut. 186 147	11-mut. 61 398	12-mut. 78 402	13-mut. 12 300	14-mut. 7 668	11
		15-mut. 522	16-mut. 270	17-mut. 3			

Table 5.1: Summary of results for planar collections of Feynman diagrams for $k = 3$ and up to $n = 9$. The second column gives the total numbers of planar collections. The third column provides the numbers of collections for each kind, classified by the number of mutations. The fourth column indicates how many layers of mutations are necessary to find the complete set of collections starting with the C_{n-2} initial collections.

[2] Here we assume that the set of all of planar collections is connected. We have checked this to be the case up to $n = 9$.

Using all such C_{n-2} collections as starting points one can then apply mutations to each and start filling out the space of planar collections in n-points. When the method is applied to $(k, n) = (3, 5)$ we obtain all planar collections without the need of any mutations since every single planar collection in this case is dual to a $(2, 5)$ Feynman diagram. Next, we apply the technique to reproduce the known results for $(3, 6)$ starting from the $C_4 = 14$ initial collections. We find that after only three layers of mutations we get all planar collections. Repeating the procedure for $(3, 7)$ we find all 693 planar collections stating from the initial $C_5 = 42$ collections after four layers of mutations.

Our first new results in this work are the computation of all 13 612 planar collections in $(3, 8)$ and all 346 710 in $(3, 9)$. Details on the results and the ancillary files where the collections were presented and provided in [74, section 4]. All results are summarized in table 5.1. We classify the planar collections according to their numbers of mutations and count the numbers of collections for each kind as well. The precise definition of metrics and degenerations of planar collections of Feynman diagrams was given in [42].

5.3 Planar Matrices of Feynman Diagrams

In the previous section we introduced an efficient algorithm for finding all planar collections of Feynman diagrams based on a pruning-mutation procedure. Such collections compute $k = 3$ biadjoint amplitudes. The next natural question is what replaces planar collections for $k = 4$ biadjoint amplitudes. Inspired by the way a single planar Feynman diagram defines a collection by pruning one leaf at a time, we start with a matrix of Feynman diagrams where the i, j element is obtained by pruning the i^{th} and j^{th} leaves of an n-point planar Feynman diagrams as the relevant objects for $k = 4$,

$$\mathcal{M} = \begin{bmatrix} \emptyset & T^{(1,2)} & \dots & T^{(1,n-1)} & T^{(1,n)} \\ T^{(2,1)} & \emptyset & \dots & T^{(2,n-1)} & T^{(2,n)} \\ \vdots & \vdots & \ddots & \vdots & \vdots \\ T^{(n-1,1)} & T^{(n-1,2)} & \dots & \emptyset & T^{(n-1,n)} \\ T^{(n,1)} & T^{(n,2)} & \dots & T^{(n,n-1)} & \emptyset \end{bmatrix}, \tag{5.7}$$

as first proposed in [42]. We denote the Feynman diagram in the i^{th} row and j^{th} column, where labels i and j are absent, by $T^{(i,j)}$. We add a metric to every Feynman diagram $T^{(i,j)}$ in the matrix, and denote the lengths of internal and external edges as $f_I^{(ij)}$ and $e_m^{(ij)}$ respectively. Correspondingly, we can use $d_{kl}^{(ij)}$ to denote the minimal distance between two leaves k and l. Up to this point, the edge lengths and hence distances $d_{kl}^{(ij)}$ of different Feynman diagrams in the matrix have no relations. We can relate them by imposing compatibility conditions analogous to those for collections of Feynman diagrams. This leads to the following definition.

Definition 5.3.1. *A planar matrix of Feynman diagrams is an $n \times n$ matrix $\mathcal{M}$ with component $\mathcal{M}_{ij}$ given by a metric tree with leaves $\{1, 2, \dots, n\} \setminus \{i, j\}$ and planar with respect to the ordering $(1, 2, \cdots, \not{i}, \cdots, \not{j}, \cdots, n)$ satisfying the following conditions*

- *Diagonal entries are the empty tree $\mathcal{M}_{ii} = \emptyset$.*
- *Compatibility* (5.6)

$$d_{kl}^{(ij)} = d_{jl}^{(ik)} = d_{kj}^{(il)} = d_{ij}^{(kl)} = d_{ik}^{(jl)} = d_{il}^{(kj)}.$$

Note that the compatibility condition has several important consequences. The first is that since a given metric is symmetric in their labels, i.e. $d^{(ij)}_{kl} = d^{(ij)}_{lk}$ which is obvious from its definition as the minimum distance from k to l, one finds that the matrix $\mathcal{M}$ must be symmetric as stated in the following lemma.

Lemma 5.3.2. *Planar matrices of Feynman diagrams are symmetric.*

Proof. The symmetry of the matrix follows from realizing that the compatibility condition requires that $d^{(ij)}_{kl} = d^{(kl)}_{ij}$ and therefore the symmetry of the metric on the left hand side in the leave labels k and l implies that of the right hand side is symmetric in the matrix labels k and l. In order to complete the proof, it is enough to note that a binary metric tree is uniquely determined by its metric as we show in appendix G. □

Planar collections of Feynman diagrams have $(n-4)n$ internal edges; $n-4$ for each of the n trees in the collection. However, only $2(n-4)$ are independent once the compatibility condition is imposed on the metrics as reviewed in [42]. In the case of planar matrices of Feynman diagrams there are $\binom{n}{2}(n-4)$ internal lengths $f^{(ij)}_I$ with $1 \leq i < j \leq n, 1 \leq I \leq n-5$ while the compatibility conditions (5.6) reduce the number down to $3(n-5)$ independent ones. This means that a planar matrix has at least $3(n-5)$ possible degenerations. The precise number depends on the structure of the trees in the matrix.

In analogy with planar collections, we say that two planar matrices are related via a mutation if they share a co-dimension one degeneration. Recall that an initial planar collection is obtained by pruning a leaf of the same n-point planar Feynman diagram to produce n different $(n-1)$-point trees. We can also get an *initial planar matrix* by pruning two different leaves at a time from the same n-point planar Feynman diagram. See figure 5.3 for an example. Using all such C_{n-2} matrices as starting points one can then apply mutations to each and start filling out the space of planar matrices in n-points.

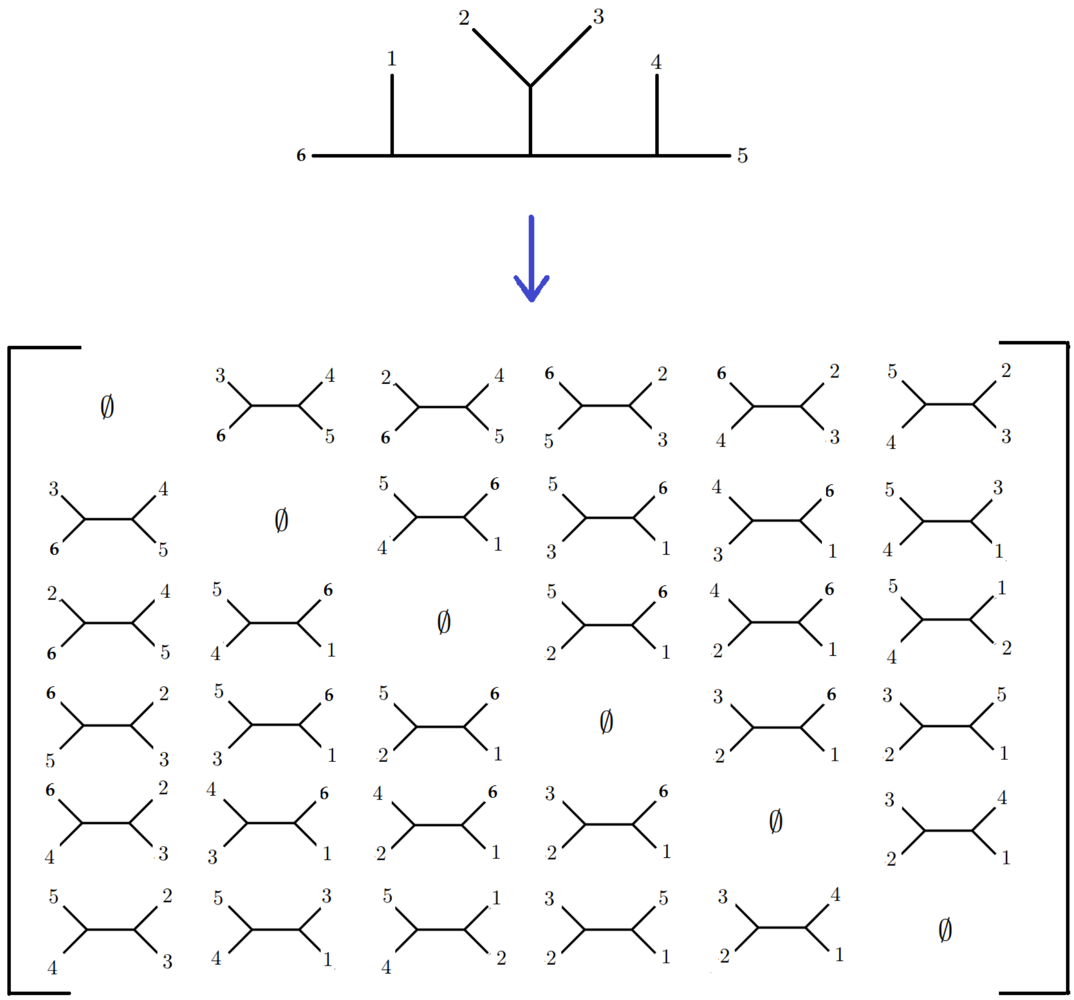

Figure 5.3: An example for a 6-point initial planar matrix. Above we show a 6-point Feynman diagram. Below there is a symmetric matrix of 4-point Feynman diagrams obtained by pruning two leaves from the set $1, 2, \cdots, 6$ at a time of the above Feynman diagram. The Feynman diagram from the i^{th} column and j^{th} row has the i^{th} and j^{th} leaves pruned.

The contribution to the amplitudes of every planar matrix can be calculated individually. Consider the function of a planar matrix of Feynman diagrams $\mathcal{M}$,

$$\mathcal{F}(\mathcal{M}) := \sum_{1\leq i,j,k,l\leq n} \pi_{ijkl}\, \mathsf{s}_{ijkl}, \tag{5.8}$$

with $\pi_{ijkl} := d_{kl}^{(ij)}$. Here s_{ijkl} are the generalized symmetric Mandelstam invariants introduced in [71]. These satisfy the conditions

$$\mathsf{s}_{iijk} = 0, \qquad \sum_{j,k,l=1}^{n} \mathsf{s}_{ijkl} = 0 \quad \forall i. \tag{5.9}$$

At this point it is not obvious but these conditions make it possible to write $\mathcal{F}(\mathcal{M})$ in a form free of any length of leaves $e_m^{(ij)}$. In section 5.4 we explain this phenomenon in more generality for any value of k.

An integral of $\mathcal{F}(\mathcal{M})$ over independent internal lengths $\{f_1, f_2, \cdots, f_{3(n-5)}\}$ gives the contribution to $k = 4$ biadjoint amplitudes

$$\mathcal{R}(\mathcal{M}) = \int_\Delta d^{3(n-5)} f_I \exp \mathcal{F}(\mathcal{M})\,, \tag{5.10}$$

where the domain Δ is defined by the condition that all $\binom{n}{2}(n-4)$ internal lengths are positive and not only the $3(n-5)$ independent ones. For future use we comment that it is possible to consider (5.10) also for degenerate matrices and in such cases it integrates to zero as its domain is a set of measure zero.

Another important observation is that, in the j-th column or row of a planar matrix, all Feynman diagrams are free of particle j and the compatibility condition (5.6) requires

$$d_{kl}^{(ij)} = d_{li}^{(kj)} = d_{ik}^{(lj)}, \tag{5.11}$$

for every three different particles i, k, l of the remaining $n-1$ particles. This means the j-th column or row is nothing but a planar collection of Feynman diagrams. Each column of a planar matrix is therefore made out of planar collections of $(3, n-1)$. Besides, once several columns have been fixed, the remaining columns have much less choices because of the symmetry requirement of the matrix. This simple but powerful observation leads to the second kind of combinatorial bootstrap, which we describe next.

5.3.1 Second Combinatorial Bootstrap

Suppose we have obtained all of the N planar collections for the ordering $(1, 2, \cdots, n-1)$. Let us denote the set of all such collections as $E_{3,n-1} = \{\mathcal{C}_1, \mathcal{C}_2, \cdots, \mathcal{C}_N\}$. The last column $\{T^{(1,n)}, T^{(2,n)}, \cdots, T^{(n-1,n)}\}$ (here we have omitted the trivial empty tree $\emptyset$) of any planar matrix $\mathcal{M}$, where by definition particles $1, 2, \cdots, n-1$ are deleted respectively in addition to the common missing particle n, must be an element of $E_{3,n-1}$.

Now we consider a cyclic permutation with respect to the order $(1, 2, \cdots, n-1, n)$ of particle labels of the set $E_{3,n-1}$,

$$E_{3,n-1}^{(a)} = \{\mathcal{C}_1^{(a)}, \mathcal{C}_2^{(a)}, \cdots, \mathcal{C}_N^{(a)}\} := E_{3,n-1}\big|_{i \to i+a}\,. \tag{5.12}$$

Clearly, particle labels are to be understood modulo n. One can see that $E_{3,n-1}^{(a)}$ is the set of all planar collections for the ordering $(1, 2, \cdots, a-1, a+1, \cdots, n)$ with particle a absent. By definition, we have $E_{3,n-1}^{(n)} \equiv E_{3,n-1}^{(0)} \equiv E_{3,n-1}$. The a-th column $\{T^{(1,a)}, T^{(2,a)}, \cdots, T^{(a-1,a)}, T^{(a+1,a)}, \cdots, T^{(n-1,a)}\}$ (here we have once again omitted the trivial tree $\emptyset$) of a planar matrix $\mathcal{M}$ must belong to the set $E_{3,n-1}^{(a)}$. Thus any planar matrix of Feynman diagrams must take the form

$$\mathcal{M} = [\mathcal{C}^{(1)}_{i_1}, \mathcal{C}^{(2)}_{i_2}, \cdots, \mathcal{C}^{(n)}_{i_n}]\,, \quad \text{with } 1 \leq i_1, \cdots, i_n \leq N\,. \tag{5.13}$$

Naively, we have N choices for each column and hence N^n candidate planar matrices. In principle, one could take this set of N^n matrices and impose the compatibility condition on the metrics thus reducing the set to that of all planar matrices of Feynman diagrams. However, this procedure is impractical already for $n = 7$ where $N = 693$.

Luckily, according to the Lemma 5.3.2, the symmetry requirement of a planar matrix reduces this number dramatically. It is much more efficient to find possible planar matrices from all of the symmetric matrices of the form (5.13). Using this method we have obtained all planar matrices up to $n = 9$. Table 5.2 is a summary of our results.

	$(\mathbf{4,6})$	$(\mathbf{4,7})$	$(\mathbf{4,8})$	$(\mathbf{4,9})$
Planar Matrices	14	693	90 608	30 659 424
Degenerate Matrices	0	0	888	2 523 339

Table 5.2: Number of planar matrices of Feynman diagrams and number of degenerate matrices for different values of n.

More explicitly, when this method is applied to $(k, n) = (4, 6)$, we obtain exactly all 14 planar matrices, which are dual to the $C_4 = 14$ planar Feynman diagrams of $(2, 6)$. As there are 693 planar collections in $(3, 7)$, the duality between $(3, 7)$ and $(4, 7)$ implies that there should be 693 planar matrices in (4,7) as well. In fact, our combinatorial bootstrap procedure results in exactly that number! Moreover, in section 5.4 we explain how the 693 planar matrices of Feynman diagrams map one to one onto the 693 planar collections via the duality.

Our second set of new results corresponds to the more interesting cases of $(4, 8)$ and $(4, 9)$, where our procedure leads to 91 416 and 33 182 763 symmetric matrices respectively.

Having the set of all possible candidate matrices, we further determined that 90 608 and 30 659 424 of them respectively satisfy the compatibility conditions (5.6) while not becoming degenerate and thus get these numbers of planar matrices of Feynman diagrams. We see that in both cases, the combinatorial bootstrap came very close to the correct answer. We comment that the extra 888 and 2 523 339 "offending" symmetric matrices are actually degenerate planar matrices. This means that if we were to use all matrices obtained from the bootstrap in the formula for the amplitude we would still get the correct answer since the extra matrices integrate to zero under the formula (5.10). So we can just use all of the symmetric matrices to calculate the biadjoint amplitudes for $k = 4$ as well.

Below we show two explicit examples for $n = 6, 7$ in order to illustrate the procedure. These examples show why this is an efficient technique for getting planar matrices from collections of $(3, n-1)$. Details on the results for $(4, 8)$ and $(4, 9)$ and the ancillary files where the collections are presented are provided in the original paper [74].

5.3.2 A Simple Example: From $(3, 5)$ to $(4, 6)$

Now we proceed to show an explicit example of how to obtain planar matrices of Feynman diagrams for $(4, 6)$. In this example, given the duality $(4, 6) \sim (2, 6)$, we could obtain the planar matrices by picking $n = 6$ Feynman diagrams in $k = 2$ and remove two leaves in a systematic way as shown in figure 5.3. Here, however, we introduce an algorithm to get the matrices using a second bootstrap approach constrained by the consistency conditions explained above, thus obtaining planar matrices from planar collections of Feynman diagrams of $(3, 5)$.

This algorithm works for general n, i.e. it obtains planar matrices of $(4, n)$ from planar collections of $(3, n-1)$, and is going to be particularly useful for larger n, where the number of matrices is considerably large.

Before going through the algorithm, let's review the planar collections of $(3,5)$. There are 5 planar collections of Feynman diagrams $E_{3,5} = \{\mathcal{C}_1, \mathcal{C}_2, \mathcal{C}_3, \mathcal{C}_4, \mathcal{C}_5\}$ [42]. These can come from the caterpillar tree in $n = 5$ and its 4 cyclic permutations, shown in figure 5.4.

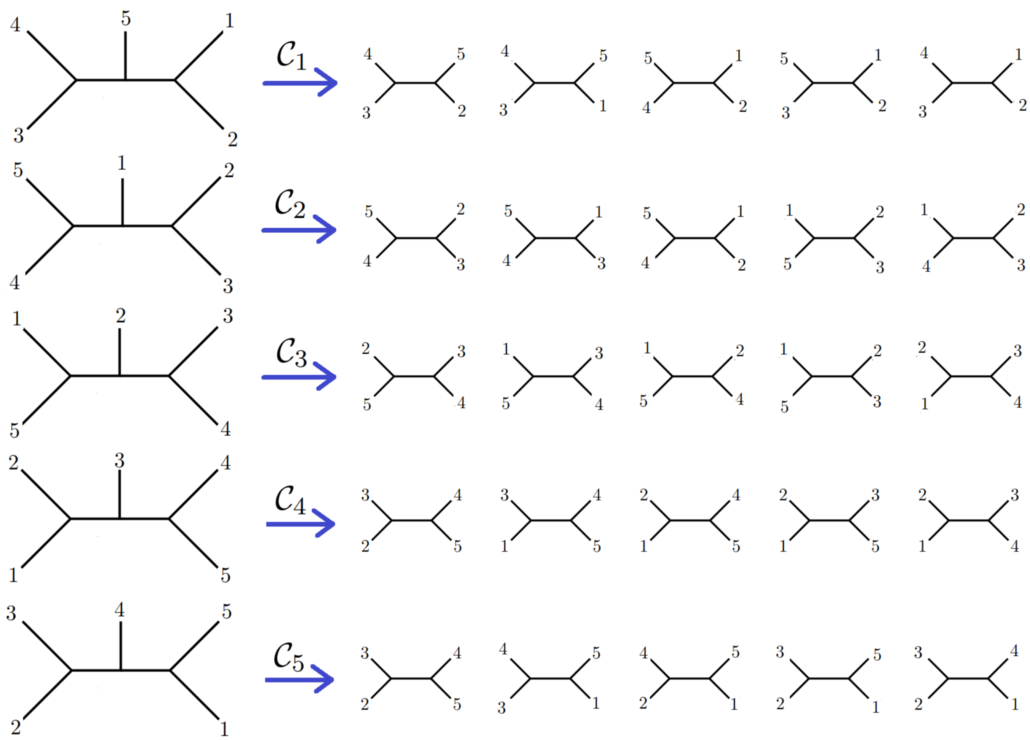

Figure 5.4: The five $k = 2$ planar Feynman diagrams and their corresponding collections in $(k,n) = (3,5)$.

In what follows, we will adopt the notation $T[ab|cd]$ for a 4-point Feynman diagram with a, b and c, d sharing a vertex, i.e.

$$T[ab|cd] := \tag{5.14}$$

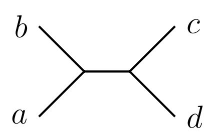

By applying cyclic permutations (5.12) on $E_{3,5}$ we get the set $E_{3,5}^{(1)}$, $E_{3,5}^{(2)}$, $\cdots$, $E_{3,5}^{(6)}$ with $E_{3,5}^{(6)} = E_{3,5}$. In the more compact notation defined above we have, for instance [3]

$$
\begin{aligned}
E_{3,5}^{(1)} &= \{\mathcal{C}_1^{(1)}, \mathcal{C}_2^{(1)}, \mathcal{C}_3^{(1)}, \mathcal{C}_4^{(1)}, \mathcal{C}_5^{(1)}\} \\
&= \left\{ \begin{matrix} T[45|63] \\ T[45|62] \\ T[23|56] \\ T[23|46] \\ T[23|45] \end{matrix} \,,\, \begin{matrix} T[34|56] \\ T[24|56] \\ T[23|56] \\ T[34|62] \\ T[34|52] \end{matrix} \,,\, \begin{matrix} T[45|63] \\ T[45|62] \\ T[35|62] \\ T[34|62] \\ T[23|45] \end{matrix} \,,\, \begin{matrix} T[34|56] \\ T[24|56] \\ T[23|56] \\ T[23|46] \\ T[23|45] \end{matrix} \,,\, \begin{matrix} T[34|56] \\ T[45|62] \\ T[35|62] \\ T[34|62] \\ T[34|52] \end{matrix} \right\} ,
\end{aligned} \tag{5.15}
$$

$$
\begin{aligned}
E_{3,5}^{(2)} &= \{\mathcal{C}_1^{(2)}, \mathcal{C}_2^{(2)}, \mathcal{C}_3^{(2)}, \mathcal{C}_4^{(2)}, \mathcal{C}_5^{(2)}\} \\
&= \left\{ \begin{matrix} T[34|56] \\ T[14|56] \\ T[13|56] \\ T[34|61] \\ T[34|51] \end{matrix} \,,\, \begin{matrix} T[45|63] \\ T[45|61] \\ T[35|61] \\ T[34|61] \\ T[13|45] \end{matrix} \,,\, \begin{matrix} T[34|56] \\ T[14|56] \\ T[13|56] \\ T[13|46] \\ T[13|45] \end{matrix} \,,\, \begin{matrix} T[34|56] \\ T[45|61] \\ T[35|61] \\ T[34|61] \\ T[34|51] \end{matrix} \,,\, \begin{matrix} T[45|63] \\ T[45|61] \\ T[13|56] \\ T[13|46] \\ T[13|45] \end{matrix} \right\} .
\end{aligned} \tag{5.16}
$$

The idea of the second bootstrap is that each column of a planar matrix is a planar collection. In other words, a planar matrix must take the form

$$
\mathcal{M} = [\mathcal{C}_{i_1}^{(1)}, \mathcal{C}_{i_2}^{(2)}, \cdots, \mathcal{C}_{i_6}^{(6)}] , \quad \text{with } 1 \le i_1, \cdots, i_6 \le 5 , \tag{5.17}
$$

[3]Here, for example, one can see the cyclic permutation $\{1 \to 3, 2 \to 4, 3 \to 5, 4 \to 6, 5 \to 1, 6 \to 2\}$ of $\mathcal{C}_1$ as $\{T[45|63], T[45|62], T[23|56], T[23|46], T[23|45]\}$ with the leaves 3, 4, 5, 6 and 1 pruned, respectively, in addition to the common missing leaf 2. We rotate the list from right by 1 to get a planar collection $\mathcal{C}_1^{(2)}$ with the leaves 1, 3, 4, 5 and 6 pruned, respectively.

where each element in $\mathcal{M}$ corresponds to a column, thus the i-th column belongs to the set $E_{3,5}^{(i)}$ subject to the i-th permutation. There are five choices for the first column, since there are five collections in $(3,5)$. However, once one of the collections is chosen, the choices for the remaining five columns get substantially reduced. For example, let's choose the first column of the matrix to be the first collection $\mathcal{C}_1^{(1)}$. The symmetry of the matrix implies $T^{(1,2)} = T^{(2,1)}$, thus the first tree of the second column $\mathcal{C}_{i_2}^{(2)}$ must be the first tree of the first column, i.e. $T[45|63]$ [4]. By looking at (5.15) and (5.16) we find that only $\mathcal{C}_2^{(2)}$ and $\mathcal{C}_5^{(2)}$ satisfy this requirement. Similarly, we select candidates from $E_{3,5}^{(i)}$ by again imposing the symmetry condition $T^{(1,i)} = T^{(i,1)}$ now for $i = 3,4,5,6$ (see figure 5.5 for a sketch).

$$
\begin{array}{cccccc}
E_{3,5}^{(1)} & E_{3,5}^{(2)} & E_{3,5}^{(3)} & E_{3,5}^{(4)} & E_{3,5}^{(5)} & E_{3,5}^{(6)} \\
\text{Choose } \mathcal{C}_1^{(1)} \text{ as } \xrightarrow{} \text{ the first column} & \downarrow & \downarrow & \downarrow & \downarrow & \downarrow \\
 & \{\mathcal{C}_2^{(2)}, \mathcal{C}_5^{(2)}\} & \{\mathcal{C}_1^{(3)}, \mathcal{C}_4^{(3)}\} & \{\mathcal{C}_1^{(4)}, \mathcal{C}_2^{(4)}, \mathcal{C}_4^{(4)}\} & \{\mathcal{C}_1^{(5)}, \mathcal{C}_3^{(5)}, \mathcal{C}_5^{(5)}\} & \{\mathcal{C}_2^{(6)}, \mathcal{C}_4^{(6)}, \mathcal{C}_5^{(6)}\} \\
 & \text{Choose } \mathcal{C}_2^{(2)} \text{ as } \xrightarrow{} \text{ the second column} & \downarrow & \downarrow & \downarrow & \downarrow \\
 & & \{\mathcal{C}_1^{(3)}, \mathcal{C}_4^{(3)}\} & \{\mathcal{C}_2^{(4)}\} & \{\mathcal{C}_1^{(5)}\} & \{\mathcal{C}_2^{(6)}, \mathcal{C}_4^{(6)}\} \\
 & & \text{Choose } \mathcal{C}_1^{(3)} \text{ as } \xrightarrow{} \text{ the third column} & \downarrow & \downarrow & \downarrow \\
 & & & \{\mathcal{C}_2^{(4)}\} & \{\mathcal{C}_1^{(5)}\} & \{\mathcal{C}_2^{(6)}\}
\end{array}
$$

Figure 5.5: Illustration of the second combinatorial bootstrap for obtaining planar matrices of Feynman diagrams. Here we choose $\mathcal{C}_1^{(1)}$, $\mathcal{C}_2^{(2)}$ and $\mathcal{C}_1^{(3)}$ as the first three columns and then get a symmetric planar matrix by filling in the remaining three columns with $\mathcal{C}_2^{(4)}$, $\mathcal{C}_1^{(5)}$ and $\mathcal{C}_2^{(6)}$. See also table 5.3.

With this approach, the number of choices for the remaining 5 columns has been reduced from the naive $5^5 = 3\,125$ to $2 \times 2 \times 3 \times 3 \times 3 = 108$. Therefore, we can now forget about the first column and focus on the possible 108 choices for the remaining 5 columns. Let's

[4] Recall that $\mathcal{C}_1^{(1)} = \{T[45|63], T[45|62], T[23|56], T[23|46], T[23|45]\}$.

for instance choose $\mathcal{C}_2^{(2)} = \{T[45|63], T[45|61], T[35|61], T[34|61], T[13|45]\}$ for the second column of the matrix. Because of the symmetry condition $T^{(2,i)} = T^{(i,2)}$ in (5.7), only one or two candidates are selected for each of the remaining four columns, see third row in figure 5.5.

By going on with the procedure above, we end up with a planar matrix of Feynman diagrams

$$
\begin{aligned}
&[\mathcal{C}_1^{(1)}, \mathcal{C}_2^{(2)}, \mathcal{C}_1^{(3)}, \mathcal{C}_2^{(4)}, \mathcal{C}_1^{(5)}, \mathcal{C}_2^{(6)}] \\
&= \begin{bmatrix}
\emptyset & T[45|63] & T[45|62] & T[23|56] & T[23|46] & T[23|45] \\
T[45|63] & \emptyset & T[45|61] & T[35|61] & T[34|61] & T[13|45] \\
T[45|62] & T[45|61] & \emptyset & T[25|61] & T[24|61] & T[12|45] \\
T[23|56] & T[35|61] & T[25|61] & \emptyset & T[23|61] & T[23|51] \\
T[23|46] & T[34|61] & T[24|61] & T[23|61] & \emptyset & T[23|41] \\
T[23|45] & T[13|45] & T[12|45] & T[23|51] & T[23|41] & \emptyset
\end{bmatrix},
\end{aligned}
\tag{5.18}
$$

which happens to be $\mathcal{M}_1$ in table 5.3 on the next page and is also the example shown in figure 5.3.

Had we chosen $\mathcal{C}_5^{(2)}$ for the second column instead of $\mathcal{C}_2^{(2)}$, we would have found another two planar matrices using the same procedure, which correspond to $\mathcal{M}_2$ and $\mathcal{M}_3$ in table 5.3. Hence, we find a total of 3 planar matrices for the initial choice $\mathcal{C}_1^{(1)}$.

Likewise, one finds 3, 2, 4 and 2 planar matrices for the initial choices $\mathcal{C}_2^{(1)}$, $\mathcal{C}_3^{(1)}$, $\mathcal{C}_4^{(1)}$ and $\mathcal{C}_5^{(1)}$, respectively, thus giving 14 planar matrices in total. One can check that all these 14 matrices satisfy the compatibility conditions (5.6). Therefore, all of them contribute to the biadjoint amplitude in $k = 3$.

In table 5.3 we present all 14 planar matrices of Feynman diagrams in $(4, 6)$, explicitly showing the corresponding collections in each column.

Matrix	Collections	Matrix	Collections
$\mathcal{M}_1$	$[\mathcal{C}_1, \mathcal{C}_2, \mathcal{C}_1, \mathcal{C}_2, \mathcal{C}_1, \mathcal{C}_2]$	$\mathcal{M}_8$	$[\mathcal{C}_3, \mathcal{C}_2, \mathcal{C}_1, \mathcal{C}_5, \mathcal{C}_4, \mathcal{C}_4]$
$\mathcal{M}_2$	$[\mathcal{C}_1, \mathcal{C}_5, \mathcal{C}_4, \mathcal{C}_4, \mathcal{C}_3, \mathcal{C}_2]$	$\mathcal{M}_9$	$[\mathcal{C}_4, \mathcal{C}_4, \mathcal{C}_3, \mathcal{C}_2, \mathcal{C}_1, \mathcal{C}_5]$
$\mathcal{M}_3$	$[\mathcal{C}_1, \mathcal{C}_5, \mathcal{C}_4, \mathcal{C}_1, \mathcal{C}_5, \mathcal{C}_4]$	$\mathcal{M}_{10}$	$[\mathcal{C}_4, \mathcal{C}_1, \mathcal{C}_5, \mathcal{C}_4, \mathcal{C}_1, \mathcal{C}_5]$
$\mathcal{M}_4$	$[\mathcal{C}_2, \mathcal{C}_4, \mathcal{C}_3, \mathcal{C}_2, \mathcal{C}_4, \mathcal{C}_3]$	$\mathcal{M}_{11}$	$[\mathcal{C}_4, \mathcal{C}_3, \mathcal{C}_2, \mathcal{C}_4, \mathcal{C}_3, \mathcal{C}_2]$
$\mathcal{M}_5$	$[\mathcal{C}_2, \mathcal{C}_1, \mathcal{C}_5, \mathcal{C}_4, \mathcal{C}_4, \mathcal{C}_3]$	$\mathcal{M}_{12}$	$[\mathcal{C}_4, \mathcal{C}_3, \mathcal{C}_2, \mathcal{C}_1, \mathcal{C}_5, \mathcal{C}_4]$
$\mathcal{M}_6$	$[\mathcal{C}_2, \mathcal{C}_1, \mathcal{C}_2, \mathcal{C}_1, \mathcal{C}_2, \mathcal{C}_1]$	$\mathcal{M}_{13}$	$[\mathcal{C}_5, \mathcal{C}_4, \mathcal{C}_4, \mathcal{C}_3, \mathcal{C}_2, \mathcal{C}_1]$
$\mathcal{M}_7$	$[\mathcal{C}_3, \mathcal{C}_2, \mathcal{C}_4, \mathcal{C}_3, \mathcal{C}_2, \mathcal{C}_4]$	$\mathcal{M}_{14}$	$[\mathcal{C}_5, \mathcal{C}_4, \mathcal{C}_1, \mathcal{C}_5, \mathcal{C}_4, \mathcal{C}_1]$

Table 5.3: Planar matrices of Feynman diagrams in $(4,6)$. Here we abbreviate $[\mathcal{C}_{i_1}^{(1)}, \mathcal{C}_{i_2}^{(2)}, \cdots, \mathcal{C}_{i_6}^{(6)}]$ as $[\mathcal{C}_{i_1}, \mathcal{C}_{i_2}, \cdots, \mathcal{C}_{i_6}]$ since the superscripts can be inferred from the position of $\mathcal{C}_i$ in the brackets.

5.3.3 A More Interesting Example: From $(3,6)$ to $(4,7)$

Now we comment on another example, in this case on how to obtain planar matrices of Feynman diagrams for $(4,7)$ using the second bootstrap again. The starting point are the 48 planar collections of (3,6), i.e. $E_{3,6} = \{\mathcal{C}_1, \mathcal{C}_2, \cdots, \mathcal{C}_{48}\}$, which can be obtained from the first bootstrap. The cyclic permutations (5.12) give the set $E_{3,6}^{(1)}$, $E_{3,6}^{(2)}$, $\cdots$, $E_{3,6}^{(7)}$ with $E_{3,6}^{(7)} = E_{3,6}$. Then a planar matrix must take the form

$$\mathcal{M} = [\mathcal{C}_{i_1}^{(1)}, \mathcal{C}_{i_2}^{(2)}, \cdots, \mathcal{C}_{i_7}^{(7)}], \quad \text{with } 1 \le i_1, \cdots, i_7 \le 48, \tag{5.19}$$

where the i-th column belongs to the set $E_{3,6}^{(i)}$. Now we have 48 choices for the first column. Once again, we repeat the same procedure as before but now for 7 columns, and we get 693 planar matrices. One can check that all these 693 symmetric matrices satisfy the compatibility conditions (5.6). Therefore, all of them are planar matrices and contribute to the biadjoint amplitude in $k = 4$.

After summing over every choice of the first column as well as every possible choice for the remaining columns allowed by the candidates at each step, we get 693 symmetric matrices in total, which are much more than the 42 initial planar matrices for $(4, 7)$ used in the pruning-mutation procedure of section 5.2. There are 693 planar collections in $(3, 7)$ as well and how they are dual to 693 planar matrices is explained in section 5.4.

The ordering of collections in $E_{3,6}$ is not relevant as long as its cyclic permutations $E_{3,6}^{(1)}, \cdots, E_{3,6}^{(7)}$ change covariantly. For the readers' convenience, we borrow Table 1 from [42] containing all 48 collections and place it as table H.1 in appendix H. We adopt the same ordering notation as in [42] so that we can present more details of the second bootstrap. A collection in table H.1 is given by 6 trees characterized by 6 numbers. For example, the first collection $\mathcal{C}_1$ expressed by $[4, 4, 4, 3, 3, 3]$ means the collection given in figure 5.2, where the "middle leaves" are 4, 4, 4, 3, 3 and 3 respectively. Its cyclic permutations give $\mathcal{C}_1^{(1)}, \mathcal{C}_1^{(2)}, \cdots, \mathcal{C}_1^{(7)}$ with $\mathcal{C}_1^{(7)} = \mathcal{C}_1$, which act as the first element of $E_{3,6}^{(1)}, E_{3,6}^{(2)}, \cdots, E_{3,6}^{(7)}$ respectively.

If we choose $\mathcal{C}_1^{(1)}$ as the first column, it happens that from each $E_{3,6}^{(2)}, \cdots, E_{3,6}^{(7)}$ there are 14 collections satisfying the symmetry requirement $T^{(1,i)} = T^{(i,1)}$. For example, for the second and third column, their 14 possible choices of collections are

$$\mathcal{C}_1^{(2)}, \mathcal{C}_{15}^{(2)}, \mathcal{C}_{19}^{(2)}, \mathcal{C}_{24}^{(2)}, \mathcal{C}_{26}^{(2)}, \mathcal{C}_{34}^{(2)}, \mathcal{C}_{39}^{(2)}, \mathcal{C}_{42}^{(2)}, \mathcal{C}_{43}^{(2)}, \mathcal{C}_{44}^{(2)}, \mathcal{C}_{45}^{(2)}, \mathcal{C}_{46}^{(2)}, \mathcal{C}_{47}^{(2)}, \mathcal{C}_{48}^{(2)}, \tag{5.20}$$

$$\mathcal{C}_3^{(3)}, \mathcal{C}_7^{(3)}, \mathcal{C}_{10}^{(3)}, \mathcal{C}_{14}^{(3)}, \mathcal{C}_{17}^{(3)}, \mathcal{C}_{21}^{(3)}, \mathcal{C}_{28}^{(3)}, \mathcal{C}_{31}^{(3)}, \mathcal{C}_{32}^{(3)}, \mathcal{C}_{33}^{(3)}, \mathcal{C}_{36}^{(3)}, \mathcal{C}_{38}^{(3)}, \mathcal{C}_{41}^{(3)}, \mathcal{C}_{48}^{(3)}. \tag{5.21}$$

We see that the naive number of choices for the remaining 6 columns reduces from $48^6 \sim 1 \times 10^{10}$ down to $14^6 \sim 8 \times 10^6$.

Now we can forget the first column and focus on the 14^6 candidates for the remaining 6 columns. If we choose $\mathcal{C}_1^{(2)}$ from (5.20) as the second column, we find only one collection

$\mathcal{C}_{48}^{(3)}$ from (5.21) that satisfies the requirement $T^{(2,3)} = T^{(3,2)}$. Similarly, we find that there is only one collection from 14 candidates for the remaining 4 columns satisfying the requirement $T^{(2,i)} = T^{(i,2)}$ as well for $i = 4, 5, 6, 7$. This time we see that the naive number of choices for the remaining five columns dramatically reduces from $14^5 \sim 5 \times 10^5$ to 1. Hence the only choice that makes up a planar matrix of the form (5.19) is

$$[\mathcal{C}_1^{(1)}, \mathcal{C}_1^{(2)}, \mathcal{C}_{48}^{(3)}, \mathcal{C}_{41}^{(4)}, \mathcal{C}_{27}^{(5)}, \mathcal{C}_{18}^{(6)}, \mathcal{C}_8^{(7)}] \,. \tag{5.22}$$

Had we chosen the remaining collections $\mathcal{C}_{15}^{(2)}, \cdots, \mathcal{C}_{47}^{(2)}$ or $\mathcal{C}_{48}^{(2)}$ in (5.20) as the second column instead of $\mathcal{C}_1^{(2)}$, we would have found 1, 2, 1, 2, 1, 2, 2, 2, 1, 2, 3, 3 and 9 planar matrices respectively. Thus there are 32 planar matrices in total with $\mathcal{C}_1^{(1)}$ as the first column. Similarly, we can get all of the planar matrices with $\mathcal{C}_2^{(1)}, ..., \mathcal{C}_{47}^{(1)}$ or $\mathcal{C}_{48}^{(1)}$ as the first column of the matrix. By adding them up, including the 32 ones for $\mathcal{C}_1^{(1)}$, we obtain all the 693 planar matrices in $(4, 7)$.

We computed all the planar collections of Feynman diagrams for the cases $(3, 6)$, $(3, 7)$, $(3, 8)$ and $(3, 9)$ using the first combinatorial bootstrap, as well as all the planar matrices of Feynman diagrams for $(4, 7)$, $(4, 8)$ and $(4, 9)$ using the second combinatorial bootstrap, and we refer the reader to [74, section 4] for a detailed explanation.

5.4 Higher k or Planar Arrays of Feynman Diagrams and Duality

Planar collections can be thought of as one-dimensional arrays while planar matrices as two-dimensional arrays of Feynman diagrams satisfying certain conditions. It is natural to propose that the computation of generalized biadjoint amplitudes for any (k, n) can be done using $k-2$ dimensional arrays of Feynman diagrams.

Definition 5.4.1. *A planar array of Feynman diagrams is a $(k-2)$-dimensional array $\mathcal{A}$ with dimensions of size n. The array has as component $\mathcal{A}_{i_1,i_2,\ldots,i_{k-2}}$ a metric tree with leaves in the set $\{1,2,\ldots,n\}\setminus\{i_1,i_2,\ldots,i_{k-2}\}$ and which is planar with respect to the ordering $(1,2,\cdots,\not{i}_1,\cdots,\not{i}_2,\cdots,\not{i}_{k-2},\cdots,n)$ satisfying the following conditions*

- *Diagonal entries are the empty tree $\mathcal{A}_{\ldots,i,\ldots,i,\ldots}=\emptyset$.*
- *Compatibility: $d_{i_1 i_2}^{(i_3,\ldots,i_k)}$ is completely symmetric in all k indices.*

A point which has not been explained so far is why each element in a collection, matrix or in general an array is called a Feynman diagram. We now turn to this point. The contribution to an amplitude of a given planar array of Feynman diagrams is computed using the function

$$\mathcal{F}(\mathcal{A})=\sum_{i_1,i_2,\ldots,i_k}\mathsf{s}_{i_1 i_2\cdots i_k}d_{i_1 i_2}^{(i_3,\ldots,i_k)}. \tag{5.23}$$

For $k=2$ it is easy to show that this function is independent of the external edge's lengths by writing $d_{ij}=e_i+e_j+d_{ij}^{\text{internal}}$ and using momentum conservation. For $k=3$ it was noted in [42] that the function $\mathcal{F}(\mathcal{C})$ can also be written in a way that it is also independent of the external edges. However, the proof is not as straightforward. In order to easily see this property all we have to do is to treat each tree in the array as a true Feynman diagram with its own kinematics.

The element in the array $\mathcal{A}_{i_1,i_2\ldots,i_{k-2}}$ is an $(n-k+2)$-particle Feynman diagram with particle labels $\{1,2,\ldots,n\}\setminus\{i_1,i_2\ldots,i_{k-2}\}$. As such, one has to associate the proper kinematic invariants satisfying momentum conservation. Let us introduce the notation

$\mathcal{I} := \{i_1, i_2 \ldots, i_{k-2}\}$ and $\overline{\mathcal{I}}$ for its complement. Then we have

$$s_{ii}^{(\mathcal{I})} = 0, \quad \sum_{j\in\overline{\mathcal{I}}} s_{ij}^{(\mathcal{I})} = 0 \quad \forall i \in \overline{\mathcal{I}}. \tag{5.24}$$

Using these kinematic invariants one can parametrize the (k, n) invariants as

$$\mathsf{s}_{i_1 i_2 \ldots i_k} := \sum_{\mathcal{I}\cup\{j_1,j_2\}=\{i_1,i_2,\ldots,i_k\}} s_{j_1,j_2}^{(\mathcal{I})}, \tag{5.25}$$

where the sum is over all possible ways of decomposing $\{i_1, i_2, \ldots, i_k\}$ into two sets of $k-2$ and 2 elements respectively. To illustrate the notation consider $k = 3$ where

$$\mathsf{s}_{ijk} := s_{jk}^{(i)} + s_{ki}^{(j)} + s_{ij}^{(k)}. \tag{5.26}$$

This parametrization is very redundant but as any good redundancy it makes at least one property of the relevant object manifest. In this case it is the independence of the external edges of $\mathcal{F}(\mathcal{A})$. Let us continue with the $k = 3$ case in order not to clutter the notations but the general k version is clear. Using (5.26) one can write

$$\mathcal{F}(\mathcal{C}) = \sum_{i,j,k} \mathsf{s}_{ijk} d_{jk}^{(i)} \tag{5.27}$$

as

$$\mathcal{F}(\mathcal{C}) = \frac{1}{3}\sum_{i=1}^{n}\sum_{j,k} s_{jk}^{(i)} d_{jk}^{(i)}. \tag{5.28}$$

Here we used the symmetry property of $d_{jk}^{(i)}$ to identify all three terms coming from using (5.26). The new form is nothing but a sum over the functions $F(T)$ for each of the trees in the collection and therefore it is clearly independent of the external edges as expected.

Let us now discuss how the two kinds of combinatorial bootstraps work for general planar arrays of Feynman diagrams. The first kind of combinatorial bootstrap, which we called pruning-mutating in section 5.2, is simply the process of producing C_{n-2} initial arrays of Feynman diagrams by starting with any given n-point planar Feynman diagram and pruning $k-2$ of its leaves in all possible ways to end up with an array of $(n-k+2)$-point Feynman diagrams. Starting from these initial planar arrays, one computes the corresponding metrics and find all their possible degenerations. Approaching each degeneration one at a time one can produce a new planar array by resolving the degeneration only in the other planar possible way. Repeating the mutation procedure on all new arrays generated until no new array is found leads to the full set of planar arrays of Feynman diagrams.

The second kind of combinatorial bootstrap, as described in section 5.3 for planar matrices, is the idea that the compatibility conditions on the metrics of the trees making the array force it to be completely symmetric. This simple observation together with the fact that any subarray where some indices are fixed must in itself be a valid planar array of Feynman diagrams for some smaller values of k and n gives strong constrains on the objects. As it should be clear from the examples presented in section 5.3, the second bootstrap approach is more efficient than the first one if all planar arrays in $(k-1, n-1)$ are known. This means that one could start with $(3,6)$ and produce the following sequence:

$$(3,6) \to (4,7) \to (5,8) \to (6,9) \to (7,10)\dots \tag{5.29}$$

The reason to consider this sequence is that after obtaining all its elements, one can construct all $(3,n)$ planar collections via duality. Of course, in order to do that efficiently one has to find a combinatorial way of performing the duality directly at the level of the graphs.

5.4.1 Combinatorial Duality

Let us start by defining some notation that will be used in this section. We will denote T_n as a planar tree in $(2,n)$, $\mathcal{C}_n$ as a planar collection in $(3,n)$ and $\mathcal{M}_n$ as a planar matrix in $(4,n)$. In general, a planar array $\mathcal{A}_n$ will correspond to a $(k-2)$-dimensional array with dimensions of size n. In order to understand how the combinatorial duality works, we also introduce the concept of combinatorial soft limit. The combinatorial soft limit for particle i applied to $\mathcal{A}_n$ is defined by removing the i-th $(k-3)$-dimensional array from $\mathcal{A}_n$, as well as removing the i-th label to the remaining $(k-3)$-dimensional arrays. Therefore, the combinatorial soft limit takes us from $(k,n) \to (k,n-1)$.

It is useful to introduce a superscript $\mathcal{A}_n^{(i)}$ to refer to an array obtained from a combinatorial soft limit for particle i. Notice that this notation slightly differs from the one we use in earlier sections.

With this in hand, we can define the particular duality $(2,n) \sim (n-2,n)$ as taking the tree T_n of $(2,n)$ and applying the combinatorial soft limit to particles $i_1,...,i_{n-2}$ in order to remove $n-2$ leaves to obtain the corresponding dual $\mathcal{A}_{n-2}^{(i_1,...,i_{n-2})}$ of $(n-2,n)$.

For general (k,n) with $k < n-2$ the duality works as follows. Consider a $(k-2)$-dimensional planar array $\mathcal{A}_n$ of (k,n). By taking the combinatorial soft limit for particle i, we end up with $\mathcal{A}_{n-1}^{(i)}$ of $(k,n-1)$. Apply this step n times for all the n particles. Now dualize each of the n objects to directly obtain the corresponding $(n-k-2)$-dimensional array $\mathcal{A}_n$ of $(n-k,n)$, hence the duality. The combinatorial duality can be simply summarized as

$$(k,n) \xrightarrow[\text{limit}]{\text{soft}} n \times (k,n-1) \xrightarrow[\text{dualize}]{} (n-k,n) \tag{5.30}$$

Illustrative example: $(3,7) \sim (4,7)$

Now we proceed to show the explicit example for $(3,7) \sim (4,7)$. The combinatorial soft limit for particle i applied to a planar collection $\mathcal{C}_n$ corresponds to removing the i-th tree in $\mathcal{C}_n$ as well as removing the i-th label in all the rest of the trees in $\mathcal{C}_n$. Therefore, it implies $\mathcal{C}_n \to \mathcal{C}_{n-1}^{(i)}$. Similarly, the combinatorial soft limit for particle i applied to a planar matrix $\mathcal{M}_n$ corresponds to removing the i-th column and row in $\mathcal{M}_n$ as well as removing the i-th label in all the rest of the trees in $\mathcal{M}_n$. Therefore, it implies $\mathcal{M}_n \to \mathcal{M}_{n-1}^{(i)}$.

Before studying $(3,7) \sim (4,7)$ let us consider $(3,6) \sim (3,6)$ as this will be useful below. Using (5.30) we can see

$$(3,6) \xrightarrow[\text{limit}]{\text{soft}} 6 \times (3,5) \xrightarrow[\text{dualize}]{} (3,6) \tag{5.31}$$

where the duality $(2,5) \sim (3,5)$ is one of the most basic ones which was used as a motivation for introducing planar collections in [42].

Now consider one planar collection $\mathcal{C}_{n=7}$ of $(3,7)$. By taking the combinatorial soft limit for particle i, we end up with a collection $\mathcal{C}_{n=6}^{(i)}$ in $(3,6)$. Given that $(3,6) \sim (3,6)$, this collection is dual to another collection $\tilde{\mathcal{C}}_{n=6}^{(i)}$, which corresponds to the i-th column of a planar matrix $\mathcal{M}_{n=7}$ in $(4,7)$. This means that if we now take the combinatorial soft limit for the other particles in $\mathcal{C}_{n=7}$ we end up with the full matrix $\mathcal{M}_{n=7}$. Hence, the objects $\mathcal{C}_{n=7}$ and $\mathcal{M}_{n=7}$ are dual.

We can also see this by following an equivalent path. Consider one planar matrix $\mathcal{M}_{n=7}$ of $(4,7)$. By taking the combinatorial soft limit for particle i, we end up with a planar matrix $\mathcal{M}_{n=6}^{(i)}$ of $(4,6)$. Notice that this matrix is dual to the planar tree $T_{n=6}^{(i)}$ of $(2,6)$ which is an element of $\mathcal{C}_{n=7}$, so by repeating the soft limit for all the remaining particles we end up with the full $\mathcal{C}_{n=7}$ of $(3,7)$.

5.5 Outlook

Generalized biadjoint amplitudes as defined by a CHY integral over the configuration space of n points in $\mathbb{CP}^{k-1}$ with $k > 2$ provide a very natural step beyond standard quantum field theory [71]. An equally natural generalization of quantum field theory amplitudes is obtained by first identifying standard Feynman diagrams with metric trees and their connection to $\mathrm{Trop}\, G(2,n)$. In [140], arrangements of metric trees where introduced as objects corresponding to $\mathrm{Trop}\, G(3,n)$. A special class of such arrangement, called planar collections of Feynman diagrams were then proposed as the simplest generalization of Feynman diagrams in [42]. In this work we introduced $(k-2)$-dimensional planar arrays of Feynman diagrams as the all k generalization. One of the most exciting phenomena is that these $(k-2)$-dimensional arrays define generalized biadjoint amplitudes.

The fact that both definitions of generalized amplitudes, either as a CHY integral or as a sum over arrays, coincide is non-trivial. In fact, a rigorous proof of this connection, perhaps along the lines of the proof for $k = 2$ given by Dolan and Goddard [94, 95], is a pressing problem. One possible direction is hinted by the observations made in section 5.4, where each Feynman diagram in an array was given its own kinematics along with its own metric. Of course, what makes the planar array interesting is the compatibility conditions for the metrics of the various trees in the array. Understanding the physical meaning of such conditions is also a very important problem. However, this already gives a hint as to what to do with the CHY integral. Borrowing the $k = 3$ example in section 5.4, the kinematics is parameterized as $\mathsf{s}_{ijk} = s^{(i)}_{jk} + s^{(j)}_{ik} + s^{(k)}_{ij}$. Recall that in the CHY formulation on $\mathbb{CP}^2$ introduced in [71] one starts with a potential function

$$\mathcal{S}^{(3)}_n := \sum_{i,j,k} \mathsf{s}_{ijk} \log |ijk| \tag{5.32}$$

with $|ijk|$ Plücker coordinates in $G(3,n)$. Even though the object is antisymmetric in all its indices, only its absolute value is relevant in $\mathcal{S}_n^{(3)}$ since the way it enters in the CHY formula is only via the equations needed for the computation of its critical points. This means that $|ijk|$ can be used to define "effective" $k=2$ Plücker coordinates of the form $|jk|^{(i)} := |ijk|$. In other words, once a label is selected, say i, then all other points in $\mathbb{CP}^2$ can be projected onto a $\mathbb{CP}^1$ using the i^{th}-point. This means that the potential $\mathcal{S}_n^{(3)}$ can be written as a sum over n $k=2$ potentials in a way completely analogous to $\mathcal{F}(\mathcal{C})$ in (5.28), i.e.

$$\mathcal{S}_n^{(3)} = \frac{1}{3}\sum_{i=1}^{n}\sum_{j,k} s_{jk}^{(i)}\,|jk|^{(i)}. \tag{5.33}$$

One can then write a $k=3$ CHY formula as a product over n $k=2$ CHY integrals linked by the "compatibility constraints" imposing that the absolute value of $|jk|^{(i)}$, $|ij|^{(k)}$, $|ik|^{(j)}$ all be equal.

The CEGM formula has paved the way for investigating a natural generalization of quantum field theory. Another generalization of quantum field theory, known as string theory, also also offered deep insights into various aspects of physical theories owing to its rich structure. One notable contribution of string theory comes from its ability to express a theory of quantum gravity as a conventional quantum field theory, an idea we will explore further in the upcoming chapter. It is exhilarating to contemplate the possibility of significant advancements resulting from the CEGM generalization. Some other recent developments partly related to the higher-k framework, which have not been mentioned in this thesis, can be found in [133, 97, 21, 67, 115, 2, 119, 3, 175, 139, 132, 135, 137, 17, 68, 43].

PART III

Holographic Quark Gluon Plasmas

In the third part of the thesis, we shift our focus from examining aspects of perturbative quantum field theory and its CEGM generalization and delve into the non-perturbative realm of strongly coupled gauge theories using the AdS/CFT correspondence introduced in chapter 1. In particular, and in the only chapter of this part, we use top-down holographic models to study the thermal equation of state of strongly coupled quark-gluon plasmas in an external magnetic field. We identify different conformal and non-conformal theories within consistent truncations of $\mathcal{N}=8$ gauged supergravity in five dimensions (including STU models and gauged $\mathcal{N}=2^*$ theory) and show that the ratio of the transverse to the longitudinal pressure P_T/P_L as a function of $T/\sqrt{B}$ can be collapsed to a "universal" curve for a wide range of the adjoint hypermultiplet masses m. We stress that this does not imply any hidden universality in magnetoresponse, as other observables do not exhibit any universality. Instead, the observed collapse in P_T/P_L is simply due to a strong dependence of the equation of state on the (freely adjustable) renormalization scale: in other words, it is simply a fitting artifact. Remarkably, we do uncover a different universality in $\mathcal{N}=2^*$ gauge theory in the external magnetic field: we show that the magnetized $\mathcal{N}=2^*$ plasma has a critical point at $T_{crit}/\sqrt{B}$ whose value varies by 2% (or less) as $m/\sqrt{B}\in[0,\infty)$. At criticality, and for large values of $m/\sqrt{B}$, the effective central charge of the theory scales as $\propto \sqrt{B}/m$.

Chapter 6

Quark-Gluon Plasmas in a Magnetic Field

6.1 Introduction and summary

In [112] the authors used the recent lattice QCD equation of state (EOS) data in the presence of a background magnetic field [27, 28], and the holographic EOS results[1] for the strongly coupled $\mathcal{N} = 4$ $SU(N)$ maximally supersymmetric Yang-Mills (SYM) to argue for a universal magnetoresponse. While $\mathcal{N} = 4$ SYM is conformal, the scale invariance is explicitly broken by the background magnetic field B and its thermal equilibrium stress-energy tensor is logarithmically sensitive to the choice of the renormalization scale. It was shown in [112] that both the QCD and the $\mathcal{N} = 4$ SYM data (with optimally adjusted

[1] Studied for the first time in [92].

renormalization scale) for the pressure anisotropy R,

$$R \equiv \frac{P_T}{P_L}\,, \tag{6.1}$$

i.e. defined as a ratio of the transverse P_T to the longitudinal P_L pressure, collapse onto a single universal curve as a function of $T/\sqrt{B}$, at least for $T/\sqrt{B} \gtrsim 0.2$ or correspondingly for $R \gtrsim 0.5$, see [112, figure 6]. The authors do mention that the "universality" is somewhat fragile: besides the obvious fact that large-N $\mathcal{N}=4$ SYM is not QCD (leading to inherent ambiguities as to how precisely one would match the renormalization schemes in both theories — hence the authors opted for the freely-adjustable renormalization scale in SYM), one observes the universality in R, but not in other thermodynamic quantities (e.g. $P_T/\mathcal{E}$ — the ratio of the transverse pressure to the energy density).

So, is there a universal magnetoresponse? In this chapter we address this question in a controlled setting: specifically, we consider holographic models of gauge theory/string theory correspondence [160, 8] where all the four-dimensional strongly coupled gauge theories discussed have the same ultraviolet fixed point: $\mathcal{N}=4$ SYM. We discuss two classes of theories:

- conformal gauge theories corresponding to different consistent truncations of $\mathcal{N}=8$ gauged supergravity in five dimensions[2] [41];
- nonconformal $\mathcal{N}=2^*$ gauge theory ($\mathcal{N}=4$ SYM with a mass term for the $\mathcal{N}=2$ hypermultiplet) [177, 61, 41] (PW).

In the former case, the anisotropic thermal equilibrium states are characterized by the

[2] In this class of theories there is a well motivated choice of the renormalization scale — namely, it is natural to have it be the same for all the theories in the class.

temperature T, the background magnetic field B and the renormalization scale μ; in the latter case, we have additionally a hypermultiplet mass scale m.

Before we present results, we characterize more precisely the models studied.

- $\mathbb{CFT}_{diag}$: $\mathcal{N}=4$ SYM has a global $SU(4)$ R-symmetry. In this model the magnetic field is turned on for the diagonal $U(1)$ of the R-symmetry. This is the model of [112], see also [92]. See section 6.2.1 for technical details.
- $\mathbb{CFT}_{STU}$: Holographic duals of $\mathcal{N}=4$ SYM with $U(1)^3 \subset SU(4)$ global symmetry are known as STU models [32, 89]. In this conformal theory the background magnetic field is turned on for one of the $U(1)$'s. This model is a consistent truncation of $\mathcal{N}=8$ five-dimensional gauged supergravity with two scalar fields dual to two dimension $\Delta=2$ operators. As we show in section 6.2.2, in the presence of the background magnetic field these operators will develop thermal expectation values.
- $n\mathbb{CFT}_m$: As we show in section 6.2.3, within consistent truncation of $\mathcal{N}=8$ five-dimensional gauged supergravity presented in [41], it is possible to identify a holographic dual to $\mathcal{N}=2^*$ gauge theory with a single $U(1)$ global symmetry. In this model the background magnetic field is turned on in this $U(1)$. The label $m\in(0,+\infty)$ denotes the hypermultiplet mass of the $\mathcal{N}=2^*$ gauge theory.
- $\mathbb{CFT}_{PW,m=0}$: This conformal gauge theory is a limiting case of the nonconformal $n\mathbb{CFT}_m$ model:

$$\mathbb{CFT}_{PW,m=0} = \lim_{m/\sqrt{B}\to 0} n\mathbb{CFT}_m\,.$$

Its bulk gravitational dual contains two scalar fields dual to dimension $\Delta=2$ and $\Delta=3$ operators of the $\mathcal{N}=2^*$ gauge theory. As we show in section 6.2.3, in the presence of the background magnetic field these operators will develop thermal expectation values.

- $\mathbb{CFT}_{PW,m=\infty}$: This conformal gauge theory is a limiting case of the nonconformal $n\mathbb{CFT}_m$

model:

$$\mathbb{CFT}_{PW,m=\infty} = \lim_{m/\sqrt{B}\to\infty} n\mathbb{CFT}_m\,.$$

Its holographic dual can be obtained from the $\mathcal{N}=8$ five dimensional gauged supergravity of [41] using the "near horizon limit" of [144][3], followed by the uplift to six dimensions — the resulting holographic dual is Romans $F(4)$ gauged supergravity in six dimensions [183, 90][4]. The six dimensional gravitational bulk contains a single scalar, dual to dimension $\Delta = 3$ operator of the effective CFT_5. There is no conformal anomaly in odd dimensions. Furthermore, there is no invariant dimension-five operator that can be constructed only with the magnetic field strength — as a result, the anisotropic stress-energy tensor of $\mathbb{CFT}_{PW,m=\infty}$ plasma is traceless, and is *free* from renormalization scheme ambiguities. Details on the $\mathbb{CFT}_{PW,m=\infty}$ model are presented in section 6.2.3. The renormalization scheme-independence of $\mathbb{CFT}_{PW,m=\infty}$ is a welcome feature: we will use the pressure anisotropy (6.1) of the theory as a benchmark to compare with the other conformal and nonconformal models.

And now the results. There is no universal magnetoresponse. Qualitatively, among conformal/nonconformal models we observe three different IR regimes (i.e. when $T/\sqrt{B}$ is small):

- In $\mathbb{CFT}_{diag}$ it is possible to reach deep IR, i.e. the $T/\sqrt{B}\to 0$ limit. For $T/\sqrt{B}\lesssim 0.1$ the thermodynamics is BTZ-like with the entropy density[5] [92]

$$s \to \frac{N^2}{3}\,BT\,,\qquad \text{as}\qquad \frac{T}{\sqrt{B}}\to 0\,. \tag{6.2}$$

[3]See appendix D of [53] for details of the isotropic (no magnetic field) thermal states of $\mathcal{N}=2^*$ plasma in the limit $m/T\to\infty$. The first hint that $\mathcal{N}=2^*$ plasma in the infinite mass limit is an effective five dimensional CFT appeared in [52].

[4]See [86] for a recent discussion.

[5]We independently reproduce this result.

■ Both in $\mathbb{CFT}_{PW,m=0}$ and $\mathbb{CFT}_{PW,m=\infty}$ (and in fact in all $n\mathbb{CFT}_m$ models) there is a terminal critical temperature T_{crit} which separates thermodynamically stable and unstable phases of the anisotropic plasma. Remarkably, this T_{crit} is universally determined by the magnetic field B, (almost) independently[6] of the mass parameter m of $n\mathbb{CFT}_m$:

$$
\begin{array}{cccccc}
 & \mathbb{CFT}_{PW,m=0} & \longrightarrow & n\mathbb{CFT}_m & \longrightarrow & \mathbb{CFT}_{PW,m=\infty} \\[2em]
\frac{T_{crit}}{\sqrt{B}}: & 0.29823(5) & \longrightarrow & [0.29823(6), 0.30667(1)] & \longrightarrow & 0.30673(9) \\[2em]
\frac{m}{\sqrt{2B}}: & 0 & \longrightarrow & [1/100, 10] & \longrightarrow & \infty\,,
\end{array}
$$

i.e. the variation of $T_{crit}/\sqrt{B}$ with mass about its mean value is 2% or less, see figure 6.7 (left panel). We leave the extensive study of this critical point to future work, and only point out that the specific heat at constant B at criticality has a critical exponent[7] $\alpha = \frac{1}{2}$:

$$
c_B = -T \frac{\partial^2 \mathcal{F}}{(\partial T)^2}\bigg|_B = \frac{\partial s}{\partial \ln T}\bigg|_B \propto \ (T - T_{crit})^{-1/2} \,, \tag{6.3}
$$

where $\mathcal{F}$ is the free energy density, see figure 6.6.

■ The $\mathbb{CFT}_{STU}$ model in the IR is different from the other ones. We obtained reliable numerical results in this model for $T/\sqrt{B} \gtrsim 0.06$: we neither observe the critical point as in the $\mathbb{CFT}_{PW,m=0}$ and $\mathbb{CFT}_{PW,m=\infty}$ models, nor the BTZ-like behavior (6.2) as in the $\mathbb{CFT}_{diag}$ model, see figure 6.3 (left panel).

[6] A very weak dependence on the mass parameter has been also observed for the equilibration rates in $\mathcal{N} = 2^*$ isotropic plasma in [55].

[7] The critical point with the same mean-field exponent α has been observed in isotropic thermodynamics of $\mathcal{N} = 2^*$ plasma with different masses for the bosonic and fermionic components of the hypermultiplet [60].

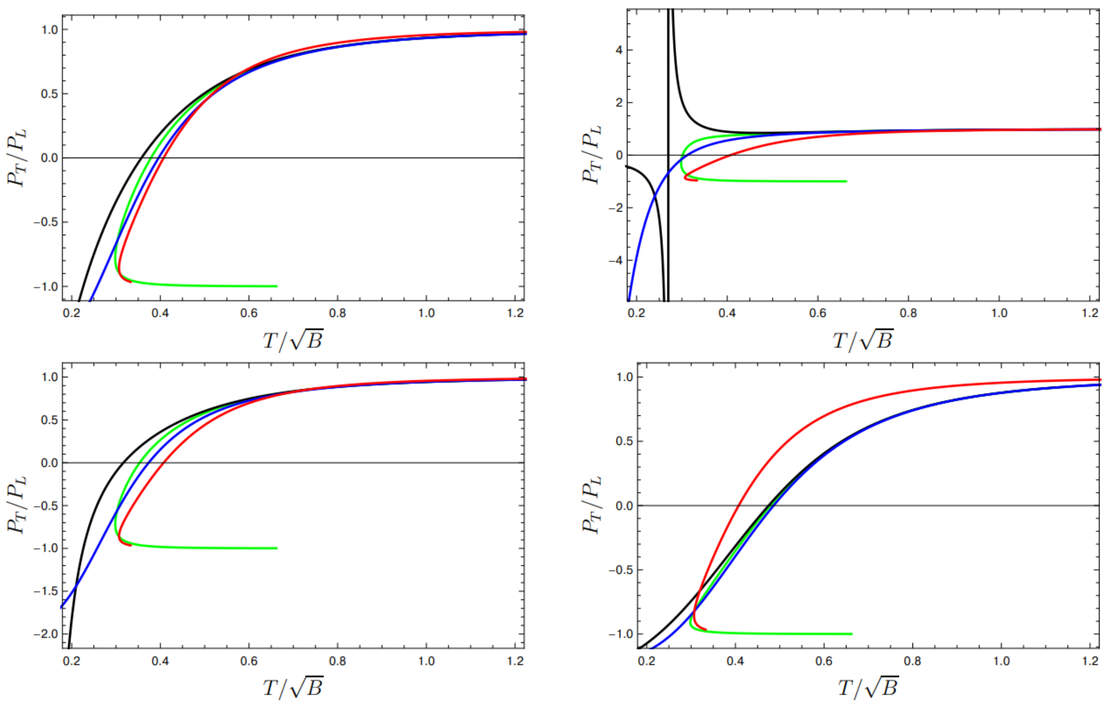

Figure 6.1: Anisotropy parameter $R = P_T/P_L$ for conformal models $\mathbb{CFT}_{diag}$ (black curves), $\mathbb{CFT}_{STU}$ (blue curves), $\mathbb{CFT}_{PW,m=0}$ (green curves) and $\mathbb{CFT}_{PW,m=\infty}$ (red curves) as a function of $T/\sqrt{B}$. $R_{\mathbb{CFT}_{PW,m=\infty}}$ is renormalization scheme independent; for the other models there is a strong dependence on the renormalization scale $\delta = \ln \frac{B}{\mu^2}$: different panels represent different choices for δ; all the models in the same panel have the same value of δ, leading to identical high-temperature asymptotics, $T/\sqrt{B} \gg 1$.

In figure 6.1 we present the pressure anisotropy parameter R (6.1) for the conformal theories: $\mathbb{CFT}_{diag}$ (black curves), $\mathbb{CFT}_{STU}$ (blue curves), $\mathbb{CFT}_{PW,m=0}$ (green curves) and $\mathbb{CFT}_{PW,m=\infty}$ (red curves) as a function of[8] $T/\sqrt{B}$. R is renormalization scheme independent in the $\mathbb{CFT}_{PW,m=\infty}$ model, while in the former three conformal models it is sensitive to

$$\delta \equiv \ln \frac{B}{\mu^2}\,, \tag{6.4}$$

[8]We use the same normalization of the magnetic field in holographic models as in [112].

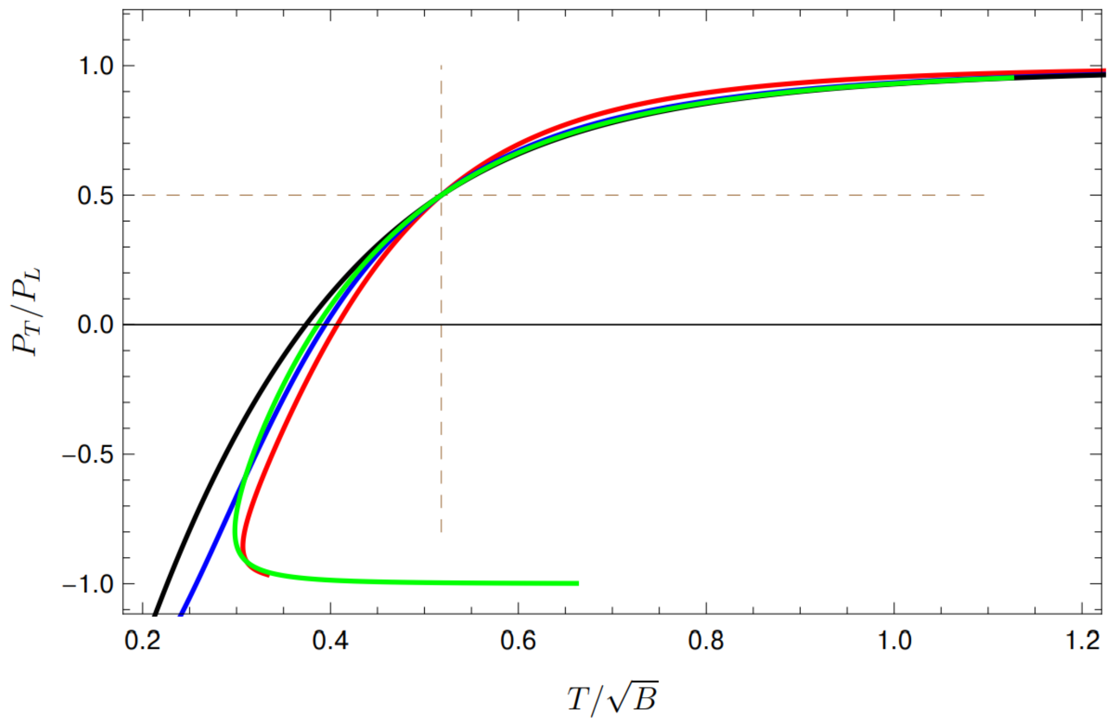

Figure 6.2: Renormalization scale δ is adjusted separately for the $\mathbb{CFT}_{diag}$, $\mathbb{CFT}_{STU}$ and $\mathbb{CFT}_{PW,m=0}$ models (see (6.7)) to ensure that in all these models the pressure anisotropy $R = 0.5$ occurs for the same value of $\frac{T}{\sqrt{B}}$ as in the $\mathbb{CFT}_{PW,m=\infty}$ model (see (6.6)). This matching point is highlighted with the dashed brown lines.

where μ is the renormalization scale. We performed high-temperature perturbative analysis, i.e. as $T/\sqrt{B} \gg 1$, to ensure that the definition of δ is consistent across all the conformal models sensitive to it, see appendix J. In the { top left, top right, bottom left, bottom right } panel of figure 6.1 we set $\{\delta = 4\,, \delta = 2.5\,, \delta = 3.5\,, \delta = 7\}$ (correspondingly) for $R_{\mathbb{CFT}_{diag}}$, $R_{\mathbb{CFT}_{STU}}$ and $R_{\mathbb{CFT}_{PW,m=0}}$ — notice that while all the curves exhibit the same high-temperature asymptotics, the anisotropy parameter R is quite sensitive to δ; in fact, $R_{\mathbb{CFT}_{diag}}$ diverges for $\delta = 2.5$ (because P_L crosses zero with P_T remaining finite). Varying δ, it is easy to achieve $R_{\mathbb{CFT}_{diag}}$, $R_{\mathbb{CFT}_{STU}}$ and $R_{\mathbb{CFT}_{PW,m=0}}$ in the IR to be "to the left" of the scheme-independent (red) curve $R_{\mathbb{CFT}_{PW,m=\infty}}$ (top panels and the bottom left panel); or "to the right" of the scheme-independent (red) curve $R_{\mathbb{CFT}_{PW,m=\infty}}$ (the bottom right panel).

In figure 6.1 we kept δ the same for the conformal models $\mathbb{CFT}_{diag}$, $\mathbb{CFT}_{STU}$ and $\mathbb{CFT}_{PW,m=0}$. This is very reasonable given that one can match δ across all the models by comparing the UV, i.e. $T/\sqrt{B} \gg 1$ thermodynamics (see appendix J) — there are no other scales besides T and B, and thus by dimensional analysis[9],

$$P_{T/L} = T^4 \ \hat{P}_{T/L}\left(\frac{T}{\sqrt{B}}, \frac{\mu}{\sqrt{B}}\right). \tag{6.5}$$

If we give up on maintaining the same renormalization scale for all the conformal models, it is easy to "collapse" all the curves for the pressure anisotropy, see figure 6.2. We will not perform sophisticated fits as in [112], and instead, adjusting δ independently for each model, we require that in all models the pressure anisotropy $R = 0.5$ is attained at the same value of $T/\sqrt{B}$ (represented by the dashed brown lines):

$$\frac{T}{\sqrt{B}}\bigg|_{\mathbb{CFT}_{diag},\mathbb{CFT}_{STU},\mathbb{CFT}_{PW,m=0}} = \frac{T}{\sqrt{B}}\bigg|_{\mathbb{CFT}_{PW,m=\infty}} = 0.51796(7)\,. \tag{6.6}$$

Specifically, we find that (6.6) is true, provided

$$\left\{\delta_{\mathbb{CFT}_{STU}}\,, \delta_{\mathbb{CFT}_{diag}}\,, \delta_{\mathbb{CFT}_{PW,m=0}}\right\} = \{3.9592(4)\,,\, 4.2662(0)\,,\, 4.1659(8)\}\,. \tag{6.7}$$

In a nutshell, this is what was done in [112] to claim a universal magnetoresponse for $R \gtrsim 0.5$. Rather, we interpret the collapse in figure 6.2 as nothing but a fitting artifact, possible due to a strong dependence of the anisotropy parameter R on the renormalization scale.

[9]The asymptotic AdS_5 radius L always scales out from the final formulas.

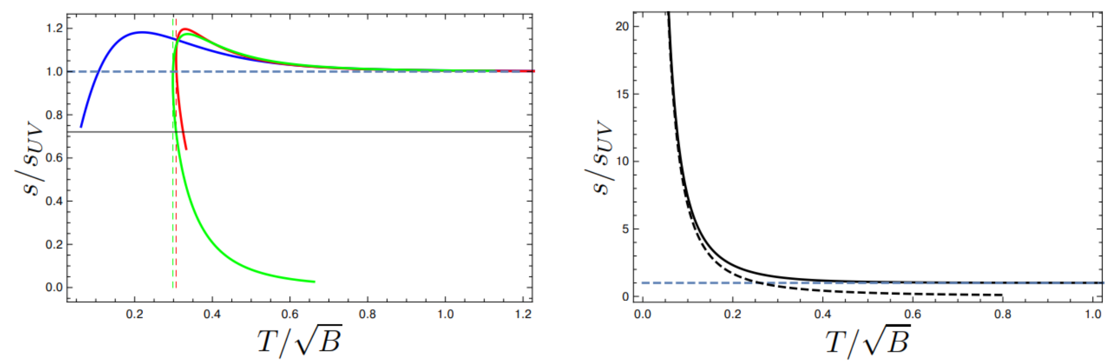

Figure 6.3: Entropy densities s in conformal models, relative to the entropy densities of the UV fixed points s_{UV} at the corresponding temperature (see (6.8)), as functions of $T/\sqrt{B}$: $\mathbb{CFT}_{diag}$ (black), $\mathbb{CFT}_{STU}$ (blue), $\mathbb{CFT}_{PW,m=0}$ (green) and $\mathbb{CFT}_{PW,m=\infty}$ (red). Left panel: vertical dashed lines indicate critical temperatures T_{crit} separating thermodynamically stable and unstable phases of $\mathbb{CFT}_{PW,m=0}$ (green) and $\mathbb{CFT}_{PW,m=\infty}$ (red) models. Right panel: the dashed black line is the small-T asymptote of the relative entropy in the $\mathbb{CFT}_{diag}$ model, see (6.9).

To further see that there is no universal physics, we can compare renormalization scheme-independent anisotropic thermodynamic quantities of the models: the entropy densities, see figure 6.3. The color coding is as before: $\mathbb{CFT}_{diag}$ (black curves), $\mathbb{CFT}_{STU}$ (blue curves), $\mathbb{CFT}_{PW,m=0}$ (green curves) and $\mathbb{CFT}_{PW,m=\infty}$ (red curves). We plot the entropy densities relative to the entropy density of the UV fixed point at the corresponding temperature (see equation (D.13) for the $\mathbb{CFT}_{PW,m=\infty}$ model in [53]):

$$s_{UV}\bigg|_{\mathbb{CFT}_{diag},\mathbb{CFT}_{STU},\mathbb{CFT}_{PW,m=0}} = \frac{1}{2}\pi^2 N^2 T^3\,, \qquad (m\times s_{UV})\bigg|_{\mathbb{CFT}_{PW,m=\infty}} = \frac{432}{625}\pi^3 N^2 T^4\,. \quad (6.8)$$

The dashed vertical lines in the left panel indicate the terminal (critical temperature) $T_{crit}/\sqrt{B}$ for $\mathbb{CFT}_{PW,m=0}$ (green) and $\mathbb{CFT}_{PW,m=\infty}$ (red) models which separates thermodynamically stable (top) and unstable (bottom) branches. Notice that s/s_{UV} diverges for

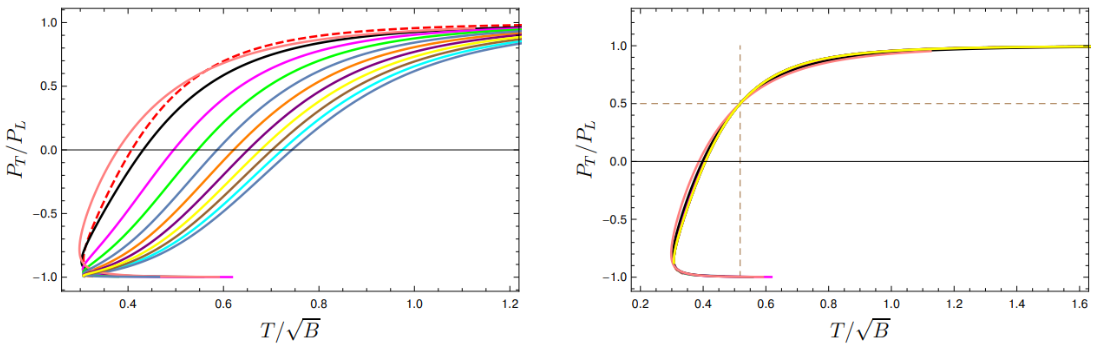

Figure 6.4: Anisotropy parameter $R = P_T/P_L$ for nonconformal models $n\mathbb{CFT}_m$ for select values of the hypermultiplet mass m, see (6.10), as a function of $T/\sqrt{B}$ (solid curves; from pink to dark blue as m increases). The dashed red curve is a benchmark model $\mathbb{CFT}_{PW,m=\infty}$ — where the anisotropy parameter is renormalization scale independent. In the left panel the renormalization scale is set to $\delta = 4$ for all $n\mathbb{CFT}_m$ models; in the right panel it is separately adjusted for each $n\mathbb{CFT}_m$ model to ensure that all the curves pass through the matching point, highlighted with dashed brown lines.

the $\mathbb{CFT}_{diag}$ model as $T/\sqrt{B} \to 0$ — this is reflection of the IR BTZ-like thermodynamics (6.2); the dashed black line is the IR asymptote

$$\frac{s}{s_{UV}}\bigg|_{\mathbb{CFT}_{diag}} \to \frac{2}{3\pi^2}\,\frac{B}{T^2}\,, \qquad \text{as} \qquad \frac{T}{\sqrt{B}} \to 0\,. \tag{6.9}$$

In $n\mathbb{CFT}_m$ models it is equally easy to 'collapse' the data for the pressure anisotropy. In these models we have an additional scale m — the mass of the $\mathcal{N} = 2$ hypermultiplet. In the absence of the magnetic field, i.e. for isotropic $\mathcal{N} = 2^*$ plasma, the thermodynamics is renormalization scheme-independent[10] [54]. Once we turn on the magnetic field, there is a scheme-dependence. In figure 6.4 we show the pressure anisotropy for $\mathcal{N} = 2^*$ gauge

[10]Scheme-dependence arises once we split the masses of the fermionic and bosonic components of the $\mathcal{N} = 2^*$ hypermultiplet [54].

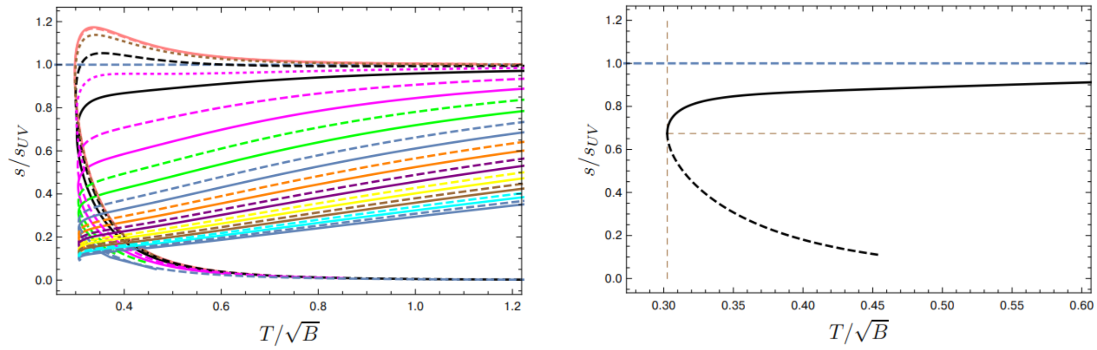

Figure 6.5: Left panel: entropy densities s in $n\mathbb{CFT}_m$ models, relative to the entropy density of the UV fixed point (the $\mathcal{N}=4$ SYM in this case) s_{UV} at the corresponding temperature (see (6.8)), as functions of $T/\sqrt{B}$. Color coding of the solid curves agrees with that in figure 6.4 — see (6.10) for the set of the hypermultiplet masses. Additional dashed and dotted curves correspond to additional values of m, within the same interval (6.10). Each $n\mathbb{CFT}_m$ model has a terminal critical point. In the right panel we show this for the model with $m/\sqrt{2B}=1$: the brown lines identify the critical temperature $T_{crit}/\sqrt{B}$ and the relative entropy at the criticality s^{crit}/s_{UV} (these quantities are presented in figure 6.7). “Top” solid black curve denotes the thermodynamically stable branch and "bottom” dashed black curve denotes the thermodynamically unstable branch (see figure 6.6 for further details).

theory for select values of m (solid curves from pink to dark blue),

$$\frac{m}{\sqrt{2B}} = \left\{\frac{1}{100}, 1, 2, 3, 4, 5, 6, 7, 8, 9, 10\right\} . \tag{6.10}$$

The dashed red curve represents the anisotropy parameter of the conformal $\mathbb{CFT}_{PW,m=\infty}$ model, which is renormalization scheme-independent. In the left panel the renormalization scale $\delta = 4$ for all the $n\mathbb{CFT}_m$ models. In the right panel, we adjusted $\delta = \delta_m$ for each $n\mathbb{CFT}_m$ model independently, so that the pressure anisotropy $R_{n\mathbb{CFT}_m} = 0.5$ at the same temperature as in the $\mathbb{CFT}_{PW,m=\infty}$ model, see (6.6). This matching point is denoted by dashed brown lines.

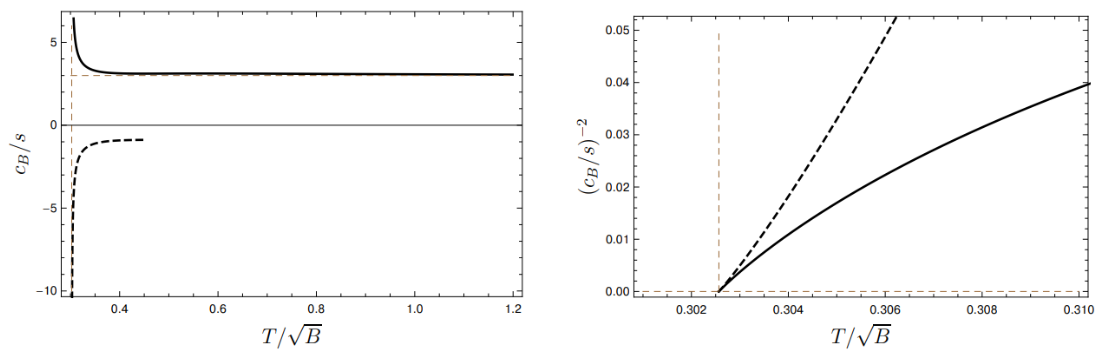

Figure 6.6: $n\mathbb{CFT}_m$ model with $m/\sqrt{2B} = 1$ is used to highlight phases of the anisotropic plasma. Following (6.3) we evaluate the constant-B specific heat of the plasma. The dashed brown lines highlight the location of the critical point. Left panel: the specific heat diverges as one approaches the critical temperature; it is negative for the branch denoted by the dashed black curve (see also the right panel of figure 6.5), indicating the thermodynamic instability. Right panel: $(c_B/s)^{-2}$ vanishes at criticality, with nonvanishing slope. This implies that the critical exponent $\alpha = \frac{1}{2}$, see (6.11).

As in conformal models, the entropy densities (which are renormalization scheme independent thermodynamic quantities) are rather distinct, see left panel of figure 6.5. The color coding is as in figure 6.4, except that we collected more data[11] in addition to (6.10): these are the dashed and dotted curves. The entropy density of the UV fixed point is defined as in (6.8). All the $n\mathbb{CFT}_m$ models studied, as well as the $\mathbb{CFT}_{PW,m=0}$ and $\mathbb{CFT}_{PW,m=\infty}$ conformal models, have a terminal critical point T_{crit} that separates the thermodynamically stable (top solid) and unstable (bottom dashed) branches, which we presented for the $\frac{m}{\sqrt{2B}} = 1$ $n\mathbb{CFT}_m$ model in the right panel. The dashed brown lines identify the critical temperature T_{crit} and the entropy density s^{crit} at criticality. In figure 6.6 we present results for the specific heat c_B in this model defined as in (6.3). Indeed, the (lower) thermodynamically unstable branch has a negative specific heat (left panel); approaching the critical

[11] To have a better characterization of the critical points.

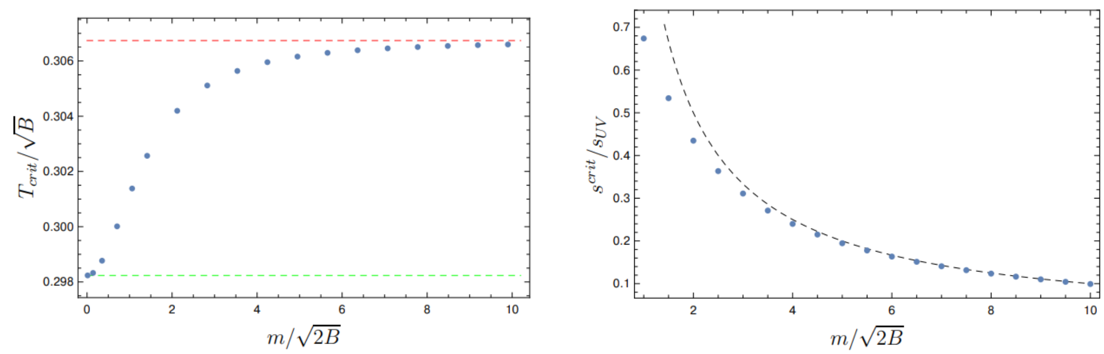

Figure 6.7: $n\mathbb{CFT}_m$ models as well as the conformal models $\mathbb{CFT}_{PW,m=0}$ and $\mathbb{CFT}_{PW,m=\infty}$ have terminal critical temperature, separating thermodynamically stable and unstable phases. In the left panel we present $T_{crit}/\sqrt{B}$ as function of $m/\sqrt{2B}$; in the right panel we present the relative entropy at criticality $\gamma = s^{crit}/s_{UV}$ (6.13). The dots represent results for the $n\mathbb{CFT}_m$ models; the dashed horizontal lines (left panel) represent the critical temperature for the $\mathbb{CFT}_{PW,m=0}$ model (green) and the $\mathbb{CFT}_{PW,m=\infty}$ model (red). The dashed black curve (right panel) represents the asymptote of γ as $m/\sqrt{B} \to \infty$, see (6.14).

temperature from above we observe the divergence in the specific heat, both for the stable and the unstable branches. To extract a critical exponent α, defined as

$$c_B \propto \left(\frac{T}{T_{crit}} - 1\right)^{-\alpha}, \qquad T \to T_{crit} + 0\,, \tag{6.11}$$

we plot (right panel) the dimensionless quantity c_B^2/s^2 as a function of $T/\sqrt{B}$. Both the stable (solid) and the unstable (dashed) curves approach zero, signaling the divergence of the specific heat at the critical temperature (vertical dashed brown line), with a finite slope — this implies that the critical exponent is

$$\alpha = \frac{1}{2}\,. \tag{6.12}$$

There is a remarkable universality of the critical points in $n\mathbb{CFT}_m$ and conformal

$\mathbb{CFT}_{PW,m=0}$ and $\mathbb{CFT}_{PW,m=\infty}$ models. In figure 6.7 (left panel) we present the results for the critical temperature as a function of $m/\sqrt{2B}$ in $n\mathbb{CFT}_m$ models (points). The horizontal dashed lines indicate the location of the critical points for the $\mathbb{CFT}_{PW,m=0}$ (green) and $\mathbb{CFT}_{PW,m=\infty}$ (red) conformal models. In the right panel the dots represent the relative entropy,

$$\gamma = \gamma(m/\sqrt{B}) \equiv \frac{s^{crit}}{s_{UV}}\,, \tag{6.13}$$

at criticality for the $n\mathbb{CFT}_m$ models. Effectively, γ as in (6.13) measures the number of DOF at critical point in anisotropic plasma relative to the number of DOF (or the central charge) of the UV fixed point ($\mathcal{N}=4$ SYM). The dashed black line is a simple asymptotic for γ as $m/\sqrt{B}\to\infty$, γ_∞,

$$\gamma_\infty = \frac{\sqrt{2B}}{m}\,. \tag{6.14}$$

One can understand the origin of the asymptote (6.13) from the fact that $n\mathbb{CFT}_m$ models in the large m limit should resemble the conformal model $\mathbb{CFT}_{PW,m=\infty}$; thus, we expect that $\gamma_\infty \approx \gamma_{\mathbb{CFT}_{PW,m=\infty}}$. Indeed,

$$\begin{aligned}\gamma_{\mathbb{CFT}_{PW,m=\infty}} =&\frac{s^{crit}_{\mathbb{CFT}_{PW,m=\infty}}}{s_{UV,\mathbb{CFT}_{diag}}} = \underbrace{\frac{s^{crit}}{s_{UV}}\bigg|_{\mathbb{CFT}_{PW,m=\infty}}}_{1.0603(7)} \times \underbrace{\frac{s_{UV,\mathbb{CFT}_{PW,m=\infty}}}{s_{UV,\mathbb{CFT}_{diag}}}}_{\frac{864\pi}{625}\times\frac{T_{crit}}{m}} \\ =&1.0603(7) \times \frac{864\pi}{625\sqrt{2}} \times \underbrace{\frac{T_{crit}}{\sqrt{B}}}_{0.30673(9)} \times \frac{\sqrt{2B}}{m} = 0.99883(9) \times \frac{\sqrt{2B}}{m}\,,\end{aligned} \tag{6.15}$$

where we extracted numerically the value of $\frac{s^{crit}}{s_{UV}}$ for the $\mathbb{CFT}_{PW,m=\infty}$ conformal model, used (6.8) to analytically compute the second factor in the first line, and substituted the numerical value for $T_{crit}/\sqrt{B}$ of the $\mathbb{CFT}_{PW,m=\infty}$ model in the second line.

We now outline the rest of the chapter, containing technical details necessary to obtain the results reported above. In section 6.2 we introduce the holographic theory of [41] and explain how the various models discussed here arise as consistent truncations of the latter: $\mathbb{CFT}_{diag}$ in section 6.2.1, $\mathbb{CFT}_{STU}$ in section 6.2.2, and $n\mathbb{CFT}_m$ in section 6.2.3. The conformal models $\mathbb{CFT}_{PW,m=0}$ and $\mathbb{CFT}_{PW,m=\infty}$ are special limits of the $n\mathbb{CFT}_m$ model and are discussed in sections 6.2.3 and 6.2.3 correspondingly. Holographic renormalization is by now a standard technique [191], and we only present the results for the boundary gauge theory observables. Due to the numerical character of this work, it is important to validate the numerical results in the limits where perturbative computations (analytical or numerical) are available. We have performed such validations in appendix J, i.e. when $\frac{T}{\sqrt{B}} \gg 1$. We did not want to overburden the reader with details, and so we did not present the checks of the agreement of the numerical parameters (e.g. as in (6.38)) with the corresponding perturbative counterparts — but we have performed such checks in all models. There are further important constraints on the numerically obtained energy density, pressure, entropy, etc., of the anisotropic plasma: the first law of the thermodynamics $d\mathcal{E} = Tds$ (at constant magnetic field and the mass parameter, if available), and the thermodynamic relation between the free energy density and the longitudinal pressure $\mathcal{F} = -P_L$. The latter relation can be proved (see appendix I) at the level of the equations of motion, borrowing the holographic arguments of [57] used to establish the universality of the shear viscosity to the entropy density in the holographic plasma models. Still, as the first law of thermodynamics, it provides an important consistency check on the numerical data — we verified these constraints in all the models, both perturbatively in the high-temperature limit, to $\mathcal{O}\left(\frac{B^4}{T^8}\right)$ inclusive, see appendix J, and for finite values of $B/\sqrt{T}$, see appendix J.1 – once again, we present only partial results of the full checks.

This chapter is a step in broadening the class of strongly coupled magnetized gauge theory plasmas (both conformal and massive) amenable to controlled holographic analysis.

We focused on the equation of state, extending the work of [112]. The next step is to analyze the magneto-transport in these models, in particular the magneto-transport at criticality.

6.2 Technical details

The starting point for the holographic analysis is the effective action of [41]:

$$\begin{aligned}
S_5 = \frac{1}{4\pi G_5}\int_{\mathcal{M}_5} d^5\xi\sqrt{-g}\Bigg[\frac{R}{4} - \frac{1}{4}\Big(\rho^4\nu^{-4}F^{(1)}_{\mu\nu}F^{(1)\mu\nu} + \rho^4\nu^4 F^{(2)}_{\mu\nu}F^{(2)\mu\nu} + \rho^{-8}F^{(3)}_{\mu\nu}F^{(3)\mu\nu}\Big) \\
- \frac{1}{2}\sum_{j=1}^{4}\left(\partial_\mu\phi_j\right)^2 - 3\left(\partial_\mu\alpha\right)^2 - \left(\partial_\mu\beta\right)^2 - \frac{1}{8}\sinh^2(2\phi_1)\left(\partial_\mu\theta_1 + \left(A^{(1)}_\mu + A^{(2)}_\mu - A^{(3)}_\mu\right)\right)^2 \\
- \frac{1}{8}\sinh^2(2\phi_2)\left(\partial_\mu\theta_2 + \left(A^{(1)}_\mu - A^{(2)}_\mu + A^{(3)}_\mu\right)\right)^2 - \frac{1}{8}\sinh^2(2\phi_3)(\partial_\mu\theta_3 + (-A^{(1)}_\mu + A^{(2)}_\mu \\
+ A^{(3)}_\mu))^2 - \frac{1}{8}\sinh^2(2\phi_4)\left(\partial_\mu\theta_4 - \left(A^{(1)}_\mu + A^{(2)}_\mu + A^{(3)}_\mu\right)\right)^2 - \mathcal{P}\Bigg],
\end{aligned} \tag{6.16}$$

where the $F^{(J)}$ are the field strengths of the $U(1)$ gauge fields, $A^{(J)}$, and $\mathcal{P}$ is the scalar potential. We introduced

$$\rho \equiv e^{\alpha}\,, \qquad \nu \equiv e^{\beta}\,. \tag{6.17}$$

The scalar potential, $\mathcal{P}$, is given in terms of a superpotential

$$\mathcal{P} = \frac{g^2}{8}\left[\,\sum_{j=1}^{4}\left(\frac{\partial W}{\partial\phi_j}\right)^2 + \frac{1}{6}\left(\frac{\partial W}{\partial\alpha}\right)^2 + \frac{1}{2}\left(\frac{\partial W}{\partial\beta}\right)^2\,\right] - \frac{g^2}{3}W^2\,, \tag{6.18}$$

where

$$W = -\frac{1}{4\rho^2\nu^2}\Big[\big(1+\nu^4-\nu^2\rho^6\big)\cosh(2\phi_1)+\big(-1+\nu^4+\nu^2\rho^6\big)\cosh(2\phi_2) \\ +\big(1-\nu^4+\nu^2\rho^6\big)\cosh(2\phi_3)+\big(1+\nu^4+\nu^2\rho^6\big)\cosh(2\phi_4)\Big]\,. \tag{6.19}$$

In what follows we set gauged supergravity coupling $g = 1$, this corresponds to setting the asymptotic AdS_5 radius to $L = 2$. The five dimensional gravitational constant G_5 is related to the rank of the supersymmetric $\mathcal{N} = 4$ $SU(N)$ UV fixed point as

$$G_5 = \frac{4\pi}{N^2}\,. \tag{6.20}$$

6.2.1 $\mathbb{CFT}_{diag}$

The holographic dual to the $\mathbb{CFT}_{diag}$ conformal model is a consistent truncation of (6.16) with

$$\alpha = \beta = \phi_j = \theta_j = 0\,, \qquad A_\mu^{(1)} = A_\mu^{(2)} = A_\mu^{(3)} = \frac{2}{\sqrt{3}}\,A_\mu\,, \tag{6.21}$$

leading to

$$S_{\mathbb{CFT}_{diag}} = \frac{1}{16\pi G_5}\int_{\mathcal{M}_5} d^5\xi\sqrt{-g}\Big[R - 4F_{\mu\nu}F^{\mu\nu}+3\Big]\,, \tag{6.22}$$

where we used the normalization of the bulk $U(1)$ to be consistent with [112].

This model has been extensively studied in [92, 112] and we do not review it here.

6.2.2 $\mathbb{CFT}_{STU}$

The holographic dual to the $\mathbb{CFT}_{STU}$ is a special case of the STU model [31, 32, 89], a consistent truncation of the effective action (6.16) with

$$\theta_j = \phi_j = 0\,, \tag{6.23}$$

leading to

$$\begin{aligned} S_{STU} =& \frac{1}{4\pi G_5}\int_{\mathcal{M}_5} d^5\xi\sqrt{-g}\bigg[\frac{R}{4} - \frac{1}{4}\Big(\rho^4\nu^{-4}F^{(1)}_{\mu\nu}F^{(1)\mu\nu} + \rho^4\nu^4 F^{(2)}_{\mu\nu}F^{(2)\mu\nu} \\ &+ \rho^{-8}F^{(3)}_{\mu\nu}F^{(3)\mu\nu}\Big) - 3\left(\partial_\mu\alpha\right)^2 - \left(\partial_\mu\beta\right)^2 - \mathcal{P}_{STU}\bigg]\,, \end{aligned} \tag{6.24}$$

and the scalar potential

$$\mathcal{P}_{STU} = -\frac{1}{4}(\rho^2\nu^2 + \rho^2\nu^{-2} + \rho^{-4})\,. \tag{6.25}$$

We would like to keep a single bulk gauge field, so we can set two of them to zero and work with the remaining one. The symmetries of the action allow us to choose whichever gauge field we want. To see this, notice that the action (6.24) is invariant under $F^{(1)}_{\mu\nu} \to F^{(2)}_{\mu\nu}$ together with $\nu \to \nu^{-1}$. Moreover, (6.24) with $F^{(1)}_{\mu\nu} \equiv 2F_{\mu\nu}$ and $F^{(2)}_{\mu\nu} = F^{(3)}_{\mu\nu} = 0$ is the same as with $F^{(3)}_{\mu\nu} \equiv 2F_{\mu\nu}$ and $F^{(1)}_{\mu\nu} = F^{(2)}_{\mu\nu} = 0$ for the gauge fields and with the scalar field redefinitions $\rho \to \nu^{1/2}\rho^{-1/2}$ and $\nu \to \nu^{1/2}\rho^{1/2}$. Thus, we arrive to the holographic dual of $\mathbb{CFT}_{STU}$ as

$$S_{\mathbb{CFT}_{STU}} = \frac{1}{4\pi G_5}\int_{\mathcal{M}_5} d^5\xi\sqrt{-g}\bigg[\frac{R}{4} - \rho^4\nu^{-4}F_{\mu\nu}F^{\mu\nu} - 3\left(\partial_\mu\alpha\right)^2 - \left(\partial_\mu\beta\right)^2 - \mathcal{P}_{STU}\bigg]\,, \tag{6.26}$$

where once again we used the normalization of the remaining gauge field as in [112].

Solutions to the gravitational theory (6.26) representing magnetic black branes dual to anisotropic magnetized $\mathbb{CFT}_{STU}$ plasma correspond to the following background ansatz[12]:

$$ds_5^2 = -c_1^2\ dt^2 + c_2^2\ \left(dx^2 + dy^2\right) + \left(\frac{r}{2}\right)^2\ dz^2 + c_4^2\ dr^2\,, \qquad F = B\ dx \wedge dy\,, \tag{6.27}$$

where all the metric warp factors c_i as well as the bulk scalars ρ and ν are functions of the radial coordinate r,

$$r\ \in\ [r_0, +\infty)\,, \tag{6.28}$$

where r_0 is a location of a regular Schwarzschild horizon, and $r \to +\infty$ is the asymptotic AdS_5 boundary. Introducing a new radial coordinate

$$x \equiv \frac{r_0}{r}\,, \qquad x\ \in\ (0, 1]\,, \tag{6.29}$$

and denoting

$$\begin{aligned} &c_1 = \frac{r}{2}\ \left(1 - \frac{r_0^4}{r^4}\right)^{1/2}\ a_1\,, \qquad c_2 = \frac{r}{2}\ \ a_2\,, \qquad c_4 = \frac{2}{r}\ \left(1 - \frac{r_0^4}{r^4}\right)^{-1/2}\ a_4 \\ &B = \frac{1}{2} r_0^2\ b\,, \end{aligned} \tag{6.30}$$

[12]Note that we fixed the radial coordinate r with the choice of the metric warp factor in front of dz^2.

we obtain the following system of ODEs (in a radial coordinate x, $' = \frac{d}{dx}$):

$$
\begin{aligned}
0 = a_1' + &\frac{a_1}{\nu^4\rho^4 a_2^3 x(3a_2 - 2a_2' x)(1-x^4)}\bigg(\nu^4\rho^4 a_2^2 x a_2' \left((x^4-1)x a_2' - 2(x^4-3)a_2\right) \\
&- 2\nu^2\rho^2 a_2^4 x^2 (x^4-1)\left(3\nu^2(\rho')^2 + \rho^2(\nu')^2\right) - 256\rho^8 a_4^2 x^4 b^2 + 2\nu^2 a_2^4 \left(a_4^2(\nu^4\rho^6 + \rho^6 + \nu^2)\right. \\
&\left. - 3\nu^2\rho^4\right)\bigg) ,
\end{aligned}
\tag{6.31}
$$

$$
\begin{aligned}
0 = a_4' + &\frac{a_4}{3\nu^4\rho^4 a_2^4 x(3a_2 - 2a_2' x)(x^4-1)}\bigg(9\nu^4\rho^4 a_2^3 x^2 (x^4-1)(a_2')^2 + 6\nu^2\rho^2 a_2^5 x^2 (x^4-1) \\
&\times \left(3\nu^2(\rho')^2 + \rho^2(\nu')^2\right) + 256 a_4^2 \rho^8 x^4 \left(9a_2 - 4a_2' x\right) b^2 - 4\nu^2 a_2^4 x (2a_4^2(\nu^4\rho^6 + \rho^6 + \nu^2) \\
&+ 3\nu^2\rho^4(x^4-2))a_2' + 6\nu^2 a_2^5 (a_4^2(\nu^4\rho^6 + \rho^6 + \nu^2) - 3\nu^2\rho^4)\bigg) ,
\end{aligned}
\tag{6.32}
$$

$$
\begin{aligned}
0 = a_2'' - \frac{(a_2')^2}{a_2} - \frac{512 a_4^2\rho^4 x^2 (3a_2 - a_2' x)}{3\nu^4 a_2^4 (x^4-1)} b^2 + \frac{a_2'}{3x\rho^4\nu^2(x^4-1)}\bigg(4a_4^2(\rho^6\nu^4 + \rho^6 + \nu^2) \\
+ 3\rho^4\nu^2(x^4-1)\bigg) ,
\end{aligned}
\tag{6.33}
$$

$$
\begin{aligned}
0 = \rho'' - \frac{(\rho')^2}{\rho} + \frac{256 a_4^2\rho^4 x^2 (2\rho' x + \rho)}{3\nu^4 a_2^4 (x^4-1)} b^2 + \frac{\rho'}{3x\nu^2\rho^4(x^4-1)}\bigg(4a_4^2(\rho^6\nu^4 + \rho^6 + \nu^2) \\
+ 3\rho^4\nu^2(x^4-1)\bigg) - \frac{a_4^2(\rho^6\nu^4 + \rho^6 - 2\nu^2)}{3\rho^3\nu^2 x^2 (x^4-1)} ,
\end{aligned}
\tag{6.34}
$$

$$
\begin{aligned}
0 = \nu'' - \frac{(\nu')^2}{\nu} - \frac{256 a_4^2\rho^4 x^2 (3\nu - 2\nu' x)}{3\nu^4 a_2^4 (x^4-1)} b^2 + \frac{\nu'}{3\rho^4\nu^2 x(x^4-1)}\bigg(4a_4^2(\rho^6\nu^4 + \rho^6 + \nu^2) \\
+ 3\rho^4\nu^2(x^4-1)\bigg) - \frac{a_4^2\rho^2(\nu^4-1)}{\nu x^2(x^4-1)} .
\end{aligned}
\tag{6.35}
$$

Notice that r_0 is completely scaled out from all the equations of motion. equations (6.31)-(6.35) have to be solved subject to the following asymptotics:

- in the UV, i.e. as $x \to 0_+$,

$$
\begin{aligned}
&a_1 = 1 + a_{1,2}\ x^4 + \mathcal{O}(x^8 \ln x)\,, \qquad a_2 = 1 + \left(a_{2,2} - 32 b^2 \ln x\right)\ x^4 + \mathcal{O}(x^6)\,,\\
&a_4 = 1 + \left(-a_{1,2} + \frac{64}{3} b^2 - \frac{4}{3} n_1^2 - 4 r_1^2 - 2 a_{2,2} + 64 b^2 \ln x\right)\ x^4 + \mathcal{O}(x^6)\,,\\
&\rho = 1 + r_1\ x^2 + \mathcal{O}(x^4)\,, \qquad \nu = 1 + n_1\ x^2 + \mathcal{O}(x^4)\,;
\end{aligned}
\tag{6.36}
$$

- in the IR, i.e. as $y \equiv 1 - x \to 0_+$,

$$
\begin{aligned}
&a_1 = a_{1,h,0} + \mathcal{O}(y)\,, \qquad a_2 = a_{2,h,0} + \mathcal{O}(y)\,, \qquad \rho = r_{h,0} + \mathcal{O}(y)\,, \qquad \nu = n_{h,0} + \mathcal{O}(y)\,,\\
&a_4 = \frac{3 a_{2,h,0}^2 r_{h,0}^2 n_{h,0}^2}{(3 a_{2,h,0}^4 n_{h,0}^6 r_{h,0}^6 + 3 a_{2,h,0}^4 n_{h,0}^2 r_{h,0}^6 + 96 b^2 r_{h,0}^8 + 3 a_{2,h,0}^4 n_{h,0}^4)^{1/2}} + \mathcal{O}(y)\,.
\end{aligned}
\tag{6.37}
$$

In total, given b — roughly the ratio $\frac{\sqrt{B}}{T}$, the asymptotic expansions are specified by 8 parameters:

$$
\{a_{1,2}\,,\ a_{2,2}\,,\ r_1\,,\ n_1\,,\ a_{1,h,0}\,,\ a_{2,h,0}\,,\ r_{h,0}\,,\ n_{h,0}\}\,,
\tag{6.38}
$$

which is the correct number of parameters necessary to provide a solution to a system of three second order and two first order equations, $3 \times 2 + 2 \times 1 = 8$. The parameters n_1 and r_1 correspond to the expectation value of two dimension $\Delta = 2$ operators of the boundary $\mathbb{CFT}_{STU}$; the other two parameters, $a_{1,2}$ and $a_{2,2}$, determine the expectation value of its stress-energy tensor. Using the standard holographic renormalization we find:

$$\begin{aligned}
\langle T_{tt}\rangle &\equiv \mathcal{E} = \frac{r_0^4}{512\pi G_5}\left(3-6a_{1,2}-128b^2\ln r_0+128b^2\ln 2+4a_{2,2}+64b^2\ \kappa\right)\,,\\
\langle T_{xx}\rangle &= \langle T_{yy}\rangle \equiv P_T = \frac{r_0^4}{512\pi G_5}\left(3-6a_{1,2}-128b^2\ln r_0+128b^2\ln 2+4a_{2,2}+64b^2\ \kappa\right)\,,\\
\langle T_{zz}\rangle &\equiv P_L = \frac{r_0^4}{512\pi G_5}\left(3-6a_{1,2}-128b^2\ln r_0+128b^2\ln 2+4a_{2,2}+64b^2\ \kappa\right)\,,
\end{aligned} \tag{6.39}$$

for the components of the boundary stress-energy tensor, and

$$s=\frac{r_0^3a_{2,h,0}^2}{32G_5}\,,\qquad T=\frac{\sqrt{3}\left[a_{2,h,0}^4n_{h,0}^2(n_{h,0}^4r_{h,0}^6+r_{h,0}^6+n_{h,0}^2)+32b^2r_{h,0}^8\right]^{1/2}a_{1,h,0}r_0}{12\pi r_{h,0}^2n_{h,0}^2a_{2,h,0}^2}\,, \tag{6.40}$$

for the entropy density and the temperature. Note that, as in $\mathcal{N}=4$ SYM [112],

$$\langle T^{\mu}{}_{\mu}\rangle = -\frac{r_0^4b^2}{4\pi G_5} = -\frac{N^2}{4\pi^2}\ B^2\,, \tag{6.41}$$

where we used (6.30) and (6.20). The (holographic) free energy density is given by the standard relation

$$\mathcal{F}=\mathcal{E}-Ts\,. \tag{6.42}$$

The constant parameter κ in (6.39) comes from the finite counterterm of the holographic renormalization; we find it convenient to relate it to the renormalization scale μ in (6.4) as

$$\kappa = 2\ln(2\pi\mu)\,. \tag{6.43}$$

As shown in appendix J.0.1, the renormalization scheme choice (6.43) implies that in the high-temperature limit $T^2 \gg B$,

$$R_{\mathbb{CFT}_{STU}} = 1 - \frac{4B^2}{\pi^4 T^4}\ \ln \frac{T}{\mu\sqrt{2}} + \mathcal{O}\left(\frac{B^4}{T^8}\ \ln^2 \frac{T}{\mu}\right) . \tag{6.44}$$

We can not solve the equations (6.31)-(6.35) analytically; adapting numerical techniques developed in [7], we solve these equations (subject to the asymptotics (6.36) and (6.37)) numerically. The results of numerical analysis are data files assembled of parameters (6.38), labeled by b. It is important to validate the numerical data (in addition to the standard error analysis). There are two important constraints that we verified for $\mathbb{CFT}_{STU}$ (and in fact all the other models):

- The first law of thermodynamics (FL), $d\mathcal{E}/(Tds) - 1$ (with B kept fixed), leads to the differential constrain on data sets (6.38) (here $' = \frac{d}{db}$):

$$\text{FL} : 0 = \frac{\sqrt{3} r_{h,0}^2 n_{h,0}^2 a_{2,h,0}((2a_{2,2}' - 3a_{1,2}')b + 32b^2 + 6a_{1,2} - 4a_{2,2} - 3)}{(4a_{2,h,0}' b - 3a_{2,h,0}) a_{1,h,0} \sqrt{a_{2,h,0}^4 n_{h,0}^2 ((n_{h,0}^4 + 1) r_{h,0}^6 + n_{h,0}^2) + 32b^2 r_{h,0}^8}} - 1 . \tag{6.45}$$

- Anisotropy introduced by the external magnetic field results in $P_T \neq P_L$. From the elementary anisotropic thermodynamics (see [112] for a recent review), the free energy density of the system $\mathcal{F}$ is given by

$$\mathcal{F} = -P_L \qquad \Longrightarrow \qquad 0 = \frac{\mathcal{E} + P_L}{sT} - 1 . \tag{6.46}$$

We emphasize that holographic renormalization (even anisotropic one) naturally enforces (6.42) (see [50] for one of the first demonstrations), but not (6.46). In appendix

I we present a holographic proof[13] of the thermodynamic relation (TR) (6.46). Applying it to $\mathbb{CFT}_{STU}$ model we arrive at the constraint

$$\mathrm{TR}:0=\frac{\sqrt{3}(1-2a_{1,2})r_{h,0}^2n_{h,0}^2}{a_{1,h,0}\sqrt{a_{2,h,0}^4n_{h,0}^2((n_{h,0}^4+1)r_{h,0}^6+n_{h,0}^2)+32b^2r_{h,0}^8}}-1\,. \tag{6.47}$$

In appendix J.0.1 we have verified FT and TR in the $\mathbb{CFT}_{STU}$ model to order $\mathcal{O}(b^4)\sim\mathcal{O}(B^4/T^8)$ inclusive[14].

Technical details presented here are enough to generate the $\mathbb{CFT}_{STU}$ model plots reported in section 6.1.

6.2.3 $n\mathbb{CFT}_m$

There is a simple consistent truncation of the effective action (6.16) to that of the PW action [177], supplemented with a single bulk $U(1)$ gauge field. Indeed, setting

$$\begin{aligned}&\beta=0\Longrightarrow\nu=1\,,\qquad \phi_2=\phi_3\equiv\chi\,,\qquad \phi_1=\phi_4=0\,,\\&A^{(1)}=A^{(2)}\equiv\sqrt{2}A\,,\qquad A^{(3)}=0\,,\qquad \theta_J=0\,.\end{aligned} \tag{6.48}$$

we find

$$S_{n\mathbb{CFT}_m}=\frac{1}{4\pi G_5}\int_{\mathcal{M}_5}d^5\xi\sqrt{-g}\left[\frac{R}{4}-3\left(\partial_\mu\alpha\right)^2-\left(\partial_\mu\chi\right)^2-\mathcal{P}_{PW}-\rho^4F_{\mu\nu}F^{\mu\nu}\right], \tag{6.49}$$

[13] The proof follows the same steps as in the first proof of the universality of the shear viscosity to the entropy density in holography [57].

[14] Additionally, as in the $n\mathbb{CFT}_m$ model with $m/\sqrt{2B}=1$ (see appendix J.1), we checked both relations for finite b.

where $\mathcal{P}_{PW}$ is the Pilch-Warner scalar potential of the gauged supergravity:

$$\begin{aligned}\mathcal{P}_{PW} =& \frac{1}{48}\left(\frac{\partial W_{PW}}{\partial\alpha}\right)^2 + \frac{1}{16}\left(\frac{\partial W_{PW}}{\partial\chi}\right)^2 - \frac{1}{3}W_{PW}^2\,,\\ W_{PW} =& -\frac{1}{\rho^2} - \frac{1}{2}\rho^4\cosh(2\chi)\,.\end{aligned} \tag{6.50}$$

We use the same holographic background ansatz, the same radial coordinate x, as for the $\mathbb{CFT}_{STU}$ model (6.27)-(6.30); except that now we have the bulk scalar fields α and χ (here $' = \frac{d}{dx}$):

$$\begin{aligned}0 =& a_1' + \frac{2a_1a_2x}{3a_2 - 2a_2'x}\left((\chi')^2 + 3(\alpha')^2\right) + \frac{a_1a_2'}{2a_2} - \frac{a_1(x^4-9)}{4x(x^4-1)} + \frac{64a_1a_4^2e^{4\alpha}x^3b^2}{a_2^3(3a_2-2a_2'x)(x^4-1)}\\ &- \frac{a_1a_2a_4^2}{8x(3a_2-2a_2'x)(x^4-1)}\left(2e^{8\alpha} + 16e^{-4\alpha} - e^{8\alpha-4\chi} + 16e^{2\alpha+2\chi} + 16e^{2\alpha-2\chi} - e^{8\alpha+4\chi}\right)\\ &+ \frac{3a_1a_2}{4x(3a_2-2a_2'x)}\,,\end{aligned} \tag{6.51}$$

$$\begin{aligned}0 =& a_4' + \frac{2a_4a_2x}{3a_2 - 2a_2'x}\left((\chi')^2 + 3(\alpha')^2\right) - \frac{3a_4a_2'}{2a_2} + \frac{64a_4^3e^{4\alpha}x^3(9a_2-4a_2'x)b^2}{3a_2^4(3a_2-2a_2'x)(x^4-1)}\\ &+ \frac{a_4^3(3a_2-4xa_2')}{24x(3a_2-2a_2'x)(x^4-1)}\left(2e^{8\alpha} + 16e^{2\alpha+2\chi} - e^{8\alpha-4\chi} + 16e^{2\alpha-2\chi} + 16e^{-4\alpha} - e^{8\alpha+4\chi}\right)\\ &- \frac{a_4(12a_2 - a_2'x(x^4+7)x)}{2(x^4-1)(3a_2-2a_2'x)x}\,,\end{aligned} \tag{6.52}$$

$$\begin{aligned}0 =& a_2'' - \frac{(a_2')^2}{a_2} - \frac{128a_4^2e^{4\alpha}x^2(3a_2-a_2'x)b^2}{3a_2^4(x^4-1)} + \frac{a_2'}{12x(x^4-1)}\Big(12(x^4-1) + a_4^2(2e^{8\alpha}\\ &+ 16e^{2\alpha+2\chi} - e^{8\alpha-4\chi} + 16e^{2\alpha-2\chi} + 16e^{-4\alpha} - e^{8\alpha+4\chi})\Big)\,,\end{aligned} \tag{6.53}$$

$$
\begin{aligned}
0 &= \alpha'' + \frac{64a_4^2e^{4\alpha}x^2(2\alpha'x+1)b^2}{3a_2^4(x^4-1)} + \frac{\alpha'}{12x(x^4-1)}\bigg(12(x^4-1) + a_4^2(2e^{8\alpha} + 16e^{2\alpha+2\chi} \\
&- e^{8\alpha-4\chi} + 16e^{2\alpha-2\chi} + 16e^{-4\alpha} - e^{8\alpha+4\chi})\bigg) - \frac{a_4^2}{12x^2(x^4-1)}\bigg(2e^{8\alpha} + 4e^{2\alpha+2\chi} - e^{8\alpha-4\chi} \\
&+ 4e^{2\alpha-2\chi} - 8e^{-4\alpha} - e^{8\alpha+4\chi}\bigg)\,,
\end{aligned}
\tag{6.54}
$$

$$
\begin{aligned}
0 &= \chi'' + \frac{128a_4^2\chi'e^{4\alpha}x^3b^2}{3a_2^4(x^4-1)} + \frac{\chi'}{12x(x^4-1)}\bigg(12(x^4-1) + a_4^2(2e^{8\alpha} + 16e^{2\alpha+2\chi} - e^{8\alpha-4\chi} \\
&+ 16e^{2\alpha-2\chi} + 16e^{-4\alpha} - e^{8\alpha+4\chi})\bigg) - \frac{a_4^2\,(8e^{2\alpha+2\chi} + e^{8\alpha-4\chi} - 8e^{2\alpha-2\chi} - e^{8\alpha+4\chi})}{8x^2(x^4-1)}\,.
\end{aligned}
\tag{6.55}
$$

As in the $\mathbb{CFT}_{STU}$ model, r_0 is completely scaled out from all the equations of motion. equations (6.51)-(6.55) have to be solved subject to the following asymptotics:

- in the UV, i.e. as $x \to 0_+$,

$$
\begin{aligned}
a_1 &= 1 - x^4\left(4\alpha_{1,0}^2 + 2\alpha_{1,0}\alpha_{1,1} + \frac{\alpha_{1,1}^2}{2} - \frac{64b^2}{3} + 2\chi_0\chi_{1,0} + 2a_{2,2,0} + a_{4,2,0}\right) + \mathcal{O}(x^6)\,, \\
a_2 &= 1 + x^4\left(-32b^2\ln x + a_{2,2,0}\right) + \mathcal{O}\left(x^6\ln x\right)\,, \\
a_4 &= 1 - \frac{2}{3}x^2\chi_0^2 + x^4\bigg(-4\alpha_{1,1}^2\ \ln^2 x + \left(-8\alpha_{1,0}\alpha_{1,1} + 64b^2 - \frac{8}{3}\chi_0^4 - 2\alpha_{1,1}^2\right)\ln x \\
&+ a_{4,2,0}\bigg) + \mathcal{O}\left(x^6\ln^3 x\right)\,, \\
\alpha &= x^2\left(\alpha_{1,1}\ \ln x + \alpha_{1,0}\right) + \mathcal{O}\left(x^4\ln^2 x\right)\,, \\
\chi &= \chi_0 x + \left(\frac{4}{3}\chi_0^3\ \ln x + \chi_{1,0}\right)x^3 + \mathcal{O}\left(x^5\ln^2 x\right)\,;
\end{aligned}
\tag{6.56}
$$

- in the IR, i.e. as $y \equiv 1 - x \to 0_+$,

$$
\begin{split}
&a_1 = a_{1,h,0} + \mathcal{O}(y)\,,\ a_2 = a_{2,h,0} + \mathcal{O}(y)\,,\ \alpha = \ln r_{h,0} + \mathcal{O}(y)\,,\ \chi = \ln c_{h,0} + \mathcal{O}(y)\,,\\
&a_4 = 4\sqrt{3} a_{2,h,0}^2 r_{h,0}^2 c_{h,0}^2 \, \Big(a_{2,h,0}^4 (r_{h,0}^6 (16 c_{h,0}^6 - r_{h,0}^6 (1 - c_{h,0}^4)^2) + 16 c_{h,0}^2 (r_{h,0}^6 + c_{h,0}^2)) \\
&\qquad\qquad + 512 b^2 c_{h,0}^4 r_{h,0}^8 \Big)^{-1/2} + \mathcal{O}(y)\,.
\end{split}
\tag{6.57}
$$

The non-normalizable coefficients $\alpha_{1,1}$ (of the dimension $\Delta = 2$ operator) and χ_0 (of the dimension $\Delta = 3$ operator) are related to the masses of the bosonic and the fermionic components of the hypermultiplet of $\mathcal{N} = 2^*$ gauge theory. When both masses are the same (see [54])

$$
\alpha_{1,1} = \frac{2}{3}\, \chi_0^2\,. \tag{6.58}
$$

Furthermore, carefully matching to the extremal PW solution [177, 61] (following the same procedure as in [54]) we find

$$
\frac{B}{m^2} = \frac{2b}{\chi_0^2}\,, \tag{6.59}
$$

where m is the hypermultiplet mass. We find it convenient to use

$$
\eta \equiv \frac{m}{\sqrt{2B}} \qquad \Longrightarrow \qquad \chi_0 = 2\sqrt{b}\ \eta\,, \tag{6.60}
$$

to label different mass parameters in $n\mathbb{CFT}_m$ models, see (6.10). In total, given η and b, the asymptotics expansions are specified by 8 parameters:

$$
\{a_{2,2,0}\,,\ a_{4,2,0}\,,\ \alpha_{1,0}\,,\ \chi_{1,0}\,,\ a_{1,h,0}\,,\ a_{2,h_0}\,,\ r_{h,0}\,,\ c_{h,0}\}\,, \tag{6.61}
$$

which is the correct number of parameters necessary to provide a solution to a system of three second order and two first order equations, $3 \times 2 + 2 \times 1 = 8$. Parameters $\alpha_{1,0}$ and $\chi_{1,0}$ correspond to the expectation values of dimensions $\Delta = 2$ ($\mathcal{O}_2$) and $\Delta = 3$ ($\mathcal{O}_3$) operators (correspondingly) of the boundary $n\mathbb{CFT}_m$; the other two parameters, $a_{2,2,0}$ and $a_{4,2,0}$, determine the expectation value of its stress-energy tensor. Using the standard holographic renormalization [31] we find:

$$
\begin{split}
\langle T_{tt}\rangle \equiv \mathcal{E} = \frac{r_0^4}{1536\pi G_5}\biggl(& 9 - 64b^2\left(\eta^4 + 6\ln r_0 - 6\ln 2 - 3\kappa + 6\right) + 192\alpha_{1,0}b\eta^2 + 72\alpha_{1,0}^2 \\
& + 48a_{2,2,0} + 18a_{4,2,0} + 48\sqrt{b}\eta\chi_{1,0}\biggr)\,, \\
\langle T_{xx}\rangle = \langle T_{yy}\rangle \equiv P_T = \frac{r_0^4}{4608\pi G_5}\biggl(& 9 - 64b^2(-7\eta^4 + 18\ln r_0 - 18\ln 2 - 9\kappa + 15) \\
& - 192\alpha_{1,0}b\eta^2 + 72\alpha_{1,0}^2 + 144\sqrt{b}\eta\chi_{1,0} + 72a_{2,2,0} + 18a_{4,2,0}\biggr)\,, \\
\langle T_{zz}\rangle \equiv P_L = \frac{r_0^4}{4608\pi G_5}\biggl(& 9 + 64b^2\left(7\eta^4 + 18\ln r_0 - 18\ln 2 - 9\kappa - 6\right) - 192\alpha_{1,0}b\eta^2 \\
& + 72\alpha_{1,0}^2 + 144\sqrt{b}\eta\chi_{1,0} + 18a_{4,2,0}\biggr)\,,
\end{split}
\tag{6.62}
$$

for the components of the boundary stress-energy tensor,

$$
\mathcal{O}_2 = \frac{r_0^2}{8\pi G_5}\ \left(\alpha_{1,0} - \frac{2}{3}\eta^2 b\right)\,, \qquad \mathcal{O}_3 = -\frac{r_0^3}{16\pi G_5}\left(\chi_{1,0} + \frac{8}{3}\eta^3 b^{3/2}\right)\,, \tag{6.63}
$$

for the expectation values of the relevant operators, and

$$
s=\frac{r_0^3a_{2,h,0}^2}{32G_5}\,,\qquad T=\frac{\sqrt{3}r_0a_{1,h,0}}{48\pi a_{2,h,0}^2c_{h,0}^2r_{h,0}^2}\biggl[a_{2,h,0}^4(16c_{h,0}^2(r_{h,0}^6+c_{h,0}^2)-r_{h,0}^6((c_{h,0}^4-1)^2r_{h,0}^6
$$
$$
-16c_{h,0}^6))+512b^2c_{h,0}^4r_{h,0}^8\biggr]^{1/2}\,, \tag{6.64}
$$

for the entropy density and the temperature. Note that, as expected [60],

$$
\begin{aligned}
\langle T^\mu{}_\mu\rangle =&-\frac{r_0^4}{4\pi G_5}\left(b^2\left(1-\frac{4}{3}\eta^4\right)+\alpha_{1,0}b\eta^2-\frac{1}{4}\sqrt{b}\eta\chi_{1,0}\right)\\
=&-2m^2\,\mathcal{O}_2-m\,\mathcal{O}_3-\frac{N^2}{4\pi^2}B^2\,,
\end{aligned} \tag{6.65}
$$

where in the second equality we used (6.30), (6.20), (6.63) and (6.60). The (holographic) free energy density is directly given by the standard relation (6.42). The constant parameter κ in (6.62) comes from the finite counterterm of the holographic renormalization; we fix it as in (6.43).

We can not solve the equations (6.51)-(6.55) analytically; adapting numerical techniques developed in [7], we solve these equations (subject to the asymptotics (6.56) and (6.57)) numerically. The results of numerical analysis are data files assembled of parameters (6.61), labeled by b and η. As for the $\mathbb{CFT}_{STU}$ model, we validate the numerical data verifying the differential constraint from the first law of the thermodynamics $d\mathcal{E}=Tds$ (FL) and the algebraic constraint from the thermodynamic relation $\mathcal{F} = -P_L$ (TR):

$$
\begin{split}
\text{FL}: 0 =& \frac{4\sqrt{3}a_{2,h,0}c_{h,0}^2 r_{h,0}^2}{a_{1,h,0}(3a_{2,h,0}-4ba'_{2,h,0})}\biggl(8(4b\eta^2+3\alpha_{1,0})(\alpha_{1,0}-\alpha'_{1,0}b)-4\sqrt{b}(2\chi'_{1,0}b-3\chi_{1,0})\eta \\
&-3a'_{4,2,0}b-8a'_{2,2,0}b-32b^2+6a_{4,2,0}+16a_{2,2,0}+3\biggr)\biggl(a_{2,h,0}^4(16c_{h,0}^2(r_{h,0}^6+c_{h,0}^2) \\
&-r_{h,0}^6((c_{h,0}^4-1)^2 r_{h,0}^6-16c_{h,0}^6))+512b^2c_{h,0}^4r_{h,0}^8\biggr)^{-1/2}-1\,,
\end{split}
\tag{6.66}
$$

$$
\begin{split}
\text{TR}: 0 =& \frac{4\sqrt{3}r_{h,0}^2c_{h,0}^2}{9a_{1,h,0}}\biggl(64b^2\eta^4+96\alpha_{1,0}b\eta^2+72\sqrt{b}\eta\chi_{1,0}+72\alpha_{1,0}^2-384b^2+36a_{2,2,0} \\
&+18a_{4,2,0}+9\biggr)\biggl(a_{2,h,0}^4(16c_{h,0}^2(r_{h,0}^6+c_{h,0}^2)-r_{h,0}^6((c_{h,0}^4-1)^2r_{h,0}^6-16c_{h,0}^6)) \\
&+512b^2c_{h,0}^4r_{h,0}^8\biggr)^{-1/2}-1\,.
\end{split}
\tag{6.67}
$$

In appendix J.1 we have verified FT and TR in the $n\mathbb{CFT}_m$ model with $m/\sqrt{2B} = 1$ numerically.

Technical details presented here are enough to generate $n\mathbb{CFT}_m$ model plots reported in section 6.1.

$\mathbb{CFT}_{PW,m=0}$

The $\mathbb{CFT}_{PW,m=0}$ model is a special case of the $n\mathbb{CFT}_m$ model when the hypermultiplet mass m is set to zero. This necessitates setting the non-normalizable coefficients $\alpha_{1,1}$ and χ_0 to zero $\Longrightarrow$ $\eta = 0$ in (6.60). From (6.55) it is clear that this $m = 0$ limit is consistent with

$$
\eta(x) \equiv 0 \qquad \Longrightarrow \qquad \chi_{1,0} = 0\,,
\tag{6.68}
$$

implying that the $\mathbb{Z}_2$ symmetry of the holographic dual, i.e. the symmetry associated with $\chi \leftrightarrow -\chi$, is unbroken. In what follows, we study the $\mathbb{Z}_2$-symmetric phase of the $\mathbb{CFT}_{PW,m=0}$ anisotropic thermodynamics[15],

$$\mathcal{O}_3 = 0\,. \tag{6.69}$$

In appendix J.0.2 we verified FT and TR in $\mathbb{CFT}_{PW,m=0}$ to order $\mathcal{O}(b^4)$ inclusive; we also present $\mathcal{O}(B^4/T^8)$ results for $R_{\mathbb{CFT}_{PW,m=0}}$ and confirm that the renormalization scheme choice of κ as in (6.43) leads to

$$R_{\mathbb{CFT}_{PW,m=0}} = R_{\mathbb{CFT}_{STU}} + \mathcal{O}\left(\frac{B^4}{T^8}\right)\,. \tag{6.70}$$

$\mathbb{CFT}_{PW,m=\infty}$

The holographic dual to the $\mathbb{CFT}_{PW,m=\infty}$ model can be obtained as a particular decoupling limit $\chi \to \infty$ of the effective action (6.49). As emphasized originally in [144], the supersymmetric vacuum, and the isotropic thermal equilibrium states of the theory [53, 52] are locally that of the $4+1$ dimensional conformal plasma. We derive the $5+1$ dimensional holographic effective action $S_{\mathbb{CFT}_{PW,m=\infty}}$ (trivially) generalizing the arguments of [144].

It is the easiest to start with the $\mathcal{N} = 2^*$ vacuum in a holographic dual, the PW geometry [177]. The IR limit corresponds to $\chi \to \infty$, thus, introducing a new radial coordinate $u \to \infty$,

$$e^{2\chi} \simeq 2u\,, \qquad e^{6\alpha} \simeq \frac{2}{3u}\,, \qquad e^{A} \simeq \left(\frac{2}{3u^4}\right)^{1/3} \mathrm{k}\,, \tag{6.71}$$

[15] It is interesting to investigate whether this $\mathbb{Z}_2$ symmetry can be spontaneously broken, and if so, what is the role of the magnetic field. This, however, is outside the scope of the current paper.

the background metric becomes

$$ds^2_{PW} \simeq \left(\frac{3}{2u^2}\right)^{4/3}\left[4du^2 + \left(\frac{2\mathrm{k}}{3}\right)^2 \eta_{\mu\nu}dx^\mu dx^\nu\right]. \tag{6.72}$$

The parameter $\mathrm{k} = 2m$ here is defined as in PW [177, 61]. Introducing [144]

$$e^{4\phi_2} \equiv e^{2(\alpha-\chi)} \simeq \left(\frac{1}{12u^4}\right)^{1/3}, \qquad e^{4\phi_1} \equiv e^{6\alpha+2\chi} \simeq \frac{4}{3}, \tag{6.73}$$

the metric (6.72) can be understood as a KK reduction of the locally AdS_6 metric on a compact $x_6 \sim x_6 + L_6$:

$$ds^2_6 = e^{-2\phi_2}ds^2_{PW} + e^{6\phi_2}dx_6^2 \;\simeq\; \frac{3^{3/2}}{2u^2}\left[4du^2 + \left(\frac{2\mathrm{k}}{3}\right)^2 \eta_{\mu\nu}dx^\mu dx^\nu + \frac{1}{9}dx_6^2\right]. \tag{6.74}$$

The metric (6.74) and the scalar ϕ_1 (6.73) is a solution [144] to $d = 6$ $\mathcal{N} = (1,1)$ $F(4)$ SUGRA [183]

$$S_{F(4)} = \frac{1}{16\pi G_6}\int_{\mathcal{M}_6} d\xi^6\sqrt{-g_6}\left(R_6 - 4(\partial\phi_1)^2 + e^{-2\phi_1} + e^{2\phi_1} - \frac{1}{16}e^{6\phi_1}\right), \tag{6.75}$$

where, using the PW five-dimensional Newton's constant G_5,

$$\frac{L_6}{G_6} = \frac{1}{G_5}. \tag{6.76}$$

Notice that the bulk gauge field in (6.49) can be reinterpreted as a gauge field in the six-dimensional metric (6.74)

$$\underbrace{\sqrt{-g_{PW}}\;\rho^4 F_{\mu\nu}F^{\mu\nu}}_{\text{in } ds^2_{PW}} \qquad = \qquad \underbrace{\sqrt{-g_6}\;e^{2\phi_1}F_{[6]\mu\nu}F^{\mu\nu}_{[6]}}_{\text{in } ds^2_6}, \tag{6.77}$$

leading to

$$S_{\mathbb{CFT}_{PW,m=\infty}} = \frac{1}{16\pi G_6}\int_{\mathcal{M}_6} d\xi^6 \sqrt{-g_6}\biggl(R_6 - 4(\partial\phi_1)^2 + e^{-2\phi_1} + e^{2\phi_1} - \frac{1}{16}e^{6\phi_1} - 4e^{2\phi_1}F_{[6]\mu\nu}F_{[6]}^{\mu\nu}\biggr)\,, \tag{6.78}$$

which is precisely the (truncated) effective action of the $F(4)$ gauged supergravity of [86][16].

Solutions to the gravitational theory (6.78) representing magnetic branes dual to anisotropic magnetized $\mathbb{CFT}_{PW,m=\infty}$ plasma correspond to the following background ansatz:

$$ds_5^2 = -c_1^2\, dt^2 + c_2^2\, \left(d\hat{x}^2 + d\hat{y}^2\right) + c_3^3\left(d\hat{z}^2 + d\hat{x}_6\right) + c_4^2\, dr^2\,, \qquad F_{[6]} = B_{[6]}\, d\hat{x}\wedge d\hat{y}\,, \tag{6.79}$$

where all the metric warp factors c_i as well as the bulk scalar ϕ_1 are functions of the radial coordinate r. The rescaled, i.e. $\hat{}$ coordinates, are related to PW coordinates x^μ and the KK direction x_6 as follows (compare with (6.74)):

$$\{\hat{t},\hat{\boldsymbol{x}}\} \equiv \hat{x}^\mu = \frac{2\mathrm{k}}{3}x^\mu\,, \qquad \hat{x}_6 = \frac{1}{3}x_6\,. \tag{6.80}$$

It is convenient to fix the radial coordinate r and redefine the metric warp factor, the bulk scalar, and the magnetic field as

$$\begin{aligned} c_1 &= \frac{3^{3/4}r}{2^{1/2}}\, \left(1-\frac{r_0^5}{r^5}\right)^{1/2}\, a_1\,, \qquad c_2 = \frac{3^{3/4}r}{2^{1/2}}\, a_2\,, \qquad c_3 = \frac{3^{3/4}r}{2^{1/2}}\,,\\ c_4 &= \frac{3^{3/4}2^{1/2}}{r}\, \left(1-\frac{r_0^5}{r^5}\right)^{-1/2}\, a_4\,, \qquad B_{[6]} = \frac{1}{2}r_0^2\,\hat{b}\,, \qquad \phi_1 = \frac{1}{4}\ln\frac{4}{3} + p\,. \end{aligned} \tag{6.81}$$

[16]The identification is as follows: $A^i = 0$, $B = 0$, $X = e^{-\phi_1}$, $m = \frac{1}{4}$ and $g^2 = \frac{1}{2}$.

The radial coordinate r changes

$$r \in [r_0, +\infty), \tag{6.82}$$

where r_0 is a location of a regular Schwarzschild horizon, and $r \to +\infty$ is the asymptotic AdS_6 boundary[17]. The bulk scalar field p is dual to a dimension $\Delta = 3$ of the effective five-dimensional boundary conformal theory. Introducing a radial coordinate x as in (6.29) we obtain the following system of ODEs (in a radial coordinate x, $' = \frac{d}{dx}$):

$$\begin{aligned}
0 = a_1' + \frac{a_1}{36a_2^3 x(x^5-1)(2a_2 - a_2'x)}\biggl(&18x^2a_2^2(x^5-1)(2a_2^2(p')^2 - (a_2')^2) \\
&+ 18xa_2^3(3x^5-8)a_2' - 4a_4^2(27a_2^4 - 8\hat{b}^2x^4)e^{2p} - 9a_2^4(9a_4^2e^{-2p} - e^{6p}a_4^2 - 20)\biggr),
\end{aligned} \tag{6.83}$$

$$\begin{aligned}
0 = a_4' - \frac{a_4}{36a_2^4 x(x^5-1)(2a_2 - a_2'x)}\biggl(&18a_2^3x^2(1-x^5)(2a_2^2(p')^2 + 3(a_2')^2) \\
&+ x(90a_2^4(x^5-2) + a_4^2(32e^{2p}\hat{b}^2x^4 + 9a_2^4(12e^{2p} + 9e^{-2p} - e^{6p})))a_2' \\
&- 3a_2(a_4^2(32e^{2p}\hat{b}^2x^4 + 3a_2^4(12e^{2p} + 9e^{-2p} - e^{6p})) - 60a_2^4)\biggr),
\end{aligned} \tag{6.84}$$

$$\begin{aligned}
0 = a_2'' - \frac{(a_2')^2}{a_2} + \frac{1}{36(x^5-1)xa_2^4}\biggl(&a_4^2(32e^{2p}\hat{b}^2x^4 + 9a_2^4(12e^{2p} + 9e^{-2p} - e^{6p})) \\
&+ 36a_2^4(x^5-1)\biggr)a_2' - \frac{32e^{2p}a_4^2\hat{b}^2x^2}{9a_2^3(x^5-1)},
\end{aligned} \tag{6.85}$$

$$\begin{aligned}
0 = p'' &+ \frac{1}{36(x^5-1)xa_2^4}\biggl(a_4^2(32e^{2p}\hat{b}^2x^4 + 9a_2^4(12e^{2p} + 9e^{-2p} - e^{6p})) + 36a_2^4(x^5-1)\biggr)p' \\
&+ \frac{a_4^2}{36a_2^4x^2(x^5-1)}\biggl(32e^{2p}\hat{b}^2x^4 - 27a_2^4(4e^{2p} - 3e^{-2p} - e^{6p})\biggr).
\end{aligned} \tag{6.86}$$

As before, r_0 is completely scaled out of all the equations of motion. Equations. (6.83)-

[17] AdS_6 of radius $L_{AdS_6} = 3^{3/4}2^{1/2}$ is a solution with $r_0 = 0$, $\hat{b} = 0$ and $a_1 = a_2 = a_4 \equiv 1$ and $p \equiv 0$.

(6.86) have to be solved subject to the following asymptotics:

- in the UV, i.e. as $x \to 0_+$,

$$
\begin{aligned}
a_1 =&1 + a_{1,5}x^5 + \mathcal{O}(x^9)\,, \qquad a_2 = 1 + \frac{8}{9}\hat{b}^2 x^4 + a_{2,5}x^5 + \mathcal{O}(x^7)\,, \\
a_4 =&1 - \frac{4}{3}\hat{b}^2 x^4 - (a_{1,5} + 2a_{2,5})x^5 + \mathcal{O}(x^6)\,, \qquad p = p_3 x^3 + \frac{4}{9}\hat{b}^2 x^4 + \mathcal{O}(x^6)\,;
\end{aligned}
\tag{6.87}
$$

- in the IR, i.e. as $y \equiv 1 - x \to 0_+$,

$$
\begin{aligned}
&a_1 = a_{1,h,0} + \mathcal{O}(y)\,, \qquad a_2 = a_{2,h,0} + \mathcal{O}(y)\,, \qquad p = \ln p_{h,0} + \mathcal{O}(y)\,, \\
&a_4 = \frac{30a_{2,h,0}^2 p_{h,0}}{(5p_{h,0}^4(9a_{2,h,0}^4(12 - p_{h,0}^4) + 32\hat{b}^2) + 405a_{2,h,0}^4)^{1/2}} + \mathcal{O}(y)\,.
\end{aligned}
\tag{6.88}
$$

In total, given $\hat{b}$, the asymptotic expansions are specified by 6 parameters:

$$
\{a_{1,5}\,,\ a_{2,5}\,,\ p_3\,,\ a_{1,h,0}\,,\ a_{2,h,0}\,,\ p_{h,0}\}\,,
\tag{6.89}
$$

which is the correct number of parameters necessary to provide a solution to a system of two second order and two first order equations, $2 \times 2 + 2 \times 1 = 6$. The parameter p_3 corresponds to the expectation value of a dimension $\Delta = 3$ operator of the boundary theory; the other two parameters, $a_{1,5}$ and $a_{2,5}$, determine the expectation value of its stress-energy tensor. Using the standard holographic renormalization we find:

$$
\begin{aligned}
&\langle T_{[5]\hat{t}\hat{t}} \rangle \equiv \mathcal{E}_{[5]} = \frac{27r_0^5}{32\pi G_6}(1 - 2a_{1,5} + a_{2,5})\,, \\
&\langle T_{[5]\hat{x}\hat{x}} \rangle = \langle T_{[5]\hat{y}\hat{y}} \rangle \equiv P_{[5]T} = \frac{27r_0^5}{128\pi G_6}(1 - 2a_{1,5} + 6a_{2,5})\,, \\
&\langle T_{\hat{z}\hat{z}} \rangle = \langle T_{[5]\hat{x}_6\hat{x}_6} \rangle \equiv P_{[5]L} = \frac{27r_0^5}{128\pi G_6}(1 - 2a_{1,5} - 4a_{2,5})\,,
\end{aligned}
\tag{6.90}
$$

for the components of the boundary stress-energy tensor, and

$$s_{[5]} = \frac{27 r_0^4 a_{2,h,0}^2}{16 G_6}\,, \qquad T_{[5]} = \frac{\sqrt{5} r_0 a_{1,h,0}}{48\pi a_{2,h,0}^2 p_{h,0}} \left[9 a_{2,h,0}^4 (9 - p_{h,0}^8 + 12 p_{h,0}^4) + 32 \hat{b}^2 p_{h,0}^4 \right]^{1/2}\,, \tag{6.91}$$

for the entropy density and the temperature. Note that,

$$\langle T^{\mu}_{[5]\ \mu} \rangle = 0\,. \tag{6.92}$$

There is no renormalization scheme dependence in (6.90), and the trace of the stress-energy tensor vanishes — there is no invariant dimension-five operator that can be constructed only with the magnetic field strength. The (holographic) free energy density is given by the standard relation (6.42). In (6.90)-(6.91) we used the subscript ${}_{[5]}$ to indicate that the thermodynamic quantities are measured from the perspective of the effective five-dimensional boundary conformal theory; to convert to the four-dimensional perspective, we need to account for (6.80), see also [53],

$$\begin{split} &\Big\{ \mathcal{E}, P_T, P_L \Big\} = \Big\{ \mathcal{E}_{[5]}, P_{[5]T}, P_{[5]L} \Big\} \times \underbrace{\left(\frac{2\mathrm{k}}{3}\right)^4}_{(d\hat{t}\cdot d\hat{vol}_3)/(dt\cdot dvol_3)} \times \underbrace{\frac{L_6}{3}}_{\oint d\hat{x}_6}\,, \\ &s = s_{[5]} \times \underbrace{\left(\frac{2\mathrm{k}}{3}\right)^3}_{d\hat{vol}_3/dvol_3} \times \underbrace{\frac{L_6}{3}}_{\oint d\hat{x}_6}\,, \qquad T = T_{[5]} \times \underbrace{\left(\frac{2\mathrm{k}}{3}\right)}_{d\hat{t}/dt}\,, \qquad b = \hat{b} \times \underbrace{\left(\frac{2\mathrm{k}}{3}\right)^2}_{d\hat{x}\wedge d\hat{y}/dx\wedge dy}\,. \end{split} \tag{6.93}$$

As for the other models discussed in this paper, the first law of thermodynamics $d\mathcal{E} = Tds$ (at fixed magnetic field) and the thermodynamic relation $\mathcal{F} = -P_L$ lead to constraints on the numerically obtained parameter set (6.89) (here $' = \frac{d}{d\hat{b}}$):

$$
\text{FL} : 0 = \frac{6(2\hat{b}a'_{2,5} - 4\hat{b}a'_{1,5} - 5a_{2,5} + 10a_{1,5} - 5)\sqrt{5}a_{2,h,0}p_{h,0}}{5a_{1,h,0}(32\hat{b}^2p_{h,0}^4 - 9a_{2,h,0}^4(p_{h,0}^8 - 12p_{h,0}^4 - 9))^{1/2}(a'_{2,h,0}\hat{b} - a_{2,h,0})} - 1\,, \tag{6.94}
$$

$$
\text{TR} : 0 = \frac{6(1 - 2a_{1,5})p_{h,0}\sqrt{5}}{a_{1,h,0}(32\hat{b}^2p_{h,0}^4 - 9a_{2,h,0}^4(p_{h,0}^8 - 12p_{h,0}^4 - 9))^{1/2}} - 1\,. \tag{6.95}
$$

In appendix J.0.3 we verified FT and TR in the $\mathbb{CFT}_{PW,m=\infty}$ model to order $\mathcal{O}(\hat{b}^4)$ inclusive; we also present $\mathcal{O}(B^4/T^8)$ results for $R_{\mathbb{CFT}_{PW,m=\infty}}$.

Chapter 7

Conclusion

In this thesis we studied several aspects of quantum field theory. We started uncovering a novel behavior developed by tree-level scattering amplitudes, finding that on the (i, j, k) split kinematic subspace amplitudes in the biadjoint scalar, NLSM and special Galileon theories split semi-locally into the product of three amputated currents without becoming singular. The semi-local property of these 3-splits makes an important difference from standard factorization, in which the particle set partitions. However, when one imposes further conditions on the kinematic space in order to turn currents into amplitudes, i.e. into observables, at least one of them vanishes, and in this sense locality is protected. We also found that, for the cases of NLSM and special Galileon amplitudes, smooth splits provide an alternative way to discover their extended theories by simply exploring subspaces of the kinematic space. Moreover, we used 3-splits to reconstruct NLSM amplitudes from novel recursion relations without resorting on soft limits. As far as we know, 3-splits are not derivable from unitarity arguments and therefore represent a new phenomenon in quantum field theory.

The smooth split phenomenon happens in all the theories that we studied, and it is important to ask whether other theories analogously split. Our analysis and proofs of 3-splits using CHY suggest that this could very well be the case. The reason is that the CHY potential and the integrands in the CHY formulas had a very interesting behavior under split kinematics, one which made the split very transparent. For example, it is tempting to start studying smooth splits for the Born-Infeld theory, as it admits a CHY formulation which contains the same matrix $\mathbf{A}_n$ that appears in both the NLSM and special Galileon representations. As we previously comment, reproducing 3-splits for Born-Infeld amplitudes would open the door for amplitudes in other theories like Yang-Mills and Einstein gravity to smoothly split, although new conditions on the polarization vectors are expected for this to happen. It is also intriguing that the 3-split behavior is very similar to the residue of one of the possible factorizations that higher-k amplitudes can have. It would be very interesting to dig further into this connection, and see if this behavior is indeed coming from the CEGM generalization of quantum field theory. This would imply that we could gain new insights into quantum field theory by studying the higher-k framework.

We then extended the global Schwinger construction, which computes the partial biadjoint amplitude $m_n(\mathbb{I},\mathbb{I})$ as an integral over the positive tropical Grassmannian $\text{Trop}^+G(2,n)$, to all amplitudes $m_n(\alpha,\beta)$ and proposed a formula for general ϕ^p theories, making use of non-crossing chord diagrams along the way. We found that ϕ^p amplitudes can be thought of as a sum of products of cubic amplitudes, and presented a formula for this general schematic structure based on the Lagrange inversion procedure. The different global Schwinger constructions provide an alternative way for computing scattering amplitudes, from geometrical and combinatorial considerations. It would be interesting to extend the study to loop level and even to other theories. An exciting possibility would be to find a way to include numerators, as this could provide a new transparent way to find and prove important properties of scattering amplitudes, like the double copy. One of the reasons to expect this is that, as we saw in this thesis, the global Schwinger formula already proved to be useful for studying well known properties of scattering amplitudes like factorization or soft limits. Furthermore, as there is a global Schwinger formula for general $\mathrm{Trop}^+G(k,n)$, one could try to define ϕ^p-like amplitudes for higher-k theories or start studying how the global Schwinger formula for higher-k behaves at poles, as this could be instructive for learning more about factorizations in CEGM amplitudes.

In fact, this thesis has also uncovered novel perspectives regarding the CEGM generalization of quantum field theory. First, let us recall that a key aspect of the CHY formula are the scattering equations, which connect the space of n points on $\mathbb{CP}^1$ with the space of kinematic invariants. The scattering equations possess $(n-3)!$ solutions and localize the CHY integral on them. The CEGM formulation contains analogous generalized scattering equations on $X(k,n)$, and one natural question was to determine their number of solutions. We found all the singular solutions —i.e. the solutions in which the n points do not remain in a generic configuration in a soft limit— for the cases $X(3,7)$, $X(4,7)$, $X(3,8)$ and $X(5,8)$. We also proposed a general classification for all singular solutions for any k and n. Since the scattering equations have been a powerful tool for studying properties of scattering amplitudes via CHY, like KLT orthogonality or the color-kinematics duality, it would be fascinating to find new physical applications from the generalized scattering equations, which could also help in constructing analogous Yang-Mills and gravity generalized amplitudes.

Since Feynman diagrams make spacetime properties like local interactions manifest, knowing about the analogous objects to Feynman diagrams that compute CEGM amplitudes could be of physical interest. Building up on work by Borges and Cachazo, who described generalized Feynman diagrams for $k=3$, we extended the study to any k, finding that in general they correspond to planar arrays of lower-point Feynman diagrams satisfying some compatibility conditions. These objects compute the higher-k amplitudes, and they are in bijection with the maximal cones of the positive tropical Grassmannian $\mathrm{Trop}^+G(k,n)$. It turns out that every Feynman diagram in quantum field theory has a dual description in terms of planar arrays. We also found a combinatorial bootstrap approach to obtain all these objects. One intriguing aspect of these results is that the planar arrays actually correspond to groups of standard Feynman diagrams, each with its own kinematics and its own metric. It could be important to understand the physical meaning of the compatibility conditions for the metrics of all the trees in the group. Moreover, as CEGM amplitudes factorize in exotic ways, e.g. into three pieces, in contrast with factorizations of standard amplitudes into two lower-point ones, it would be important to have a better combinatorial understanding of how planar arrays behave at poles. This could provide hints of what the notion of locality is in the CEGM formulation, and could help us obtain a field theoretic-like description of it. For example, a fascinating possibility would be to find a quantum theory that inevitably entails the planar arrays.

Finally, we moved on to study nonperturbative aspects of quantum field theory and analyzed various holographic models under a background magnetic field. These models describe the quark gluon plasma state of matter which shares some properties with the deconfined phase of the QCD plasma that prevailed in the early universe. In particular, we focused on conformal gauge theories as consistent truncations of $\mathcal{N}=8$ gauged supergravity in 5 dimensions, and on the nonconformal $\mathcal{N}=2^*$ gauge theory. We performed numerical simulations to show that there was no universal magnetoresponse as claimed in a previous article, since their results were due to a strong dependence on the renormalization scale, as well as other thermodynamic quantities did not show any universality. We found, however, a different universality for the $\mathcal{N}=2^*$ gauge theory in a magnetic field background: the corresponding plasma has a critical point for some $T_c/\sqrt{B}$, where T_c corresponds to a critical temperature and B is the magnetic field, which barely varies for different values of $m/\sqrt{B}$, where m is the hypermultiplet mass.

Bibliography

[1] Georges Aad et al. Observation of a new particle in the search for the Standard Model Higgs boson with the ATLAS detector at the LHC. *Phys. Lett. B*, 716:1–29, 2012.

[2] Md. Abhishek, Subramanya Hegde, Dileep P. Jatkar, and Arnab Priya Saha. Double soft theorem for generalised biadjoint scalar amplitudes. *SciPost Phys.*, 10(2):036, 2021.

[3] Md. Abhishek, Subramanya Hegde, and Arnab Priya Saha. One-loop integrand from generalised scattering equations. *JHEP*, 05:012, 2021.

[4] Stephen L. Adler. Consistency conditions on the strong interactions implied by a partially conserved axial-vector current. II. *Phys. Rev.*, 139:B1638–B1643, 1965.

[5] Nima Afkhami-Jeddi. Soft Graviton Theorem in Arbitrary Dimensions. 2014.

[6] Daniele Agostini, Taylor Brysiewicz, Claudia Fevola, Lukas Kühne, Bernd Sturmfels, and Simon Telen. Likelihood Degenerations. 7 2021.

[7] Ofer Aharony, Alex Buchel, and Patrick Kerner. The Black hole in the throat: Thermodynamics of strongly coupled cascading gauge theories. *Phys. Rev.*, D76:086005, 2007.

[8] Ofer Aharony, Steven S. Gubser, Juan Martin Maldacena, Hirosi Ooguri, and Yaron Oz. Large N field theories, string theory and gravity. *Phys. Rept.*, 323:183–386, 2000.

[9] P. B. Aneesh, Pinaki Banerjee, Mrunmay Jagadale, Renjan Rajan, Alok Laddha, and Sujoy Mahato. On positive geometries of quartic interactions: Stokes polytopes, lower forms on associahedra and world-sheet forms. *JHEP*, 04:149, 2020.

[10] P. B. Aneesh, Mrunmay Jagadale, and Nikhil Kalyanapuram. Accordiohedra as positive geometries for generic scalar field theories. *Phys. Rev. D*, 100(10):106013, 2019.

[11] Y. Aoki, G. Endrodi, Z. Fodor, S. D. Katz, and K. K. Szabo. The Order of the quantum chromodynamics transition predicted by the standard model of particle physics. *Nature*, 443:675–678, 2006.

[12] Nima Arkani-Hamed, Yuntao Bai, Song He, and Gongwang Yan. Scattering Forms and the Positive Geometry of Kinematics, Color and the Worldsheet. *JHEP*, 05:096, 2018.

[13] Nima Arkani-Hamed, Freddy Cachazo, and Jared Kaplan. What is the Simplest Quantum Field Theory? *JHEP*, 09:016, 2010.

[14] Nima Arkani-Hamed, Song He, and Thomas Lam. Stringy canonical forms. *JHEP*, 02:069, 2021.

[15] Nima Arkani-Hamed, Song He, Thomas Lam, and Hugh Thomas. Binary Geometries, Generalized Particles and Strings, and Cluster Algebras. 2019.

[16] Nima Arkani-Hamed, Song He, Giulio Salvatori, and Hugh Thomas. Causal Diamonds, Cluster Polytopes and Scattering Amplitudes. 12 2019.

[17] Nima Arkani-Hamed, Aaron Hillman, and Sebastian Mizera. Feynman polytopes and the tropical geometry of UV and IR divergences. *Phys. Rev. D*, 105(12):125013, 2022.

[18] Nima Arkani-Hamed, Tzu-Chen Huang, and Yu-tin Huang. Scattering amplitudes for all masses and spins. *JHEP*, 11:070, 2021.

[19] Nima Arkani-Hamed and Jared Kaplan. On Tree Amplitudes in Gauge Theory and Gravity. *JHEP*, 04:076, 2008.

[20] Nima Arkani-Hamed, Thomas Lam, and Marcus Spradlin. Non-perturbative geometries for planar $\mathcal{N} = 4$ SYM amplitudes. 2019.

[21] Nima Arkani-Hamed, Thomas Lam, and Marcus Spradlin. Positive configuration space. *Commun. Math. Phys.*, 384(2):909–954, 2021.

[22] Nima Arkani-Hamed and Jaroslav Trnka. The Amplituhedron. *JHEP*, 10:030, 2014.

[23] Peter Brockway Arnold, Guy D. Moore, and Laurence G. Yaffe. Transport coefficients in high temperature gauge theories. 1. Leading log results. *JHEP*, 11:001, 2000.

[24] Peter Brockway Arnold, Guy D Moore, and Laurence G. Yaffe. Transport coefficients in high temperature gauge theories. 2. Beyond leading log. *JHEP*, 05:051, 2003.

[25] Christian Baadsgaard, N. E. J. Bjerrum-Bohr, Jacob L. Bourjaily, and Poul H. Damgaard. Scattering Equations and Feynman Diagrams. *JHEP*, 09:136, 2015.

[26] Christian Baadsgaard, N. E. J. Bjerrum-Bohr, Jacob L. Bourjaily, and Poul H. Damgaard. String-Like Dual Models for Scalar Theories. *JHEP*, 12:019, 2016.

[27] G. S. Bali, F. Bruckmann, G. Endrodi, F. Gruber, and A. Schaefer. Magnetic field-induced gluonic (inverse) catalysis and pressure (an)isotropy in QCD. *JHEP*, 04:130, 2013.

[28] G. S. Bali, F. Bruckmann, G. Endrödi, S. D. Katz, and A. Schäfer. The QCD equation of state in background magnetic fields. *JHEP*, 08:177, 2014.

[29] Pinaki Banerjee, Alok Laddha, and Prashanth Raman. Stokes polytopes: the positive geometry for ϕ^4 interactions. *JHEP*, 08:067, 2019.

[30] Yuliy Baryshnikov. On stokes sets. *New developments in singularity theory (Cambridge, 2000)*, 21:65–86, 2001.

[31] K. Behrndt, Ali H. Chamseddine, and W. A. Sabra. BPS black holes in N=2 five-dimensional AdS supergravity. *Phys. Lett.*, B442:97–101, 1998.

[32] K. Behrndt, Mirjam Cvetic, and W. A. Sabra. Nonextreme black holes of five-dimensional N=2 AdS supergravity. *Nucl. Phys.*, B553:317–332, 1999.

[33] Paolo Benincasa and Alex Buchel. Hydrodynamics of Sakai-Sugimoto model in the quenched approximation. *Phys. Lett. B*, 640:108–115, 2006.

[34] Paolo Benincasa, Alex Buchel, and Roman Naryshkin. The Shear viscosity of gauge theory plasma with chemical potentials. *Phys. Lett. B*, 645:309–313, 2007.

[35] Paolo Benincasa and Freddy Cachazo. Consistency Conditions on the S-Matrix of Massless Particles. 5 2007.

[36] Arkady Berenstein, Sergey Fomin, and Andrei Zelevinsky. Cluster algebras III: Upper bounds and double Bruhat cells. *arXiv Mathematics e-prints*, page math/0305434, May 2003.

[37] Z. Bern, J. J. M. Carrasco, and Henrik Johansson. New Relations for Gauge-Theory Amplitudes. *Phys. Rev. D*, 78:085011, 2008.

[38] Z. Bern, Lance J. Dixon, M. Perelstein, and J. S. Rozowsky. Multileg one loop gravity amplitudes from gauge theory. *Nucl. Phys. B*, 546:423–479, 1999.

[39] Louis J. Billera, Susan P. Holmes, and Karen Vogtmann. Geometry of the space of phylogenetic trees. *Adv. Appl. Math.*, 27(4):733–767, November 2001.

[40] N. E. J. Bjerrum-Bohr, Poul H. Damgaard, Thomas Sondergaard, and Pierre Vanhove. The Momentum Kernel of Gauge and Gravity Theories. *JHEP*, 01:001, 2011.

[41] Nikolay Bobev, Arnab Kundu, Krzysztof Pilch, and Nicholas P. Warner. Supersymmetric Charged Clouds in AdS_5. *JHEP*, 03:070, 2011.

[42] Francisco Borges and Freddy Cachazo. Generalized Planar Feynman Diagrams: Collections. *JHEP*, 11:164, 2020.

[43] L. Bossinger, J. M. Drummond, and R. Glew. Adjacency for scattering amplitudes from the Gröbner fan. 12 2022.

[44] Raphael Bousso. The Holographic principle. *Rev. Mod. Phys.*, 74:825–874, 2002.

[45] E. Brezin, C. Itzykson, G. Parisi, and J. B. Zuber. Planar Diagrams. *Commun. Math. Phys.*, 59:35, 1978.

[46] Ruth Britto, Freddy Cachazo, and Bo Feng. Generalized unitarity and one-loop amplitudes in N=4 super-Yang-Mills. *Nucl. Phys. B*, 725:275–305, 2005.

[47] Ruth Britto, Freddy Cachazo, and Bo Feng. New recursion relations for tree amplitudes of gluons. *Nucl. Phys. B*, 715:499–522, 2005.

[48] Ruth Britto, Freddy Cachazo, Bo Feng, and Edward Witten. Direct proof of tree-level recursion relation in Yang-Mills theory. *Phys. Rev. Lett.*, 94:181602, 2005.

[49] Johannes Broedel, Oliver Schlotterer, and Stephan Stieberger. Polylogarithms, Multiple Zeta Values and Superstring Amplitudes. *Fortsch. Phys.*, 61:812–870, 2013.

[50] Alex Buchel. N=2* hydrodynamics. *Nucl. Phys.*, B708:451–466, 2005.

[51] Alex Buchel. On universality of stress-energy tensor correlation functions in supergravity. *Phys. Lett. B*, 609:392–401, 2005.

[52] Alex Buchel. Bulk viscosity of gauge theory plasma at strong coupling. *Phys. Lett.*, B663:286–289, 2008.

[53] Alex Buchel. Entanglement entropy of $\mathcal{N} = 2^*$ de Sitter vacuum. 2019.

[54] Alex Buchel, Stan Deakin, Patrick Kerner, and James T. Liu. Thermodynamics of the N=2* strongly coupled plasma. *Nucl. Phys.*, B784:72–102, 2007.

[55] Alex Buchel, Michal P. Heller, and Robert C. Myers. Equilibration rates in a strongly coupled nonconformal quark-gluon plasma. *Phys. Rev. Lett.*, 114(25):251601, 2015.

[56] Alex Buchel, Luis Lehner, Robert C. Myers, and Anton van Niekerk. Quantum quenches of holographic plasmas. *JHEP*, 05:067, 2013.

[57] Alex Buchel and James T. Liu. Universality of the shear viscosity in supergravity. *Phys. Rev. Lett.*, 93:090602, 2004.

[58] Alex Buchel and James T. Liu. Gauged supergravity from type IIB string theory on Y**p,q manifolds. *Nucl. Phys. B*, 771:93–112, 2007.

[59] Alex Buchel, James T. Liu, and Andrei O. Starinets. Coupling constant dependence of the shear viscosity in N=4 supersymmetric Yang-Mills theory. *Nucl. Phys. B*, 707:56–68, 2005.

[60] Alex Buchel and Chris Pagnutti. Critical phenomena in N=2* plasma. *Phys. Rev.*, D83:046004, 2011.

[61] Alex Buchel, Amanda W. Peet, and Joseph Polchinski. Gauge dual and noncommutative extension of an N=2 supergravity solution. *Phys.Rev.*, D63:044009, 2001.

[62] Alex Buchel and Bruno Umbert. QGP universality in a magnetic field? *JHEP*, 06:149, 2020.

[63] Freddy Cachazo. Combinatorial Factorization. 10 2017.

[64] Freddy Cachazo. Diagonally Embedded Sets of $\mathrm{Trop}^{+}G(2,n)$'s in $\mathrm{Trop}\,G(2,n)$: Is There a Critical Value of n? 4 2021.

[65] Freddy Cachazo, Peter Cha, and Sebastian Mizera. Extensions of Theories from Soft Limits. *JHEP*, 06:170, 2016.

[66] Freddy Cachazo and Nick Early. Planar Kinematics: Cyclic Fixed Points, Mirror Superpotential, k-Dimensional Catalan Numbers, and Root Polytopes. 10 2020.

[67] Freddy Cachazo and Nick Early. Minimal Kinematics: An All k and n Peek into $\mathrm{Trop}^{+}\mathrm{G}(k,n)$. *SIGMA*, 17:078, 2021.

[68] Freddy Cachazo and Nick Early. Biadjoint Scalars and Associahedra from Residues of Generalized Amplitudes. 4 2022.

[69] Freddy Cachazo, Nick Early, and Bruno Giménez Umbert. Smoothly splitting amplitudes and semi-locality. *JHEP*, 08:252, 2022.

[70] Freddy Cachazo, Nick Early, Alfredo Guevara, and Sebastian Mizera. Δ-algebra and scattering amplitudes. *JHEP*, 02:005, 2019.

[71] Freddy Cachazo, Nick Early, Alfredo Guevara, and Sebastian Mizera. Scattering Equations: From Projective Spaces to Tropical Grassmannians. *JHEP*, 06:039, 2019.

[72] Freddy Cachazo, Nick Early, and Yong Zhang. Color-Dressed Generalized Biadjoint Scalar Amplitudes: Local Planarity. 12 2022.

[73] Freddy Cachazo and Yvonne Geyer. A 'Twistor String' Inspired Formula For Tree-Level Scattering Amplitudes in N=8 SUGRA. 6 2012.

[74] Freddy Cachazo, Alfredo Guevara, Bruno Umbert, and Yong Zhang. Planar Matrices and Arrays of Feynman Diagrams. 12 2019.

[75] Freddy Cachazo, Song He, and Ellis Ye Yuan. Scattering equations and Kawai-Lewellen-Tye orthogonality. *Phys. Rev.*, D90(6):065001, 2014.

[76] Freddy Cachazo, Song He, and Ellis Ye Yuan. Scattering of Massless Particles in Arbitrary Dimensions. *Phys. Rev. Lett.*, 113(17):171601, 2014.

[77] Freddy Cachazo, Song He, and Ellis Ye Yuan. Scattering of Massless Particles: Scalars, Gluons and Gravitons. *JHEP*, 07:033, 2014.

[78] Freddy Cachazo, Song He, and Ellis Ye Yuan. Scattering Equations and Matrices: From Einstein To Yang-Mills, DBI and NLSM. *JHEP*, 07:149, 2015.

[79] Freddy Cachazo, Lionel Mason, and David Skinner. Gravity in Twistor Space and its Grassmannian Formulation. *SIGMA*, 10:051, 2014.

[80] Freddy Cachazo, Sebastian Mizera, and Guojun Zhang. Scattering Equations: Real Solutions and Particles on a Line. *JHEP*, 03:151, 2017.

[81] Freddy Cachazo and Jairo M. Rojas. Notes on Biadjoint Amplitudes, Trop $G(3,7)$ and $X(3,7)$ Scattering Equations. 2019.

[82] Freddy Cachazo and David Skinner. Gravity from Rational Curves in Twistor Space. *Phys. Rev. Lett.*, 110(16):161301, 2013.

[83] Freddy Cachazo and Andrew Strominger. Evidence for a New Soft Graviton Theorem. 2014.

[84] Freddy Cachazo, Bruno Umbert, and Yong Zhang. Singular Solutions in Soft Limits. 2019.

[85] Freddy Cachazo and Bruno Giménez Umbert. Connecting Scalar Amplitudes using The Positive Tropical Grassmannian. 5 2022.

[86] Kevin Chen and Michael Gutperle. Holographic line defects in F(4) gauged supergravity. *Phys. Rev.*, D100(12):126015, 2019.

[87] Clifford Cheung, Karol Kampf, Jiri Novotny, Chia-Hsien Shen, and Jaroslav Trnka. On-Shell Recursion Relations for Effective Field Theories. *Phys. Rev. Lett.*, 116(4):041601, 2016.

[88] Clifford Cheung, Karol Kampf, Jiri Novotny, and Jaroslav Trnka. Effective Field Theories from Soft Limits of Scattering Amplitudes. *Phys. Rev. Lett.*, 114(22):221602, 2015.

[89] Mirjam Cvetic and Steven S. Gubser. Phases of R charged black holes, spinning branes and strongly coupled gauge theories. *JHEP*, 04:024, 1999.

[90] Mirjam Cvetic, Hong Lu, and C. N. Pope. Gauged six-dimensional supergravity from massive type IIA. *Phys. Rev. Lett.*, 83:5226–5229, 1999.

[91] Sumit R. Das, Gary W. Gibbons, and Samir D. Mathur. Universality of low-energy absorption cross-sections for black holes. *Phys. Rev. Lett.*, 78:417–419, 1997.

[92] Eric D'Hoker and Per Kraus. Magnetic Brane Solutions in AdS. *JHEP*, 10:088, 2009.

[93] Lance J. Dixon. Calculating scattering amplitudes efficiently. In *Theoretical Advanced Study Institute in Elementary Particle Physics (TASI 95): QCD and Beyond*, pages 539–584, 1 1996.

[94] Louise Dolan and Peter Goddard. Proof of the Formula of Cachazo, He and Yuan for Yang-Mills Tree Amplitudes in Arbitrary Dimension. *JHEP*, 05:010, 2014.

[95] Louise Dolan and Peter Goddard. The Polynomial Form of the Scattering Equations. *JHEP*, 07:029, 2014.

[96] James Drummond, Jack Foster, Omer Gurdogan, and Chrysostomos Kalousios. Tropical Grassmannians, cluster algebras and scattering amplitudes. 2019.

[97] James Drummond, Jack Foster, Ömer Gürdoğan, and Chrysostomos Kalousios. Tropical fans, scattering equations and amplitudes. *JHEP*, 11:071, 2021.

[98] James Drummond, Jack Foster, Omer Gürdogan, and Chrysostomos Kalousios. Algebraic singularities of scattering amplitudes from tropical geometry. 2019.

[99] G. R. Dvali, Gregory Gabadadze, and Massimo Porrati. 4-D gravity on a brane in 5-D Minkowski space. *Phys. Lett. B*, 485:208–214, 2000.

[100] F. J. Dyson. The Radiation theories of Tomonaga, Schwinger, and Feynman. *Phys. Rev.*, 75:486–502, 1949.

[101] F. J. Dyson. The S matrix in quantum electrodynamics. *Phys. Rev.*, 75:1736–1755, 1949.

[102] Nicholas Early and Victor Reiner. On configuration spaces and whitehouse's lifts of the eulerian representations. *Journal of Pure and Applied Algebra*, 223(10):4524–4535, 2019.

[103] Nick Early. Combinatorics and Representation Theory for Generalized Permutohedra I: Simplicial Plates. *arXiv e-prints*, page arXiv:1611.06640, November 2016.

[104] Nick Early. Generalized permutohedra in the kinematic space. 4 2018.

[105] Nick Early. Honeycomb tessellations and canonical bases for permutohedral blades. 10 2018.

[106] Nick Early. From weakly separated collections to matroid subdivisions. 2019.

[107] Nick Early. Planar kinematic invariants, matroid subdivisions and generalized Feynman diagrams. 2019.

[108] Nick Early. Weighted blade arrangements and the positive tropical Grassmannian. 5 2020.

[109] Nick Early. Planarity in Generalized Scattering Amplitudes: PK Polytope, Generalized Root Systems and Worldsheet Associahedra. 6 2021.

[110] Henriette Elvang and Yu-tin Huang. *Scattering Amplitudes in Gauge Theory and Gravity*. Cambridge University Press, 2015.

[111] Roberto Emparan. Absorption of scalars by extended objects. *Nucl. Phys. B*, 516:297–314, 1998.

[112] Gergely Endrodi, Matthias Kaminski, Andreas Schafer, Jackson Wu, and Laurence Yaffe. Universal Magnetoresponse in QCD and $\mathcal{N}=4$ SYM. *JHEP*, 09:070, 2018.

[113] D. B. Fairlie and D. E. Roberts. DUAL MODELS WITHOUT TACHYONS - A NEW APPROACH. 1972.

[114] David B. Fairlie. A Coding of Real Null Four-Momenta into World-Sheet Coordinates. *Adv. Math. Phys.*, 2009:284689, 2009.

[115] Livia Ferro and Tomasz Lukowski. Amplituhedra, and beyond. *J. Phys. A*, 54(3):033001, 2021.

[116] R. P. Feynman. Space-time approach to quantum electrodynamics. *Phys. Rev.*, 76:769–789, Sep 1949.

[117] Sergey Fomin and Andrei Zelevinsky. Cluster algebras I: Foundations. *arXiv Mathematics e-prints*, page math/0104151, Apr 2001.

[118] Sergey Fomin and Andrei Zelevinsky. Cluster algebras II: Finite type classification. *Inventiones Mathematicae*, 154(1):63–121, Oct 2003.

[119] Jack Alexander Foster. *On the singularities of scattering amplitudes : From cluster adjacency tropical geometry*. PhD thesis, Southampton U., 2020.

[120] H Frost. Biadjoint scalar tree amplitudes and intersecting dual associahedra. *JHEP*, 06:153, 2018.

[121] Y. Fukuda et al. Evidence for oscillation of atmospheric neutrinos. *Phys. Rev. Lett.*, 81:1562–1567, 1998.

[122] Xiangrui Gao, Song He, and Yong Zhang. Labelled tree graphs, Feynman diagrams and disk integrals. *JHEP*, 11:144, 2017.

[123] Diego García Sepúlveda and Alfredo Guevara. A Soft Theorem for the Tropical Grassmannian. 2019.

[124] Israel M Gelfand, Mark I Graev, and Alexander Postnikov. Combinatorics of hypergeometric functions associated with positive roots. In *The Arnold-Gelfand mathematical seminars*, pages 205–221. Springer, 1997.

[125] Murray Gell-Mann and M Levy. The axial vector current in beta decay. *Nuovo Cim.*, 16:705, 1960.

[126] David J. Gross and Paul F. Mende. The High-Energy Behavior of String Scattering Amplitudes. *Phys. Lett. B*, 197:129–134, 1987.

[127] David J. Gross and Paul F. Mende. String Theory Beyond the Planck Scale. *Nucl. Phys. B*, 303:407–454, 1988.

[128] S. S. Gubser, Igor R. Klebanov, and A. W. Peet. Entropy and temperature of black 3-branes. *Phys. Rev. D*, 54:3915–3919, 1996.

[129] S. S. Gubser, Igor R. Klebanov, and Alexander M. Polyakov. Gauge theory correlators from noncritical string theory. *Phys. Lett. B*, 428:105–114, 1998.

[130] Steven S. Gubser, Igor R. Klebanov, and Arkady A. Tseytlin. Coupling constant dependence in the thermodynamics of N=4 supersymmetric Yang-Mills theory. *Nucl. Phys. B*, 534:202–222, 1998.

[131] Alfredo Guevara and Yong Zhang. Planar Matrices and Arrays of Feynman Diagrams: Poles for Higher k. 7 2020.

[132] Song He, Zhenjie Li, and Qinglin Yang. Truncated cluster algebras and Feynman integrals with algebraic letters. *JHEP*, 12:110, 2021. [Erratum: JHEP 05, 075 (2022)].

[133] Song He, Zhenjie Li, and Chi Zhang. Two-loop octagons, algebraic letters and $\bar{Q}$ equations. *Phys. Rev. D*, 101(6):061701, 2020.

[134] Song He, Lecheng Ren, and Yong Zhang. Notes on polytopes, amplitudes and boundary configurations for Grassmannian string integrals. *JHEP*, 04:140, 2020.

[135] Song He, Yihong Wang, Yong Zhang, and Peng Zhao. Notes on worldsheet-like variables for cluster configuration spaces. 9 2021.

[136] Song He and Qinglin Yang. An Etude on Recursion Relations and Triangulations. *JHEP*, 05:040, 2019.

[137] Niklas Henke. *Applications of tropical geometry and cluster algebras to multi-particle scattering amplitudes.* PhD thesis, Hamburg U., 2022.

[138] Niklas Henke and Georgios Papathanasiou. How tropical are seven- and eight-particle amplitudes? 2019.

[139] Niklas Henke and Georgios Papathanasiou. Singularities of eight- and nine-particle amplitudes from cluster algebras and tropical geometry. *JHEP*, 10:007, 2021.

[140] Sven Herrmann, Anders Jensen, Michael Joswig, and Bernd Sturmfels. How to draw tropical planes. *the electronic journal of combinatorics*, 16(2):6, 2009.

[141] Christopher P. Herzog. The Hydrodynamics of M theory. *JHEP*, 12:026, 2002.

[142] Kurt Hinterbichler. Theoretical Aspects of Massive Gravity. *Rev. Mod. Phys.*, 84:671–710, 2012.

[143] Kurt Hinterbichler and Austin Joyce. Hidden symmetry of the Galileon. *Phys. Rev. D*, 92(2):023503, 2015.

[144] Carlos Hoyos. Higher dimensional conformal field theories in the Coulomb branch. *Phys. Lett.*, B696:145–150, 2011.

[145] Simon C. Huot, Sangyong Jeon, and Guy D. Moore. Shear viscosity in weakly coupled N = 4 super Yang-Mills theory compared to QCD. *Phys. Rev. Lett.*, 98:172303, 2007.

[146] Mrunmay Jagadale and Alok Laddha. Towards positive geometry of multi scalar field amplitudes. Accordiohedron and effective field theory. *JHEP*, 04:100, 2022.

[147] Renjan Rajan John, Ryota Kojima, and Sujoy Mahato. Weights, Recursion relations and Projective triangulations for Positive Geometry of scalar theories. *JHEP*, 10:037, 2020.

[148] Nikhil Kalyanapuram. On Polytopes and Generalizations of the KLT Relations. *JHEP*, 12:057, 2020.

[149] Nikhil Kalyanapuram. Stokes Polytopes and Intersection Theory. *Phys. Rev. D*, 101(10):105010, 2020.

[150] Nikhil Kalyanapuram and Raghav G. Jha. Positive Geometries for all Scalar Theories from Twisted Intersection Theory. *Phys. Rev. Res.*, 2(3):033119, 2020.

[151] Karol Kampf, Jiri Novotny, and Jaroslav Trnka. Tree-level Amplitudes in the Nonlinear Sigma Model. *JHEP*, 05:032, 2013.

[152] Karol Kampf and Jiří Novotny. Unification of Galileon Dualities. *JHEP*, 10:006, 2014.

[153] H. Kawai, D. C. Lewellen, and S. H. H. Tye. A Relation Between Tree Amplitudes of Closed and Open Strings. *Nucl. Phys. B*, 269:1–23, 1986.

[154] Ryota Kojima. Weights and recursion relations for ϕ^p tree amplitudes from the positive geometry. *JHEP*, 08:054, 2020.

[155] P. Kovtun, Dan T. Son, and Andrei O. Starinets. Viscosity in strongly interacting quantum field theories from black hole physics. *Phys. Rev. Lett.*, 94:111601, 2005.

[156] Karl Landsteiner and Javier Mas. The Shear viscosity of the non-commutative plasma. *JHEP*, 07:088, 2007.

[157] Tomasz Lukowski, Matteo Parisi, and Lauren K. Williams. The positive tropical Grassmannian, the hypersimplex, and the m=2 amplituhedron. 2 2020.

[158] Kengo Maeda, Makoto Natsuume, and Takashi Okamura. Viscosity of gauge theory plasma with a chemical potential from AdS/CFT. *Phys. Rev. D*, 73:066013, 2006.

[159] Carlos R. Mafra. Berends-Giele recursion for double-color-ordered amplitudes. *JHEP*, 07:080, 2016.

[160] Juan Martin Maldacena. The Large N limit of superconformal field theories and supergravity. *Int. J. Theor. Phys.*, 38:1113–1133, 1999. [Adv. Theor. Math. Phys.2,231(1998)].

[161] Michelangelo L. Mangano and Stephen J. Parke. Multiparton amplitudes in gauge theories. *Phys. Rept.*, 200:301–367, 1991.

[162] Thibault Manneville and Vincent Pilaud. Geometric realizations of the accordion complex of a dissection. *arXiv e-prints*, page arXiv:1703.09953, March 2017.

[163] J. Mas. Shear viscosity from R-charged AdS black holes. *JHEP*, 03:016, 2006.

[164] David Mateos, Robert C. Myers, and Rowan M. Thomson. Holographic phase transitions with fundamental matter. *Phys. Rev. Lett.*, 97:091601, 2006.

[165] David Mateos, Robert C. Myers, and Rowan M. Thomson. Holographic viscosity of fundamental matter. *Phys. Rev. Lett.*, 98:101601, 2007.

[166] David Mateos, Robert C. Myers, and Rowan M. Thomson. Thermodynamics of the brane. *JHEP*, 05:067, 2007.

[167] Sebastian Mizera. Combinatorics and Topology of Kawai-Lewellen-Tye Relations. *JHEP*, 08:097, 2017.

[168] Sebastian Mizera. Inverse of the String Theory KLT Kernel. *JHEP*, 06:084, 2017.

[169] Sebastian Mizera. *Aspects of Scattering Amplitudes and Moduli Space Localization*. PhD thesis, Perimeter Inst. Theor. Phys., 2019.

[170] Stephen G. Naculich. CHY representations for gauge theory and gravity amplitudes with up to three massive particles. *JHEP*, 05:050, 2015.

[171] V. P. Nair. A Current Algebra for Some Gauge Theory Amplitudes. *Phys. Lett. B*, 214:215–218, 1988.

[172] J. C. Novelli and J. Y. Thibon. Hopf Algebras of m-permutations, (m+1)-ary trees, and m-parking functions. *arXiv e-prints*, page arXiv:1403.5962, March 2014.

[173] Brian C. Odom, D. Hanneke, B. D'Urso, and G. Gabrielse. New Measurement of the Electron Magnetic Moment Using a One-Electron Quantum Cyclotron. *Phys. Rev. Lett.*, 97:030801, 2006.

[174] OEIS Foundation Inc. (2019), The On-Line Encyclopedia of Integer Sequences. . http://oeis.org.

[175] Matteo Parisi. *Combinatorial aspects of scattering amplitudes: amplituhedra, T-duality, and cluster algebras.* PhD thesis, Oxford U., Inst. Math., 2021.

[176] Stephen J. Parke and T. R. Taylor. Amplitude for n-gluon scattering. *Phys. Rev. Lett.*, 56:2459–2460, Jun 1986.

[177] Krzysztof Pilch and Nicholas P. Warner. N=2 supersymmetric RG flows and the IIB dilaton. *Nucl. Phys.*, B594:209–228, 2001.

[178] Joseph Polchinski. Dirichlet Branes and Ramond-Ramond charges. *Phys. Rev. Lett.*, 75:4724–4727, 1995.

[179] B. Pontecorvo. Neutrino Experiments and the Problem of Conservation of Leptonic Charge. *Zh. Eksp. Teor. Fiz.*, 53:1717–1725, 1967.

[180] Alexander Postnikov. Total positivity, Grassmannians, and networks. *arXiv Mathematics e-prints*, page math/0609764, September 2006.

[181] Prashanth Raman. The positive geometry for ϕ^p interactions. *JHEP*, 10:271, 2019.

[182] Radu Roiban, Marcus Spradlin, and Anastasia Volovich. On the tree level S matrix of Yang-Mills theory. *Phys. Rev. D*, 70:026009, 2004.

[183] L. J. Romans. The F(4) Gauged Supergravity in Six-dimensions. *Nucl. Phys.*, B269:691, 1986. [,691(1985)].

[184] Paul Romatschke and Ulrike Romatschke. Viscosity Information from Relativistic Nuclear Collisions: How Perfect is the Fluid Observed at RHIC? *Phys. Rev. Lett.*, 99:172301, 2007.

[185] Giulio Salvatori. 1-loop Amplitdues from the Halohedron. 2018.

[186] Giulio Salvatori and Stefan Stanojevic. Scattering Amplitudes and Simple Canonical Forms for Simple Polytopes. *JHEP*, 03:067, 2021.

[187] Francisco Santos, Christian Stump, and Volkmar Welker. Noncrossing sets and a grassmann associahedron. In *Forum of Mathematics, Sigma*, volume 5. Cambridge University Press, 2017.

[188] Omid Saremi. The Viscosity bound conjecture and hydrodynamics of M2-brane theory at finite chemical potential. *JHEP*, 10:083, 2006.

[189] Burkhard U. W. Schwab and Anastasia Volovich. Subleading Soft Theorem in Arbitrary Dimensions from Scattering Equations. *Phys. Rev. Lett.*, 113(10):101601, 2014.

[190] Jiro Sekiguchi and Masaaki Yoshida. W (e6)-action on the configuration space of six lines on the real projective plane. *Kyushu Journal of Mathematics*, 51(2):297–354, 1997.

[191] Kostas Skenderis. Lecture notes on holographic renormalization. *Class. Quant. Grav.*, 19:5849–5876, 2002.

[192] Alexei N Skorobogatov. On the number of representations of matroids over finite fields. *Designs, Codes and Cryptography*, 9(2):215–226, 1996.

[193] Dam T. Son and Andrei O. Starinets. Hydrodynamics of r-charged black holes. *JHEP*, 03:052, 2006.

[194] David Speyer and Bernd Sturmfels. The tropical Grassmannian. *Advances in Geometry*, 4(3):389–411, 2004.

[195] David Speyer and Lauren K. Williams. The tropical totally positive Grassmannian. *arXiv Mathematics e-prints*, page math/0312297, December 2003.

[196] Ishan Srivastava. Constraining the weights of Stokes polytopes using BCFW recursions for ϕ^4. *JHEP*, 04:064, 2021.

[197] Bernd Sturmfels and Simon Telen. Likelihood Equations and Scattering Amplitudes. 12 2020.

[198] Leonard Susskind. The World as a hologram. *J. Math. Phys.*, 36:6377–6396, 1995.

[199] Leonard Susskind and G. Frye. Algebraic aspects of pionic duality diagrams. *Phys. Rev. D*, 1:1682–1686, 1970.

[200] Gerard 't Hooft. A Planar Diagram Theory for Strong Interactions. *Nucl. Phys. B*, 72:461, 1974.

[201] Gerard 't Hooft. Dimensional reduction in quantum gravity. *Conf. Proc. C*, 930308:284–296, 1993.

[202] Derek Teaney. The Effects of viscosity on spectra, elliptic flow, and HBT radii. *Phys. Rev. C*, 68:034913, 2003.

[203] Steven Weinberg. Infrared photons and gravitons. *Phys. Rev.*, 140:B516–B524, 1965.

[204] Edward Witten. Anti-de Sitter space and holography. *Adv. Theor. Math. Phys.*, 2:253–291, 1998.

[205] Edward Witten. Anti-de Sitter space, thermal phase transition, and confinement in gauge theories. *Adv. Theor. Math. Phys.*, 2:505–532, 1998.

[206] Edward Witten. Perturbative gauge theory as a string theory in twistor space. *Commun. Math. Phys.*, 252:189–258, 2004.

[207] R. L. Workman et al. Review of Particle Physics. *PTEP*, 2022:083C01, 2022.

[208] Donovan Young. Linear k-Chord Diagrams. *arXiv e-prints*, page arXiv:2004.06921, April 2020.

APPENDICES

Appendix A

Definition of Amputated Currents

Throughout chapter 2, we have used amputated currents in various quantum field theories of scalars in order to characterize the behavior of the corresponding amplitudes when restricted to the split kinematic subspace. In this appendix we give a formal definition of the objects.

Currents are objects in quantum field theory which appear when one interpolates between correlation functions and scattering amplitudes. Recall that the LSZ formalism starts with a correlation function of operators in coordinate space $G(x_1, x_2, \ldots, x_n)$. Fourier transforming to momentum space produces a distribution localized on the momentum conservation loci

$$\delta^D(p_1 + p_2 + \cdots + p_n)\tilde{G}(p_1, p_2, \ldots, p_n)\,.$$

This is due to translational invariance of the correlation function $G(x_1, x_2, \ldots, x_n)$. The function $\tilde{G}(p_1, p_2, \ldots, p_n)$ has simple poles of the form $1/p_i^2$ and a scattering amplitude is obtained by the limiting procedure (or multidimensional residue computation)

$$A(p_1, p_2, \ldots, p_n) = \left(\prod_{i=1}^{n} \lim_{p_i^2 \to 0} p_i^2 \right) \tilde{G}(p_1, p_2, \ldots, p_n). \tag{A.1}$$

The process of multiplying by p_i^2 is called "amputating" the i^{th}-leg. A current is defined by performing all but one of the operations in (A.1). Let us assume that the n^{th}-leg is spared. Then,

$$J(p_1, p_2, \ldots, p_{n-1}) := \left(\prod_{i=1}^{n-1} \lim_{p_i^2 \to 0} p_i^2 \right) \tilde{G}(p_1, p_2, \ldots, p_{n-1}, p_n). \tag{A.2}$$

Note that the current still possesses the $1/p_n^2$ pole and hence the n^{th} leg is said to remain off-shell, i.e. $p_n^2 \neq 0$. In chapter 2, the relevant object is the amputated current, i.e.

$$\mathcal{J}(p_1, p_2, \ldots, p_{n-1}) := p_n^2 J(p_1, p_2, \ldots, p_{n-1}). \tag{A.3}$$

In general, (amputated) currents are not unique. This is most apparent in gauge theories where currents are not even gauge invariant. The reason is that physical observables are obtained from scattering amplitudes and therefore any two currents that differ by something that vanishes when $p_n^2 = 0$ lead to the same physical consequences. Here, however, we are using currents to determine the behavior of amplitudes and as such there can be no ambiguity. Luckily, for scalar theories there is a natural prescription which provides the required definition. The Feynman diagrams used to compute correlation functions in momentum space and amplitudes are combinatorially identical. The prescription is to write each Feynman diagram in terms of a basis of Mandelstam invariants provided by the planar ones with respect to the canonical order $\mathbb{I}$. Each such invariant can be made to depend on only a set of particles not containing label n. Each Feynman diagram is then fully amputated.

While this definition is precise, it is not very effective in practice as computing amplitudes or currents using Feynman diagrams quickly becomes impractical as n increases. This is why we provide a definition using the CHY formalism. In fact, this definition leads exactly to the amputated currents that appear in smooth splittings.

Consider the most general CHY potential for n particles and we will allow three of them to be off-shell, say particles i, j, k. Of course, we are only interested in the case with a single off-shell particles but the construction is more uniform is we allow all three to be off-shell. Following Naculich's construction [170], we define the modified CHY potential[1]

$$\begin{aligned}\mathcal{S}_n = &\sum_{a<b} 2p_a \cdot p_b \log(\sigma_a - \sigma_b) + (p_i^2 + p_j^2 - p_k^2)\log(\sigma_i - \sigma_j) + \\ &(p_k^2 + p_i^2 - p_j^2)\log(\sigma_k - \sigma_i) + (p_j^2 + p_k^2 - p_i^2)\log(\sigma_j - \sigma_k).\end{aligned} \tag{A.4}$$

Note that this potential was designed as to preserve $\mathrm{SL}(2,\mathbb{C})$ invariance. This means that three of the punctures can be fixed and it is natural to take the set $\{\sigma_i, \sigma_j, \sigma_k\}$ to be $\{0, 1, \infty\}$. Let us choose $\sigma_i = 0, \sigma_j = 1$, and $\sigma_k = \infty$. In this case the potential becomes

$$\mathcal{S}_n = \sum_{a<b\,:\,a,b\notin\{i,j,k\}} s_{ab}\log(\sigma_a - \sigma_b) + \sum_{a\notin\{i,j\}} \left(2p_a \cdot p_i \log(\sigma_a) + 2p_a \cdot p_j \log(1 - \sigma_a)\right). \tag{A.5}$$

Note that any term containing σ_k drops out while $\log(\sigma_i - \sigma_j) = \log 1 = 0$.

Having constructed the CHY potential it is possible to give the CHY formula for the five kinds of amputated currents used in the main text. We present them in the form of a lemma. In the lemma the CHY potential $\mathcal{S}_n$ is always the one defined in (A.5). We also use $\mathbf{A}_n^{[p\,q]}$ to denote the submatrix of the matrix $\mathbf{A}_n$ obtained by removing the p^{th} and q^{th} rows and columns. The entries of the $n \times n$ matrix $\mathbf{A}_n$ that do not involve off-shell legs

[1] Naculich works directly with the scattering equations and not with the potential but it is straightforward to translate.

are given by the standard expression $A_{ab} = s_{ab}/(\sigma_a - \sigma_b)$. Likewise, $\mathbf{A}_n^{[i\,j\,k]}$ denotes the submatrix of the matrix $\mathbf{A}_n$ obtained by removing the i^{th}, j^{th} and k^{th} rows and columns.

Before proceeding, a comment on notation is required. An amputated current is often written in a form in which the n^{th} particle corresponds to the off-shell leg and to indicate this the n^{th} label is not shown as in (A.3). However, in the statement of the lemma we allow the off-shell leg to be any leg in a given set and therefore all labels are shown in the currents.

Lemma A.0.1. *Let $q \in \{i, j, k\}$ represent the off-shell leg of the current. Then the CHY representation of a biadjoint amputated current is given by,*

$$\mathcal{J}(1, 2, \ldots, n) = \int \prod_{a \notin \{i,j,k\}} d\sigma_a \delta\left(\frac{\partial \mathcal{S}_n}{\partial \sigma_a}\right) \left(\frac{|i\,j||j\,k||k\,i|}{|1\,2||2\,3| \cdots |n-1\,n||n\,1|}\right)^2 . \tag{A.6}$$

The CHY representation of a NLSM amputated current is,

$$\mathcal{J}^{\text{NLSM}}(1, 2, \ldots, n) = \int \prod_{a \notin \{i,j,k\}} d\sigma_a \delta\left(\frac{\partial \mathcal{S}_n}{\partial \sigma_a}\right) \left(\frac{|i\,j||j\,k||k\,i|}{|1\,2||2\,3| \cdots |n-1\,n||n\,1|}\right) \frac{|i\,j||j\,k||k\,i|}{|p\,q|^2} \det \boldsymbol{A}_n^{[p\,q]} . \tag{A.7}$$

Here q is arbitrary (with $q \neq p$), although in practise it is convenient to choose it in the set $\{i, j, k\}$.

Similarly, the CHY representation of a mixed NLSM amputated current is given by,

$$\mathcal{J}^{\text{NLSM}\oplus\phi^3}(1, 2, \ldots, n|i, j, k) = \int \prod_{a \notin \{i,j,k\}} d\sigma_a \delta\left(\frac{\partial \mathcal{S}_n}{\partial \sigma_a}\right) \left(\frac{|i\,j||j\,k||k\,i|}{|1\,2||2\,3| \cdots |n-1\,n||n\,1|}\right) \det \boldsymbol{A}_n^{[i\,j\,k]} . \tag{A.8}$$

The CHY representation of a special Galileon amputated current is,

$$\mathcal{J}^{\mathrm{sGal}} = \int \prod_{a \notin \{i,j,k\}} d\sigma_a \delta\left(\frac{\partial \mathcal{S}_n}{\partial \sigma_a}\right) \left(\frac{|i\,j||j\,k||k\,i|}{|p\,q|^2} \det \boldsymbol{A}_n^{[p\,q]}\right)^2 \tag{A.9}$$

and finally the CHY representation of a mixed special Galileon amputated current is,

$$\mathcal{J}^{\mathrm{sGal}\oplus\phi^3}(i,j,k) = \int \prod_{a \notin \{i,j,k\}} d\sigma_a \delta\left(\frac{\partial \mathcal{S}_n}{\partial \sigma_a}\right) \left(\det \boldsymbol{A}_n^{[i\,j\,k]}\right)^2. \tag{A.10}$$

Proof. To prove the lemma it is required to show that the corresponding CHY formulas reproduce the amputated currents as defined using Feynman diagrams. However, for scalar field theories, this is evident from the Dolan-Goddard proof of biadjoint amplitudes [94] and from Naculich's general construction [170].

□

Appendix B

Proof of Determinantal Product Formula: Lemma 2.4.1

In chapter 2 we proved the smooth splitting formula for NSLM and special Galileon amplitudes using Lemma 2.4.1. In this appendix we provide the proof. For the reader's convenience we rewrite the statement of the Lemma.

Lemma B.0.1. *Let $M \in \mathbb{C}^{2m\times 2m}$ be antisymmetric, $L \in \mathbb{C}^{r\times r}$, and $W \in \mathbb{C}^{(2m+r)\times(2m+r)}$*

defined in terms of M and L as follows

$$W := \left[\begin{array}{ccccc|ccccc} 0 & M_{1,2} & \cdots & M_{1,2m-1} & M_{1,2m} & 0 & 0 & 0 & \cdots & 0 \\ -M_{1,2} & 0 & \cdots & M_{2,2m-1} & M_{2,2m} & 0 & 0 & 0 & \cdots & 0 \\ \vdots & \vdots & \vdots & \ddots & \vdots & \vdots & \vdots & \vdots & \ddots & \vdots \\ -M_{1,2m-1} & -M_{2,2m-1} & \cdots & 0 & M_{2m-1,2m} & 0 & 0 & 0 & \cdots & 0 \\ -M_{1,2m} & -M_{2,2m} & \cdots & -M_{2m-1,2m} & 0 & c_1 & c_2 & c_3 & \cdots & c_r \\ \hline 0 & 0 & \cdots & 0 & d_1 & L_{1,1} & L_{1,2} & \cdots & L_{1,r-1} & L_{1,r} \\ 0 & 0 & \cdots & 0 & d_2 & L_{2,1} & L_{2,2} & \cdots & L_{2,r-1} & L_{2,r} \\ \vdots & \vdots & \ddots & \vdots & \vdots & \vdots & \vdots & \ddots & \vdots & \vdots \\ 0 & 0 & \cdots & 0 & d_r & L_{r,1} & L_{r,2} & \cdots & L_{r,r-1} & L_{r,r} \end{array}\right] \tag{B.1}$$

with d_a and c_a arbitrary complex numbers, then the following holds

$$det(W) = det(M)\,det(L). \tag{B.2}$$

Proof. Let us compute the determinant on the LHS of (B.0.1) using the $2m$-th column to expand. Note that the contribution from any d_a is of the form

$$\det \left[\begin{array}{c|c} P & Q \\ \hline 0 & R \end{array}\right] = \det(P)\det(R) \tag{B.3}$$

where

$$P = \begin{bmatrix} 0 & M_{1,2} & M_{1,3} & \cdots & M_{1,2m-1} \\ -M_{1,2} & 0 & M_{2,3} & \cdots & M_{2,2m-1} \\ -M_{1,3} & -M_{2,3} & 0 & \cdots & M_{3,2m-1} \\ \vdots & \vdots & \vdots & \ddots & \vdots \\ -M_{1,2m-1} & -M_{2,2m-1} & -M_{3,2m-1} & \cdots & 0 \end{bmatrix}. \tag{B.4}$$

Since P is an odd-dimensional antisymmetric matrix, its determinant is zero and therefore the determinant (B.3) vanishes. This implies that the determinant on the LHS of (B.0.1) is independent of d_a. Likewise, the determinant can also be shown to be independent of c_a.

Having proved that (B.3) is independent of the values of d_a and c_a, it is possible to set them to any convenient values. In this case, it is clear that by setting $d_a = c_a = 0$ for all $a \in \{1, 2, \ldots, r\}$ one is left with the determinant of a block diagonal matrix. Using the elementary property of determinants that the determinant of a block-diagonal matrix is the product of the determinants of the blocks the result follows. □

Appendix C

Lagrange Inversion Formula and Fuss-Catalan Numbers

Given a function $f(x)$ that admits a series expansion around $x = 0$ and $f(0) = 0$ while $f'(0) \neq 0$, the Lagrange inversion formula gives a series expansion for the compositional inverse of $f(x)$, i.e. for a function $g(x)$ such that $g(f(x)) = x$, in terms of the series coefficients of $f(x)$.

Let us review one particular formulation which is relevant for this work. Start by defining an auxiliary function $h(x)$ such that $h(x) = x/f(x)$. Let

$$h(x) = \sum_{i=0}^{\infty} h_i x^i \tag{C.1}$$

be the series expansion of $h(x)$ around $x = 0$. Now define

$$g_r := \frac{1}{2\pi i} \oint_{|z|=\epsilon} \frac{dz}{r+1} \left(\frac{h(z)}{z} \right)^{r+1}. \tag{C.2}$$

The Lagrange inversion formula states that the series expansion of $g(x)$ is of the form

$$g(x) = x\sum_{r=0}^{\infty} g_r x^r\,. \tag{C.3}$$

The proof is fairly simple. Consider the RHS of (C.2) and write it in terms of $f(z)$ and then write $z = g(u)$,

$$\frac{1}{2\pi i}\oint_{|z|=\epsilon}\frac{dz}{r+1}\left(\frac{1}{f(z)}\right)^{r+1} = \frac{1}{2\pi i}\oint_{|u|=\epsilon}\frac{du}{r+1}g'(u)\left(\frac{1}{f(g(u))}\right)^{r+1} = \frac{1}{2\pi i}\oint_{|u|=\epsilon}\frac{du}{(r+1)}\frac{g'(u)}{u^{r+1}}. \tag{C.4}$$

Now, taking the derivative of (C.3),

$$g'(x) = \sum_{r=0}^{\infty}(r+1)g_r x^r \tag{C.5}$$

and plugging in it into the last expression on the right in (C.4) one finds (C.2).

Before seeing explicitly how this works in the context of interest, let us review some well-known facts about generating functions of Fuss-Catalan numbers, in particular, how they are interconnected via the Lagrange inversion formula.

Let $B_k(x)$ be the generating of the Fuss-Catalan numbers $\mathrm{FC}_n(k,1)$. The function $B_k(x)$ satisfies the equation $B_k(x) = 1 + xB_k(x)^k$. Now let us prove that

$$f(x) := \frac{x}{B_{k-1}(x)}, \quad g(x) := xB_k(x) \tag{C.6}$$

are compositional inverses of each other. Start with $B_k(x) = 1 + xB_k(x)^k$ and multiply by x^{k-1} so that we get an equation for $g(x)$ of the form $x^{k-2}g(x) = x^{k-1} + g(x)^k$. Now let $p(x)$ be the compositional inverse of $g(x)$, i.e., $g(p(x)) = x$. Letting $x = p(u)$ in

$x^{k-2}g(x) = x^{k-1} + g(x)$ leads to $u\,p(u)^{k-2} = p(u)^{k-1} + u^k$. Let us prove that $f(x)$ satisfies the same equation as $p(x)$. Starting with $B_{k-1}(x) = 1 + xB_{k-1}(x)^{k-1}$ and substituting $B_{k-1}(x) = x/f(x)$ gives $x/f(x) = 1 + x^k/f(x)^{k-1}$. Multiplying by $f(x)^{k-1}$ we obtain the same equation satisfied by $p(x)$.

In the case at hand, we are interested in $k = 3$ so that

$$h(x) = B_2(x) = \frac{1-\sqrt{1-4z}}{2z} \tag{C.7}$$

is the generating function of Catalan numbers, and g_r becomes the Fuss-Catalan number $\mathrm{FC}_r(3,1)$. In this case (C.2) reads

$$\mathrm{FC}_r(3,1) = \frac{1}{2\pi i}\oint_{|z|=\epsilon} \frac{dz}{r+1}\left(\frac{1-\sqrt{1-4z}}{2z^2}\right)^{r+1} \tag{C.8}$$

with

$$g(x) = xB_3(x), \quad \text{with} \quad B_3(x) := \sum_{r=0}^{\infty} \mathrm{FC}_r(3,1)x^r\,. \tag{C.9}$$

Let us see how this applies to our construction in section 3.6. Let us consider the following choice for the function $h(x)$

$$h(x) = \sum_{i=0}^{\infty} m_{i+2}x^i \tag{C.10}$$

where m_{i+2} represents a generic $(i+2)$-particle amplitude in the biadjoint ϕ^3 scalar theory of the form $m_{i+2}(\mathbb{I},\mathbb{I})$. Since the mass dimension of $m_{i+2}(\mathbb{I},\mathbb{I})$ is $-2(i-1)$ we are motivated to define $m_2 := P^2$ and $m_3 := 1$. Here $1/P^2$ represents a generic propagator. We will soon see why this somewhat strange definition of m_2 is useful. Let us start by noticing that the number of Feynman diagrams contributing to $m_{i+2}(\mathbb{I},\mathbb{I})$ is the Catalan number C_i.

The claim is that the form of the amplitude $A_n^{\phi^4}$ is determined by the coefficient $g_{n/2-1}$

divided by $h_0^{n/2-1}$. Let us compute the first few cases of (C.2) in order to illustrate the use of the formula,

$$
\begin{aligned}
A_4^{\phi^4} &= \frac{g_1}{h_0} = h_1 = m_3 \\
A_6^{\phi^4} &= \frac{g_2}{h_0^2} = \frac{h_0^2 h_2 + h_0 h_1^2}{h_0^2} = m_4 + m_3^2 \frac{1}{P^2} \\
A_8^{\phi^4} &= \frac{g_3}{h_0^3} = \frac{h_3 h_0^3 + 3h_1 h_2 h_0^2 + h_1^3 h_0}{h_0^3} = m_5 + 3m_3 m_4 \frac{1}{P^2} + m_3^3 \left(\frac{1}{P^2}\right)^2 .
\end{aligned}
$$

Finally, specializing to what is called *planar kinematics*, in which all planar invariants are set to unity, one finds that $A_n^{\phi^4}$ counts the number of Feynman diagrams contributing to the amplitude. This is the number of ternary planar unrooted trees with n leaves which is known to be the given by the Fuss-Catalan numbers. Applying the same kinematics to the ϕ^3 amplitudes one can replace each by the corresponding Catalan numbers and therefore we reproduce the relation (C.2).

C.0.1 Extension to ϕ^p: Iterated Structure

Let us explicitly construct the iteration used in section 3.7.2 to propose the schematic structure of ϕ^p amplitudes.

Let us start by defining generating functions

$$
h_k(x) = \sum_{j=0}^{\infty} h_{k,j} x^j \, . \tag{C.11}
$$

The goal is to construct a recursive procedure that determines all coefficients $h_{k,j}$ as functions of the base case defined to be

$$h_3(x) = \sum_{j=0}^{\infty} h_j x^j \,. \tag{C.12}$$

Note that for the base function we have denoted the coefficients by h_j instead of $h_{3,j}$. This was done in order not clutter the formulas. Using the expression in (3.85)

$$h_k(x) = \sum_{j=0}^{\infty} h_{k,j} x^j := \sum_{j=0}^{\infty} \frac{1}{2\pi i} \oint_{|z|=\epsilon} \frac{dz}{j+1} \left(\frac{h_{k-1}(z)}{z} \right)^{j+1} x^j \tag{C.13}$$

let us present some results for the expansions.

For ϕ^4 amplitudes we have $h_4(x)$ with coefficients

$$\begin{aligned}
&h_0\\
&h_0 h_1\\
&h_0 h_1^2 + h_0^2 h_2\\
&h_0 h_1^3 + 3h_0^2 h_1 h_2 + h_0^3 h_3\\
&h_0 h_1^4 + 6h_0^2 h_1^2 h_2 + 2h_0^3 h_2^2 + 4h_0^3 h_1 h_3 + h_0^4 h_4\\
&h_0 h_1^5 + 10h_0^2 h_1^3 h_2 + 10h_0^3 h_1 h_2^2 + 10h_0^3 h_1^2 h_3 + 5h_0^4 h_2 h_3 + 5h_0^4 h_1 h_4 + h_0^5 h_5.
\end{aligned} \tag{C.14}$$

These coefficients are a refinement of the Narayana numbers. Let us see this more explicitly. Consider first the table of coefficients (see OEIS entry A134264, [174]),

$$\begin{aligned}
&1\\
&1\\
&1,1\\
&1,3,1\\
&1,6,2,4,1\\
&1,10,10,10,5,5,1\\
&1,15,30,5,20,30,3,15,6,6,1\\
&1,21,70,35,35,105,21,21,35,42,7,21,7,7,1.
\end{aligned}\tag{C.15}$$

If we now set $h_0 = x$ and all other $h_i = 1$, then terms with the same power of h_0 are combined. For example, $2h_2^2h_0^3+4h_1h_3h_0^3$ in the fifth row of (C.14) becomes $2x^3+4x^3 = 6x^3$. Carrying this out one gets

$$\begin{aligned}
&x\\
&x\\
&x^2 + x\\
&x^3 + 3x^2 + x\\
&x^4 + 6x^3 + 6x^2 + x\\
&x^5 + 10x^4 + 20x^3 + 10x^2 + x\\
&x^6 + 15x^5 + 50x^4 + 50x^3 + 15x^2 + x\\
&x^7 + 21x^6 + 105x^5 + 175x^4 + 105x^3 + 21x^2 + x.
\end{aligned}\tag{C.16}$$

These coefficients are the Narayana numbers (OEIS entry A001263, [174]).

Let us consider ϕ^5 amplitudes, so we have $h_5(x)$ with coefficients

$$
\begin{aligned}
&h_0 \\
&h_0^2 h_1 \\
&2h_0^3 h_1^2 + h_0^4 h_2 \\
&5h_0^4 h_1^3 + 6h_0^5 h_1 h_2 + h_0^6 h_3 \\
&14h_0^5 h_1^4 + 28h_0^6 h_1^2 h_2 + 4h_0^7 h_2^2 + 8h_0^7 h_1 h_3 + h_0^8 h_4 \\
&42h_0^6 h_1^5 + 120h_0^7 h_1^3 h_2 + 45h_0^8 h_1 h_2^2 + 45h_0^8 h_1^2 h_3 + 10h_0^9 h_2 h_3 + 10h_0^9 h_1 h_4 + h_0^{10} h_5.
\end{aligned}
\tag{C.17}
$$

Listing only the coefficient allows us to present one more row (OEIS entry A338135, [174]),

$$
\begin{aligned}
&1 \\
&1 \\
&2, 1 \\
&5, 6, 1 \\
&14, 28, 4, 8, 1 \\
&42, 120, 45, 45, 10, 10, 1 \\
&132, 495, 330, 22, 220, 132, 6, 66, 12, 12, 1.
\end{aligned}
\tag{C.18}
$$

Once again, if we set $h_0 = x$ and all other $h_i = 1$, then (C.17) becomes the generating functions for the 2-Narayana numbers. In general one finds the triangle of m-Narayana numbers, where the standard ones correspond to $m = 1$. The 2-Narayana numbers are then given by the coefficients in (see e.g. section 6.8 of [172])

$$
\begin{aligned}
&x \\
&x^2 \\
&x^4 + 2x^3 \\
&x^6 + 6x^5 + 5x^4 \\
&x^8 + 12x^7 + 28x^6 + 14x^5 \\
&x^{10} + 20x^9 + 90x^8 + 120x^7 + 42x^6 \\
&x^{12} + 30x^{11} + 220x^{10} + 550x^9 + 495x^8 + 132x^7
\end{aligned}
\tag{C.19}
$$

C.0.2 One Function to Compute Them All

There is one more interesting property of these representation of ϕ^p amplitudes which interconnects them. Consider the coefficients of the function $h_4(x)$. Some of them are explicitly shown in (C.14).

The claim is that the coefficients of the function $h_k(x)$ can be obtained from those of $h_4(x)$ by simply setting to zero all h_a with $a \notin (k-3)\mathbb{Z}$ (see text in OEIS entry A338135 for $k = 5$ case, [174]). For example, $h_5(x)$ is obtained by setting all h_a with a odd to zero. Of course, every other coefficient of $h_4(x)$ vanishes completely but the ones that do not reproduce $h_5(x)$.

One direct way to understand the relation among the different generating functions $h_k(x)$ is by recalling the combinatorial problem they solve. As explained in the discussions, set $m = k - 3$ and place mq points on a disk. Now count all possible ways of clustering the points in non-overlapping sets so that there are r_1 groups of m points each, r_2 groups of $2m$ points, etc. Clearly, $h_4(x)$, for which $m = 1$, contains all other problems counted by $h_k(x)$ with $k > 4$ as special cases.

Appendix D

Computing a Region for $n = 12$ that Leads to $m_7(1234576, \mathbb{I})$

Directly computing amplitudes $A_n^{\phi^4}$, using the global Schwinger formula presented in chapter 3 becomes harder as n grows. In this appendix, we show how to use the global Schwinger formula to find an explicit map from a region to $m_{n/2+1}(\alpha, \mathbb{I})$. Having the precise bijection of kinematic invariants, one gets the contribution of the region without ever carrying out an integral. The region under consideration is

$$R = \{x_0 = x_3 < x_1 = x_2,\, x_4 = x_5,\, x_6 = x_7,\, x_8 = x_9\}\,. \tag{D.1}$$

Let us consider the behavior of the $G_{12}(x)$ part of the tropical potential on a region R_{ext} where the condition $x_3 < x_1$ is relaxed an therefore contains R, i.e.,

$$R \subset R_{\text{ext}} = \{x_0 = x_3\, x_1 = x_2,\, x_4 = x_5,\, x_6 = x_7,\, x_8 = x_9\}\,. \tag{D.2}$$

The function $G_{12}(x)$ can be seen to be a linear combination of the following 14 piecewise linear functions

$$\begin{aligned}
&\min(x_1, x_3), \min(x_3, x_5), \min(x_5, x_7), \min(x_7, x_9),\\
&\min(x_1, x_3, x_5), \min(x_3, x_5, x_7), \min(x_5, x_7, x_9),\\
&\min(x_1, x_3, x_5, x_7), \min(x_3, x_5, x_7, x_9), \min(x_1, x_3, x_5, x_7, x_9),\\
&x_1, x_5, x_7, x_9.
\end{aligned}$$

Note that x_1 is always accompanied by x_3 when it is an argument in a min function. This means that when restricting to R, i.e. imposing $x_3 < x_1$ on the functions, x_1 drops out and we are left with the following 11 functions,

$$\begin{aligned}
&\min(x_3, x_5), \min(x_5, x_7), \min(x_7, x_9),\\
&\min(x_3, x_5, x_7), \min(x_5, x_7, x_9),\\
&\min(x_3, x_5, x_7, x_9), x_1, x_3, x_5, x_7, x_9.
\end{aligned}$$

It is easy to compute the coefficients of each of the 11 functions to be

$$\begin{aligned}
&t_{[2,8]} - t_{[2,6]} - t_{[6,8]}, -t_{[6,8]} + t_{[6,10]} - t_{[8,10]}, -t_{[8,10]} + t_{[8,12]} - t_{[10,12]},\\
&t_{[2,10]} - t_{[2,8]} + t_{[6,8]} - t_{[6,10]}, -t_{[6,10]} + t_{[6,12]} + t_{[8,10]} - t_{[8,12]},\\
&t_{[6,10]} - t_{[2,10]} - t_{[6,12]}, t_{[3,5]}, t_{[2,6]} - t_{[3,5]}, t_{[6,8]}, t_{[8,10]}, t_{[10,12]}.
\end{aligned}$$

Note that the coefficient of x_1 is $t_{[3,5]}$, which is precisely the invariant in the propagator that must appear according to the rules for the non-crossing diagram corresponding to the region R. The only other place where $t_{[3,5]}$ appears is in the coefficient of x_3. This means that we can write the integral over x_1 as

$$\int_{-\infty}^{\infty} dx_1 \theta(x_1 - x_3) \exp\left(-t_{[3,5]}(x_1 - x_3)\right) = \frac{1}{t_{[3,5]}} \,. \tag{D.3}$$

Combining the left over terms and relabeling variables so that $x_a \to x_{(a-3)/2}$ one finds the "effective" potential

$$\begin{aligned}
F_6 &= (t_{[2,8]} - t_{[2,6]} - t_{[6,8]}) \min(x_0, x_1) + (-t_{[6,8]} + t_{[6,10]} - t_{[8,10]}) \min(x_1, x_2) \\
&\quad + (-t_{[8,10]} + t_{[8,12]} - t_{[10,12]}) \min(x_2, x_3) + (t_{[2,10]} - t_{[2,8]} + t_{[6,8]} - t_{[6,10]}) \min(x_0, x_1, x_2) \\
&\quad + (-t_{[6,10]} + t_{[6,12]} + t_{[8,10]} - t_{[8,12]}) \min(x_1, x_2, x_3) \\
&\quad + (t_{[6,10]} - t_{[2,10]} - t_{[6,12]}) \min(x_0, x_1, x_2, x_3) + t_{[2,6]} x_0 + t_{[6,8]} x_1 + t_{[8,10]} x_2 + t_{[10,12]} x_3 \,.
\end{aligned}$$

It is a simple exercise to match the coefficients with that of the tropical potential function for $m_6(\mathbb{I}, \mathbb{I})$. The non-trivial fact is that the result is not only a map but a bijection between the corresponding sets of planar invariants. This is left as an exercise for the reader.

Appendix E

Singular Solutions in $X(3, n)$ from Bounded Chambers Counting

In this appendix, related to chapter 4, we show how to visualize and count the number of singular solutions in $X(3, 7)$ and the number of ($\texttt{regular}_7, \texttt{singular}_8$) solutions in X(3,8) with positive kinematics.

E.0.1 Singular Solutions in $X(3, 7)$

We have seen in section 4.4.1 that with positive kinematic data all the solutions we obtain are real. This means we can analyze them by counting bounded chambers in $\mathbb{RP}^2$ space when $|147|$, $|257|$ and $|367|$ vanish. We expect to find 12 bounded chambers, which would correspond to the 12 solutions for each of the 15 existing configurations.

The bounded chambers come in the following way. First, we use the same gauge fixing for the first four particles as explained in section 4.4.1. This creates 5 repelling lines, one of them crossing the diagonal of the square $[0,1]^2$ created by particles 1 and 4. It is precisely on this line where the soft particle 7 must be. We can have solutions where particle 7 is outside the square $[0,1]^2$, since particles 5 and 6 can simultaneously create bounded chambers for each other. We represent this situation in figure E.1.

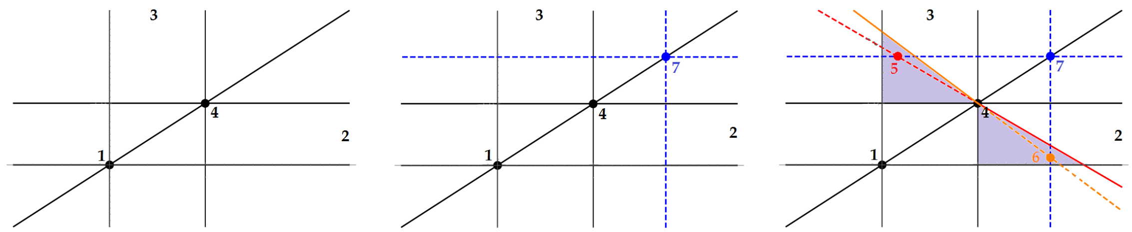

Figure E.1: *Left*: the first four particles are gauge-fixed. This creates 5 repelling lines, drawn in black, and particle 7 must be on the line that passes through 1 and 4. *Center*: we now consider the situation in which the soft particle 7 is in the outside-right(left) of the square $[0,1]^2$. *Right*: particles 5 and 6 must lie on the blue dashed lines created by particles 7, 2 and 3. This only happens if both particles bound each other through particle 4(1) (red and orange lines). The two grey bounded chambers are those where particles 5 and 6 can be.

This configuration gives rise to 2 different solutions, since particles 5 and 6 can bound each other through particles 1 and 4 when particle 7 is outside the square $[0,1]^2$.

Next, we also find solutions in the particular situation in which the soft particle 7 is inside the square $[0,1]^2$, but particles 5 and 6 are both outside of it. In this case, particles 5 and 6 also bound each other. We represent this situation in figure E.2.

This configuration also gives rise to 2 different solutions, since particles 5 and 6 can bound each other through particles 1 and 4.

Finally, we also find solutions coming from having the soft particle 7 and the two remaining hard particles inside the square $[0,1]^2$. We represent this situation in figure E.3:

This last situation gives rise to 3 solutions where both hard particles are in the same

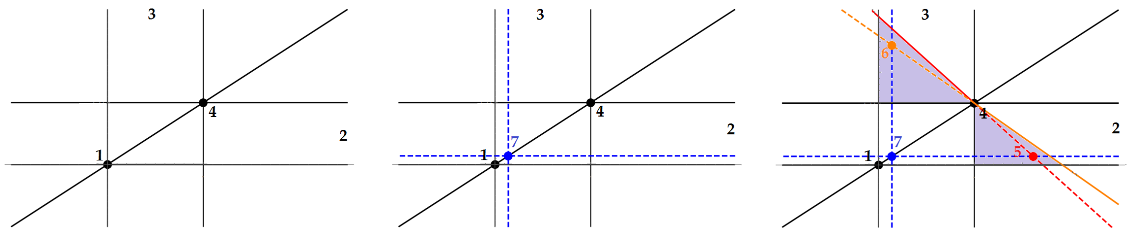

Figure E.2: *Left*: the first four particles are gauge-fixed. This creates 5 repelling lines, drawn in black, and particle 7 must be on the line that passes through 1 and 4. *Center*: we now consider the situation in which the soft particle 7 is inside the square $[0,1]^2$. *Right*: particles 5 and 6 must lie on the blue dashed lines created by particles 7, 2 and 3. This only happens if both particles bound each other through particle 4(1) (red and orange lines). The two grey bounded chambers are those where particles 5 and 6 can be.

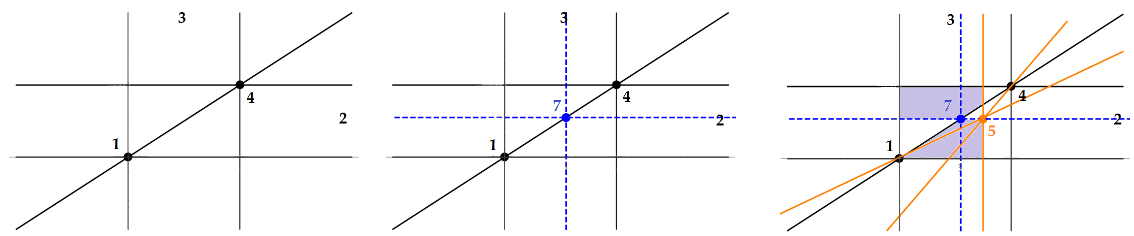

Figure E.3: *Left*: the first four particles are gauge-fixed. This creates 5 repelling lines, drawn in black, and particle 7 must be on the line that passes through 1 and 4. *Center*: we now consider the situation in which the soft particle 7 is inside the square $[0,1]^2$. This means that e.g. particle 5 must be in one of the two existing bounded chambers. *Right*: particles 5 and 6 must lie on the blue dashed lines created by particles 7, 2 and 3. If we choose particle 5 to be e.g. in the lower-right bounded chamber, this creates 3 additional repelling lines, drawn in orange, which leave four bounded chambers where particle 6 can be, shown in grey.

original bounded chamber, and 1 solution where both are in the different two original bounded chambers. Hence, there are a total of $2 \times (3+1) = 8$ solutions, since we can also choose particle 5 to be in the upper-left bounded chamber at first. Therefore, for this configuration, we count $2+2+8=12$ different solutions which correspond to the singular solutions already found before.

E.0.2 $(\texttt{regular}_7, \texttt{singular}_8)$ Solutions in X(3,8)

It turns out that the $(\texttt{regular}_7, \texttt{singular}_8)$ solutions studied in section 4.5.1 are all real too. This opens the possibility to count them in $\mathbb{RP}^2$ space in the same way as in appendix E.0.1. If we use the same gauge-fixing as in section 4.4.1 and consider the singular situation in which e.g. $|148|$, $|258|$ and $|368|$ vanish, we find ourselves in a similar fashion as in E.0.1, i.e. with 12 different situations. Yet, now we deal with one more particle (in this case particle 7) which is decoupled from the other hard particles. This particle can be found in 41 different equilibrium points, which gives the $12 \times 41 = 492$ solutions. Below we give an explicit visualization of one of the 12 different situations we can have:

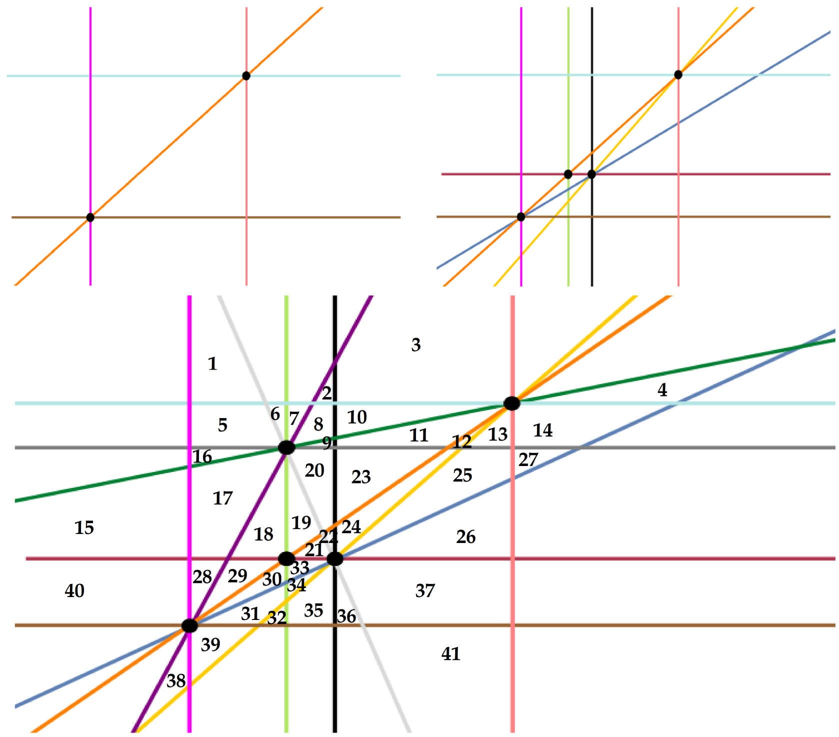

Figure E.4: *Top-Left*: particles 1, 2, 3 and 4 are gauge-fixed. This creates 5 repelling lines, and particle 8 must be on the line that passes through the two black points, which correspond to particles 1 and 4. Particles 2 and 3 are sent to infinity. *Top-Right*: we now consider e.g. the third situation seen in E.0.1. The two new black points correspond to particles 5 and 8, and new repelling lines appear due to their interaction with the other particles. *Bottom*: if we choose particles 5 and 6 to be e.g. on the two different original bounded chambers (see *Top-Left* figure), this leaves us with 41 bounded chambers where particle 7 can be.

Appendix F

Geometry Descriptions of Type 3 and 4 Configurations in $X(5,8)$

F.1 Geometry Descriptions of Type 3 and 4 Configurations in $X(5,8)$

We can use the positive kinematic data to help us visualize the geometry underlying the singular solutions of the topologies type 3 and type 4 in table 4.1 in chapter 4. For the topology type 3, there are two bounded chambers formed by the six dominating 3-planes. See their projections in figure F.1.

The F-vectors of bounded chambers are both $\{8,16,14,6\}$. The 8 vertices of each bounded chamber are labelled by $\{9,10,11,12,13,14,15,16\}$ and $\{9,10,11,12,17,18,19,20\}$, respectively. For convenience, let's call the two bounded chambers as blue and red. Among the six facets of each bounded chamber, two are tetrahedrons and the remaining four are

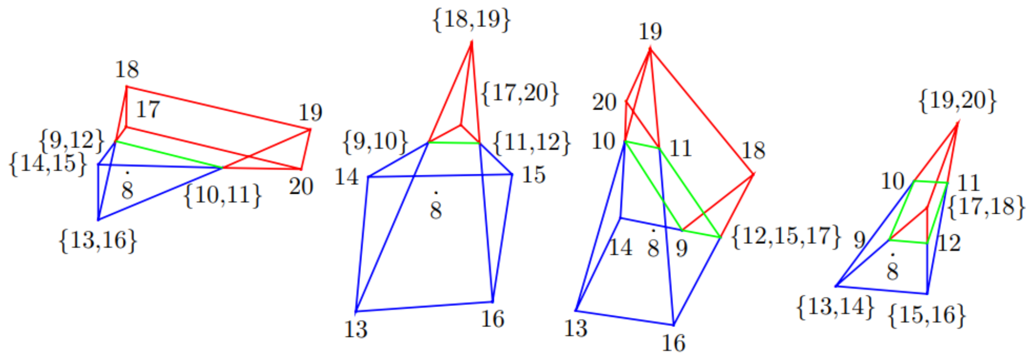

Figure F.1: Four projections from the viewpoint of particles 2, 3, 4 and 5, respectively, of the two bounded chambers (shown in blue and red) for the topology type 3 in table 4.1 and near the soft limit. Here we represent the case in which the soft particle is bounded by the blue chamber. The green edges correspond to shared edges by the blue and red chambers. In the strict soft limit, the two bounded chambers collapse to a point where the soft particle lies.

truncated triangular prisms. The two bounded chambers don't share any facet but a dim-2 boundary of vertices $\{9, 10, 11, 12\}$. Any dominating 3-plane passes through both facets of different bounded chambers, see table F.1. Particles 1, 4, 6 and 7 lie in the lines that

Particles to determine dominating 3−planes	Vertices of the facet passed by the blue chamber	Vertices of the facet passed by the red chamber
{1,2,3,7}	{9,10,11,12,13,16}	{9,10,11,12,18,19}
{1,2,4,5}	{9,12,13,14,15,16}	{9,12,17,18}
{1,3,5,6}	{9,10,13,14}	{9,10,17,18,19,20}
{2,3,4,6}	{9,10,11,12,14,15}	{9,10,11,12,17,20}
{2,5,6,7}	{10,11,13,14,15,16}	{10,11,19,20}
{3,4,5,7}	{11,12,15,16}	{11,12,17,18,19,20}

Table F.1: Dominating 3-planes and the facets they pass by in figure F.1.

pass through $\{9, 13, 18\}$, $\{12, 15, 17\}$, $\{10, 14, 20\}$ and $\{11, 16, 19\}$, respectively. Whilst particles 2, 3, and 5, which are sent to infinity, can be thought of as the intersections of four lines determined by four pairs of vertices. See the first, second and fourth projections in figure F.1.

The auxiliary points have proven to be very useful to understand the relative positions of the hard particles. Alternatively, now we can ignore them and imagine how these hard particles form some dominating planes to bound the soft particle.

In the strict soft limit, the two bounded chambers collapse to a point. Some sets of four dominating 3-planes share a point where the soft particle lies, while some share a line. For example, the four dominating 3-planes $\overline{1237}$, $\overline{1245}$, $\overline{2346}$, and $\overline{2567}$ share a common line where particles 2 and 8 lie.

There are 8 solutions of variables u, v, p, q, r, s, x_7 and z_7 for the new set of scattering equations,

$$\left\{\lim_{\tau\to 0}\frac{\partial\mathcal{S}_5}{\partial x_i}\,,\quad \lim_{\tau\to 0}\frac{\partial\mathcal{S}_5}{\partial y_i}\,,\quad \lim_{\tau\to 0}\frac{\partial\mathcal{S}_5}{\partial z_i}\,,\quad \lim_{\tau\to 0}\frac{\partial\mathcal{S}_5}{\partial w_i}\right\}\bigg|_{(4.44)}=0,\quad \text{for}\quad i=1,\ldots 8. \tag{F.1}$$

These 8 solutions can be divided into four pairs. Although the two solutions of each pair are different, using the reparameterization (4.44), they produce the same set of values for $\{x_7, y_7, z_7, w_7, x_8, y_8, z_8, w_8\}$, which corresponds to the fact that the two bounded chambers collapse to a single point.

For the topology type 4, there are two bounded 4-simplices formed by the dominating 3-planes using positive kinematic data. See their projections in figure F.2.

As summarized in table F.2, these two bounded chambers share a tetrahedron of vertices $\{9, 10, 11, 12\}$ as a common facet, which is passed by the dominating 3-plane determined by $\{1, 2, 3, 6\}$. Another three dominating 3-planes pass both facets of different bounded chambers. Two dominating 3-planes only pass a facet of either the blue or red bounded chamber. As for the last dominating 3-plane, it just passes a dim-2 boundary determined by $\{9, 10, 11\}$ of the shared facet.

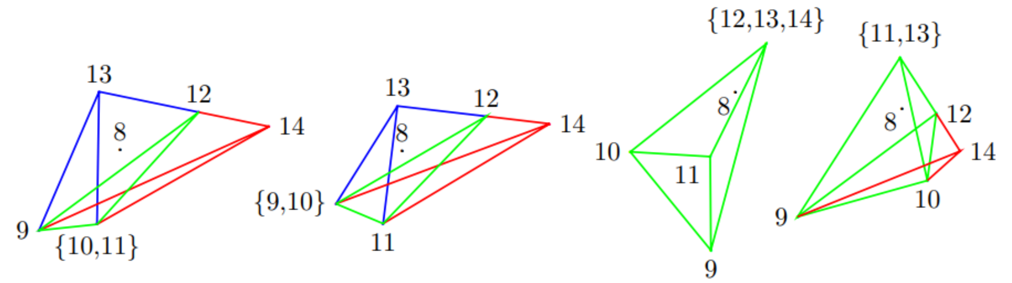

Figure F.2: Four projections from the viewpoint of particles 2, 3, 4 and 5, respectively, of the two bounded 4-simplices (shown in blue and red) for the topology type 4 in table 4.1 and near the soft limit. In the strict soft limit, the two bounded chambers collapse to a point where the soft particle lies.

The six hard particles 1, 2, 3, 5, 6 and 7 lie on the lines determined by {9,11}, {10,11}, {9,10}, {11,12}, {9,13}, {10,14}, respectively, while particle 4 lies on the line that passes $\{12, 13, 14\}$ at the same time.

Particles to determine dominating 3−planes	Vertices of the facet passed by the blue chamber	Vertices of the facet passed by the red chamber
{1,2,3,6}	{9,10,11,12}	{9,10,11,12}
{1,4,5,6}	{9,11,12,13}	{9,11,12,14}
{2,4,5,7}	{10,11,12,13}	{10,11,12,14}
{3,4,6,7}	{9,10,12,13}	{9,10,12,14}
{1,2,3,5}	{9,10,11,13}	-
{1,2,3,7}	-	{9,10,11,14}
{1,2,3,4}	-	-

Table F.2: Dominating 3-planes and the facets they pass by in figure F.2.

Appendix G

Proof of One-to-one Map of a Binary Tree and its Metric

Lemma G.0.1. *Given that two cubic trees T_A and T_B have the same valid non-degenerate metric d_{ij}, then $T_A = T_B$.*

Proof. We are going to provide a proof by induction. First, consider the base case where T_A and T_B are 3-point trees. It is clear that there exists a unique solution to $d_{12} = e_1 + e_2$, $d_{13} = e_1 + e_3$ and $d_{23} = e_2 + e_3$. Since T_A and T_B have the same non-degenerate metric, the lengths $e_i^{(A)} = e_i^{(B)}$ must be identical, thus $T_A = T_B$.

Now let us assume that the lemma is true for all $(n-1)$-point cubic metric trees and consider two n-point cubic trees T_A and T_B that have the same non-degenerate metric d_{ij}. Next let us find leaves i and j such that $d_{il} - d_{jl}$ is l independent. Such a pair of leaves must exist because the condition is true for any pair of leaves which belong to the same "cherry" as shown in the diagrams in figure G.1. Moreover, only leaves in cherries satisfy this condition in a cubic non-degenerate tree.

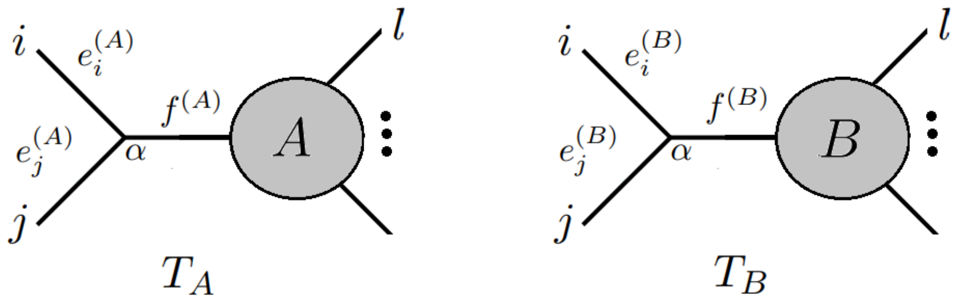

Figure G.1: Two n-point cubic trees with pairs i and j joined by the vertex α.

Removing the cherries from both trees and introducing a new leaf α one can define a metric for the the $(n-1)$-point cubic trees in figure G.2, whose leaves are given by $(\{1, 2, \ldots, n\} \setminus \{i, j\}) \cup \{\alpha\}$.

Figure G.2: Two $(n-1)$-point cubic trees with external edges $e_\alpha^{(A)} = f^{(A)}$ and $e_\alpha^{(B)} = f^{(B)}$ such that $d_{kl}^{(A)} = d_{kl}^{(B)}$.

Such a metric is defined in terms of the metric of the parent trees as follows. $d_{kl}^{(A)} = d_{kl}$ if $k, l \neq \alpha$ and $d_{k\alpha}^{(A)} = d_{ki} - e_i^{(A)}$. Likewise $d_{kl}^{(B)} = d_{kl}$ if $k, l \neq \alpha$ and $d_{k\alpha}^{(B)} = d_{ki} - e_i^{(B)}$. It is easy to see from the figure that the two metrics are identical, i.e. $d_{kl}^{(A)} = d_{kl}^{(B)}$.

Using the induction hypothesis, the two metric trees in figure G.2 must be the same. In order to complete the proof all we need is to show that $e_i^{(A)} = e_i^{(B)}$ and $e_j^{(A)} = e_j^{(B)}$. The fact that $d_{il} = e_i^{(A)} + d_{\alpha l}^{(A)} = e_i^{(B)} + d_{\alpha l}^{(B)}$ immediately implies $e_i^{(A)} = e_i^{(B)}$, hence $T_A = T_B$. $\square$

Appendix H

All Planar Collections of Feynman Diagrams for $(3, 6)$

Below we reproduce for the reader's convenience table 1 of [42] which contains all 48 planar collections of Feynman diagrams for $(3, 6)$. The notation in this case is very compact and requires some explanation. Each collection for $(3, 6)$ is made out of 5-point trees. The tree in the i^{th}-position must be planar with respect to the ordering $(1, 2, \ldots, \not{i}, \ldots, n)$. There is a single topology of five-point trees, i.e. a caterpillar tree with two cherries and one leg. Therefore it is possible to specify it by giving the label of the leaf attached to the leg. Using this, each collection becomes a one-dimensional array of six numbers.

Planar collections of trees in $k = 3$ and $n = 6$			
Collection	Trees	Collection	Trees
$\mathcal{C}_1$	$[4, 4, 4, 3, 3, 3]$	$\mathcal{C}_{25}$	$[6, 6, 6, 5, 4, 1]$
$\mathcal{C}_2$	$[4, 4, 4, 3, 6, 5]$	$\mathcal{C}_{26}$	$[6, 6, 6, 6, 6, 3]$
$\mathcal{C}_3$	$[4, 4, 4, 3, 2, 2]$	$\mathcal{C}_{27}$	$[6, 6, 6, 1, 1, 1]$
$\mathcal{C}_4$	$[4, 4, 4, 1, 4, 4]$	$\mathcal{C}_{28}$	$[6, 6, 6, 2, 2, 1]$
$\mathcal{C}_5$	$[4, 4, 4, 1, 1, 1]$	$\mathcal{C}_{29}$	$[6, 3, 2, 5, 4, 1]$
$\mathcal{C}_6$	$[4, 4, 6, 6, 6, 5]$	$\mathcal{C}_{30}$	$[6, 3, 2, 1, 1, 1]$
$\mathcal{C}_7$	$[4, 4, 6, 6, 2, 2]$	$\mathcal{C}_{31}$	$[6, 3, 2, 2, 2, 1]$
$\mathcal{C}_8$	$[4, 5, 5, 5, 4, 4]$	$\mathcal{C}_{32}$	$[2, 5, 5, 5, 2, 2]$
$\mathcal{C}_9$	$[4, 6, 6, 5, 4, 4]$	$\mathcal{C}_{33}$	$[2, 5, 2, 2, 2, 2]$
$\mathcal{C}_{10}$	$[4, 6, 6, 2, 2, 4]$	$\mathcal{C}_{34}$	$[2, 1, 4, 3, 3, 3]$
$\mathcal{C}_{11}$	$[4, 1, 1, 1, 4, 4]$	$\mathcal{C}_{35}$	$[2, 1, 4, 3, 6, 5]$
$\mathcal{C}_{12}$	$[4, 1, 1, 1, 1, 1]$	$\mathcal{C}_{36}$	$[2, 1, 4, 3, 2, 2]$
$\mathcal{C}_{13}$	$[4, 3, 2, 5, 4, 4]$	$\mathcal{C}_{37}$	$[2, 1, 6, 6, 6, 5]$
$\mathcal{C}_{14}$	$[4, 3, 2, 2, 2, 4]$	$\mathcal{C}_{38}$	$[2, 1, 6, 6, 2, 2]$
$\mathcal{C}_{15}$	$[5, 5, 4, 3, 3, 3]$	$\mathcal{C}_{39}$	$[2, 1, 1, 1, 3, 3]$
$\mathcal{C}_{16}$	$[5, 5, 4, 3, 6, 5]$	$\mathcal{C}_{40}$	$[2, 1, 1, 1, 6, 5]$
$\mathcal{C}_{17}$	$[5, 5, 5, 5, 2, 5]$	$\mathcal{C}_{41}$	$[2, 1, 1, 1, 2, 2]$

Planar collections of trees in $k = 3$ and $n = 6$			
Collection	Trees	Collection	Trees
$\mathcal{C}_{18}$	$[5, 5, 6, 6, 6, 5]$	$\mathcal{C}_{42}$	$[3, 5, 5, 5, 4, 3]$
$\mathcal{C}_{19}$	$[5, 5, 1, 1, 3, 3]$	$\mathcal{C}_{43}$	$[3, 5, 5, 1, 1, 3]$
$\mathcal{C}_{20}$	$[5, 5, 1, 1, 6, 5]$	$\mathcal{C}_{44}$	$[3, 3, 6, 3, 3, 3]$
$\mathcal{C}_{21}$	$[5, 5, 2, 2, 2, 5]$	$\mathcal{C}_{45}$	$[3, 3, 6, 6, 6, 3]$
$\mathcal{C}_{22}$	$[6, 5, 5, 5, 4, 1]$	$\mathcal{C}_{46}$	$[3, 3, 2, 5, 4, 3]$
$\mathcal{C}_{23}$	$[6, 5, 5, 1, 1, 1]$	$\mathcal{C}_{47}$	$[3, 3, 2, 1, 1, 3]$
$\mathcal{C}_{24}$	$[6, 6, 6, 3, 3, 3]$	$\mathcal{C}_{48}$	$[3, 3, 2, 2, 2, 3]$

Table H.1: All 48 planar collections of trees for $n = 6$ in a compact notation tailored to this case and explained in the text.

Appendix I

Proof of $-P_L = \mathcal{E} - sT$ in holographic magnetized plasma

The proof follows the argument for the universality of the shear viscosity to the entropy density in holographic plasma [57].

Consider a holographic dual to a four dimensional[1] gauge theory in an external magnetic field. We are going to assume that the magnetic field is along the z-direction, as in (6.27). We take the (dimensionally reduced — again, this can be relaxed) holographic background geometry to be

$$ds_5^2 = -c_1^2\ dt^2 + c_2^2\ \left(dx^2 + dy^2\right) + c_3^2\ dz^2 + c_4^2\ dr^2\,, \qquad c_i = c_i(r)\,. \tag{I.1}$$

At extremality (whether or not the extremal solution is singular or not within the trunca-

[1] Generalization to other dimensions is straightforward.

tion is irrelevant), the Poincaré symmetry of the background geometry guarantees that

$$R_{tt} + R_{zz} = 0\,, \tag{I.2}$$

where $R_{\mu\nu}$ is the Ricci tensor in the orthonormal frame. Clearly, an analogous condition must be satisfied for the full gravitational stress tensor of the matter supporting the geometry

$$T_{tt} + T_{zz} = 0\,. \tag{I.3}$$

Because turning on the nonextremality will not modify (I.3), we see that (I.2) is valid away from extremality as well. Computing the Ricci tensor for (I.1) reduces (I.2) to

$$0 = R_{tt} + R_{zz} = \frac{1}{c_1 c_2^2 c_3 c_4} \frac{d}{dr}\left[\left(\frac{c_1}{c_3}\right)' \frac{c_2^2 c_3^2}{c_4}\right] \qquad \Longrightarrow \qquad \left(\frac{c_1}{c_3}\right)' \frac{c_2^2 c_3^2}{c_4} = \text{const}\,. \tag{I.4}$$

Explicitly evaluating the ratio of the const in (I.4) in the UV ($r \to \infty$) and IR ($r \to r_{horizon}$) we recover

$$0 = \frac{\mathcal{E} + P_L}{sT} - 1\,, \tag{I.5}$$

for each of the models we study.

We should emphasize that the condition (I.2) can be explicitly verified using the equations of motion in each model studied. The point of the argument above (as the related one in [57]) is that this relation is true based on the symmetries of the problem alone.

Appendix J

Conformal models in the limit $T/\sqrt{B} \gg 1$

In holographic models, supersymmetry at extremality typically guarantees that equilibrium isotropic thermodynamics is renormalization scheme independent (compare the $\mathcal{N} = 2^*$ model with the same masses for the bosonic and the fermionic components $m_b^2 = m_f^2$, versus the same model with $m_b^2 \neq m_f^2$ [54]). This is not the case for the holographic magnetized gauge theory plasma in four space-time dimensions, see [112] for $\mathcal{N} = 4$ SYM. In this appendix we discuss the high temperature anisotropic equilibrium thermodynamics of the conformal (supersymmetric in vacuum) models. For the (locally) four dimensional models ($\mathbb{CFT}_{diag}$, $\mathbb{CFT}_{STU}$ and $\mathbb{CFT}_{PW,m=0}$) matching high-temperature equations of state is a natural way to relate renormalization schemes in various theories. In the $\mathbb{CFT}_{PW,m=\infty}$ model, which is locally five dimensional, magnetized thermodynamics is scheme independent.

J.0.1 $\mathbb{CFT}_{STU}$

The high temperature expansion corresponds to the perturbative expansion in b. In what follows we study anisotropic thermodynamics to order $\mathcal{O}(b^4)$ inclusive. Introducing

$$
\begin{split}
&a_1 = 1 + \sum_{n=1}^{\infty} a_{1,(n)}\ b^{2n}\,, \qquad a_2 = 1 + \sum_{n=1}^{\infty} a_{2,(n)}\ b^{2n}\,, \qquad a_4 = 1 + \sum_{n=1}^{\infty} a_{4,(n)}\ b^{2n}\,, \\
&\rho = 1 + \sum_{n=1}^{\infty} \rho_{(n)}\ b^{2n}\,, \qquad \nu = 1 + \sum_{n=1}^{\infty} \nu_{(n)}\ b^{2n}\,,
\end{split}
\tag{J.1}
$$

so that (see (6.36) and (6.37) for the asymptotics)

$$
\begin{split}
&a_{1,2} = \sum_{n=1}^{\infty} a_{1,2,(n)}\ b^{2n}\,, \qquad a_{2,2} = \sum_{n=1}^{\infty} a_{2,2,(n)}\ b^{2n}\,, \qquad r_1 = \sum_{n=1}^{\infty} r_{1,(n)}\ b^{2n}\,, \\
&n_1 = \sum_{n=1}^{\infty} n_{1,(n)}\ b^{2n}\,, \qquad a_{1,h,0} = 1 + \sum_{n=1}^{\infty} a_{1,h,0,(n)}\ b^{2n}\,, \qquad a_{2,h,0} = 1 + \sum_{n=1}^{\infty} a_{2,h,0,(n)}\ b^{2n}\,, \\
&r_{h,0} = 1 + \sum_{n=1}^{\infty} r_{h,0,(n)}\ b^{2n}\,, \qquad n_{h,0} = 1 + \sum_{n=1}^{\infty} n_{h,0,(n)}\ b^{2n}\,,
\end{split}
\tag{J.2}
$$

we find

- at order $n = 1$:

$$
0 = a''_{2,(1)} + \frac{x^4+3}{x(x^4-1)} a'_{2,(1)} - \frac{128x^2}{x^4-1}\,, \tag{J.3}
$$

$$
0 = a'_{4,(1)} - \frac{4x^4}{3(x^4-1)} a'_{2,(1)} + \frac{4(16x^4 + a_{4,(1)})}{x(x^4-1)}\,, \tag{J.4}
$$

$$
0 = a'_{1,(1)} + \frac{2(x^4-3)}{3(x^4-1)} a'_{2,(1)} + \frac{4(16x^4 - 3a_{4,(1)})}{3x(x^4-1)}\,, \tag{J.5}
$$

$$0 =\rho''_{(1)} + \frac{x^4+3}{x(x^4-1)}\rho'_{(1)} + \frac{4(16x^4-3\rho_{(1)})}{3x^2(x^4-1)}\,, \tag{J.6}$$

$$0 =\nu''_{(1)} + \frac{x^4+3}{x(x^4-1)}\nu'_{(1)} - \frac{4(16x^4+\nu_{(1)})}{x^2(x^4-1)}\,; \tag{J.7}$$

- and at order $n = 2$ (we will not need $\rho_{(2)}$ and $\nu_{(2)}$):

$$\begin{aligned}0 =&a''_{2,(2)} + \frac{x^4+3}{x(x^4-1)}a'_{2,(2)} - (a'_{2,(1)})^2 + \frac{128x^4+24a_{4,(1)}}{3x(x^4-1)}a'_{2,(1)} + \frac{512x^2(\nu_{(1)}-\rho_{(1)})}{x^4-1}\\ &- \frac{128x^2(2a_{4,(1)}-3a_{2,(1)})}{x^4-1}\,,\end{aligned} \tag{J.8}$$

$$\begin{aligned}0 =&a'_{4,(2)} - \frac{4x^4}{3(x^4-1)}a'_{2,(2)} + \frac{4a_{4,(2)}}{x(x^4-1)} + 2x\left((\rho'_{(1)})^2 + \frac{1}{3}(\nu'_{(1)})^2\right) + \frac{x(x^4-9)}{9(x^4-1)}(a'_{2,(1)})^2\\ &- \frac{4(3x^4a_{4,(1)}-3a_{2,(1)}x^4-32x^4+6a_{4,(1)})}{9(x^4-1)}a'_{2,(1)} + \frac{8((\nu_{(1)})^2+3(\rho_{(1)})^2)}{3x(x^4-1)}\\ &- \frac{256x^3(\nu_{(1)}-\rho_{(1)})}{x^4-1} + \frac{2(96x^4a_{4,(1)}-128a_{2,(1)}x^4+3(a_{4,(1)})^2)}{x(x^4-1)}\,,\end{aligned} \tag{J.9}$$

$$\begin{aligned}0 =\ &a'_{1,(2)} + \frac{2(x^4-3)}{3(x^4-1)}a'_{2,(2)} - \frac{4}{x(x^4-1)}a_{4,(2)} + \frac{x(x^4-9)}{9(x^4-1)}(a'_{2,(1)})^2 - \frac{8(\nu^2_{(1)}+3\rho^2_{(1)})}{3x(x^4-1)}\\ &- \frac{2(3a_{2,(1)}x^4-3a_{1,(1)}x^4-64x^4-9a_{2,(1)}+12a_{4,(1)}+9a_{1,(1)})}{9(x^4-1)}a'_{2,(1)} - \frac{2}{x(x^4-1)}(a_{4,(1)})^2\\ &+ 2x\left((\rho'_{(1)})^2 + \frac{1}{3}(\nu'_{(1)})^2\right) + \frac{4(32x^4-3a_{1,(1)})}{3x(x^4-1)}a_{4,(1)} + \frac{64x^3(a_{1,(1)}-4a_{2,(1)})}{3(x^4-1)}\\ &- \frac{256x^3(\nu_{(1)}-\rho_{(1)})}{3(x^4-1)}\,.\end{aligned} \tag{J.10}$$

Eqs. (J.3) and (J.4) can be solved analytically:

$$
\begin{aligned}
a_{2,(1)} =& 32\Big(\ln(x)\ln(1+x) - \text{dilog}(x) + \ln(x)\ln\big(1+x^2\big) + \text{dilog}(1+x) \\
&+ \frac{1}{2}\text{dilog}(1+x^2)\Big) + \frac{16}{3}\pi^2\,, \\
a_{4,(1)} =& \frac{16x^4}{3(x^4-1)}(\pi^2 - 8\text{dilog}(x) + 8\ln(x)\ln\big(x^2+1\big) + 4\text{dilog}(x^2+1) + 8\text{dilog}(1+x) \\
&+ 8\ln(x)\ln(1+x) - 12\ln(x))\,,
\end{aligned}
\tag{J.11}
$$

while the remaining ones have to be solved numerically. We find:

(n)	$a_{1,2,(n)}$	$a_{2,2,(n)}$	$r_{1,(n)}$	$n_{1,(n)}$
(1)	$\frac{16}{3} - \frac{16\pi^2}{9}$	8	$-\frac{4}{3}\pi^2$	$4\pi^2$
(2)	1541.8(0)	-3358.0(0)		

(J.12)

(n)	$a_{1,h,0,(n)}$	$a_{2,h,0,(n)}$	$r_{h,0,(n)}$	$n_{h,0,(n)}$
(1)	-7.2270(2)	$\frac{4}{3}\pi^2$	-9.770(3)	29.310(9)
(2)	1336.5(8)	-2069.9(8)		

(J.13)

An important check on the numerical results are the first law of thermodynamics FL (6.45) and the thermodynamic relation TR (6.47). Given the perturbative expansions (J.2), we can represent

$$
\text{FL} = \sum_{n=1}^{\infty} fl_{(n)}\ b^{2n}\,, \qquad \text{TR} = \sum_{n=1}^{\infty} tr_{(n)}\ b^{2n}\,,
\tag{J.14}
$$

where

- at order $n = 1$:

$$
\begin{aligned}
fl_{(1)}: &\qquad 0 = \frac{2}{3}a_{2,h,0,(1)} - 16 - a_{1,h,0,(1)}\,, \\
tr_{(1)}: &\qquad 0 = -2a_{2,h,0,(1)} - \frac{16}{3} - 2a_{1,2,(1)} - a_{1,h,0,(1)}\,;
\end{aligned}
\tag{J.15}
$$

- and at order $n = 2$:

$$
\begin{aligned}
fl_{(2)}: \qquad 0 = {} & \frac{896}{9} - \frac{2}{3}a_{1,h,0,(1)}a_{2,h,0,(1)} + a_{1,h,0,(1)}^2 - 2r_{h,0,(1)}^2 - \frac{2}{3}n_{h,0,(1)}^2 + \frac{19}{9}a_{2,h,0,(1)}^2 \\
& + \frac{64}{3}n_{h,0,(1)} - \frac{64}{3}r_{h,0,(1)} - \frac{4}{3}a_{2,2,(2)} + \frac{32}{3}a_{2,h,0,(1)} + \frac{10}{3}a_{2,h,0,(2)} \\
& + 16a_{1,h,0,(1)} - a_{1,h,0,(2)} + 2a_{1,2,(2)}\,, \\
tr_{(2)}: \qquad 0 = {} & 2a_{1,h,0,(1)}a_{2,h,0,(1)} + 2a_{1,h,0,(1)}a_{1,2,(1)} + a_{1,h,0,(1)}^2 + 4a_{2,h,0,(1)}a_{1,2,(1)} + \frac{128}{3} \\
& + 3a_{2,h,0,(1)}^2 - 2r_{h,0,(1)}^2 - \frac{2}{3}n_{h,0,(1)}^2 + \frac{32}{3}a_{1,2,(1)} - 2a_{1,2,(2)} + \frac{16}{3}a_{1,h,0,(1)} \\
& - a_{1,h,0,(2)} + 32a_{2,h,0,(1)} - 2a_{2,h,0,(2)} - \frac{64}{3}r_{h,0,(1)} + \frac{64}{3}n_{h,0,(1)}\,.
\end{aligned}
\tag{J.16}
$$

Using the results (J.12) and (J.13) (rather, we use more precise values of the parameters reported — obtained from numerics with 40 digit precision) we find

- at order $n = 1$:

$$
fl_{(1)}: \qquad 0 = -7.7822(6)\times 10^{-15}\,, \qquad tr_{(1)}: \qquad 0 = -7.1054(3)\times 10^{-15}\,; \tag{J.17}
$$

- and at order $n = 2$:

$$
fl_{(2)}: \qquad 0 = -1.9681(5)\times 10^{-6}\,, \qquad tr_{(2)}: \qquad 0 = 2.4872(6)\times 10^{-6}\,. \tag{J.18}
$$

Using the perturbative expansion (J.2), it is straightforward to invert the relation between $T/\sqrt{B}$ and b (see (6.40) and (6.30)), and use the results (6.39) with (6.43), along with the analytical values for the parameters (J.12) and (J.13) (and the analytical expression for $a_{1,h,0,(1)}$ obtained from (J.15)) to arrive at

$$
\begin{split}
R_{\mathbb{CFT}_{STU}} =& \ 1 - \frac{4B^2}{\pi^4 T^4}\ \ln\frac{T}{\mu\sqrt{2}} + \left(\frac{\pi^2}{18} + \frac{a_{2,2,(2)}}{512} - \frac{2}{3} + 8\ \ln^2\frac{T}{\mu\sqrt{2}}\right)\ \frac{B^4}{\pi^8 T^8} + \cdots \\
=& \ 1 - \frac{4B^2}{\pi^4 T^4}\ \ln\frac{T}{\mu\sqrt{2}} + \left(-6.67694906(1) + 8\ \ln^2\frac{T}{\mu\sqrt{2}}\right)\ \frac{B^4}{\pi^8 T^8} + \mathcal{O}\left(\frac{B^6}{T^{12}}\ln^3\frac{T}{\mu}\right)\,.
\end{split}
\tag{J.19}
$$

It is important to keep in mind that the value $a_{2,2,(2)}$ is sensitive to the matter content of the gravitational dual — set of relevant operators in $\mathbb{CFT}_{STU}$ that develop expectation values in anisotropic thermal equilibrium.

J.0.2 $\mathbb{CFT}_{PW,m=0}$

The high temperature expansion of the $\mathbb{Z}_2$ symmetric, $\chi \equiv 0$ phase, of anisotropic $\mathbb{CFT}_{PW,m=0}$ plasma thermodynamics corresponds to the perturbative expansion in b. In what follows we study anisotropic thermodynamics to order $\mathcal{O}(b^4)$ inclusive. Introducing

$$
\begin{split}
& a_1 = 1 + \sum_{n=1}^{\infty} a_{1,(n)}\ b^{2n}\,, \qquad a_2 = 1 + \sum_{n=1}^{\infty} a_{2,(n)}\ b^{2n}\,, \qquad a_4 = 1 + \sum_{n=1}^{\infty} a_{4,(n)}\ b^{2n}\,, \\
& \alpha = \sum_{n=1}^{\infty} \alpha_{(n)}\ b^{2n}\,,
\end{split}
\tag{J.20}
$$

so that (see (6.56) and (6.57) for the asymptotics)

$$
\begin{aligned}
&a_{2,2,0} = \sum_{n=1}^{\infty} a_{2,2,0,(n)}\; b^{2n}\,, \qquad a_{4,2,0} = \sum_{n=1}^{\infty} a_{4,2,0,(n)}\; b^{2n}\,, \qquad \alpha_{1,0} = \sum_{n=1}^{\infty} \alpha_{1,0,(n)}\; b^{2n}\,,\\
&a_{1,h,0} = 1 + \sum_{n=1}^{\infty} a_{1,h,0,(n)}\; b^{2n}\,, \qquad a_{2,h,0} = 1 + \sum_{n=1}^{\infty} a_{2,h,0,(n)}\; b^{2n}\,,\\
&r_{h,0} = 1 + \sum_{n=1}^{\infty} r_{h,0,(n)}\; b^{2n}\,,
\end{aligned}
\tag{J.21}
$$

we find

- at order $n = 1$:

$$
0 = a''_{2,(1)} + \frac{x^4+3}{x(x^4-1)} a'_{2,(1)} - \frac{128x^2}{x^4-1}\,, \tag{J.22}
$$

$$
0 = a'_{4,(1)} - \frac{4x^4}{3(x^4-1)} a'_{2,(1)} + \frac{4(16x^4 + a_{4,(1)})}{x(x^4-1)}\,, \tag{J.23}
$$

$$
0 = a'_{1,(1)} + \frac{2(x^4-3)}{3(x^4-1)} a'_{2,(1)} + \frac{4(16x^4 - 3a_{4,(1)})}{3x(x^4-1)}\,, \tag{J.24}
$$

$$
0 = \alpha''_{(1)} + \frac{x^4+3}{x(x^4-1)} \alpha'_{(1)} + \frac{4(16x^4 - 3\alpha_{(1)})}{3x^2(x^4-1)}\,; \tag{J.25}
$$

- and at order $n = 2$ (we will not need $\alpha_{(2)}$):

$$
\begin{aligned}
0 = &a''_{2,(2)} + \frac{x^4+3}{x(x^4-1)} a'_{2,(2)} + \frac{128x^4 + 24a_{4,(1)}}{3x(x^4-1)} a'_{2,(1)} - (a'_{2,(1)})^2\\
&- \frac{128x^2(2a_{4,(1)} + 4\alpha_{(1)} - 3a_{2,(1)})}{x^4-1}\,,
\end{aligned}
\tag{J.26}
$$

$$
\begin{aligned}
0 = a'_{4,(2)} &- \frac{4x^4}{3(x^4-1)} a'_{2,(2)} + 2x(\alpha'_{(1)})^2 + \frac{x(x^4-9)}{9(x^4-1)} (a'_{2,(1)})^2 \\
&- \frac{4(x^4(3a_{4,(1)} - 3a_{2,(1)} - 32) + 6a_{4,(1)})}{9(x^4-1)} a'_{2,(1)} + \frac{8\alpha_{(1)}(32x^4 + \alpha_{(1)})}{x(x^4-1)} \\
&+ \frac{2(32x^4(3a_{4,(1)} - 4a_{2,(1)}) + 3a_{4,(1)}^2 + 2a_{4,(2)})}{x(x^4-1)} ,
\end{aligned} \tag{J.27}
$$

$$
\begin{aligned}
0 =& a'_{1,(2)} + \frac{2(x^4-3)}{3(x^4-1)} a'_{2,(2)} + \frac{x(x^4-9)}{9(x^4-1)} (a'_{2,(1)})^2 + \frac{2}{9(x^4-1)} \Big(x^4(3a_{1,(1)} - 3a_{2,(1)} + 64) \\
&- 9a_{1,(1)} - 12a_{4,(1)} + 9a_{2,(1)} \Big) a'_{2,(1)} + 2x(\alpha'_{(1)})^2 - \frac{8\alpha_{(1)}^2}{x(x^4-1)} + \frac{256x^3\alpha_{(1)}}{3(x^4-1)} \\
&- \frac{2}{3x(x^4-1)} \Big(6a_{4,(2)} + 32x^4(4a_{2,(1)} - a_{1,(1)}) + 2a_{4,(1)}(-32x^4 + 3a_{1,(1)}) + 3a_{4,(1)}^2 \Big) .
\end{aligned} \tag{J.28}
$$

Eqs. (J.22) and (J.23) can be solved analytically, see (J.11), while the remaining ones have to be solved numerically. We find:

(n)	$a_{2,2,0,(n)}$	$a_{4,2,0,(n)}$	$\alpha_{1,0,(n)}$	$a_{1,h,0,(n)}$	$a_{2,h,0,(n)}$	$r_{h,0,(n)}$
(1)	8	$\frac{16\pi^2}{9}$	$-\frac{4}{3}\pi^2$	-7.2270(2)	$\frac{4}{3}\pi^2$	-9.770(3)
(2)	-1203.9(2)	1064.0(4)		652.34(4)	-863.4(3)	

(J.29)

An important check on the numerical results are the first law of thermodynamics FL (6.66) and the thermodynamic relation TR (6.67). Given the perturbative expansions (J.21), and using the representation (J.14), we find:

- at order $n = 1$:

$$
\begin{aligned}
fl_{(1)} : \qquad & 0 = \frac{2}{3} a_{2,h,0,(1)} - 16 - a_{1,h,0,(1)} , \\
tr_{(1)} : \qquad & 0 = -2a_{2,h,0,(1)} - 48 - a_{1,h,0,(1)} + 4a_{2,2,0,(1)} + 2a_{4,2,0,(1)} ;
\end{aligned} \tag{J.30}
$$

- and at order $n = 2$:

$$
\begin{aligned}
&fl_{(2)}: \; 0 = -\frac{2}{3}a_{2,h,0,(1)}a_{1,h,0,(1)} + \frac{896}{9} + \frac{32}{3}a_{2,h,0,(1)} + \frac{10}{3}a_{2,h,0,(2)} - 2r_{h,0,(1)}^2 + \frac{19}{9}a_{2,h,0,(1)}^2 \\
&+ a_{1,h,0,(1)}^2 - 8\alpha_{1,0,(1)}^2 - a_{1,h,0,(2)} - \frac{16}{3}a_{2,2,0,(2)} - 2a_{4,2,0,(2)} + 16a_{1,h,0,(1)} - \frac{64}{3}r_{h,0,(1)}\,, \\
&tr_{(2)}: \; 0 = \frac{2432}{9} - 8a_{2,2,0,(1)}a_{2,h,0,(1)} - 4a_{2,h,0,(1)}a_{4,2,0,(1)} - 4a_{1,h,0,(1)}a_{2,2,0,(1)} \\
&- 2a_{1,h,0,(1)}a_{4,2,0,(1)} + a_{1,h,0,(1)}^2 + 48a_{1,h,0,(1)} - a_{1,h,0,(2)} + \frac{352}{3}a_{2,h,0,(1)} - 2a_{2,h,0,(2)} \\
&+ 2a_{2,h,0,(1)}a_{1,h,0,(1)} + 3a_{2,h,0,(1)}^2 - 2r_{h,0,(1)}^2 + 8\alpha_{1,0,(1)}^2 - \frac{64}{3}r_{h,0,(1)} - \frac{64}{3}a_{2,2,0,(1)} \\
&+ 4a_{2,2,0,(2)} - \frac{32}{3}a_{4,2,0,(1)} + 2a_{4,2,0,(2)}\,.
\end{aligned}
\tag{J.31}
$$

Using the results (J.29) (rather, we use more precise values of the parameters reported — obtained from numerics with 40 digit precision) we find

- at order $n = 1$:

$$
fl_{(1)}: \qquad 0 = -7.7822(6) \times 10^{-15}\,, \qquad tr_{(1)}: \qquad 0 = -2.9555(5) \times 10^{-15}\,; \tag{J.32}
$$

- and at order $n = 2$:

$$
fl_{(2)}: \qquad 0 = -1.6451(1) \times 10^{-6}\,, \qquad tr_{(2)}: \qquad 0 = 2.2505(2) \times 10^{-6}\,. \tag{J.33}
$$

Using the perturbative expansion (J.21), it is straightforward to invert the relation between $T/\sqrt{B}$ and b (see (6.64) and (6.30)), and use the results (6.62) with (6.43), along with the analytical values for the parameters (J.29), to arrive at

$$
\begin{aligned}
R_{\mathbb{CFT}_{PW,m=0}} &= 1 - \frac{4B^2}{\pi^4 T^4}\ \ln\frac{T}{\mu\sqrt{2}} + \left(\frac{\pi^2}{18} + \frac{a_{2,2,0,(2)}}{512} - \frac{2}{3} + 8\ \ln^2\frac{T}{\mu\sqrt{2}}\right)\ \frac{B^4}{\pi^8 T^8} + \cdots \\
&= 1 - \frac{4B^2}{\pi^4 T^4}\ \ln\frac{T}{\mu\sqrt{2}} + \left(-2.4697(5) + 8\ \ln^2\frac{T}{\mu\sqrt{2}}\right)\ \frac{B^4}{\pi^8 T^8} + \mathcal{O}\left(\frac{B^6}{T^{12}}\ln^3\frac{T}{\mu}\right)\,.
\end{aligned}
\tag{J.34}
$$

Note that while the first line in (J.34) is equivalent to the corresponding expression in (J.19), the numerical values (compare the second lines) are different: this is related to the fact that the value $a_{2,2,0,(2)}$ in the $\mathbb{CFT}_{PW,m=0}$ dual is "sourced" by a single dimension $\Delta = 2$ operator (the scalar field α in the holographic dual), while the value $a_{2,2,(2)}$ in the $\mathbb{CFT}_{STU}$ model is "sourced" by two dimension $\Delta = 2$ operators (the scalar fields ρ and ν in the holographic dual).

J.0.3 $\mathbb{CFT}_{PW,m=\infty}$

The high temperature expansion corresponds to the perturbative expansion in $\hat{b}$. In what follows we study anisotropic thermodynamics to order $\mathcal{O}(\hat{b}^4)$ inclusive. Introducing

$$
\begin{aligned}
&a_1 = 1 + \sum_{n=1}^{\infty} a_{1,(n)}\ \hat{b}^{2n}\,, \qquad a_2 = 1 + \sum_{n=1}^{\infty} a_{2,(n)}\ \hat{b}^{2n}\,, \qquad a_4 = 1 + \sum_{n=1}^{\infty} a_{4,(n)}\ \hat{b}^{2n}\,, \\
&p = \sum_{n=1}^{\infty} p_{(n)}\ \hat{b}^{2n}\,,
\end{aligned}
\tag{J.35}
$$

so that (see (6.36) and (6.37) for the asymptotics)

$$
\begin{aligned}
&a_{1,5} = \sum_{n=1}^{\infty} a_{1,5,(n)}\ \hat{b}^{2n}\,, \qquad a_{2,5} = \sum_{n=1}^{\infty} a_{2,5,(n)}\ \hat{b}^{2n}\,, \qquad p_3 = \sum_{n=1}^{\infty} p_{3,(n)}\ \hat{b}^{2n}\,, \\
&a_{1,h,0} = 1 + \sum_{n=1}^{\infty} a_{1,h,0,(n)}\ \hat{b}^{2n}\,, \qquad a_{2,h,0} = 1 + \sum_{n=1}^{\infty} a_{2,h,0,(n)}\ \hat{b}^{2n}\,, \\
&p_{h,0} = 1 + \sum_{n=1}^{\infty} p_{h,0,(n)}\ \hat{b}^{2n}\,,
\end{aligned}
\tag{J.36}
$$

we find

- at order $n = 1$:

$$
0 = a''_{2,(1)} + \frac{x^5+4}{(x^5-1)x} a'_{2,(1)} - \frac{32x^2}{9(x^5-1)}\,,
\tag{J.37}
$$

$$
0 = a'_{4,(1)} - \frac{1}{(x^5-1)x}\left(\frac{5}{4} a'_{2,(1)} x^6 - 5a_{4,(1)} - \frac{4}{3}x^4\right)\,,
\tag{J.38}
$$

$$
0 = a'_{1,(1)} + \frac{3x^5-8}{4(x^5-1)} a'_{2,(1)} + \frac{1}{(x^5-1)x}\left(\frac{4}{9}x^4 - 5a_{4,(1)}\right)\,,
\tag{J.39}
$$

$$
0 = p''_{(1)} + \frac{x^5+4}{x(x^5-1)} p'_{(1)} - \frac{1}{x^2(x^5-1)}\left(6p_{(1)} - \frac{8}{9}x^4\right)\,;
\tag{J.40}
$$

- and at order $n = 2$ (we will not need $p_{(2)}$):

$$
\begin{aligned}
0 = &a''_{2,(2)} + \frac{x^5+4}{x(x^5-1)} a'_{2,(2)} - (a'_{2,(1)})^2 + \frac{2(4x^4+45a_{4,(1)})}{9x(x^5-1)} a'_{2,(1)} \\
&+ \frac{32x^2}{9(x^5-1)}\left(3a_{2,(1)} - 2a_{4,(1)} - 2p_{(1)}\right)\,,
\end{aligned}
\tag{J.41}
$$

$$
\begin{aligned}
0 =& a'_{4,(2)} - \frac{1}{x(x^5-1)}\left(\frac{5}{4}a'_{2,(2)}x^6 - 5a_{4,(2)}\right) + \frac{x(x^5-6)}{8(x^5-1)}(a'_{2,(1)})^2 - \frac{1}{36(x^5-1)}\Bigg(\\
& 45a_{4,(1)}x^5 - 45a_{2,(1)}x^5 - 8x^4 + 90a_{4,(1)}\Bigg)a'_{2,(1)} + \frac{x}{2}(p'_{(1)})^2 + \frac{1}{6x(x^5-1)}\Bigg(16x^4p_{(1)} \\
& + 24x^4a_{4,(1)} - 32a_{2,(1)}x^4 + 18p^2_{(1)} + 45a^2_{4,(1)}\Bigg),
\end{aligned}
\tag{J.42}
$$

$$
\begin{aligned}
0 =& \ a'_{1,(2)} + \frac{1}{x(x^5-1)}\left(\frac{3}{4}a'_{2,(2)}x^6 - 5a_{4,(2)} - 2a'_{2,(2)}x\right) + \frac{x(x^5-6)}{8(x^5-1)}(a'_{2,(1)})^2 + \frac{x}{2}(p'_{(1)})^2 \\
& + \frac{1}{36(x^5-1)}\left(27a_{1,(1)}x^5 - 27a_{2,(1)}x^5 + 8x^4 - 72a_{1,(1)} - 90a_{4,(1)} + 72a_{2,(1)}\right)a'_{2,(1)} \\
& - \frac{1}{18x(x^5-1)}\Bigg(45a^2_{4,(1)} - 16x^4p_{(1)} - 8a_{1,(1)}x^4 - 16x^4a_{4,(1)} + 32a_{2,(1)}x^4 + 54p^2_{(1)} \\
& + 90a_{1,(1)}a_{4,(1)}\Bigg).
\end{aligned}
\tag{J.43}
$$

Eqs. (J.37) and (J.38) can be solved analytically[1], while the remaining ones have to be solved numerically. We find:

(n)	$a_{1,5,(n)}$	$a_{2,5,(n)}$	$p_{3,(n)}$	$a_{1,h,0,(n)}$	$a_{2,h,0,(n)}$	$p_{h,0,(n)}$
(1)	-0.25581(6)	$-\frac{32}{45}$	-0.645(2)	-0.12878(5)	0.27576(4)	-0.25155(9)
(2)	0.22327(6)	-0.5489(8)		0.20658(5)	-0.2934(9)	

(J.44)

An important check on the numerical results are the first law of thermodynamics FL (6.94) and the thermodynamic relation TR (6.95). Given the perturbative expansions (J.36), and using the representation (J.14), we find:

[1]However, the resulting expressions are too long to be presented here. For the same reason we report only the numerical expression for $a_{2,h,0,(1)}$.

- at order $n = 1$:

$$\begin{aligned}
fl_{(1)}: &\qquad 0 = -\frac{4}{45} - \frac{2}{5}a_{1,5,(1)} - a_{1,h,0,(1)} + \frac{1}{5}a_{2,5,(1)}\,, \\
tr_{(1)}: &\qquad 0 = -\frac{4}{45} - 2a_{2,h,0,(1)} - 2a_{1,5,(1)} - a_{1,h,0,(1)}\,;
\end{aligned} \tag{J.45}$$

- and at order $n = 2$:

$$\begin{aligned}
fl_{(2)}: &\qquad 0 = \frac{8}{675} + \frac{2}{5}a_{1,5,(1)}a_{1,h,0,(1)} - \frac{1}{5}a_{1,h,0,(1)}a_{2,5,(1)} + a^2_{1,h,0,(1)} + \frac{16}{45}a_{2,h,0,(1)} \\
&\qquad + 2a_{2,h,0,(2)} + \frac{4}{45}a_{1,h,0,(1)} - a_{1,h,0,(2)} - \frac{8}{45}p_{h,0,(1)} - \frac{4}{225}a_{2,5,(1)} \\
&\qquad - \frac{3}{5}a_{2,5,(2)} + \frac{8}{225}a_{1,5,(1)} + \frac{6}{5}a_{1,5,(2)} - \frac{3}{5}p^2_{h,0,(1)} + a^2_{2,h,0,(1)}\,, \\
tr_{(2)}: &\qquad 0 = \frac{8}{675} + \frac{8}{15}a_{2,h,0,(1)} - 2a_{2,h,0,(2)} - \frac{8}{45}p_{h,0,(1)} - \frac{3}{5}p^2_{h,0,(1)} + 3a^2_{2,h,0,(1)} \\
&\qquad + 4a_{2,h,0,(1)}a_{1,5,(1)} + 2a_{2,h,0,(1)}a_{1,h,0,(1)} + 2a_{1,5,(1)}a_{1,h,0,(1)} + a^2_{1,h,0,(1)} \\
&\qquad - 2a_{1,5,(2)} - a_{1,h,0,(2)} + \frac{4}{45}a_{1,h,0,(1)} + \frac{8}{45}a_{1,5,(1)}\,.
\end{aligned} \tag{J.46}$$

Using results (J.44) (rather, we use more precise values of the parameters reported — obtained from numerics with 40 digit precision) we find

- at order $n = 1$:

$$fl_{(1)}: \qquad 0 = 1.8010(4) \times 10^{-12}\,, \qquad tr_{(1)}: \qquad 0 = 9.8392(9) \times 10^{-12}\,; \tag{J.47}$$

- and at order $n = 2$:

$$fl_{(2)}: \qquad 0 = -1.0535(2) \times 10^{-12}\,, \qquad tr_{(2)}: \qquad 0 = -3.3646(2) \times 10^{-12}\,. \tag{J.48}$$

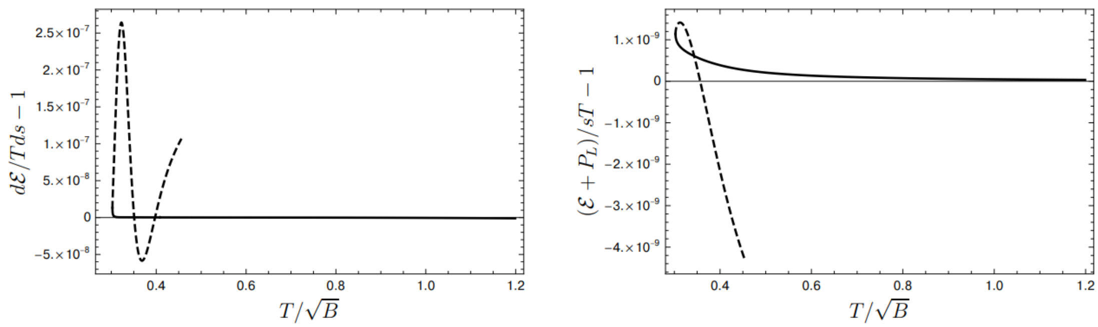

Figure J.1: Numerical checks of the first law of thermodynamics $d\mathcal{E} = Tds$ (left panel, fixed B and m) and the basic thermodynamic relation $\mathcal{F} = -P_L$ (right panel) in the $n\mathbb{CFT}_m$ model with $m = \sqrt{2B}$. The dashed parts of the curves indicate thermodynamically unstable branches of the model.

Using the perturbative expansion (J.36), it is straightforward to invert the relation between $T/\sqrt{B}$ and $\hat{b}$ (see (6.93)), and arrive at

$$\begin{aligned}
R_{\mathbb{CFT}_{PW,m=\infty}} =& 1 + \frac{3125}{512} a_{2,5,(1)} \, \frac{B^2}{\pi^4 T^4} + \frac{390625}{4718592}\bigg(90 a_{1,5,(1)} a_{2,5,(1)} + 180 a_{1,h,0,(1)} a_{2,5,(1)} \\
&+ 180 a_{2,5,(1)}^2 + 16 a_{2,5,(1)} + 45 a_{2,5,(2)} \bigg) \, \frac{B^4}{\pi^8 T^8} + \mathcal{O}\left(\frac{B^6}{T^{12}}\right) \\
=& 1 - \frac{625}{144} \, \frac{B^2}{\pi^4 T^4} + 7.2682(1) \, \frac{B^4}{\pi^8 T^8} + \mathcal{O}\left(\frac{B^6}{T^{12}}\right) .
\end{aligned} \tag{J.49}$$

J.1 FT and TR in a $n\mathbb{CFT}_m$ model

In this appendix we verified the first law of the thermodynamics (FL) and the basic thermodynamic relation $\mathcal{F} = -P_L$ (TR) in various anisotropic magnetized holographic plasma models perturbatively in $\frac{T}{\sqrt{B}} \gg 1$. In fact, we verified both constraints, in all the models considered in chapter 6, for finite values of $\frac{T}{\sqrt{B}}$. In Fig. J.1 we present the checks on these constraints in the $n\mathbb{CFT}_m$ model with $\frac{m}{\sqrt{2B}} = 1$.